# Site U1343[1]

Expedition 323 Scientists[2]

## Chapter contents



[1] Expedition 323 Scientists, 2011. Site U1343. *In* Takahashi, K., Ravelo, A.C., Alvarez Zarikian, C.A., and the Expedition 323 Scientists, *Proc. IODP,* 323: Tokyo (Integrated Ocean Drilling Program Management International, Inc.). doi:10.2204/iodp.proc.323.107.2011
[2] Expedition 323 Scientists' addresses.

## Background and objectives

The primary objective of drilling at Integrated Ocean Drilling Program (IODP) Site U1343 (proposed Site GAT-4C; Takahashi et al., 2009) was to study high-resolution Pliocene–Pleistocene paleoceanography at a location proximal to the gateway to the Arctic Ocean. Additionally, this site is closer to the current seasonal sea ice limit, and its ~2 km water depth provides information regarding the history of mid-depth water mass characteristics in the Aleutian Basin. This site is located at a depth of 1953 m on a topographic high clearly separated from the Bering shelf (Figs. **F1, F2, F3, F4, F5**). Hence, it was anticipated to have received a lower supply of reworked terrigenous sediment from the shelf during the interglacials or from subaerially exposed land during the glacials than a location directly downslope of the Bering shelf.

Site U1343 is in an area of high biological productivity called the "Green Belt." The Green Belt is formed by the Bering Slope Current (BSC), which originates from the Alaskan Stream water that flows into the Bering Sea through the western Aleutian Islands. The water that enters the Bering Sea moves eastward along the Aleutian Islands and consequently encounters the Bering shelf. The BSC is at ~300 m, and its flow is forced to turn to the northwest once it meets the slope and shelf; eddies and instabilities in its flow cause upwelling along the shelf break. Moreover, tidal mixing causes further vertical mixing of the water masses along the BSC, enhancing biological productivity within the Green Belt, which is adjacent to the northwest-trending shelf break, where high primary productivity in the surface waters and high organic carbon accumulation at the seafloor take place (Taniguchi, 1984; Springer et al., 1996). Because of the expected high organic carbon supply to the seafloor, especially during the interglacial sea level highstands, it is possible that the oxygen minimum zone (OMZ) previously extended to the depth of this site. In order to compare the vertical extent of water mass conditions across the basin and relate the OMZ to paleoproductivity, records from shallower drill sites on Bowers Ridge (IODP Site U1340, water depth = 1295 m, and IODP Site U1342, water depth = 818 m) and other slope sites will be used. This site is also located close to the maximum extent of present-day seasonal sea ice cover. Thus, this site is expected to have been covered by seasonal or perennial sea ice during the glacial sea level lowstands.


doi:10.2204/iodp.proc.323.107.2011

This drill site in the gateway region to the Arctic Ocean can also be used to study the impact of subseafloor microbes on biogeochemical fluxes in the highest surface-ocean productivity areas of the Bering Sea drill sites. Organic-fueled subseafloor respiration and its impact on biogeochemistry in such a highly productive region have not previously been quantified. To do so, drilled sediments in the gateway region were used to determine subseafloor cell abundances and to investigate the link between the mass and characteristics of subseafloor microbes and the extent of export productivity from the surface ocean (Takahashi et al., 2000).

Sedimentation rates at this site were not previously known because piston cores were unavailable. However, rates of ~180 m/m.y. were observed in an earlier site survey piston core study (Takahashi, 2005) at IODP Site U1344 (Fig. F1). Thus, we expected to recover Pleistocene to Pliocene sections.

# Operations

Five holes were cored at Site U1343 (Table T1). Hole U1343A was cored with the advanced piston corer (APC) system and drilled to 201.5 m drilling depth below seafloor (DSF). Hole U1343B was dedicated to microbiology and cored to 35.5 m DSF. Hole U1343C was cored with the APC system to 234.2 m DSF. Only a single mudline core was taken in Hole U1343D, and we decided to attempt another mudline core for stratigraphic correlation. Hole U1343E was cored with the APC and extended core barrel (XCB) systems to 744.3 m DSF. The XCB system was needed for Cores 323-U1343E-42X through 45X, where we encountered dry sediment and retrieved a destroyed core liner (42X), and for the deepest cores (323-U1343-50X through 83X). The shallower interval cored with the XCB system coincided with a bottom-simulating reflector (BSR). Coring was generally routine except for encountering biogenic methane in the cores, which complicated the curation of all cores at this site. APC coring totals for Site U1343 include 98 cores, 860.4 m penetrated, and 860.0 m recovered, for 100% core recovery. XCB coring for Site U1343 totaled 37 cores, 360.6 m penetrated, and 318.41 m recovered, for 88.3% core recovery. The total cored interval for Site U1343 was 1221.0 m with 1178.43 m of core recovered, for 96.5% total core recovery. The time spent at Site U1343 was 6.7 days.

## Hole U1343A

Hole U1343A was spudded at 0305 h on 7 August 2009 (all times are ship local time, Universal Time Coordinated [UTC] – 11 h). The first mudline core recovered 5.5 m of sediment, and the calculated seafloor was 1962.4 m drilling depth below rig floor (DRF). APC coring using nonmagnetic coring assemblies continued through Core 323-U1343A-22H to 201.5 m DSF. Temperature measurements were taken on Cores 323-U1343A-5H, 9H, and 14H with the third-generation advanced piston corer temperature tool (APCT-3). Core orientation was taken on all cores with the FlexIt orientation tool, but the data were lost when the computer running the download software was accidentally switched off during the FlexIt operations, causing the program to lose synchronization with the tool. Overall core recovery for Hole U1343A using the APC system was 101.26%, with 204.03 m recovered.

## Hole U1343B

The vessel was offset 30 m north, and Hole U1343B was spudded at 2240 h on 7 August. The first mudline core recovered 6.85 m of sediment, and the calculated seafloor was 1962.4 m DRF. Both perfluorocarbon tracer (PFT) and microsphere contamination testing methods were deployed. Four APC cores were recovered for microbiological sampling to 35.5 m DSF. Average APC core recovery for Hole U1343B was 97.4%, with 34.56 m recovered.

## Hole U1343C

The ship was offset 30 m west from the proposed site position. The APC was deployed, and Hole U1343C was spudded at 0305 h on 8 August. The first mudline core recovered 7.2 m of sediment, and the calculated seafloor was 1964.2 m DRF. APC coring using nonmagnetic coring assemblies continued through Core 323-U1343C-26H to 234.2 m DSF. Overall core recovery for Hole U1343C using the APC coring system was 98.7%, with 231.04 m recovered.

## Hole U1343D

Hole U1343D was spudded 30 m south of Hole U1343C at 0135 h on 9 August. Based on stratigraphic correlation of the first and only core, Hole U1343D was terminated at 0135 h. Overall core recovery for Hole U1343D using the APC coring system was 100.0%, with 8.5 m recovered.

## Hole U1343E

Hole U1343E was not offset from Hole U1343D and was spudded at 0215 h on 9 August. The first core barrel recovered 8.2 m of core, and an official seafloor depth was established at 1967.5 m DRF. APC coring continued through Core 323-U1343E-15H using standard steel core barrels. At Core 323-U1343E-16H the nonmagnetic barrels were put in service and used for the rest of the hole. Coring with the APC

system was suspended after Core 323-U1343E-41H was pulled with a ruptured core liner and had to be hydraulically pressed out of the core barrel. This coincided with a BSR observed in the seismic data. The core was also noticeably drier and harder at this depth. The XCB coring system was then deployed from Cores 323-U1343E-42X through 45X with good recovery. The APC coring system was put back into service for Cores 323-U1343E-46H through 49H. At that time we began to get partial strokes of the piston and were having to drillover every core. The XCB system was redeployed, and coring continued through Core 323-U1343E-83X to 744.3 m DSF. The coring tools were secured, and the hole was swept clean and displaced with 200 bbl of prepared high-viscosity logging mud. No fill was identified at total depth. Two logging strings were deployed. The triple combination (triple combo) tool string reached total depth of 745 m wireline log depth below seafloor (WSF), and good-quality logs were obtained. The second logging string consisted of the Formation MicroScanner (FMS)-sonic tool, which reached total depth of 745 m WSF and also obtained good data on both passes. Wireline logging in Hole U1343E was successfully concluded and all logging equipment was rigged down by 0745 h on 13 August. APC core recovery for Hole U1343E was 100.3%, with 381.86 m recovered. XCB core recovery for Hole U1343E was 88.3%, with 318.41 m recovered. Total core recovery for Hole U1343E was 94.47%, with 700.27 m recovered.

# Lithostratigraphy

Five holes were cored at Site U1343, reaching a maximum depth of 744.0 meters below seafloor (mbsf) in Hole U1343E. The sediments at this site are primarily composed of silt with varying amounts of clay and diatoms and minor amounts of sand, ash, foraminifers, calcareous nannofossils, and sponge spicules. Authigenic carbonates appear in all holes deeper than 35 mbsf. The sediments are predominantly dark/very dark greenish gray to dark/very dark gray. One lithologic unit spanning the early Pleistocene to the Holocene was defined at this site.

## Description of unit

### Unit I

Intervals: Sections 323-U1343A-1H-1, 0 cm, through 22H-CC, 58 cm; 323-U1343B-1H-1, 0 cm, through 4H-CC, 26 cm; 323-U1343C-1H-1, 0 cm, through 26H-CC, 31 cm; 323-U1343D-1H-1, 0 cm, through 1H-CC, 14 cm; and 323-U1343E-1H-1, 0 cm, through 83X-CC, 40 cm

Depths: Hole U1343A, 0–201.76 mbsf; Hole U1343B, 0–35.26 mbsf; Hole U1343C, 0–234.72 mbsf; Hole U1343D, 0–8.53 mbsf; and Hole U1343E, 0–744.00 mbsf

Age: early Pleistocene to Holocene

Two mainly siliciclastic and mixed siliciclastic-biogenic lithologies alternate on a decimeter to meter scale. The siliciclastic sediments (<40% biogenic components) are mostly diatom-rich clayey silt/silt/silty clay. The mixed siliciclastic-biogenic sediments (>40% biogenic components) are mixed lithologies of silt/clay and diatoms, diatom ooze, and laminated diatom ooze with varying abundances of foraminifers, calcareous nannofossils, and sponge spicules. Siliciclastic and mixed sediments vary in color from very dark greenish gray (10Y 3/1) and dark greenish gray (10Y 4/1) to dark gray (4/N) and very dark gray (5Y 3/1). Diatom oozes are generally olive-gray (5Y 4/2) and dark greenish gray (10Y 4/1). The boundaries between changes in lithologies are usually gradational, and the color and texture changes are very subtle. There is no visible soft-sediment deformation at this site.

In the main lithologies, foraminifers, calcareous nannofossils, and sponge spicules are generally rare (<5%). Sponge spicules occur frequently as sponge spicule aggregates throughout the cores and may be the remains of agglutinated benthic foraminifers. The siliciclastic fraction is composed of quartz, feldspar, rock fragments (commonly polycrystalline quartz), micas, and clay minerals. The occurrence of clay minerals at Site U1343 is generally higher than at the Bowers Ridge sites. Many millimeter-sized pyrite-rich specks occur throughout the cores. Pyrite is also abundant in the smear slides (average = 4%) (see **"Site U1343 smear slides"** in "Core descriptions"). Numerous bivalve shells and shell fragments were found at this site, especially in Hole U1343E below 500 mbsf.

Six laminated intervals occur at this site, and these can be correlated between Holes U1343A, U1343C, U1343D, and U1343E based on lithologic, reflectance, and magnetic susceptibility data (Figs. **F6, F7, F8**). In two cases the laminated intervals are correlated to bioturbated diatom ooze or diatom silt intervals in Hole U1343E. In two other cases they are laterally discontinuous and correlate to gaps between cores (Fig. **F9**). In Hole U1343A the intervals are at 1.1, 2.9, 35.9, 44.2, and 109.2 mbsf. In Hole U1343C the bases of the intervals are at 1.1, 2.7, 36.7, 108.9, and 122.7 mbsf. In Hole U1343D the base of the interval is at 1.6 mbsf. In Hole U1343E the bases of the intervals are at 30.9, 41.9, 104.1, and 117.6 mbsf. Smear slide observations show that these lamina-

tions can be foraminifer rich (as much as 40%). However, they are poor in silicoflagellates (1%–2%) and calcareous nannofossils (as much as 2%–3%). This contrasts with previous sites, where calcareous nannofossils are abundant in laminated intervals. Laminated intervals have bioturbated gradational top boundaries and either sharp or gradational lower boundaries. In the latter case, the laminations themselves are slightly bioturbated, and some laminae are consequently wavy or discontinuous. Observations that laminated sediments in one hole correlate to a bioturbated diatom ooze or diatom silt in another hole indicate spatial heterogeneity in the preservation of laminations, as observed at other sites (see the **"Site U1342"** chapter).

The induration of sediments at Site U1343 is soft throughout Holes U1343A–U1343D and the upper part of Hole U1343E. The sediments are stiff in Hole U1343E below 456 mbsf (Core 323-U1343E-54X). In this hole, two notable cores (323-U1343E-41H and 52X) contain stiff sediment, although the surrounding cores are soft. The sediments in Core 323-U1343E-52X are very stiff but abruptly change in the middle of Section 323-U1343E-53X-1 (447.0 mbsf) to soupy, water-rich material and then change back to soft sediment in the middle of Section 53X-4 (452.0 mbsf). XRD analysis did not reveal any evidence of silica diagenesis in these cores (see XRD in **"Supplementary material"**). Logging data from this interval (see **"Downhole measurements"**) show that the strata have unusually low density values, so the waterlogged sediment is a real feature that was probably disturbed during the coring process.

The sediments in Core 323-U1343E-41H are so hard that the core liner shattered. This core (346.8–354.4 mbsf) coincides with the depth of the BSR (see **"Physical properties"**). The sediments in Cores 323-U1343E-43X through 45X (360.4–388.4 mbsf) are distinct from the rest of the site. These sediments contain no diatoms, and the siliciclastic sediments are clays with a sticky texture that differ from the typically silty sediments at this site. The bulk density of these sediments is 1.6 g/cm$^3$ on average, in sharp contrast to Core 323-U1343E-41X, which reaches a maximum density of 2.0 g/cm$^3$, supporting the observed change in lithology (see **"Physical properties"**).

Bioturbation is slight to moderate throughout the cores, with the exception of the laminated intervals that do not show obvious bioturbation. The transitions between sediments with different colors or textures sometimes have centimeter-scale mottling and sometimes are gradational. In general, centimeter-scale mottles contain silty clay, sandy silt, sand, ash, and/or pyrite. There are numerous sandy patches or layers at Site U1343. Sandy lithologies are concentrated in four intervals in Hole U1343E (~58–64, ~140–180, ~300–450, and ~675–740 mbsf). In Sections 323-U1343A-1H-2 (1.56–3.00 mbsf) and 323-U1343C-1H-2 (1.83–2.02 mbsf), pervasive millimeter-scale mottling occurs at the transitions from olive-gray to dark greenish gray diatom-rich and diatom-poor lithologies, respectively. Presumably, these mottles would become less distinct with increasing burial depth and compaction and would appear as a gradual color change between the two lithologies.

Subrounded to well-rounded granule- to pebble-sized clasts occur frequently at Site U1343. The clasts are often black and fine grained and are likely of volcanic origin. An 8 cm black rounded basalt cobble was found in Section 323-U1343E-34H-CC (Fig. **F10**). There are no obvious changes in the frequency or clustering of clasts through the holes. The sediments at Site U1343 are noticeably sandier than at the other sites. The lithologies with >25% sand-sized siliciclastic grains are predominantly purely siliciclastic lithologies rather than mixed siliciclastic-biogenic ones.

Ash is less common at this site than at sites farther south. However, there are numerous thin ash layers in all holes in addition to ash-filled mottles. The ash is usually fine grained and gray in color, whereas black ash is less common.

Authigenic carbonates occur frequently at Site U1343. Authigenic euhedral crystal shapes such as rhombs, acicular crystals, and globular crystals with extreme birefringence were observed in many smear slide samples. The crystals are usually 4–10 µm long, but some are as long as 50 µm (see **"Site U1343 smear slides"** in "Core descriptions"). The sediment containing authigenic carbonates tends to be slightly lighter or more yellowish in color than the surrounding sediment. Occasionally, the authigenic carbonate–rich layers are semilithified and much paler in color and are referred to as dolostone. Smear slide samples taken from around the dolostones typically are rich in rhombic carbonate crystals, and an X-ray diffraction (XRD) sample from one such layer shows the presence of dolomite (Fig. **F11C–F11D**); another shows the presence of high-magnesium calcite (Fig. **F11A–F11B**) (see XRD in **"Supplementary material"**). Authigenic carbonates are more common in Hole U1343E below 550 mbsf, appearing in 18 of 25 cores at this interval.

Mollusk shells were found in all holes at Site U1343. The frequency of shell occurrence increases by an order of magnitude in Hole U1343E below 500 mbsf, where shells were observed every 3.6 m on average. They were observed every 34 m on average above 500 mbsf in Hole U1343E. Shells were sometimes as-

sociated with authigenic carbonates. In one case, in Section 323-U1343E-82X-6, 82 cm, a 3 cm long shell was bisected in core splitting, and the sediment within and immediately around the shell was rich in authigenic carbonates.

The presence of gas in the sediments caused several types of coring disturbance that affected the stratigraphic integrity of the sediment. Below Cores 323-U1343A-6H, 323-U1343C-5H, and 323-U1343E-8H, the sediment at the top of the sections was ejected out of the core barrel by gas expansion and 20–150 cm of sediment was extruded onto the deck. This sediment was pushed back into a core liner; however, some sediment pieces may be out of order or upside down. In all holes, punctures were made in all cores from Core 3H and down, potentially causing significant loss of sediment from extrusion. However, punctures were not always noted in core descriptions because punctures are not always visible on the cut surfaces of the cores. Below 25–30 mbsf in all holes there are numerous cracks and voids from gas expansion, which affected physical property (gamma ray attenuation [GRA] bulk density, in particular) and color reflectance measurements. In addition, wafers of sediment between wide voids were broken and jumbled during core splitting. The other common coring disturbance was biscuiting, which was common in cores recovered with the XCB from Hole U1343E (Fig. **F12**).

## Discussion

Unit I at Site U1343 encompasses a slightly longer time period than Unit I at all other sites. However, Site U1343 is distinct in having a higher proportion of siliciclastic versus biogenic grains than the Bowers Ridge sites, which is probably related to its location adjacent to the continental slope and its relative proximity to the source of terrigenous sediments. Also, at this site a higher occurrence of sand-sized grains were observed in smear slides. During glacial sea level lowstands, particularly during early stages of deglaciations, significant amounts of coarser grained detrital material may have been mobilized from the exposed Bering Sea shelf and redeposited farther down the continental slope.

Changes in the proportion of siliciclastic and mixed siliciclastic-biogenic sediments are probably related to changes in primary productivity, sea level, the proximity and flux of terrigenous sediments from rivers, and delivery by ice through glacial–interglacial cycles. The siliciclastic flux to this site may be influenced by the trajectory of the sediment load of the Yukon River, which is the largest shelf source of sediment in the Bering Sea and whose path across the shelf during times of lower sea level is unknown. Yukon-source sediment is observed to be advected southward through the Kamchatka Strait or northward through the Bering Strait as a function of glacial–interglacial changes in sea level and circulation (VanLaningham et al., 2009). The four intervals of sandy lithologies can be tentatively correlated to similar sand-rich intervals at Site U1344 (Cores 323-U1344A-5H through 8H, 21H through 25H, 48X through 50X, and 74X) (see **"Lithostratigraphy"** in the "Site U1344" chapter), a deeper site that is also just south of the continental shelf. The same deposition mechanism is likely responsible for the sandy intervals in cores from both holes. Clasts were probably transported to this site by ice, although ice can transport clay-, silt-, and sand-sized grains as well. There is not a clear correlation between sand-rich lithologies and clasts, but both kinds of grains were probably undersampled in the smear slides and visual core descriptions. Other mechanisms such as mass gravity flows can transport sand-sized and smaller grains; however, no intervals that appeared to be the result of such a mass movement were observed.

Diatom ooze and mixed diatom-siliciclastic lithologies are generally associated with low natural gamma radiation (NGR), low bulk density, and low magnetic susceptibility. More siliciclastic lithologies are associated with higher NGR, higher bulk density, and higher magnetic susceptibility. The maxima and minima of these three physical properties do not always coincide, showing that the proportion of biogenic grains is not the only parameter affecting them. For example, as the lithology varies between silt- and clay-sized grains, NGR may reflect mineralogical changes in potassium-rich feldspar and potassium clay-mineral abundance, independent of the absolute dilution of siliciclastic grains by biogenic flux. The general trends in lithologic variations with depth are similar among the holes; however, small-scale lithologic variations are harder to correlate, probably because the lithologic changes were undersampled by smear slides and the different lithologies were very similar in appearance.

The lithologies with a higher abundance of diatoms, particularly laminated intervals, are associated with higher values of color reflectance parameter b* (Figs. **F6, F7, F8**). This is analogous to the changes in diatom abundance and b* at other sites (see the **"Site U1339,"** **"Site U1341,"** and **"Site U1342"** chapters). The uppermost (Holocene) sediments at this site are diatom rich and have the highest vales of b* observed at this site. Biogenic silica flux has been observed to be higher during interglacials than glacials in the Bering Sea (Okazaki et al., 2005), so these in-

tervals of higher biogenic fraction and higher b* are interpreted as interglacials. The diatom ooze and diatom-siliciclastic mixed lithologies often correlate with higher abundances of foraminifers and calcareous nannofossils (see **"Biostratigraphy"**).

Laminations were only observed in the uppermost 130 m of sediment at this site. The laminated intervals are small, and the laminations themselves are thin (submillimeter to millimeter in scale). It is possible that laminated sediments occurred earlier in time but are no longer easily visible in the sediment because of compaction. The laminated and biogenic-rich interval in Core 323-U1343A-12H was sampled more closely for the assemblage of microfossils by the biostratigraphy group and was tentatively identified as marine isotope Stage (MIS) 11 (see **"Biostratigraphy"** for discussion).

The pattern of laminations in Sections 323-U1343A-1H-1 and 1H-2 and 323-U1343C-1H-1 and 1H-2 is similar to that observed in sediments deposited during the last deglaciation in the Bering Sea (Cook et al., 2005) and around the Pacific margin (Van Geen et al., 2003), where the Bølling-Allerød and early Holocene are laminated. The timing of the onset of laminations depends on the position and intensity of the OMZ, local export production, and the water depth of the coring site. The laminated intervals at 1.00–1.10 mbsf in Hole U1343A and 0.97–1.07 mbsf in Hole U1343C are tentatively identified as the early Holocene, and the laminated intervals at 2.17–2.87 mbsf in Hole U1343A, 1.97–2.75 mbsf in Hole U1343C, and 1.03–1.60 mbsf in Hole U1343D are tentatively identified as the Bølling-Allerød. There is a small ash layer below the Bølling-Allerød laminae in Holes U1343A, U1343C, and U1343D. Neither the ash layer nor the laminations occur in Hole U1343E, suggesting that at least 3 m of sediment is missing from the top of that hole relative to the others.

In contrast to other sites, volcaniclastic material is a minor component of sediment at Site U1343 because this site is more distant from the Aleutian arc. Thin ash layers in addition to ash-filled mottles in each hole probably represent bioturbated traces of ash layers. The ash at this site is typically lighter in color than at the Bowers Ridge or Umnak sites, which is consistent with their source being explosive rhyolitic eruptions that would be carried as far as this site.

Many of the clasts deposited at Site U1343 are volcanic. They may have originated from the Aleutian Islands and been transported by ice or they may have been from older volcanic rocks exposed on continental Alaska. Delivery of ice-rafted debris (IRD) to this site may be influenced by the strength of the BSC, which today flows from Umnak Plateau to the northwest. An increase in the occurrence of clasts in Hole U1343E may reflect an increase in ice, an increase in BSC strength, or both.

There is a shallow sulfate–methane transition zone (SMTZ) and abundant methane in the sediment column at Site U1343, as at the other slope Sites U1339 and U1345 (see **"Geochemistry and microbiology"**). This is probably a function of high export production along the Bering Slope Green Belt, where there is upwelling due to the interaction of tides and the bottom topography (Springer et al., 1996). Authigenic dolomite, high-magnesium calcite, and aragonite can form from elevated alkalinity in the SMTZ where the vertical methane flux is high (Peckmann and Thiel, 2004).

Benthic and planktonic foraminifers encrusted with yellow minerals are common at this site (see **"Biostratigraphy"**) and often coincide with samples that contain authigenic carbonates. The association of authigenic carbonates and apparent overgrowths implies that authigenic carbonates nucleated on the foraminifer tests. In this case, the stable isotope records from this site are potentially contaminated by the isotopic signature of the overgrowths, which would have anomalously low $\delta^{13}C$ and high $\delta^{18}O$.

The occurrences of mollusk shells and authigenic carbonates significantly increase below 500 mbsf, so it is possible the two are related, assuming the shells can be identified as belonging to a taxon associated with cold seeps. Interestingly, the same pattern in shells and authigenic carbonates is not observed at Site U1339 (see the **"Site U1339"** chapter)

Distinct, strongly indurated authigenic carbonate layers are largely missing at Site U1343. This implies that nonsteady-state diagenesis did not fix the SMTZ at a certain sediment depth for as long as it did at other sites, where authigenic fronts may have persisted for longer periods of time because of very low sedimentation rates. Nodules of authigenic carbonates in an SMTZ are estimated to form on a timescale of thousands of years (Ussler and Paull, 2008). The high sediment accumulation rates at Site U1343 may have precluded concretions of authigenic carbonates from forming here.

## Biostratigraphy

All core catcher samples from Holes U1343A–U1343E and three additional paleontological samples from Hole U1343A (Samples 323-U1343A-8H-4, 55 cm; 10H-6, 52 cm; and 12H-7, 35 cm) were examined for biostratigraphic purposes. Biostratigraphic datums are derived from radiolarian, diatom, dinoflagellate, silicoflagellate, ebridian, calcareous nan-

nofossil, and planktonic foraminiferal bioevents and are summarized in Table T2. The composite age model derived from all five holes shows that the sediments recovered at Site U1343 span the last ~2.2 m.y. (Fig. F13), indicating a broadly linear trend in sedimentation rates, with values of ~26 cm/k.y. in the uppermost 400 m core composite depth below seafloor (CCSF-A) and increasing to ~56 cm/k.y. in the lowermost 350 m CCSF-A. Although this age model shows that Site U1343 contains Holocene to late Pliocene sediments, the presence of Miocene and early Pliocene species indicates that some reworking has occurred at certain levels.

Samples from Site U1343 are dominated by diatom assemblages and also contain radiolarians, silicoflagellates, ebridians, organic-walled microfossils (dinoflagellates, pollen, and spores), calcareous nannofossils, and planktonic and benthic foraminiferal assemblages. Ostracodes are also present in some samples. The preservation of different microfossil groups ranges from very good to poor, with dissolution processes and barren intervals affecting the calcareous fossil groups in the lowermost 350 m, probably related to dissolution and diagenetic recrystallization. In the uppermost 250–300 m, siliceous, calcareous, and organic fossils have relatively high abundances (Fig. F14), and all groups exhibit distinct large, frequent oscillations likely associated with fluctuations in sea ice cover (Fig. F15) and productivity in the upper water column and perhaps the deepwater environment as well.

## Calcareous nannofossils

The abundance and preservation of calcareous nannofossils was determined in all core catcher samples from Holes U1343A and U1343C and in 61 core catcher samples from Hole U1343E. Samples 323-U1343A-8H-4, 55 cm; 10H-6, 52 cm; and 12H-7, 35 cm, were also examined, as were several toothpick samples from each hole (Table T3). The abundances of specific taxa were assessed in all of the samples examined; *Coccolithus pelagicus* is the most common taxon, followed by small and medium gephyrocapsids. *Coccolithus leptoporus* (both medium and small morphotypes) was also observed at some levels. Reworked specimens of mostly Miocene and Pliocene age were found in some samples from Holes U1343A and U1343E. The preservation of calcareous nannofossils ranges from good to poor, with most samples having moderate to good preservation. Etching was the most common phenomenon observed, and it is especially prominent in Samples 323-U1343A-22H-CC, 323-U1343C-15H-CC, and 323-U1343E-73X-CC. Barren levels are common throughout the upper part of the record and are the major feature below 240 m CCSF-A (Fig. F14), except in brief intervals represented by Samples 323-U1343E-35H-CC, 41H-CC through 45X-CC, and 73X-CC.

Biostratigraphic marker species (*Emiliania huxleyi* and *Pseudoemiliania lacunosa*) were only observed in Hole U1343A (Table T3). The occurrence of *E. huxleyi* in Sample 323-U1343A-3H-CC indicates that this sample and Samples 323-U1343A-1H-CC and 2H-CC can be assigned to calcareous nannofossil Zone NN21 (Martini, 1971), which is defined by the first occurrence (FO) datum of *E. huxleyi* at 0.29 Ma. However, the occurrence of a barren interval below this level hampers the precise positioning of the FO of *E. huxleyi* and the boundary with Zone NN20. In contrast, the last occurrence (LO) datum of *P. lacunosa* at 0.44 Ma (Lourens et al., 2004) in Sample 323-U1343A-12H-7, 46 cm, which defines the upper limit of calcareous nannofossil Zone NN19, is well constrained because it is located within an interval rich in calcareous nannofossils. The lower limit of Zone NN19 at 1.93 Ma (Lourens et al., 2004) is not contained in the record recovered from Hole U1343A.

## Planktonic foraminifers

All core catcher samples from Holes U1343A–U1343E were examined for planktonic foraminifers using the >125 µm fraction (Table T4). In addition, mudline samples from the top of Core 1H in all holes were analyzed using the same size fraction. The samples display fluctuating amounts of siliciclastic grains, pyrite, and mica downcore. Yellow to brownish staining of the foraminifer tests was also observed throughout the holes (Tables T4). Mudline samples contain very low abundances of planktonic foraminifers, except for the mudline sample from Core 323-U1343D-1H, where planktonic foraminifers are abundant. Core catcher samples contain generally high abundances of planktonic foraminifers in the uppermost 250 m CCSF-A. In the lower part of the record, planktonic foraminifers are absent or low in abundance (Fig. F14). The fauna in the uppermost 250 m CCSF-A is mainly dominated by *Neogloboquadrina pachyderma* (sinistral). This species dominates modern subpolar–polar environments and is controlled by sea-surface temperature (SST) (Bé and Tolderlund, 1971). SST is also the controlling factor of the distribution of *N. pachyderma* (sinistral) in the Bering Sea today (Asahi and Takahashi, 2007). Other species present are *Globigerina bulloides*, *Globigerina umbilicata*, and *Neogloboquadrina pachyderma* (dextral). These species are also found today in the Bering Sea, reflecting subpolar–polar temperatures (Asahi and Takahashi, 2007). The faunal change observed at ~250 m CCSF-A is dated at ~1 Ma (Fig. F13), which

coincides with the mid-Pleistocene Transition. Planktonic foraminifers are absent or very low in abundance before this time, and mainly subpolar species are present. In Samples 323-U1343E-44H-CC, 46H-CC, and 47H-CC, *Neogloboquadrina atlantica* (sinistral) is present in very low numbers (1–2 specimens). The LO of this species is between 2.4 and 2.5 Ma according to high-latitude stratigraphy from the North Atlantic (Weaver and Clement, 1987; Spezzaferri, 1998). *Neogloboquadrina atlantica* was first identified in the North Pacific at Deep Sea Drilling Project (DSDP) Site 883 in the middle Pliocene (Dowsett and Ishman, 1995). However, these ages appear to be too old when compared to other datums derived at this site (Fig. **F13**). It is difficult to identify *N. atlantica* because of its preservation and the transition forms between *N. pachyderma* (sinistral) and *N. atlantica* (sinistral) (Dowsett and Poore, 1990; Dowsett and Ishman, 1995), and further taxonomic work is required. We note that the occurrence of *N. atlantica* at this site coincides with a unique lithology: clays without diatoms, which were drilled using the XCB (see **"Lithostratigraphy"**).

## Benthic foraminifers

Around 50 species of benthic foraminifers were identified in 135 samples from Holes U1343A–U1343E (Tables **T5, T6, T7**). Assemblages are of relatively low diversity (typically 4–8 species per sample) and variable abundance (abundant to dominant), with a marked decline in both diversity and abundance from Sample 323-U1343E-25H-CC downhole. Both assemblages have a similar species composition, with close similarities to assemblages from Site U1339 and within or near the OMZ in the Sea of Okhotsk (Bubenshchikova et al., 2008). Variations in species dominance are most likely linked to changes in bottom water oxygenation, with the most important mechanisms likely being surface water productivity and/or intermediate water ventilation variability. High-frequency variations in oxygenation are apparent throughout the section, but initial results show that shallow infaunal high-oxygen indicators (*Elphidium* cf. *batialis* and *Islandiella norcrossi*) are generally dominant from Sample 323-U1343E-24H-CC downhole.

### Assemblage I (*Globobulimina–Nonionella*)

Assemblage I is characterized by largely medium-diversity and high-abundance faunas between the top of the section and Sample 323-U1343E-25H-CC, with persistent occurrences of the species *Globobulimina pacifica*, *Nonionella labradorica*, *Bulimina* aff. *exilis*, *Cassidulinoides tenuis*, *E.* cf. *batialis*, and *I. norcrossi*. Other common species include *Uvigerina auberiana*, *Uvigerina* cf. *peregrina*, and *Valvulineria* sp. Fluctuations in the dominance of deep and shallow infaunal species occur and are most likely related to changes in bottom water oxygen concentrations in association with changes to surface water productivity and/or intermediate water ventilation.

### Assemblage II (*Elphidium–Islandiella*)

Assemblage II consists of low-diversity and medium-abundance faunas from Sample 323-U1343E-26H-CC downhole, characterized by the relatively persistent occurrences of *E.* cf. *batialis* and *I. norcrossi*. Other common species include *B.* aff. *exilis* and *C. tenuis*. The most dominant species are regarded as shallow infaunal species in the Sea of Okhotsk (Bubenshchikova et al., 2008) and likely have higher oxygen tolerances than those of Assemblage I, although they are still within proximity to the OMZ.

## Ostracodes

Only three ostracode taxa were found in 2 out of 135 samples studied at Site U1343: Samples 323-U1343A-8H-CC and 323-U1343E-9H-CC. The specimens are articulated (full carapace) and well preserved, suggesting that they were in situ. Their low numbers can be explained by sediment dilution. The taxa observed include *Krithe* sp., *Pseudocythere* cf. *Pseudocythere caudata*, and *Munseyella* sp. The species *P. caudata* is found worldwide in the deep ocean and is common in the Arctic Ocean (Joy and Clark, 1977) and in sediments deposited during glacial times in the subarctic North Atlantic (Didié and Bauch, 2000; Alvarez Zarikian, 2009; Alvarez Zarikian et al., 2009). *Krithe* is a dominant genus in deep-sea sediments worldwide. Species of *Krithe* have depth distributions ranging from 500 to >5000 m, but previous studies have shown that the genus is mainly associated with cold water masses and high-productivity areas (Coles et al., 1994; Rodriguez-Lázaro and Cronin, 1999). Further examination is needed to identify the third species found in the samples.

## Diatoms

Diatom biostratigraphy is based on analysis of core catcher samples from each core in Holes U1343A, U1343C, and U1343E. Depth positions and age estimates of biostratigraphic marker events are shown in Figure **F13** and Tables **T8, T9, T10,** and **T11**. Diatom preservation is moderate to good in all holes, and diatom abundance is common to very abundant throughout this record.

The LO datums of *Proboscia curvirostris* and *Thalassiosira jouseae* were observed in Holes U1343A, U1343C, and U1343E (Table **T2**), giving an age of 0.3 Ma (Bar-

ron and Gladenkov, 1995; Yanagisawa and Akiba, 1998). This age is consistent with results from IODP Site U1339 at Umnak Plateau. The drilled interval above the LO of *P. curvirostris* is assigned to *Neodenticula seminae* North Pacific Diatom (NPD) Zone 12.

In general, diversity is high throughout Zone NPD12 in each hole. This zone is dominated by *N. seminae*, *Thalassiosira* spp. (*Thalassiosira antarctica* spores and *Thalassiosira latimarginata* s.l.), *Thalassionema nitzschioides*, *Fragilariopsis* spp., *Paralia sulcata*, and, to a lesser extent, *Actinocyclus curvatulus* and *Thalassiosira oestrupii*.

The last common occurrence (LCO) datum of *Actinocyclus oculatus* was observed in Sample 323-U1343E-35H-CC (301.4 mbsf). At this time the interval between this datum level and the LO datum of *P. curvirostris* in Hole U1343E is assigned to *P. curvirostris* Zone NPD11. The interval below this datum and above the FO of *Neodenticula koizumii* is *A. oculatus* Zone NPD10. No specimens were observed in Hole U1343A, defining the bottom of the hole as Zone NPD11. In Hole U1343C, only one valve was found in Sample 323-U1343C-13H-CC; therefore, no clear datum was defined.

The FO of *P. curvirostris* was defined in Sample 323-U1343E-56X-CC and assigned the age of 1.85 ± 0.1 Ma in the *A. oculatus* Zone. This datum was not established through conventional counts because few specimens were observed on the standard smear slides. However, many valves were found on slides prepared for silicoflagellate counts. The >20 µm sieve concentrated larger diatom valves, and counts were made to obtain the datum (Table **T11**). In addition, the LO of *Stephanopyxis horridus* (1.9–2.0 Ma) was estimated in Core 323-U1343E-61X. The *A. oculatus* Zone (NPD10) is defined by *N. seminae*, *Porosira glacialis*, *Stephanopyxis* spp. (*S. horridus*, *Stephanopyxis turris*, and *Stephanopyxis zabelinae*), *Paralia sol*, *P. sulcata*, *Thalassiosira* spp. (*T. antarctica* spores and *T. jouseae*), and, to a lesser extent, *Delphineis* cf. *angustata* and *Coscinodiscus marginatus*.

In the deeper Hole U1343E, the LCO of *N. koizumii* was observed in Sample 323-U1343E-77X-CC, assigning it an age of 2.1 Ma (Yanagisawa and Akiba, 1998). In accordance with Yanagisawa and Akiba (1998), *N. koizumii* was distinguished by the open copula of the valves, which differs from the closed copula of *N. seminae*. In general, the assemblage is composed of *T. latimarginata* s.l., *T. antarctica* spores, *T. oestrupii*, and, to a lesser extent, *Rhizosolenia* spp. The absence of biostratigraphic marker species *Neodenticula kamtschatica* (Zone NPD8) means that the interval between this datum and the bottom of Hole U1343E is assigned to *N. koizumii* Zone NPD9.

## Silicoflagellates and ebridians

Silicoflagellate and ebridian counting was conducted in Holes U1343C and U1343E (Table **T12**). However, not all core catcher samples could be examined for species counts because of limited time. Therefore, only selected intervals containing datum events were processed. The abundance of silicoflagellates and ebridians at Site U1343 is typically lower than at Sites U1340 and U1341 because of the high abundance of coastal and marginal sea ice diatoms. The number of datums in Holes U1343C and U1343E are one and three, respectively. The youngest datum, LO of *Distephanus octonarius* (0.2–0.3 Ma), was estimated in Core 323-U1343E-8H (64.00–74.89 mbsf). The LO of *Dictyocha subarctios* (0.6–0.8 Ma) was estimated in Cores 323-U1343C-23H (196.16–205.35 mbsf) and 323-U1343E-23H (183.86–193.41 mbsf). The LO of *Ammodochium rectangulare* is probably located in Core 323-U1343E-64X (550.64–561.15 mbsf). Because of the trace abundance of ebridians in the lower part of Hole U1343E, the LO of *A. rectangulare* may be revised by more detailed shore-based work. The bottom age of Hole U1343C is younger than 1.9 Ma because of the absence of *A. rectangulare* throughout the record. The bottom age of Hole U1343E is younger than 2.5 Ma because of the absence of *Ebriopsis antiqua antiqua*.

*Dictyocha* spp., rather than *D. subarctios*, exhibits a relative abundance of >30% of total silicoflagellates at the base of Core 323-U1343E-27H. This common occurrence is the first record found in this offshore work. *Dictyocha* spp. is mainly observed in modern temperate–subtropical waters (Poelchau, 1976) and, according to sediment trap studies, is rare in the western subarctic Pacific (Station 50N: Onodera and Takahashi, 2005) and the southern Bering Sea (Station AB: Onodera and Takahashi, unpubl. data), whereas it is abundant in the eastern subarctic Pacific (Takahashi, 1985, 1989). Therefore, the characteristic occurrence of *Dictyocha* spp. may suggest significant temporal input of warmer, less eutrophic waters into the Bering Sea from the eastern subarctic Pacific. The high abundance of *N. seminae* also supports this contention. Because the number of examined samples was significantly limited, further analysis is warranted for postexpedition work.

## Radiolarians

Radiolarian biostratigraphy is based on the analysis of core catcher samples from Holes U1343A–U1343E. Radiolarian stratigraphy at Site U1343 (Table **T13**) extends from the *Botryostrobus aquilonaris* Zone (upper Quaternary) to the *Eucyrtidium matuyamai* Zone (middle Quaternary) in the subarctic Pacific (Kamikuri et al., 2007). Six radiolarian datums common in

the subarctic Pacific were identified at this site (Table T13). These datums indicate high sedimentation rates (~20 cm/k.y.) in the uppermost 200 m of each hole. The LO and FO datums of *E. matuyamai* (0.9–1.5 Ma and 1.7–1.9 Ma, respectively) were identified in samples from Hole U1343E, providing constraints for age estimation of the lower intervals and an average sedimentation rate in Hole U1343E of 30–40 cm/k.y. This suggests sedimentation rates of >50 cm/k.y. in the intervals below 200 m.

Radiolarian abundance and preservation are shown in Table T14 and Figure F14. In general, both radiolarian abundance and preservation at Site U1343 decrease downhole. Radiolarian preservation is good to moderate in all samples from the uppermost 200 m. On the other hand, preservation in samples below 200 m is moderate to poor. Radiolarians are also abundant to common in the uppermost 200 m interval in each hole, whereas they are few in the interval below 200 m in Hole U1343E. The low abundance and poor preservation of radiolarian skeletons in the lower intervals prevents us from estimating the bottom age of Hole U1343E. Because it is not possible to find the next oldest radiolarian datum (LO of *Thecosphaera akitaensis*: 2.4–2.7 Ma), the bottom age of Hole U1343E cannot be assigned until more detailed shore-based work is accomplished.

Radiolarian assemblages at Site U1343 are mainly composed of typical subarctic Pacific species such as *Ceratospyris borealis*, *Cycladophora davisiana*, *Spongopyle osculosa*, *Spongotrochus glacialis*, and *Stylodictya validispina*.

## Palynology: dinoflagellate cysts, pollen, and other palynomorphs

Palynological assemblages were examined in 55 core catcher samples from Holes U1343A and U1343E. Additional samples (323-U1343A-8H-4, 55–57 cm; 10H-6, 52–54 cm; and 12H-7, 35–37 cm) were also analyzed (Table T15). The preservation of all palynomorphs is generally good to moderate except in a few samples (323-U1343A-19H-CC and 323-U1343E-52X-CC, 66X-CC, and 84X-CC). Abundant terrestrial palynomorphs occur throughout the sequence, with concentrations as high as 2500 grains/cm$^3$. Palynomorphs are mainly dominated by *Picea*, *Sphagnum* spores, and the freshwater algae *Botryococcus*. Their absolute abundances are variable but are usually >500 grains/cm$^3$ and can be as high 2500 grains/cm$^3$. These terrestrial palynomorph abundances can be related to significant input through atmospheric and/or ocean circulation.

Dinoflagellate cysts are common to abundant ($10^3$–$10^4$ cysts/cm$^3$) in most samples (Fig. F14). Assemblages show relatively high species diversity, with 25 taxa recorded. However, only *Brigantedinium* spp., *Islandinium minutum*, and *Filisphaera filifera* occur in significant numbers (Table T15). The occurrence of *F. filifera* in Sample 323-U1342E-44X-CC (376.6 mbsf) suggests an age of 1.41–1.7 Ma according to its LO datum in the North Pacific and the North Atlantic (Bujak, 1984; Smelror et al., unpubl. data).

In the uppermost 250 m, dinoflagellate cysts undergo high-amplitude changes in both species composition and abundance (Fig. F14). In general, typical high-productivity and upwelling assemblages dominate when abundance is high, whereas the polar species *I. minutum* dominates the assemblages when abundance is relatively low. This change in dinoflagellate assemblages indicates surface water condition changes from high productivity and upwelling to pronounced sea ice cover (Fig. F15). High variability above 250 mbsf is also observed in pollen and spore abundance, suggesting changing vegetation in adjacent land masses.

Below 250 mbsf, dinoflagellate cyst assemblages have low species diversity and low variability. However, two events marked by both high dinoflagellate cyst abundance (>5000 cysts/cm$^3$) and the dominance of *F. filifera* occur at 695 and 398 mbsf (Fig. F14). The ecological affinity of *F. filifera* is still poorly documented; however, it is considered a cold-tolerant species because it has been recorded in Arctic Pliocene–Pleistocene sediments (Mudie, 1985), although its first appearance in the northwest Atlantic coincides with the beginning of a warming episode in the late Miocene (Head et al., 1989; Aksu and Hillaire-Marcel, 1989).

## Discussion

The fossil record contained in the sequence recovered at Site U1343 displays distinct changes in the general trend of abundance and/or assemblage composition in all major fossil groups (Figs. F14, F15). These changes seem to occur gradually or abruptly between 200 and 300 m CCSF-A, which, according to the age model proposed for this site (Fig. F13), falls between 0.8 and 1.1 Ma. Thus, the trend variations recorded in all fossil groups coincide with the mid-Pleistocene Transition, when global glacial–interglacial cycles gradually shifted from a predominantly mid-amplitude 41 k.y. cycle to a high-amplitude ~100 k.y. cycle. This agrees with the increased range of variability in fossil records observed in the uppermost 250 m at Site U1343, which coincides with increased sea ice cover, upper water column productivity, and variability in the deepwater environment (Figs. F14, F15).

The diatom assemblage reveals high variability related to shifts in the overlying surface water masses at this site. Sanchetta (1982) described the pelagic species *N. seminae* as a tracer for the relatively warm Alaskan Stream waters, whose presence decreases in surface sediments north of the Aleutian Islands. Here, however, *N. seminae* is clearly in antiphase with sea ice species, suggesting it is a good indicator of open, ice-free waters. This species dominates the record, showing strong cyclicity with a major downturn after ~1 Ma, in line with subpolar planktonic foraminifers and other temperate/open water dinoflagellates and silicoflagellates. After ~1 Ma, sea ice diatoms and dinoflagellate species dominate their respective assemblages. The occurrence of intermediate-water radiolarian species *C. davisiana* also increases at this time. A comparison of diatom sea ice species and *C. davisiana* reveals a similar overall trend. However, at higher frequency the two do not always co-vary, revealing phases of opposing trends. This is also seen in a comparison of dinoflagellate sea ice species and *C. davisiana* and suggests that the overall increase in glacial–interglacial intensity after ~1 Ma invoked a colder prevailing climate at this site. This high-frequency relationship is not apparent at the Bowers Ridge sites, and therefore these interpretations require further investigation.

Benthic faunas indicate high-frequency changes in bottom water oxygen content over the entire sequence, likely related primarily to documented large changes in surface water productivity and possibly also to bottom water ventilation changes and/or methane seeps. The general increase in abundance and diversity above ~240 m CCSF-A (Assemblage I) coincides with an increase in bottom water oxygen variability. Abundance and diversity may be related to a change in sedimentation rate (Fig. **F13**), but the assemblage change marks the onset of more variable and occasionally lower oxygen conditions in the uppermost 240 m, which may be linked to regional cooling after the mid-Pleistocene Transition.

The imprint of diagenetic processes in the records of calcareous fossil groups is strong in the sequence recovered at Site U1343. Intervals barren of calcareous nannofossils are synchronous with the occurrence of microscopic to macroscopic authigenic carbonate minerals, either in the form of dolomite or authigenic carbonate (see **"Lithostratigraphy"**). Yellow-brownish stained foraminiferal tests were encountered throughout Holes U1343A–U1343E. This phenomenon was previously reported in the northwest Pacific, where it was shown to result from postdepositional authigenic carbonate formation in the foraminiferal tests (e.g., Ohkushi et al., 2005). Stable isotope measurements were affected by this carbonate formation and had slightly higher values (Ohkushi et al., 2005). The formation of authigenic carbonate is connected to the release of methane from the sediments, which may have been the cause of its formation at this site. Yellow-brown foraminifers also cooccur with layers of authigenic carbonate in the sediments (see **"Lithostratigraphy"**).

## Paleomagnetism

The archive halves of all cores recovered at Site U1343 were measured on the three-axis cryogenic magnetometer. All measurements were done at 2.5 cm intervals for APC cores and 5–20 cm intervals for XCB cores. Natural remanent magnetization (NRM) was measured before (NRM step) and/or after (demagnetization step) stepwise alternating-field (AF) demagnetization in peak fields up to 20 mT. Cores from Hole U1343A were measured at NRM step and 20 mT demagnetization step; other cores from Site U1343 were measured only at 20 mT demagnetization step to keep up with core flow.

Inclination and intensity after 20 mT AF demagnetization step from Holes U1343A, U1343C, and U1343D are plotted in Figure **F16;** data from Hole U1343E are plotted in Figure **F17.** Average inclination values are nearly 70° for the normal polarity intervals, which is close to the site axial dipole inclination (~72°), indicating that we can effectively remove overprint magnetization caused by the drill pipe and/or core barrel from the NRM records. Inclination values from Hole U1343E cores and the 60 point averages are plotted in Figure **F18.** A polarity zonation was defined from the inclination record and correlated to the polarity timescale based on micropaleontology datums (see **"Biostratigraphy"**). The Brunhes/Matuyama boundary was clearly identified in Holes U1343A, U1343C, and U1343E between 180 and 185 mbsf. Both the termination and the onset of the Jaramillo Subchron were identified in Hole U1343E. Below this depth, inclination tends to cluster around normal polarity values, which makes it hard to identify polarity zonation. The top boundary of the normal polarity zone at ~292 mbsf is tentatively identified as the termination of the Cobb Mountain Subchron. These depths and ages are listed in Table **T16.**

The relative paleointensity of cores from Site U1343 was estimated to examine potential geochronological information during the Brunhes Chron. Figure **F19** shows relative paleointensity estimates based on normalizing NRM after 20 mT AF demagnetization by magnetic susceptibility for the uppermost 100 m CCSF-A. The paleointensity variation has large amplitude and obviously shows a coherent change with

magnetic susceptibility (Fig. F19), suggesting that NRM intensity was largely influenced by environmental change. Figure F19 also shows that lower (higher) NRM intensities are always associated with lower (higher) magnetic susceptibility values. Figure F20 shows NRM intensity after 20 mT demagnetization plotted against magnetic susceptibility for Site U1343 cores. If magnetic grains in the sediments were unaffected by magnetic mineral dissolution or authigenesis and paleointensity were constant, the data in Figure F20 would be distributed linearly along a trend through the origin. A higher slope would indicate stronger paleointensity during deposition and/or finer magnetic grain size in the sediments. A lower slope would indicate weaker paleointensity and/or coarser magnetic grains in the sediments. The data distribution shows that high NRM intensities are absent in the low magnetic susceptibility range (about $<75 \times 10^{-5}$ SI), which means that the lower magnetic susceptibility sediments lack finer magnetic grains. This observation suggests that intervals of low magnetic susceptibility (Fig. F19) lack fine magnetic grains, possibly because anaerobic conditions in the sedimentary column cause fine magnetic grains to dissolve much faster than coarse magnetic grains. Consequently, NRM data from Site U1343 cores are not suitable for paleointensity reconstruction but may be useful for the study of paleoenvironmental changes.

# Geochemistry and microbiology

## Interstitial water chemistry

In Hole U1343A, 24 samples for interstitial water analyses were retrieved at a resolution of two samples per core for Cores 323-U1343A-1H and 2H, followed by one sample per core down to ~200 mbsf. High-resolution samples were taken from microbiology-dedicated Hole U1343B, with a total of 58 whole rounds. In addition, 59 samples were taken from Cores 323-U1343E-25H through 83X (207–743 mbsf) at a resolution of one per core. To prevent oxidation, whole rounds were stored in a nitrogen-filled glove box at 7°C until squeezed. Aliquot samples were processed for routine shipboard analyses (see **"Geochemistry"** in the "Methods" chapter) and collected for shore-based analyses of sulfur and oxygen isotopes of sulfate and hydrogen sulfide, trace metals, dissolved organic carbon (DOC), and fatty acids.

### Chlorinity, salinity, alkalinity, dissolved inorganic carbon, and pH

Chloride values are highly scattered but slightly decrease in the uppermost 300 m (Fig. F21C). In general, salinity decreases throughout the core but is fairly constant from 23 to 137 and 280 to 665 mbsf. Salinity ranges from 31 to 37. Alkalinity increases in the uppermost 81 m from 3.1 mM (at 0.05 mbsf) to 65 mM. Between 81 and 300 mbsf, alkalinity decreases by ~40 mM. From 300 mbsf to the bottom of Hole U1343E (743 mbsf), alkalinity slightly increases before gradually decreasing below ~460 mbsf to 16.3 mM (Fig. F22C). This trend is reflected in the dissolved inorganic carbon (DIC) profile (Fig. F22A). DIC concentrations increase from 3.3 to 66 mM in the uppermost 109 m and decrease to 16 mM at 734 mbsf. A local minimum in DIC concentrations of 20 mM occurs at ~337 mbsf. pH varies between 7.3 and 8.2 (Fig. F22B).

### Dissolved sulfate and hydrogen sulfide

Dissolved sulfate at Site U1343 decreases from concentrations close to seawater values at 0.05 mbsf to undetectable values at 7.8 mbsf and below (Fig. F22D). Hydrogen sulfide concentrations have local maxima at ~2.3 and ~8 mbsf of 63.5 and 576 µM, respectively. Except for in these intervals of increased sulfide concentrations, values are below detection limit (Fig. F22F). Sulfate and hydrogen sulfide profiles are displayed for the uppermost 15 mbsf only (Fig. F22D, F22F).

### Dissolved ammonium, phosphate, and silica

Ammonium concentrations increase with depth from 0.05 mM in the top of the sediment column to a maximum of 14.3 mM at 444 mbsf (Fig. F22H). Ammonium decreases slightly in the lowermost 140 m from 12.43 to 10.73 mM. Phosphate increases from 10 µM in the surface sediment to a maximum concentration of ~300 µM at 100 mbsf. Below this depth, phosphate decreases, most significantly from 100 to 200 mbsf (Fig. F22G). Dissolved silica concentrations are nearly constant throughout the sediment column (Fig. F21K).

### Dissolved calcium, magnesium, sodium, and potassium

Calcium concentrations decrease from seawater values in the uppermost sediment to a minimum concentration of 2 mM at 32 mbsf (Fig. F21A). Between 30 and 300 mbsf, calcium concentrations are fairly constant at <5 mM. Below 300 mbsf, calcium concentrations slightly increase to a maximum of 6.9 mM at 444 mbsf. Below this depth, calcium concentrations show a scattered distribution but remain <8 mM (Fig. F21A). Magnesium concentrations reach a maximum of 56.8 mM at 100 mbsf and decrease to 8 mM at 740 mbsf (Fig. F21B). The most significant decrease in magnesium

concentration is observed between 100 and 300 mbsf. Sodium concentrations do not show a significant trend with depth (Fig. F21D). Potassium concentrations decrease from seawater concentrations in the surface sediment to 6 mM at 740 mbsf (Fig. F21E).

### Dissolved manganese, iron, barium, boron, lithium, and strontium

Dissolved manganese and iron concentrations are higher near the top of the sediment column, with maximum values of 5.8 and 60.7 µM, respectively (Fig. F21G–F21H). The depth of maximum manganese concentrations is above the depth of maximum iron concentrations.

The lithium concentration profile shows a minimum in the uppermost ~10 m and increases steadily with depth (Fig. F21I). This profile resembles the lithium profiles of Sites U1339, U1344, and U1345. Dissolved boron concentrations increase from a minimum of 353 mM at 0.05 mbsf to a maximum of 1670 µM at 737 mbsf (Fig. F21J). Dissolved barium concentrations increase steeply in the uppermost ~10 m and vary between 40 and 80 µM below (Fig. F21L).

## Volatile hydrocarbons

Samples for volatile hydrocarbon analyses were taken from Holes U1343A, U1343B, U1343C, and U1343E at the same resolution as interstitial water samples. Methane ($C_1$) is detectable at all depths except the uppermost 8 m (Fig. F22E). Low amounts of ethane ($C_2$) were detected below 33.5 mbsf. Ethene and propane were also intermittently detected below 189.05 mbsf. The headspace $C_1/C_2$ ratios generally decrease with depth and temperature from >10,000 at shallow sediment depths to ~200 at 712.6 mbsf. The very high $C_1/C_2$ ratios indicate biological methane formation. Significant losses of methane occurred during core retrieval and processing, especially below 11–12 mbsf; therefore, we only report methane data from the uppermost 15 m of Hole U1343B.

## Sedimentary bulk geochemistry

Eighty-two samples from Holes U1343A and U1343E were analyzed for solid-phase total carbon (TC), total nitrogen (TN), total sulfur (TS), and total inorganic carbon (TIC). From these analyses, total organic carbon (TOC) and calcium carbonate ($CaCO_3$) concentrations were calculated (see "Geochemistry" in the "Methods" chapter) (Fig. F23). $CaCO_3$ content at Site U1343 ranges from 0.5 to 3.5 wt% (average = 1.6 wt%) (Fig. F23A). TOC and TN concentrations range from 0.42 to 1.56 wt% (average = 0.66 wt%) and from 0.06 to 0.16 wt% (average = 0.10 wt%), respectively (Fig. F23B–F23C). TS concentrations range from 0.14 to 0.82 wt% (average = 0.41 wt%) (Fig. F23D). $CaCO_3$ content varies downcore but does not display an overall trend. TOC and TN contents are relatively high in two samples at 2.9 and 108.7 mbsf. Splits of squeeze cakes were also collected and treated for shore-based analyses of bulk elemental composition, iron mineral phases, and iron-monosulfide and pyrite content and sulfur isotope compostion.

## Microbiology

Samples for community structure and total prokaryotic cell abundance were collected adjacent to interstitial water whole rounds in sections drilled using the APC system. Additional samples were taken from XCB Cores 323-U1343E-78X through 80X to evaluate prokaryotic cell abundance and community structure in the deepest portion of Hole U1343E. PFT analyses performed in these cores show no contamination from drill fluid in the center of the whole round where microbiology samples were taken. Samples from all cores were fixed according to the protocol described in "Microbiology" in the "Methods" chapter.

## Conclusion

Interstitial water sulfate, DIC, phosphate, and ammonium concentration profiles indicate that the sediment at Site U1343 is characterized by high rates of carbon turnover compared to the Bowers Ridge sites (U1340, U1341, and U1342). Concentrations of these interstitial water constituents are, in general, at least one order of magnitude higher than at Site U1342 (see "Geochemistry and microbiology" in the "Site U1342" chapter). Profiles of methane and sulfate suggest that sulfate reduction is largely driven by methane diffusing into the SMTZ. The sulfate profile is nearly linear in the uppermost 8 m, indicating minor sulfate consumption here. The methane flux into the SMTZ, as calculated from the methane concentration gradient between 8 and 11 mbsf, is ~50%–60% of the sulfate flux into the SMTZ. Hydrogen sulfide concentrations reach maximum values in the SMTZ. A relatively high flux of calcium into the SMTZ stresses the importance of sulfate reduction coupled to the anaerobic oxidation of methane (AOM), which commonly leads to the formation of $CaCO_3$ because of an increase in pH and alkalinity in the SMTZ. The calcium flux into the SMTZ is ~35% of the methane flux, indicating that a large fraction

of the DIC produced through AOM is deposited as $CaCO_3$.

The curvature of the ammonium profile suggests that ammonium production results from organic matter degradation throughout the sediment column. This is confirmed through preliminary modeling exercises (data not shown) and suggests organic matter degradation and hence microbial activity even at depths below 400 mbsf. Organic matter degradation also leads to the accumulation of DIC and phosphate in the interstitial water. The accumulation of these constituents, however, is much lower than that predicted by the ammonium profile, assuming steady state and a constant ratio between carbon, nitrogen, and phosphorus of remineralized organic matter. This suggests both production and consumption of DIC and phosphate in the sediment. Consumption of these species is most likely caused by the formation of apatite and calcium carbonates (e.g., dolomite). The interstitial water profiles suggest that the net consumption of phosphate is highest between 180 and 200 mbsf and net DIC consumption is highest between 300 and 350 mbsf.

The decreases in salinity and interstitial water chloride concentrations indicate freshening of the interstitial fluids with depth. A possible explanation for this trend is the dissociation of gas hydrates during core recovery, which releases freshwater and causes dilution of dissolved ion concentrations (Kastner et al., 1998; Hesse et al., 2000). This process, however, is constrained to sediment intervals with in situ gas hydrate and therefore often causes a "scattering" of the chloride profile, with chloride depletion corresponding to high methane concentrations as artifacts of core recovery. Below 200 mbsf, where salinity and chloride profiles show the most pronounced decreases, the interstitial water profiles display the least scatter. On the other hand, a "soupy" core texture was observed in cores retrieved below 200 mbsf (A.C. Ravelo, pers. comm., 2009), and such a texture is typically an indication of the dissociation of gas hydrates (Westbrook, Carson, Musgrave, et al., 1994).

Alternatively, decreases in interstitial water salinity and chloride concentrations can result from meteoric water input, clay membrane ion filtration, and clay mineral dehydration (e.g., De Lange and Brumsack, 1998; Dählmann and de Lange, 2003). The hypothesis that depletion is caused by the release of mineral-bound water by clay mineral dehydration is strengthened by the significant decrease in potassium concentrations below 200 mbsf. Clay mineral dehydration (e.g., the transformation of smectite to illite) is known to result in strong potassium depletion because of the integration of potassium into the illite mineral structure (Dählmann and de Lange, 2003). Interestingly, potassium decreases significantly at ~180 and 280 mbsf. These depths correlate well with changes in lithology (see **"Lithostratigraphy"**) characterized by increases in clay mineral content. This supports the idea that clay mineral transformations are the major cause of freshening of interstitial fluids at Site U1343. These findings highlight the potential importance of terrigenous material input at sites proximal to the Bering Sea shelf for geochemical processes during diagenesis.

## Physical properties

Site U1343 is positioned on a large canyon interfluve bordering the western side of the lower course of the exceptionally large Zhemchug submarine canyon that deeply incises the Beringian continental margin. Hole U1343A was spudded at a water depth of 1964 m (APC corrected).

Sections of cores recovered from Holes U1343A–U1343E were scanned by the "fast track" Special Task Multisensor Logger (STMSL) to record whole-round magnetic susceptibility and GRA bulk density. After warming to ambient laboratory temperature, whole-round sections were placed on the Whole-Round Multisensor Logger (WRMSL) to record GRA bulk density, magnetic susceptibility, and *P*-wave velocity. Sediment samples were collected from sections recovered from Holes U1343A and U1343E and analyzed using moisture and density (MAD) procedures to determine moisture, bulk density, grain density, and porosity properties. MAD data from Hole U1343A (0–202 mbsf) were merged vertically with the lower part of Hole U1343E (0–744 mbsf). As shown on all MAD figures, the merge or splice depth of Holes U1343A and U1343E was selected at 200 mbsf (~220 m CCSF-D). The collection of overlapping MAD data in Hole U1343E began at Core 323-U1343E-33H, the top of which is at ~183 mbsf.

Gas-expansion voids and cracks throughout Site U1343 cores disrupted core-sediment integrity and created gaps and breaks that degraded the accuracy and in situ applicability of STMSL and WRMSL recordings. The transition from APC to XCB coring began at ~354 mbsf in Hole U1343E (Core 323-U1343E-42X), a depth that closely corresponds to that of an acoustically bright band of reflection horizons at 0.46 s two-way traveltime. Based on its cross-cutting relations to dipping beds and pressure-temperature setting, the band was identified earlier as a gas hydrate BSR by Cooper et al. (1987). XCB coring below the band mechanically disrupted and injected fluidized mud into the core sediment, which further

denigrated physical property measurements with onboard magnetic susceptibility logging systems and MAD discrete sampling.

The sedimentary column cored at Site U1343 is relatively uniform in general lithology, and only one lithologic unit (Unit I) was defined (see **"Lithostratigraphy"**). Unit I varies in composition and texture from siliciclastic silt and silty clay beds to sequences of mixed siliciclastic and biogenic sediment (diatom ooze). Bulk density and *P*-wave velocity data from core measurements and logs suggest that the cored section may be more lithologically variable than one unit.

## GRA wet bulk density

WRMSL GRA readings of wet bulk density for Hole U1343E are noisy and spiky because of expanding gas disruption of recovered cores and XCB coring disturbances below ~360 mbsf (Fig. **F24A**). Below ~10 mbsf, wet bulk density increases slightly from an average of ~1.60 g/cm$^3$ to ~1.65 g/cm$^3$ at ~100 mbsf. The average value below this depth, although oscillatory, does not seem to change until ~360 mbsf, where it decreases to ~1.60 g/cm$^3$. This decrease is coincident with the change from APC to XCB coring and the consequent recovery of drilling-disturbed core sections. The transition to XCB coring also corresponds to the calculated depth (~360 mbsf) of the methane hydrate BSR identified by Cooper et al. (1987).

In contrast, the downhole triple combo logging tool string records a shift in average bulk density below the posited BSR from ~1.65 to ~1.72 g/cm$^3$ (Fig. **F24B;** see **"Downhole measurements"**). These observations imply that sediment strengthening, which necessitated a shift to XCB coring, occurs at and extends below the strong reflectors. Additionally, onboard measurements of physical properties on mechanically disturbed and mud-slurry-injected core sediment produce generally lower readings than in situ values measured by the density log. At ~520–530 mbsf both the WRMSL and the downhole logging density tool record a slight shift to higher average density, from ~1.65 to 1.75 g/cm$^3$ for whole-round GRA and from 1.72 to 1.75 g/cm$^3$ for the downhole logging tool. This change to higher readings coincides with an increase in the $V_P$ log (Fig. **F25**).

Despite gas expansion and coring degradation of sediment integrity, the downhole profile of average values recorded by the WRMSL GRA densitometer indicates cyclicity, with a dominant wavelength ranging between ~25 and ~50 m. Cyclic variations in wet bulk density are more clearly recorded by the density log (Fig. **F24B**). These oscillations likely reflect lithologic variations. If so, the downhole profile of logging-tool density implies the existence of at least two and possibly three physically distinguishable lithologic units.

## Magnetic susceptibility

Figure **F26** shows that magnetic susceptibility measured on Hole U1343E cores exhibits cyclicity, from averages of ~20–25 SI units to readings of >200 SI units. Peak readings, which are roughly separated by 30–50 m, are prominent to ~360 mbsf. Below this depth, which is coincident with the conjectured gas hydrate BSR, wavelength broadens and average values decrease. The bright band of the BSR is underlain by a deeper zone (>2 s two-way traveltime) of laterally disrupted reflection horizons, an observation commonly ascribed to acoustic scattering by interstitial gas bubbles. Diagenetic alteration of the deeper stratigraphic section through which the hydrate BSR has presumably vertically migrated may have degraded the magnetic susceptibility properties of deeper sediment.

## *P*-wave velocity

*P*-wave velocity was measured in only the first core of Hole U1343A. Because of abundant, wide cracks and breaks in core-sediment continuity caused by gas expansion, *P*-wave velocity could not be measured with any useful meaning with respect to in situ values. *P*-wave and shear wave velocities are, however, well recorded by the downhole FMS-sonic logging tool string (see **"Downhole measurements"**). The log of *P*-wave velocity readings displayed in Figure **F25** documents an increasing average velocity with depth from a near-surface value of ~1550 m/s to ~1840 m/s at the bottom of Hole U1343E at ~744 mbsf. Three gradients of increasing *P*-wave velocity are recognizable: Gradient 1 (0 to ~360 mbsf; increasing at ~110 m/s/km), Gradient 2 (360–520 mbsf; increasing at ~550 m/s/km), and Gradient 3 (~530–744 mbsf; increasing at ~890 m/s/km). The transition between Gradients 1 and 2 is coincident with the depth of the methane hydrate BSR identified by Cooper et al. (1987) along this sector of the Beringian margin and the shift from APC to XCB coring. The steepened lower gradient presumably reflects lithification, perhaps contributed to by the ascent of the BSR through the underlying sediment. The conspicuous ramp of Gradient 3 cannot be linked to a described change in dominant lithology or solely to compaction effects, although average bulk density does increase slightly on the downhole profiles of WRMSL GRA and MAD measurements (Fig. **F24**). An explorable explanation for the steep-

ness of the lower gradient is the increased abundance of authigenic carbonate minerals and shell debris observed in cores recovered in Hole U1343E below ~520 mbsf (see **"Lithostratigraphy"**).

## Thermal conductivity

Thermal conductivity was determined on whole-round core sections, typically on Sections 1 or 2 of each core recovered from Holes U1343A, U1343C, U1343D, and U1343E. Thermal conductivity readings in Hole U1343E (Fig. **F27**) vary widely between ~1.2 and ~0.6 W/(m·K) about a mean value of ~0.95 W/(m·K). Exceptionally low excursions are most likely the consequence of gas expansion and core disruption. In general, cores collected above the posited methane hydrate BSR at ~360 mbsf exhibit higher variability and are also the most gas-disrupted sections measured. Cores collected below the transition to higher carbonate content at ~520 mbsf display the highest range of thermal conductivity values (Figs. **F24, F25**).

## Natural gamma radiation

Similar to WRMSL GRA measurements of wet bulk density, NGR readings on the same core sections from Hole U1343E also track a downhole trend of increasing values from near-surface readings of ~25 counts/s to ~32 counts/s at ~100 mbsf (Fig. **F28**). Below this depth, NGR oscillates greatly and decreases slightly to ~25 counts/s at ~320 mbsf, where a significant increase to ~40 counts/s is recorded. This depth is effectively the same as that of the posited hydrate BSR and the shift to XCB coring. Deeper in Hole U1343E, average NGR decreases gradually to ~25–26 counts/s. At ~520 mbsf, readings increase to ~30 counts/s. The shift to higher NGR corresponds to the top of trends of higher readings of wet bulk density and downhole-measured *P*-wave velocities (Figs. **F24, F25**).

NGR generally tracks the abundance of clay minerals and their absorbed radioactive nuclei. Apparently, higher bulk density sediments in Hole U1343E are also richer in clay and other siliciclastic minerals. Diatoms and other siliceous microfossils that resist compaction and sediment consolidation do not make up the dominant component constructing the stratigraphic section sampled at Site U1343. Perhaps because of this circumstance, NGR readings track compaction-driven densification of clay-rich beds, an observation consistent with the progressive downhole increase in *P*-wave velocities (Fig. **F25;** see **"Downhole measurements"**).

## MAD (discrete sample) wet bulk density

Similar to downhole distribution of wet bulk density tracked by the WRMSL GRA densitometer, average values of MAD or discrete sample density increase downhole in Hole U1343A from a near-surface value of ~1.50 g/cm$^3$ to an average near 1.70 g/cm$^3$ at ~100 mbsf (Fig. **F29;** Table **T17**). The average MAD bulk density changes little below this depth, including across the transition to samples collected from Hole U1343E below 200 mbsf and at the BSR at ~360 mbsf. Significant excursions above and below this mean are probably spurious measurements. To understand the accuracy and usefulness of MAD data measured on gas- and coring-disturbed cores, it is helpful to compare MAD bulk density measurements to in situ bulk density measurements recorded by the downhole triple combo logging tool string (Fig. **F24B;** see **"GRA wet bulk density"** and **"Downhole measurements"**).

## MAD porosity and water content

Figure **F30** displays closely similar profiles of water (moisture) content and sediment porosity recorded in core samples recovered from Holes U1343A and U1343E. Near-surface porosity is ~70%, noticeably lower than that measured at Sites U1339 (~80%), U1340 (~75%), U1341 (~78%), and U1342 (~80%). This circumstance can be ascribed to the lower overall content of siliceous microfossils composing the sedimentary section cored at Site U1343. Porosity (and water content) decreases sharply downhole to ~60% at ~80 mbsf, below which it only gradually lessens to ~56% at ~744 m CCSF-D. Porosity or gradient changes are not recorded across the presumed hydrate BSR at ~360 mbsf (390 m CCSF-D) or below ~520 mbsf (547 m CCSF-D), where shifts to higher in situ *P*-wave velocity and bulk density readings occur (Figs. **F24B, F25**). The gentle downhole reduction in porosity and water content can best be ascribed to compactive dewatering, which is most prominently exhibited in the uppermost ~80 m of section.

## Grain density

Stripped of rapid excursions to single-point high and low values, average grain density seems to show three density-fluctuating (±0.2–0.3 g/cm$^3$) (Fig. **F31**) groupings: an upper group from the seafloor to ~100 mbsf with an average density of ~2.68 g/cm$^3$; a middle group between ~100 and 540 mbsf with an average density of ~2.65 g/cm$^3$; and a basal group with a lower density of ~2.55 g/cm$^3$ at ~540 mbsf that increases downhole to 2.70 g/cm$^3$ at 744 mbsf. Only

the lower group displays a clear increase with depth that matches both the downhole increase in the bulk density and *P*-wave velocity logs and the occurrence of authigenic carbonate and shell debris (Figs. **F24B, F25**). Within the groups, fluctuation in grain density appears to increase downhole. The range for the bottom group, 2.35–2.82 g/cm$^3$, is quite high, a pattern that matches the wide, oscillating swings of bulk density measured by the density log (Fig. **F24B**). The wavelength of oscillations broadens below ~320–340 mbsf, the approximated depth of the seismically identified methane hydrate BSR.

# Stratigraphic correlation

The composite depth scale and splice at Site U1343 are constructed from 0.0 to 269.92 m CCSF-A (as defined in **"Stratigraphic correlation"** in the "Methods" chapter). The splice consists of one complete and continuous interval from the mudline to 269.92 m CCSF-A. Below the splice, cores from Hole U1343E (with unknown gaps) are appended from 270.47 to 779.18 m CCSF-A.

The continuous splice ranges from the top of Core 323-U1343C-1H to interval 323-U1343E-28H-6, 79.2 cm (Tables **T18, T19**). The appended cores range from interval 323-U1343E-29H-1, 0 cm (270.42 m CCSF-A), to 83X-7, 31 cm (779.62 m CCSF-A), with a constant affine value of 35.62 m.

Correlations were accomplished using IODP Correlator software (version 1.656), and some intervals were checked with digital line-scan images with Corelyzer (version 1.3.3). The composite (CCSF-A) and splice (CCSF-D) depth scales are based primarily on the stratigraphic correlation of WRMSL magnetic susceptibility (Fig. **F32**), WRMSL GRA bulk density (Fig. **F33**), whole-round NGR (Fig. **F34**), and color reflectance parameter b* (Fig. **F35**) data. Figure **F36** shows the spliced composite record for Site U1343.

The CCSF-A and CCSF-D scales were constructed by assuming that the uppermost sediment (the mudline) in Core 323-U1343C-1H represents the sediment/water interface. The mudline was also recovered in Cores 323-U1343A-1H and 323-U1343B-1H, confirming the fidelity of the top of the recovered section. Core 323-U1343C-1H serves as the anchor in the composite depth scale and is the only core with depths that are the same on the mbsf, CCSF-A, and CCSF-D scales. From this anchor we worked downhole, correlating the variations in core logging data on a core-by-core basis using Correlator. All splice points in the interval of 0–269.92 m CCSF-A are clear and convincing based on multiple data types and are further supported with NGR wireline logging data (see **"Downhole measurements"**). Pervasive gas voids are apparent as low spikes in the GRA bulk density data and, to some extent, in other data types.

Within the splice, the composite CCSF-A depth scale is defined as the CCSF-D depth scale. Note that CCSF-D rigorously applies only to the spliced interval. Intervals outside the splice, although available with CCSF-A composite depth assignments, should not be expected to correlate precisely with fine-scale details within the splice or with other holes because of normal variation in the relative spacing of features in different holes. Such apparent depth differences may reflect coring artifacts or fine-scale variations in sediment accumulation and preservation at and below the seafloor.

The cumulative offset between the mbsf and CCSF-A depth scales is nonlinear (Fig. **F37**). The affine growth factor (a measure of the fractional stretching of the composite section relative to the drilled interval; see **"Stratigraphic correlation"** in the "Methods" chapter) at Site U1343 between 0 and 36.4 mbsf (i.e., Cores 323-U1343A-1H through 4H, 323-U1343B-1H through 4H, and 323-U1343C-1H through 4H) is 1.03. At greater depths (all cores to 234.2 mbsf, that is, through Core 323-U1343C-26H) have an affine growth factor of 1.15. A few significant anomalies around this relatively uniform affine growth relationship are explained; relatively short cores (e.g., Cores 323-U1343C-8H and 323-U1343E-5H) typically contain significant debris that fell in the borehole at the top of each Section 1; as a result, they have artificially low apparent top depths and thus artificially low affine values. The calculation of mass accumulation rates (MARs) based on CCSF-A or CCSF-D scales should account for the affine growth factor by dividing apparent depth intervals by the appropriate growth factor for the depth interval. After it is divided by the growth factor (accounting for the different depth intervals), this scaled depth scale should be referred to as CCSF-B.

Cores deeper than the spliced interval—that is, intervals 323-U1343E-29H-1, 0 cm (270.42 m CCSF-A), through 83X-7, 31 cm (779.62 m CCSF-A)—were appended to the slice with a constant affine value of 35.62 m. MARs calculated in this interval should not be divided by the affine growth factor because their depths are a linear transformation of drilling depths.

# Downhole measurements

## Logging operations

Downhole logging of Hole U1343E started after APC/XCB coring to a total depth of 743.8 m DSF (2711.3 m DRF) ended on 12 August 2009 at 0750 h (all times are ship local time, UTC – 11 h). In preparation

for logging, the hole was conditioned with a ~50 bbl sweep of high-viscosity mud and displaced with 265 bbl of logging mud. The bit was then raised to the logging depth of 99.5 m DSF (2067 m DRF).

Two tool strings were deployed in Hole U1343E: the triple combo and the FMS-sonic combination (for tool and measurement acronyms, see **"Downhole measurements"** in the "Methods" chapter). Assembly of the triple combo started at 1315 h, and the string was run in hole (RIH) at 1410 h. The tool string reached the bottom of the hole (total depth = 2711 m wireline log depth below rig floor [WRF]), and a first short (~50 m) uphole logging pass started at 900 ft/h at 1625 h. After the pass was completed, the triple combo was sent back to total depth, and the main pass started at 1650 h at 900 ft/h. The pass ended at 1945 h when the tool string crossed the seafloor, marked by a drop in natural radioactivity at 1962.5 m WRF, ~5 m shallower than that detected by the driller. The triple combo reached the rig floor at 2100 h and was rigged down at 2150 h.

Overall, the caliper of the density sonde showed an irregular borehole with several enlarged intervals above 420 m WSF but very few large washouts and very good conditions in the lower section, indicating that deployment of the FMS-sonic tool string would provide worthwhile velocity and image data. The tool string was built up and RIH at 2230 h. It reached its maximum depth at 2710 m WRF at 0020 h, August 13, and the first pass started at 900 ft/h. The pass was completed at 0233 h with the bottom of the 35 m long tool string at 2110 m WRF. After the tool string returned to the bottom of the hole, the second pass started at 2710 m WRF at 0300 h and ended at 0535 h after the last velocity measurements were recorded immediately below the bit. The FMS-sonic was rigged down after reaching the surface at 0650 h, and the rig floor resumed normal operations at 0745 h in preparation for transit to the next site.

## Downhole logging data quality

Figures **F38** and **F39** show a summary of the main logging data recorded in Hole U1343E. These data were processed and converted to depth below seafloor and matched to depths between different logging runs. The resulting depth scale is wireline log matched depth below seafloor (WMSF; see **"Downhole measurements"** in the "Methods" chapter).

The first indicators of the overall quality of the logs are the size and shape of the borehole measured by the calipers. The hole size measured by the Hostile Environment Litho-Density Sonde (HLDS) caliper during the triple combo run and by the FMS arms is shown in Figures **F38** and **F39,** respectively. Although both runs indicate an irregular hole, particularly above 430 m WSF, all of the calipers show that the tools were making contact with the formation over most of the interval logged, suggesting that the overall quality of the data is good.

Irregular hole size has an effect on measurements that require good contact with the formation, namely density and porosity. Although the HLDS caliper in Figure **F38** suggests that the tools were making good contact between 300 and 360 m WSF and that the hole was even smaller than the nominal bit size in part of this interval, the density and neutron porosity data in this interval seem questionable. The anomalously low density readings between 307 and 322 m WSF and the very high neutron porosity values between 300 and 360 m WSF suggest that the tool was not properly measuring formation properties. A comparison with density measurements made with the GRA track sensor on cores recovered from Hole U1343E and MAD measurements made on samples from Site U1343 shows generally good agreement, except in this interval, where logging data are significantly lower than core measurements.

Because this interval includes the estimated depth of one of the main seismic reflectors at this site, possibly a BSR, it is necessary to carefully assess the quality of the data recorded in this key transition interval. Figure **F40** shows a close-up comparison of hole size, gamma ray, and density data recorded over this interval by several passes and tool strings. The triple combo downlog was recorded routinely to guarantee that data were recorded even in the case of tool failure later in the deployment. The caliper was not open during this pass, and only the gamma ray and resistivity measurements taken while the tool was being lowered are generally considered to be reliable. However, the density sonde is active and can make valid measurements in places where the tool is actually making contact with the formation on its way down.

The caliper logs show that the smaller hole size between 307 and 322 m WSF was measured only during the triple combo uplog, and both FMS passes measured a larger hole in this interval. Comparison of the gamma ray logs shows that the triple combo uplog also recorded significantly higher values than any of the other passes in this same interval because it was in direct contact with the formation. The lower density values measured below 307 m WSF during both the uplog and downlog show that either the in situ density is significantly lower than the core density measured with the GRA track sensor and MAD measurements, which is unlikely, or the density sonde was not measuring the formation property despite being in apparent good contact. The good correlation between the resistivity and ve-

locity logs and the GRA density data in this interval, which is expected under normal consolidation of sediments, suggests that the GRA track measurements are more reliable than the density log in this interval. One possible explanation for this apparent contradiction is that the narrow hole size measured by the caliper was an indication of shallower material falling off and building a temporary ledge of loose sediments whose density was measured by the HLDS.

Because the triple combo uplog was the only pass to measure elevated gamma radiation between 303 and 317 m WMSF and all other passes show very good repeatability (Fig. **F40**), we consider the high readings to be the anomalous consequence of temporary fill in the borehole. We use the gamma ray log recorded during the second pass of the FMS-sonic tool string in the following figures and discussion.

Except in the interval discussed above, Figure **F38** shows that density and gamma ray measurements made downhole and on the recovered cores are in good agreement; however, they display a depth offset of ~5 m with the core data, indicating deeper depth for the same measurement. This offset was adjusted in the core measurement and recovery data shown in Figure **F40** for a more precise comparison. All logs are referenced to the seafloor depth of 1962.5 m WRF, which was identified where the gamma ray tool stopped detecting any natural radioactivity at the end of the triple combo run. This depth is 5 m shallower than the drillers estimation.

Above 370 m WSF, the resistivity values measured by the electrode spherically focused resistivity (SFLU) measurement were lower than those recorded by induction measurements (e.g., medium induction phasor-processed resistivity [IMPH] and deep induction phasor-processed resistivity [IDPH] in Fig. **F38**), probably because of current loss at the electrodes and eccentralization of the sonde. The higher induction resistivity values are more representative of the resistivity of the formation, but the higher resolution SFLU data are a good indication of finer scale variability in the formation.

The display in Figure **F39** of the high coherence in sonic waveforms used to derive compressional and shear velocities suggests that, despite the enlarged hole and the closeness of formation $V_P$ to sound velocity in the borehole fluid (~1500 m/h), the Dipole Sonic Imager (DSI) was able to capture distinct wave arrivals and measure reliable $V_P$ and $V_S$ profiles. Additional postcruise processing will be required only to refine these profiles and will likely reduce the variability of $V_P$ and $V_S$ in some intervals.

## Logging stratigraphy and correlation

The combined analysis of gamma ray, resistivity, density, and velocity logs allows for the identification of several logging units defined by characteristic trends. Because of the uniformity of the sediments at this site (see **"Lithostratigraphy"**), these units are mostly defined by subtle changes in trends and correlations rather than indications of significant changes in the formation. Because the $V_P$ log also allows for correlation with seismic stratigraphy, it was the primary guide in delimiting the units. The variations in the content of the three radioactive elements contributing to the natural radioactivity of the formation (K, U, and Th; Fig. **F41**) were also used for the definition of these units.

Logging Unit 1 (100–330 m WMSF) is characterized mainly by a steady increase with depth in velocity, whereas the other logging data remain mostly uniform despite some variability, such as in gamma radiation. Using the preliminary $V_P$ logs and a density profile composite made of the density log and the envelope of GRA bulk density between 310 and 360 m WMSF, we were able to reproduce the main reflectors observed in seismic Line Stk-1 (Sakamoto et al., 2005) crossing Site U1343. The velocity increase at the bottom of logging Unit 1 is likely responsible for the strong reflector that can be observed at 2860 ms two-way traveltime (Fig. **F42**). Although we speculated that this reflector might be a BSR that indicates the existence of gas hydrate overlying free gas, no conclusive indication from the logs supports the occurrence of gas hydrate. However, slightly higher velocity and resistivity trends and lower dipole waveform amplitudes above the reflector, as well as lower chlorinity values measured on several pore water samples (see **"Geochemistry and microbiology"**), suggest that some amount of gas hydrate might be present.

One of the ash layers (Section 323-U1343E-33H-3) recovered in this unit can be recognized in the FMS images (Fig. **F43A**).

Logging Unit 2 (330–510 m WMSF) is defined by slightly decreasing trends with depth in resistivity and slightly higher gamma ray values than those in shallower and deeper units. In the upper part of this unit (330–360 m WSF), the density values measured on the shipboard tracks were the highest recorded in this hole and were not matched by any of the density logs (Figs. **F38, F40**). These values were used in the synthetic seismogram (Fig. **F42**) and seem to be associated with the broad reflector at ~2880 ms two-way traveltime. One of the sections with the highest

density readings (Section 323-U1343E-41H-6) can be associated with a resistive mottled area in the FMS images (Fig. F43B).

The top of logging Unit 3 (510–745 m WMSF) is defined by a drop in gamma radiation, an increase in $V_P$, and a change in the trends of all the logs. The gamma ray, potassium, thorium, density, resistivity, $V_P$, and $V_S$ logs all display variability with depth of wider amplitude and lower frequency than in the upper units, suggesting a significant change in deposition history and rates. A dolostone recovered in this unit can be recognized in the FMS images (Section 323-U1343E-78X-6; Fig. F43C).

### Temperature measurements

The APCT-3 tool was successfully deployed three times in Hole U1343A. The measured temperatures range from 4.34°C at 43.5 m DSF to 8.53°C at 129.0 m DSF and closely fit a linear geothermal gradient of 49.0°C/km (Fig. F44). The temperature at the seafloor was 2.05°C based on the average of the measurements at the mudline during all APCT-3 deployments. A simple estimate of the heat flow can be obtained from the product of the geothermal gradient by the average thermal conductivity (0.985 W/[m·K]; see "Physical properties"), which gives a value of 48.2 mW/m$^2$, within the range of previous measurements in the area (the global heat flow database of the International Heat Flow Commission can be found at www.heatflow.und.edu/index.html).

Considering the variations in thermal conductivity with depth, a more accurate measure of heat flow in a conductive regime can be given by a "Bullard plot." The thermal resistance of an interval is calculated by integrating the inverse of thermal conductivity over depth. If the thermal regime is purely conductive, the heat flow will be the slope of the temperature versus the thermal resistance profile (Bullard, 1939). The thermal resistance calculated over the intervals overlying the APCT-3 measurements is shown in Table T20, and the resulting linear fit of the temperature gives a slightly lower heat flow value of 46.6 mW/m$^2$.

## References


Aksu, A.E., and Hillaire-Marcel, C., 1989. Upper Miocene to Holocene oxygen and carbon isotopic stratigraphy of Sites 646 and 647, Labrador Sea. *In* Srivastava, S.P., Arthur, M.A., Clement, B., et al., *Proc. ODP, Sci. Results,* 105: College Station, TX (Ocean Drilling Program), 689–704. doi:10.2973/odp.proc.sr.105.139.1989

Alvarez Zarikian, C.A., 2009. Data report: late Quaternary ostracodes at IODP Site U1314 (North Atlantic Ocean). *In* Channell, J.E.T., Kanamatsu, T., Sato, T., Stein, R., Alvarez Zarikian, C.A., Malone, M.J., and the Expedition 303/306 Scientists, *Proc. IODP,* 303/306: College Station, TX (Integrated Ocean Drilling Program Management International, Inc.). doi:10.2204/iodp.proc.303306.213.2009

Alvarez Zarikian, C.A., Stepanova, A.Y., and Grützner, J., 2009. Glacial–interglacial variability in deep sea ostracod assemblage composition at IODP Site U1314 in the subpolar North Atlantic. *Mar. Geol.,* 258(1–4):69–87. doi:10.1016/j.margeo.2008.11.009

Asahi, H., and Takahashi, K., 2007. A 9-year time-series of planktonic foraminifer fluxes and environmental change in the Bering Sea and the central subarctic Pacific Ocean, 1990–1999. *Prog. Oceanogr.,* 72(4):343–363. doi:10.1016/j.pocean.2006.03.021

Barron, J.A., and Gladenkov, A.Y., 1995. Early Miocene to Pleistocene diatom stratigraphy of Leg 145. *In* Rea, D.K., Basov, I.A., Scholl, D.W., and Allan, J.F. (Eds.), *Proc. ODP, Sci. Results,* 145: College Station, TX (Ocean Drilling Program), 3–19. doi:10.2973/odp.proc.sr.145.101.1995

Bé, A.W.H., and Tolderlund, D.S., 1971. Distribution and ecology of living planktonic foraminifera in surface waters of the Atlantic and Indian Oceans. *In* Funnel, B.M., and Riedel, W.R. (Eds.), *The Micropaleontology of Oceans:* Cambridge (Cambridge Univ. Press), 105–149.

Bujak, J.P., 1984. Cenozoic dinoflagellate cysts and acritarchs from the Bering Sea and northern North Pacific, DSDP Leg 19. *Micropaleontology,* 30(2):180–212. doi:10.2307/1485717

Bullard, E.C., 1939. Heat flow in South Africa. *Proc. R. Soc. London, Ser. A,* 173:474–502.

Bubenshchikova, N., Nürnberg, D., Lembke-Jene, L., and Pavlova, G., 2008. Living benthic foraminifera of the Okhotsk Sea: faunal composition, standing stocks and microhabitats. *Mar. Micropaleontol.,* 69(3–4):314–333. doi:10.1016/j.marmicro.2008.09.002

Coles, G.P., Whatley, R.C., and Moguilevsky, A., 1994. The ostracod genus *Krithe* from the Tertiary and Quarternary of the North Atlantic. *Palaeontology,* 37(1):71–120.

Cook, M.S., Keigwin, L.D., and Sancetta, C.A., 2005. The deglacial history of surface and intermediate water of the Bering Sea. *Deep-Sea Res., Part II,* 52(16–18):2163–2173. doi:10.1016/j.dsr2.2005.07.004

Cooper, A.K., Scholl, D.W., and Marlow, M.S., 1987. Structural framework, sedimentary sequences, and hydrocarbon potential of the Aleutian and Bowers Basins, Bering Sea. *In* Scholl, D.W., Grantz, A., and Vedder, J. (Eds.), *Geology and Resource Potential of the Continental Margin of Western North America and Adjacent Ocean Basins—Beaufort Sea to Baja California* (Vol. 6): *Earth Sci. Ser.* Houston (Circum-Pacific Council for Energy and Mineral Resources), 476–502.

Dählmann, A., and de Lange, G.J., 2003. Fluid–sediment interactions at Eastern Mediterranean mud volcanoes: a stable isotope study from ODP Leg 160. *Earth Planet. Sci. Lett.,* 212(3–7):377–391. doi:10.1016/S0012-821X(03)00227-9

De Lange, G.J., and Brumsack, H.-J., 1998. Pore-water indications for the occurrence of gas hydrates in Eastern

Mediterranean mud dome structures. *In* Robertson, A.H.F., Emeis, K.-C., Richter, C., and Camerlenghi, A. (Eds.), *Proc. ODP, Sci. Results,* 160: College Station, TX (Ocean Drilling Program), 569–574. **doi:10.2973/odp.proc.sr.160.042.1998**

Didié, C., and Bauch, H.A., 2000. Species composition and glacial–interglacial variations in the ostracode fauna of the northeast Atlantic during the past 200,000 years. *Mar. Micropaleontol.,* 40(1–2):105–129. **doi:10.1016/S0377-8398(00)00034-7**

Dowsett, H.J., and Ishman, S.E., 1995. Middle Pliocene planktonic and benthic foraminifers from the subarctic North Pacific: Sites 883 and 887. *In* Rea, D.K., Basov, I.A., Scholl, D.W., and Allan, J.F. (Eds.), *Proc. ODP, Sci. Results,* 145: College Station, TX (Ocean Drilling Program), 141–156. **doi:10.2973/odp.proc.sr.145.150.1995**

Dowsett, H.J., and Poore, R.Z., 1990. A new planktic foraminifer transfer function for estimating Pliocene-Holocene paleoceanographic conditions in the North Atlantic. *Mar. Micropaleontol.,* 16(1–2):1–23. **doi:10.1016/0377-8398(90)90026-I**

Head, M.J., Norris, G., and Mudie, P.J., 1989. Palynology and dinocyst stratigraphy of the upper Miocene and lowermost Pliocene, ODP Leg 105, Site 646, Labrador Sea. *In* Srivastava, S.P., Arthur, M.A., Clement, B., et al., *Proc. ODP, Sci. Results,* 105: College Station, TX (Ocean Drilling Program), 423–451. **doi:10.2973/odp.proc.sr.105.135.1989**

Hesse, R., Frape, S.K., Egeberg, P.K., and Matsumoto, R., 2000. Stable isotope studies (Cl, O, and H) of interstitial waters from Site 997, Blake Ridge gas hydrate field, West Atlantic. *In* Paull, C.K., Matsumoto, R., Wallace, P.J., and Dillon, W.P. (Eds.), *Proc. ODP, Sci. Results,* 164: College Station, TX (Ocean Drilling Program), 129–137. **doi:10.2973/odp.proc.sr.164.238.2000**

Joy, J.A., and Clark, D.L., 1977. The distribution, ecology and systematics of the benthic Ostracoda of the central Arctic Ocean. *Micropaleontology,* 23(2):129–154. **doi:10.2307/1485329**

Kamikuri, S., Nishi, H., and Motoyama, I., 2007. Effects of late Neogene climatic cooling on North Pacific radiolarian assemblages and oceanographic conditions. *Palaeogeogr., Palaeoclimatol., Palaeoecol.,* 249(3–4):370–392. **doi:10.1016/j.palaeo.2007.02.008**

Kastner, M., Kvenvolden, K.A., and Lorenson, T.D., 1998. Chemistry, isotopic composition, and origin of a methane-hydrogen sulfide hydrate at the Cascadia subduction zone. *Earth Planet. Sci. Lett.,* 156:173–183. **doi:10.1016/S0012-821X(98)00013-2**

Ling, H.Y., 1992. Late Neogene silicoflagellates and ebridians from Leg 128, Sea of Japan. *In* Pisciotto, K.A., Ingle, J.C., Jr., von Breymann, M.T., and Barron, J., et al. (Eds.), *Proc. ODP, Sci. Results,* 127/128, Pt. 1: College Station, TX (Ocean Drilling Program), 237–248. **doi:10.2973/odp.proc.sr.127128-1.126.1992**

Lourens, L.J., Hilgen, F.J., Shackleton, N.J., Laskar, J., and Wilson, D., 2004. The Neogene period. *In* Gradstein, F.M., Ogg, J.G., and Smith, A.G. (Eds.), *A Geological Time Scale 2004*. Cambridge (Cambridge Univ. Press), 409–440.

Martini, E., 1971. Standard Tertiary and Quaternary calcareous nannoplankton zonation. *In* Farinacci, A. (Ed.), *Proc. 2nd Int. Conf. Planktonic Microfossils Roma:* Rome (Ed. Tecnosci.), 2:739–785.

Mudie, P.J., 1985. Palynology of the Cesar Cores, Alpha Ridge. *In* Jackson, H.R., Mudie, P.J., and Blasco, S.M. (Eds.), *Initial Geological Report on CESAR—the Canadian Expedition to Study the Alpha Ridge, Arctic Ocean.* Pap.—Geol. Surv. Can., 84–22:149–174.

Ohkushi, K., Ahagon, N., Uchida, M., and Shibata, Y., 2005. Foraminiferal isotope anomalies from northwestern Pacific marginal sediments. *Geochem. Geophys. Geosyst.,* 6:Q04005. **doi:10.1029/2004GC000787**

Okazaki, Y., Takahashi, K., Asahi, H., Katsuki, K., Hori, J., Yasuda, H., Sagawa, Y., and Tokuyama, H., 2005. Productivity changes in the Bering Sea during the late Quaternary. *Deep-Sea Res., Part II,* 52(16–18):2150–2162. **doi:10.1016/j.dsr2.2005.07.003**

Onodera, J., and Takahashi, K., 2005. Silicoflagellate fluxes and environmental variations in the northwestern North Pacific during December 1997–May 2000. *Deep-Sea Res., Part I,* 52(2):371–388. **doi:10.1016/j.dsr.2004.10.001**

Poelchau, H.S., 1976. Distribution of Holocene silicoflagellates in North Pacific sediments. *Micropaleontology,* 22(2):164–193. **doi:10.2307/1485399**

Peckmann, J., and Thiel, V., 2004. Carbon cycling at ancient methane-seeps. *Chem. Geol.,* 205(3–4):433–467. **doi:10.1016/j.chemgeo.2003.12.025**

Rodriguez-Lázaro, J., and Cronin, T.M., 1999. Quaternary glacial and deglacial Ostracoda in the thermocline of the Little Bahama Bank (NW Atlantic): palaeoceanographic implications. *Palaeogeogr., Palaeoclimatol., Palaeoecol.,* 152(3–4):339–364. **doi:10.1016/S0031-0182(99)00048-6**

Sakamoto, T., Ikehara, M., Aoki, K., Iijima, K., Kimura, N., Nakatsuka, T., and Wakatsuchi, M., 2005. Ice-rafted debris (IRD)-based sea-ice expansion events during the past 100 kyrs in the Okhotsk Sea. *Deep Sea Res., Part II,* 52(16–18):2275–2301. **doi:10.1016/j.dsr2.2005.08.007**

Sancetta, C., 1982. Distribution of diatom species in surface sediments of the Bering and Okhotsk seas. *Micropaleontology,* 28(3):221–257. **doi:10.2307/1485181**

Spezzaferri, S., 1998. Planktonic foraminifer biostratigraphy and paleoenvironmental implications of Leg 152 sites (East Greenland margin). *In* Saunders, A.D., Larsen, H.C., and Wise, S.W., Jr. (Eds.), *Proc. ODP, Sci. Results,* 152: College Station, TX (Ocean Drilling Program), 161–189. **doi:10.2973/odp.proc.sr.152.220.1998**

Springer, A.M., McRoy, C.P., and Flint, M.V., 1996. The Bering Sea Green Belt: shelf-edge processes and ecosystem production. *Fish. Oceanogr.,* 5(3–4):205–223. **doi:10.1111/j.1365-2419.1996.tb00118.x**

Takahashi, K., 1985. Two year time-series fluxes of silicoflagellates and Actiniscus: size fractioned results from Subarctic Pacific Station PAPA, 1982–1984. *WHOI Tech. Rep.,* WHOI-85-41.

Takahashi, K., 1989. Silicoflagellates as productivity indicators: evidence from long temporal and spatial flux variability responding to hydrography in the northeastern Pacific. *Global Biogeochem. Cy.,* 3(1):43–61. **doi:10.1029/GB003i001p00043**

Takahashi, K., 2005. The Bering Sea and paleoceanography. *Deep-Sea Res., Part II,* 52(16–18):2080–2091. **doi:10.1016/j.dsr2.2005.08.003**

Takahashi, K., Fujitani, N., Yanada, M., and Maita, Y., 2000. Long-term biogenic particle fluxes in the Bering Sea and the central subarctic Pacific Ocean, 1990–1995. *Deep-Sea Res., Part I,* 47(9):1723–1759. **doi:10.1016/S0967-0637(00)00002-9**

Takahashi, K., Ravelo, A.C., and Alvarez Zarikian, C.A., 2009. Pliocene–Pleistocene paleoceanography and climate history of the Bering Sea. *IODP Sci. Prosp.,* 323. **doi:10.2204/iodp.sp.323.2009**

Taniguchi, A., 1984. Microzooplankton biomass in the arctic and subarctic Pacific Ocean in summer. *In* Hoshiai, T., and Fukuchi, M., *Proc. Sixth Symp. Polar Biol.* Mem. Natl. Inst. Polar Res. Spec. Issue (Jpn.), 32:63–76.

Ussler, W., III, and Paull, C.K., 2008. Rates of anaerobic oxidation of methane and authigenic carbonate mineralization in methane-rich deep-sea sediments inferred from models and geochemical profiles. *Earth Planet. Sci. Lett.,* 266(3–4):271–287. **doi:10.1016/j.epsl.2007.10.056**

Van Geen, A., Zheng, Y., Bernhard, J.M., Cannariato, K.G., Carriquiry, J., Dean, W.E.B., Eakins, W.,Ortiz, J.D., and Pike, J., 2003. On the preservation of laminated sediments along the western margin of North America. *Paleoceanography,* 18(4): 1098. **doi:10.1029/2003PA000911**

VanLaningham, S., Pisias, N.G., Duncan, R.A., and Clift, P.D., 2009. Glacial–interglacial sediment transport to the Meiji Drift, northwest Pacific Ocean: evidence for timing of Beringian outwashing. *Earth Planet. Sci. Lett.,* 277(1–2):64–72. **doi:10.1016/j.epsl.2008.09.033**

Weaver, P.P.E., and Clement, B.M., 1987. Magnetobiostratigraphy of planktonic foraminiferal datums: Deep Sea Drilling Project Leg 94, North Atlantic. *In* Ruddiman, W.F., Kidd, R.B., Thomas, E., et al., *Init. Repts. DSDP,* 94: Washington (U.S. Govt. Printing Office), 815–829. **doi:10.2973/dsdp.proc.94.120.1987**

Westbrook, G.K., Carson, B., Musgrave, R.J., et al., 1994. *Proc. ODP, Init. Repts.,* 146 (Pt. 1): College Station, TX (Ocean Drilling Program). **doi:10.2973/odp.proc.ir.146-1.1994**

Yanagisawa, Y., and Akiba, F., 1998. Refined Neogene diatom biostratigraphy for the northwest Pacific around Japan, with an introduction of code numbers for selected diatom biohorizons. *Chishitsugaku Zasshi,* 104:395–414.

**Publication:** 15 March 2011
**MS 323-107**

**Figure F1.** Location map for Site U1343, on a topographic high on the Bering Sea shelf.

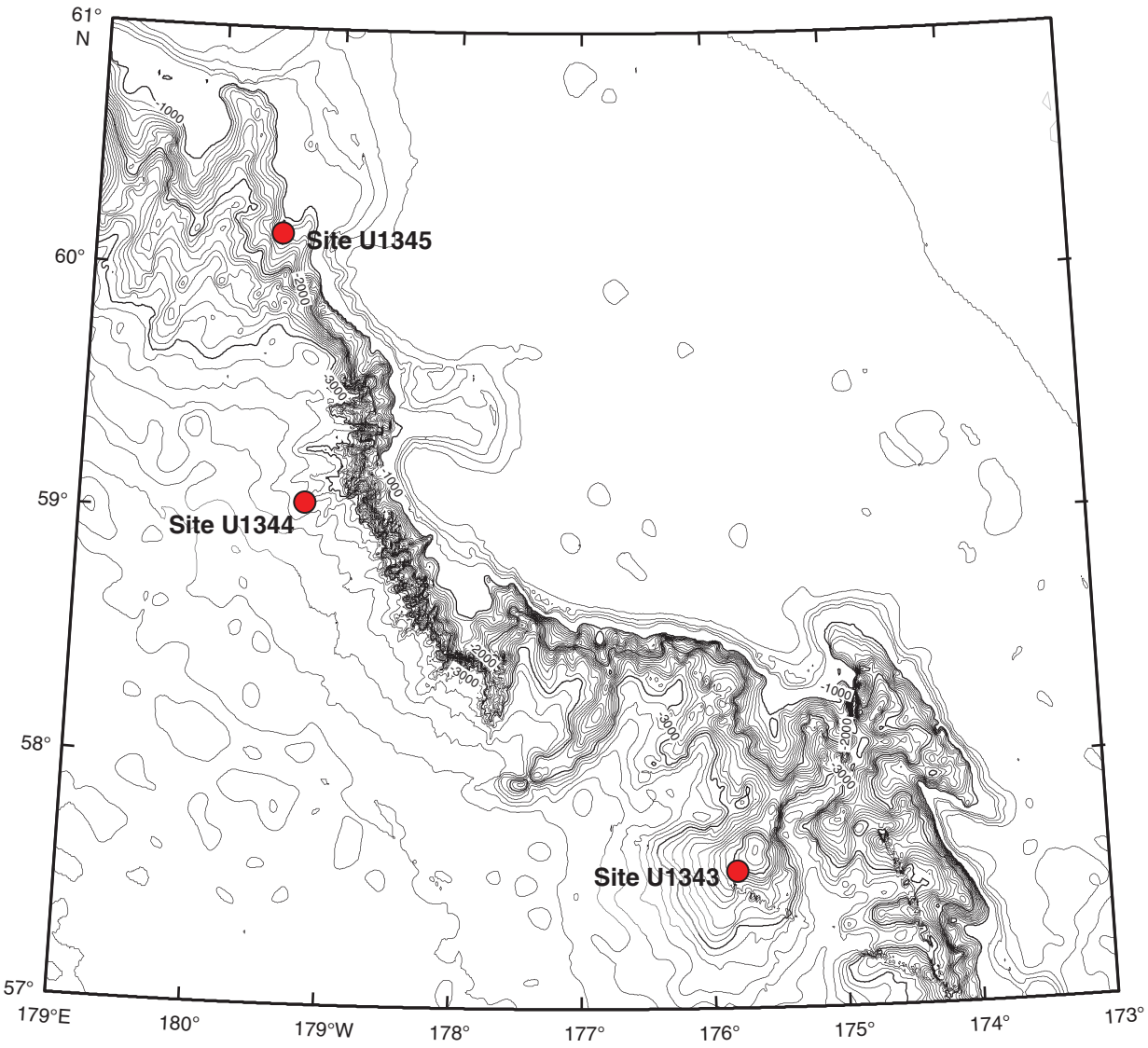

**Figure F2.** Navigation map of *Hakuhou-Maru* Cruise KH99-3 around Site U1343, including close-up seismic profiles shown in Figures F3 and F4.

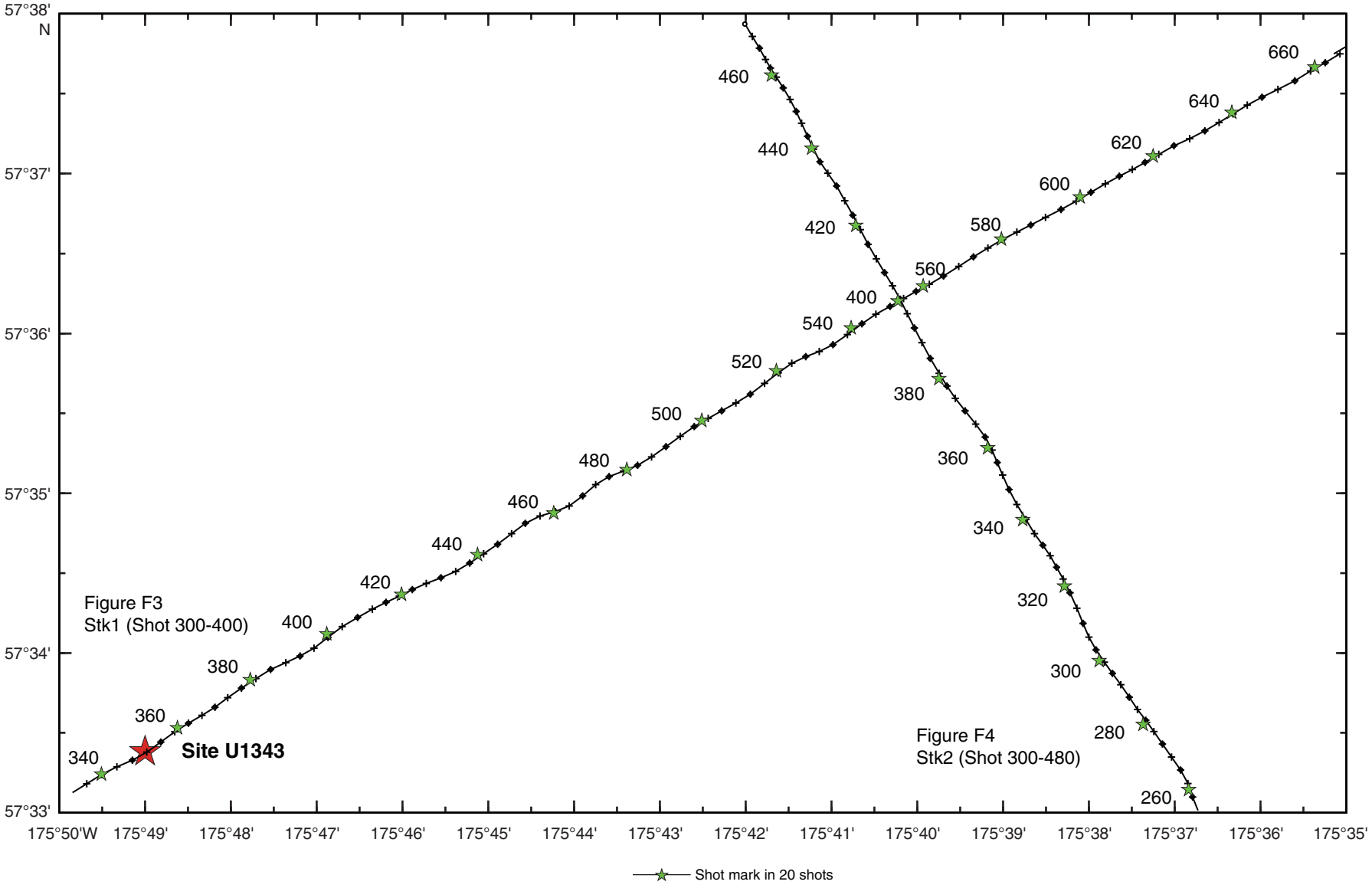

**Figure F3. A.** Close-up seismic profile of *Hakuhou-Maru* Cruise KH99-3 Line Stk1 (southwest–northeast) near Site U1343. **B.** Time-depth curve estimated from results of velocity analyses near Site U1343.

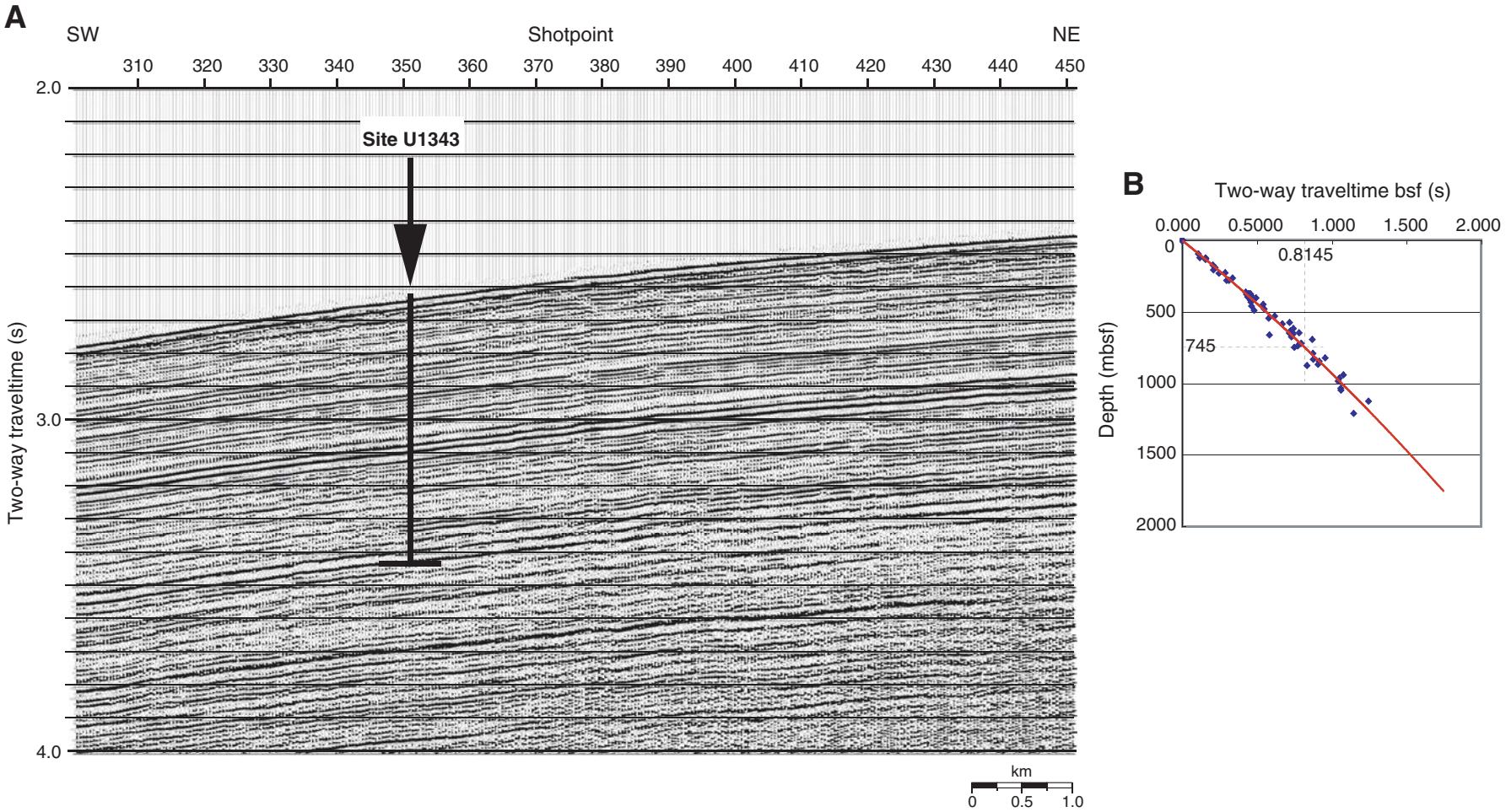

**Figure F4. A.** Close-up seismic profile of *Hakuhou-Maru* Cruise KH99-3 Line Stk2 (southeast–northwest) near Site U1343. The projected drill penetration of Site U1343 is shown by the dashed line. The cross point with Line Stk1 (southwest–northeast) is at Shotpoint 400. **B.** Time-depth curve estimated from results of velocity analyses on Lines Stk1 and Stk2 around Site U1343.

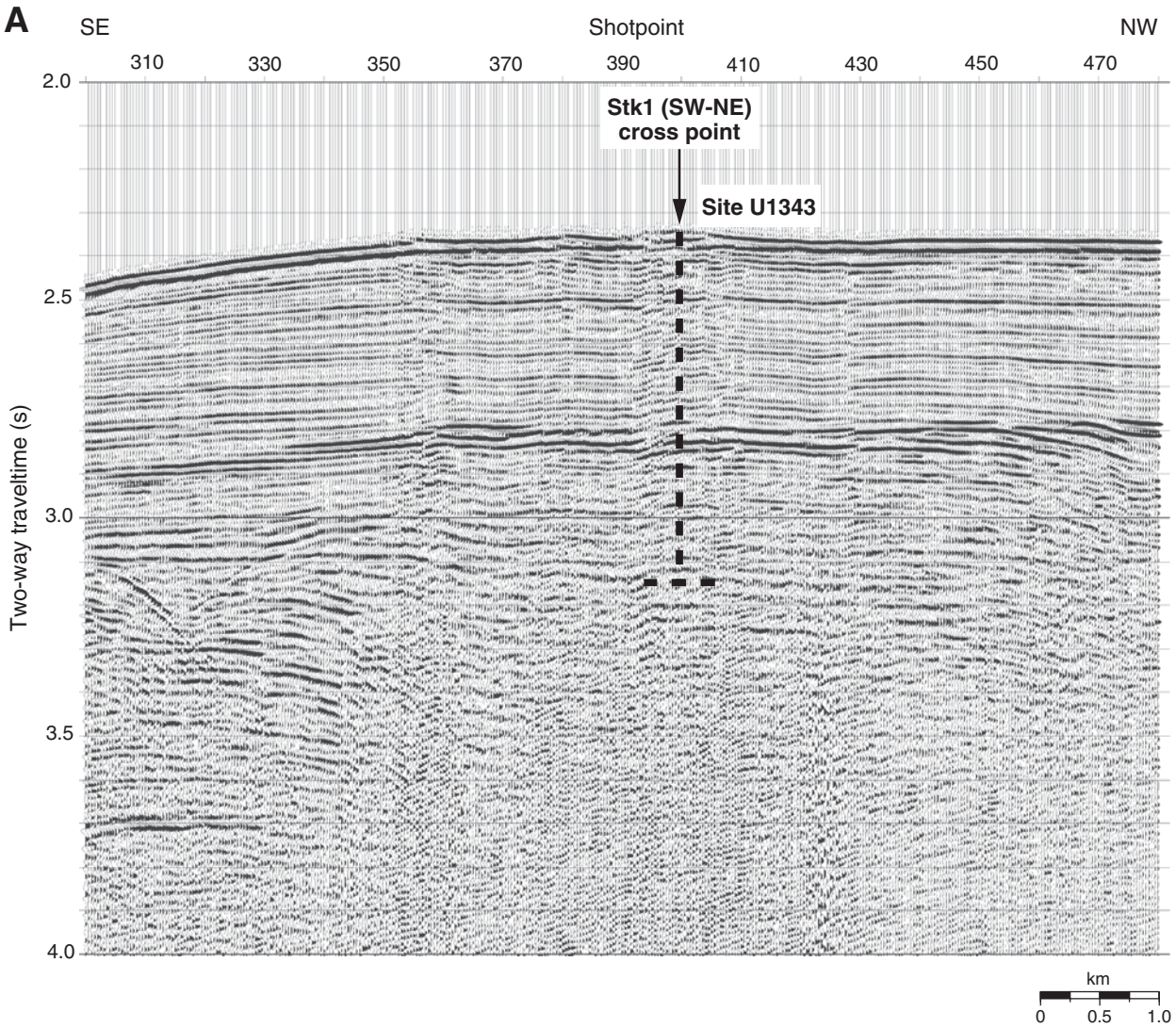


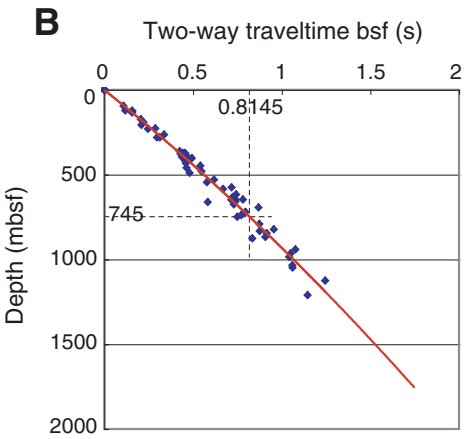

**Figure F5.** Seismic profile of *Hakuhou-Maru* Cruise KH99-3 Line Stk1 (southwest–northeast), showing the location of Site U1343. The cross point with Line Stk2 (southeast–northwest) is at Shotpoint 553.

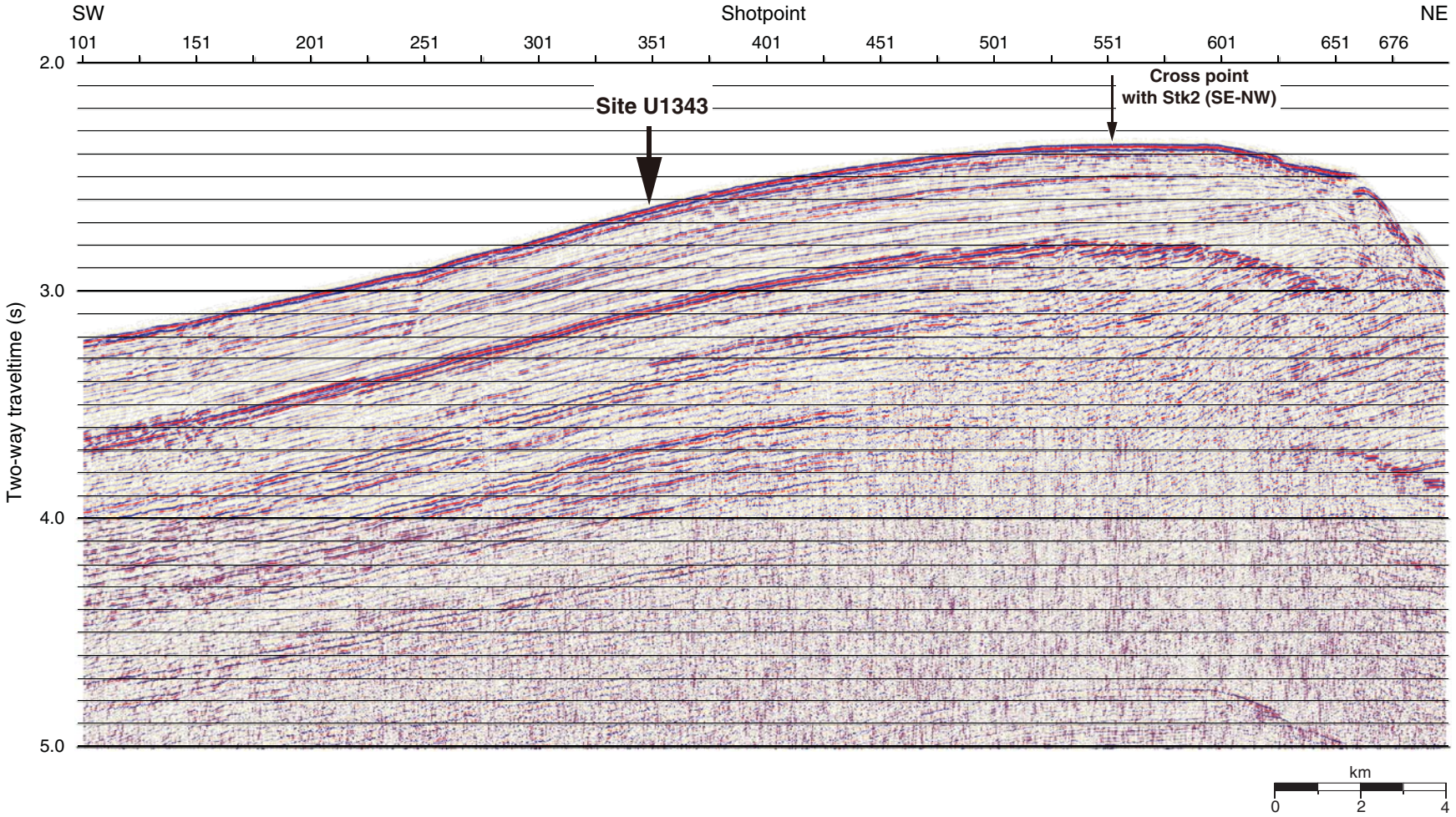

**Figure F6.** Summary of lithology, structures, accessories, microfossils, and physical properties, Hole U1343A. See legend in Figure F6 in the "Methods" chapter. Soft-sed = soft-sediment, auth = authigenic, calc = calcareous, NGR = natural gamma radiation, GRA = gamma ray attenuation, sed rate = sedimentation rate.

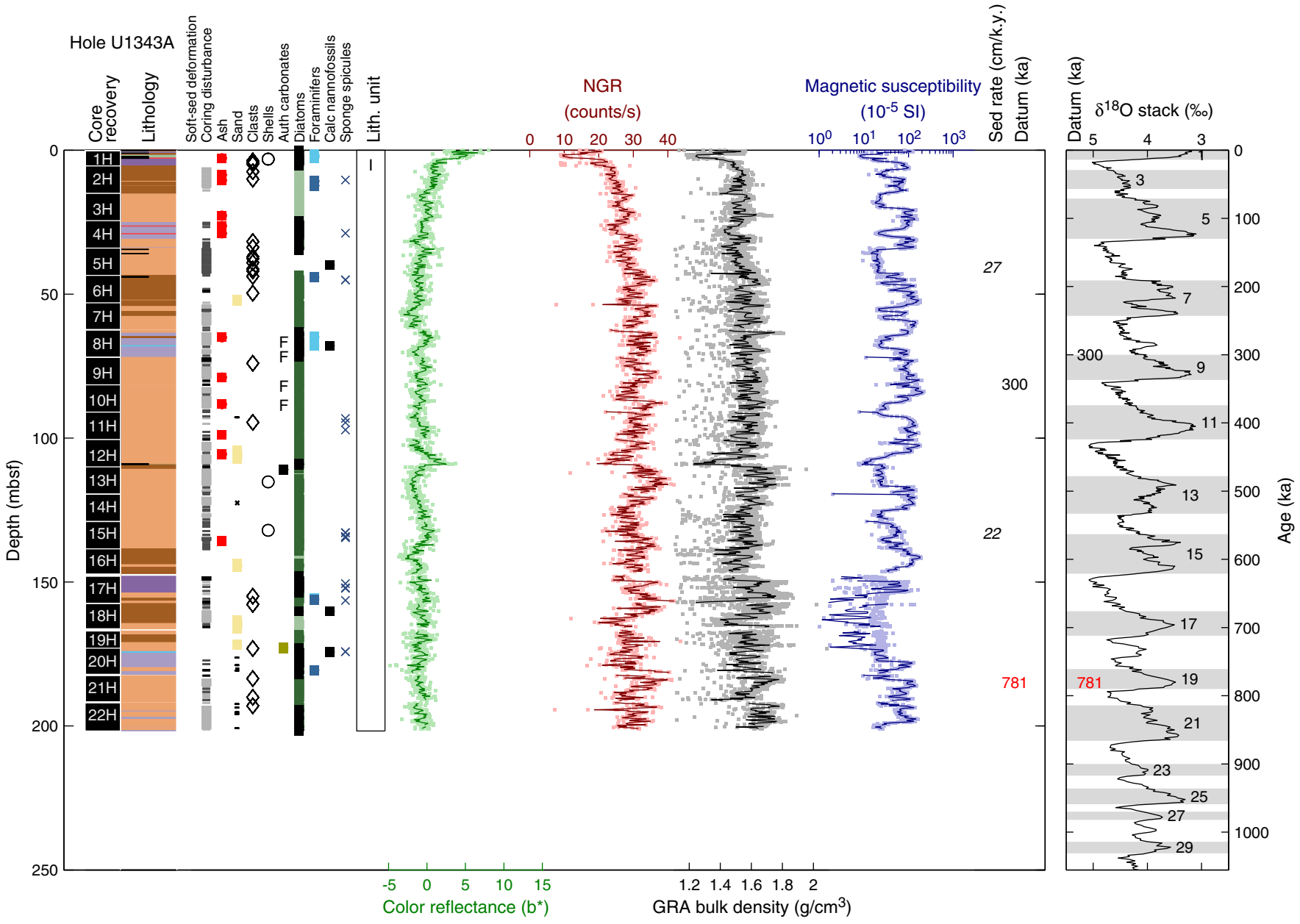

**Figure F7.** Summary of lithology, structures, accessories, microfossils, and physical properties, Hole U1343C. See legend in Figure F6 in the "Methods" chapter. Soft-sed = soft-sediment, auth = authigenic, calc = calcareous, NGR = natural gamma radiation, GRA = gamma ray attenuation, sed rate = sedimentation rate.

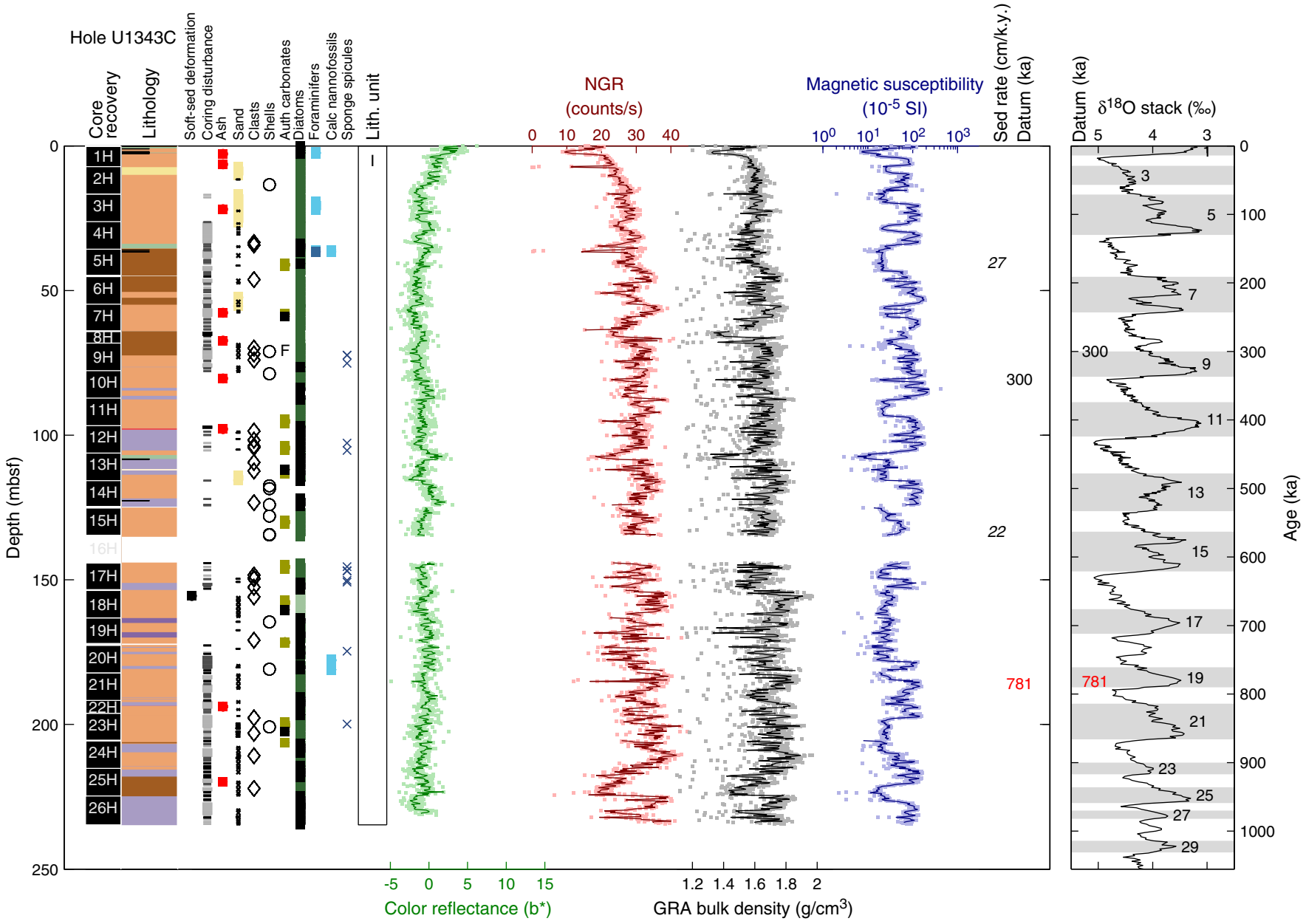

**Figure F8.** Summary of lithology, structures, accessories, microfossils, and physical properties, Hole U1343E. See legend in Figure F6 in the "Methods" chapter. Soft-sed = soft-sediment, auth = authigenic, calc = calcareous, NGR = natural gamma radiation, GRA = gamma ray attenuation, sed rate = sedimentation rate. **A.** 0–250 mbsf. (**Continued on next two pages.**)

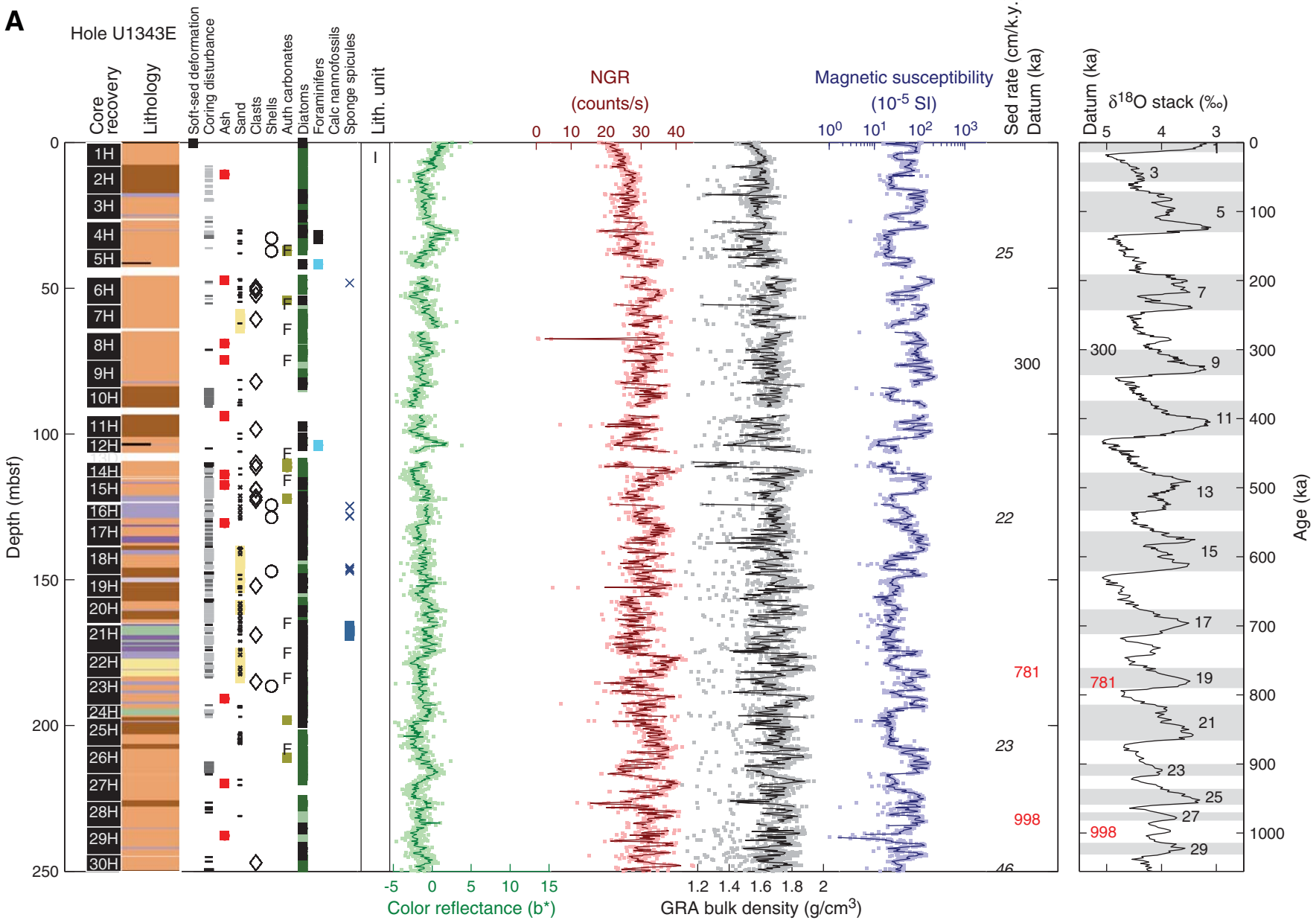

**Figure F8 (continued).** **B.** 250–500 mbsf. (Continued on next page.)

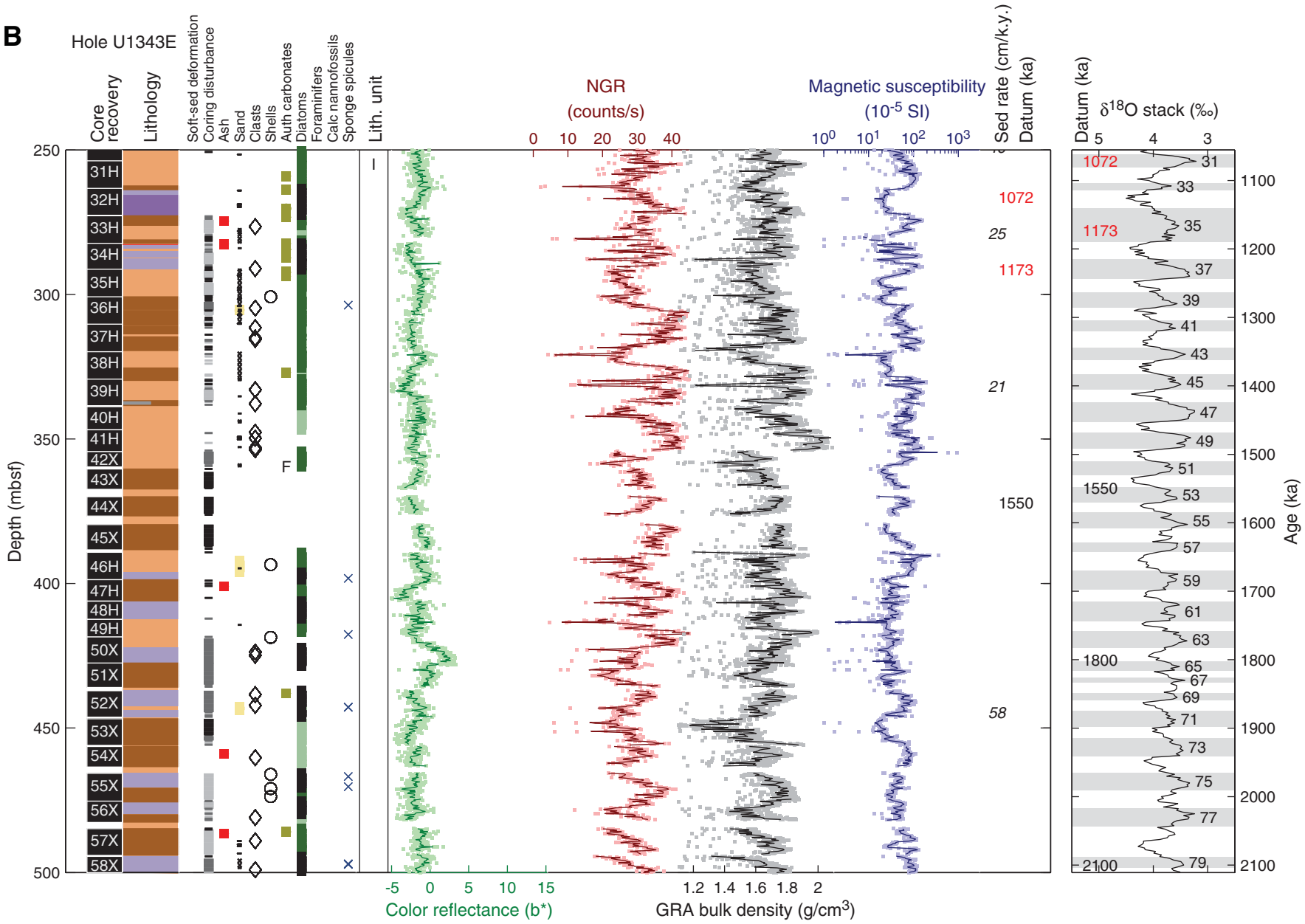

**Figure F8 (continued).** C. 500–750 mbsf.

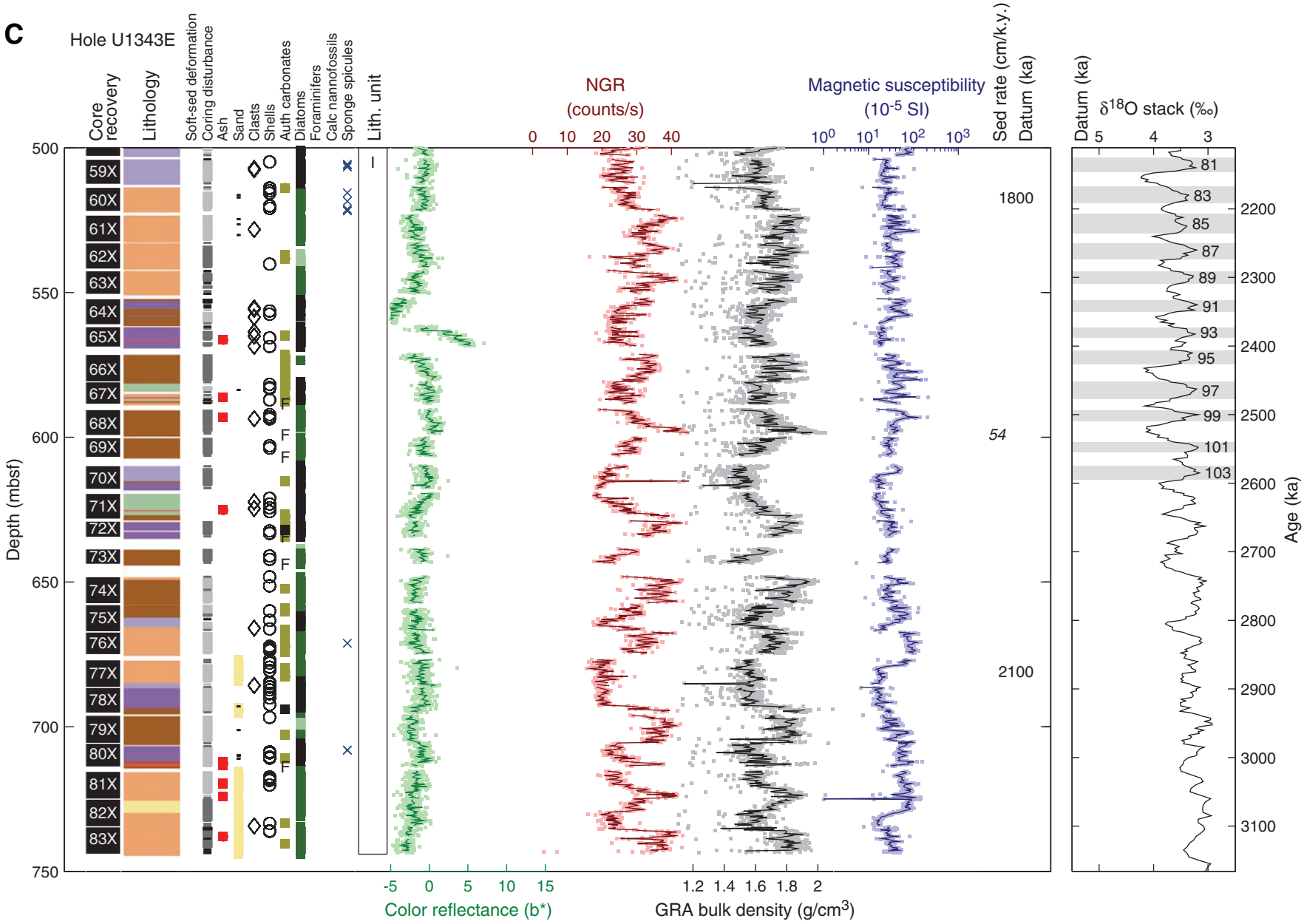

**Figure F9.** Correlation of laminated intervals, Holes U1343A, U1343C, and U1343E.

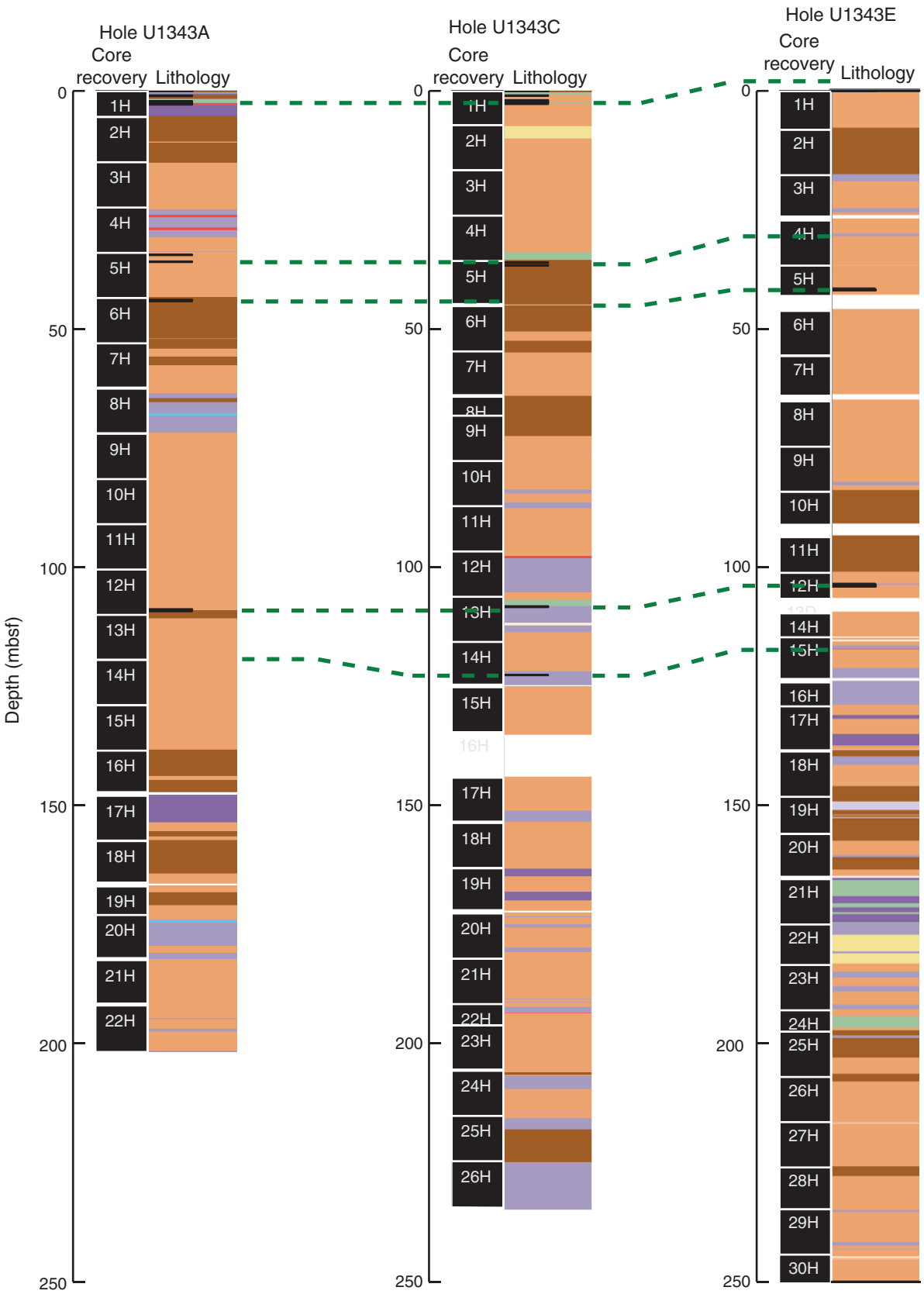

**Figure F10. A.** Core photograph of 8 cm basalt cobble at 41–47.5 cm in interval 323-U1343E-34H-CC, 31–58 cm. **B.** Thin section photomicrograph under cross-polarized light (above) and plane-polarized light (below).

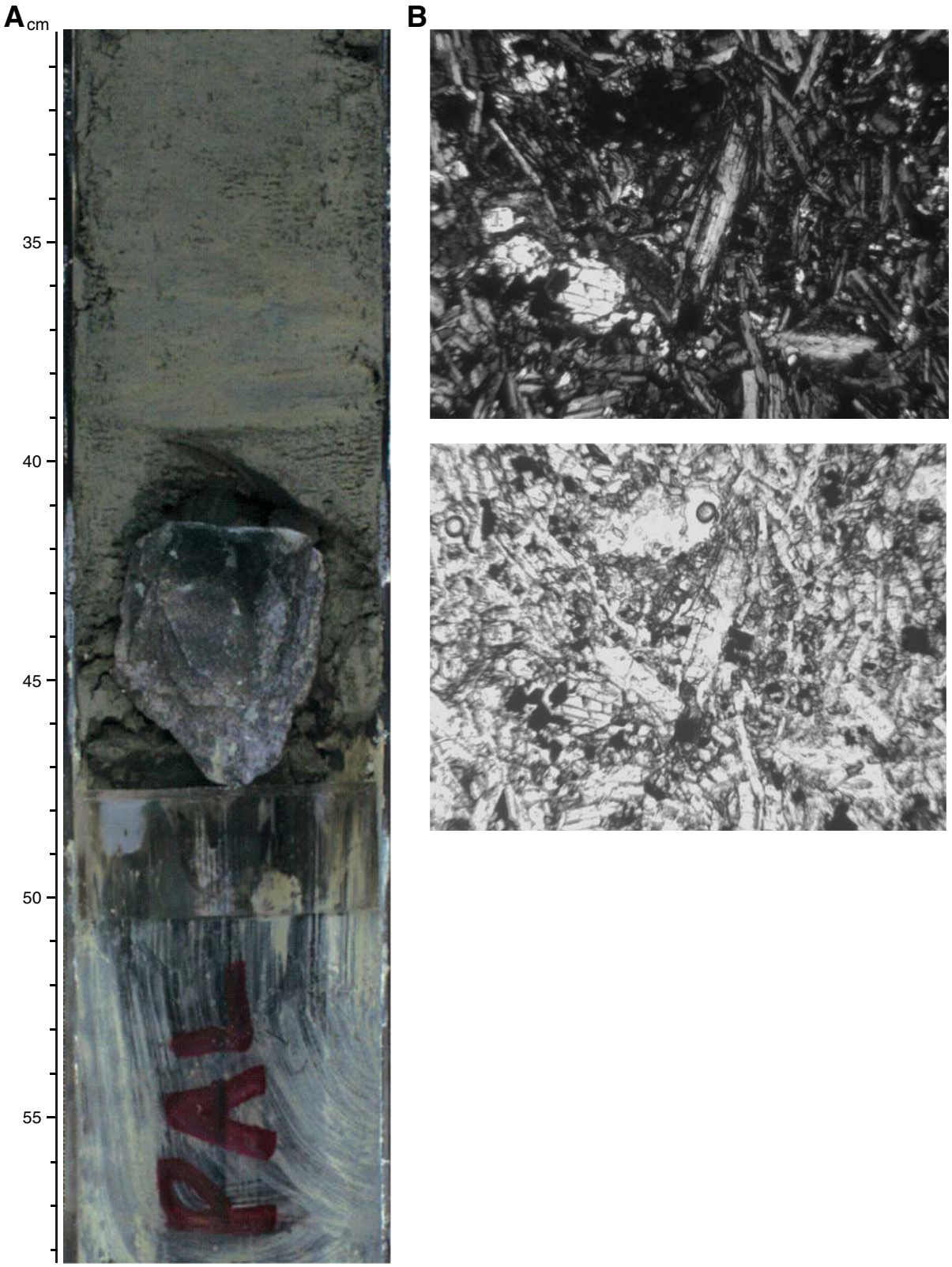

**Figure F11. A.** X-ray diffraction (XRD) analysis, Sample 323-U1343C-7H-3, 125–126 cm. **B.** Smear slide photograph of acicular authigenic carbonate crystals under cross-polarized light, Section 323-U1343C-7H-3, 47 cm. **C.** XRD analysis, Sample 323-U1343A-13H-2, 35–36 cm. **D.** Smear slide photograph of rhombs, Section 323-U1343A-13H-2, 36 cm. Q = quartz, Fsp = feldspar, I = illite, MgC = Mg-rich calcite, Chl = chlorite, D = dolomite, H = halite.

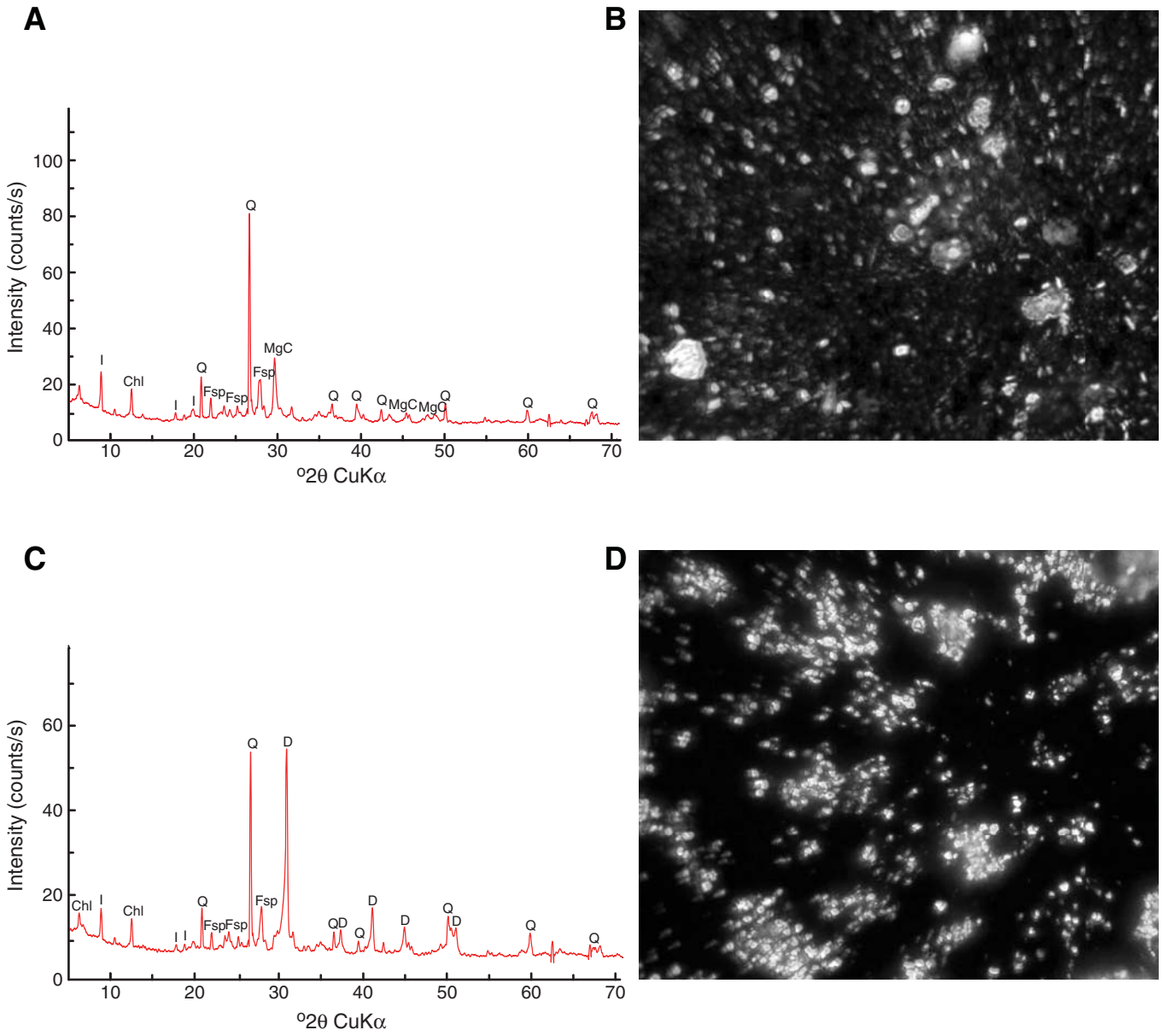

**Figure F12.** Core photograph of biscuiting (interval 323-U1343E-54X-3, 43–89 cm).

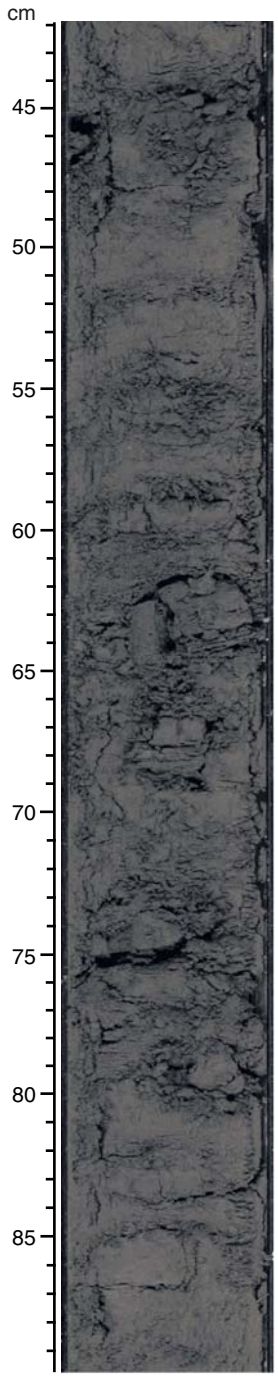

**Figure F13.** Age-depth plot for Site U1343 showing biostratigraphic datums based on radiolarians, diatoms, calcareous nannofossils, silicoflagellates, ebridians, dinoflagellates, and planktonic foraminifers. Biostratigraphic datums are listed in Table T2.

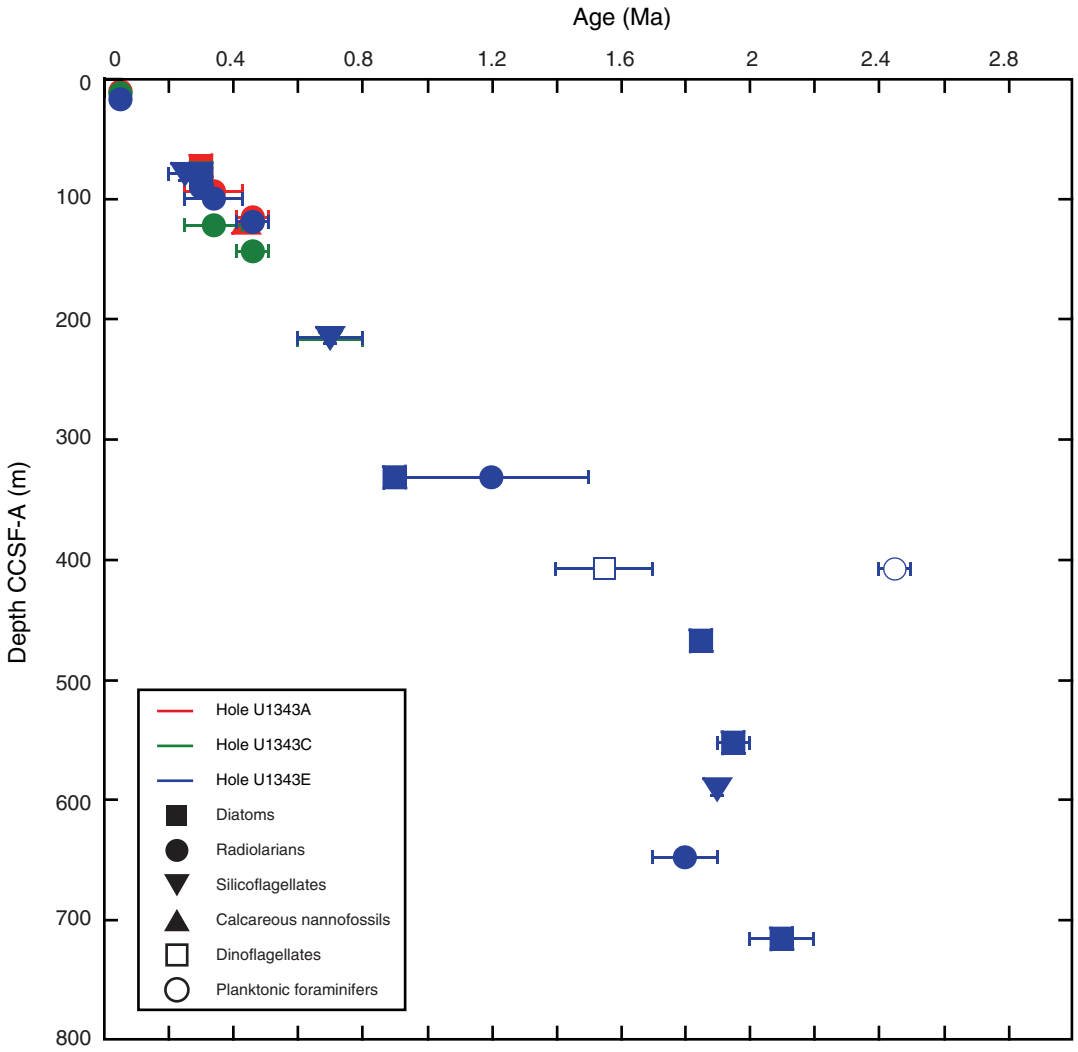

**Figure F14.** Abundance estimations for all major groups of fossils except diatoms. The data shown are from Holes U1343A–U1343E (radiolarians and planktonic and benthic foraminifers); Holes U1343A, U1343C, and part of Hole U1343E (calcareous nannofossils); and Hole U1343A and part of Hole U1343E (dinoflagellate cysts). B = barren, R = rare, F = few, C = common, A = abundant, D = dominant. For benthic foraminifer abundance estimates, see **"Biostratigraphy"** in the "Methods" chapter.

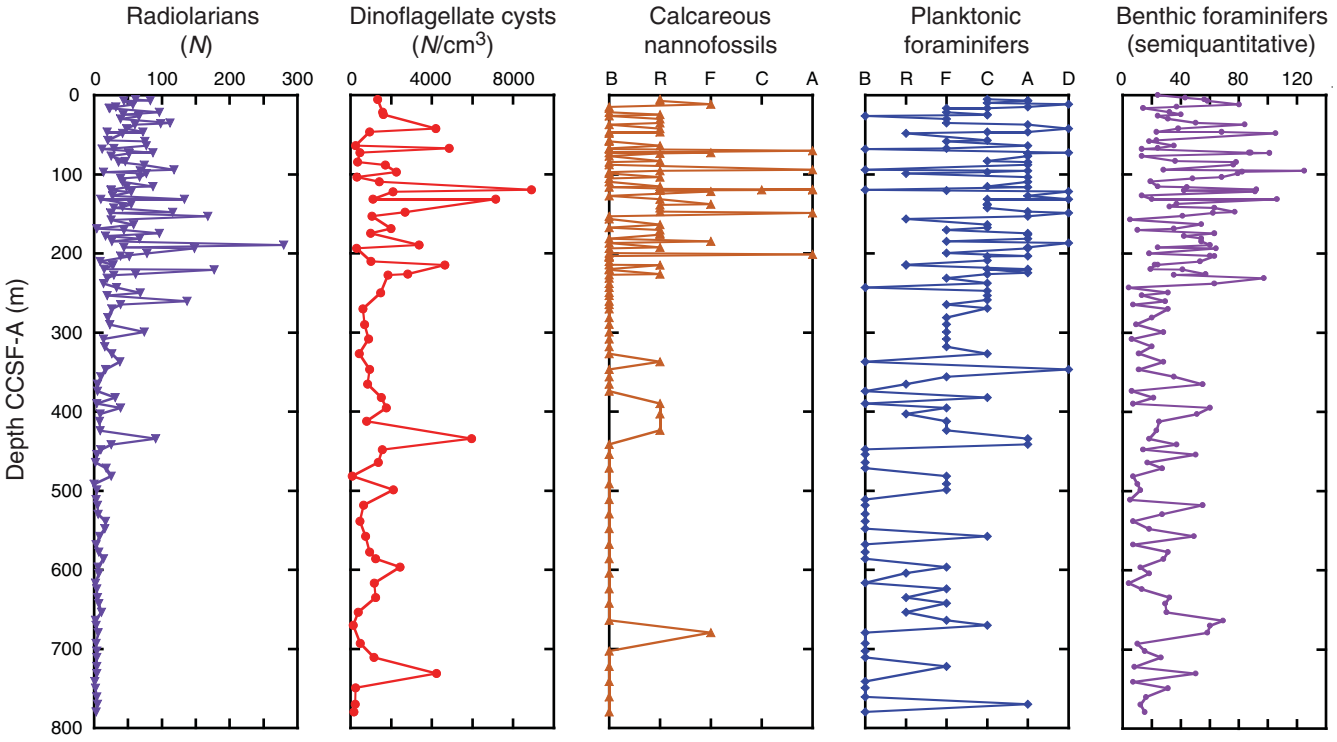

**Figure F15.** Relative abundances of sea ice dinoflagellates, sea ice diatoms, diatom species *Neodenticula seminae* (a proxy for pelagic/open water environment), and semiquantitative counts of subpolar planktonic foraminifers. Sea ice diatoms considered include *Bacteriosira fragilis*, *Detonula confervacea*, *Fragilariopsis cylindrus*, *Thalassiosira hyalina*, and *Thalassiosira antarctica* spores. Sea ice dinoflagellates considered include *Islandinium minutum*, *Operculodinium centrocarpum* (Arctic morphotype), and *Impagidinium minutum*.

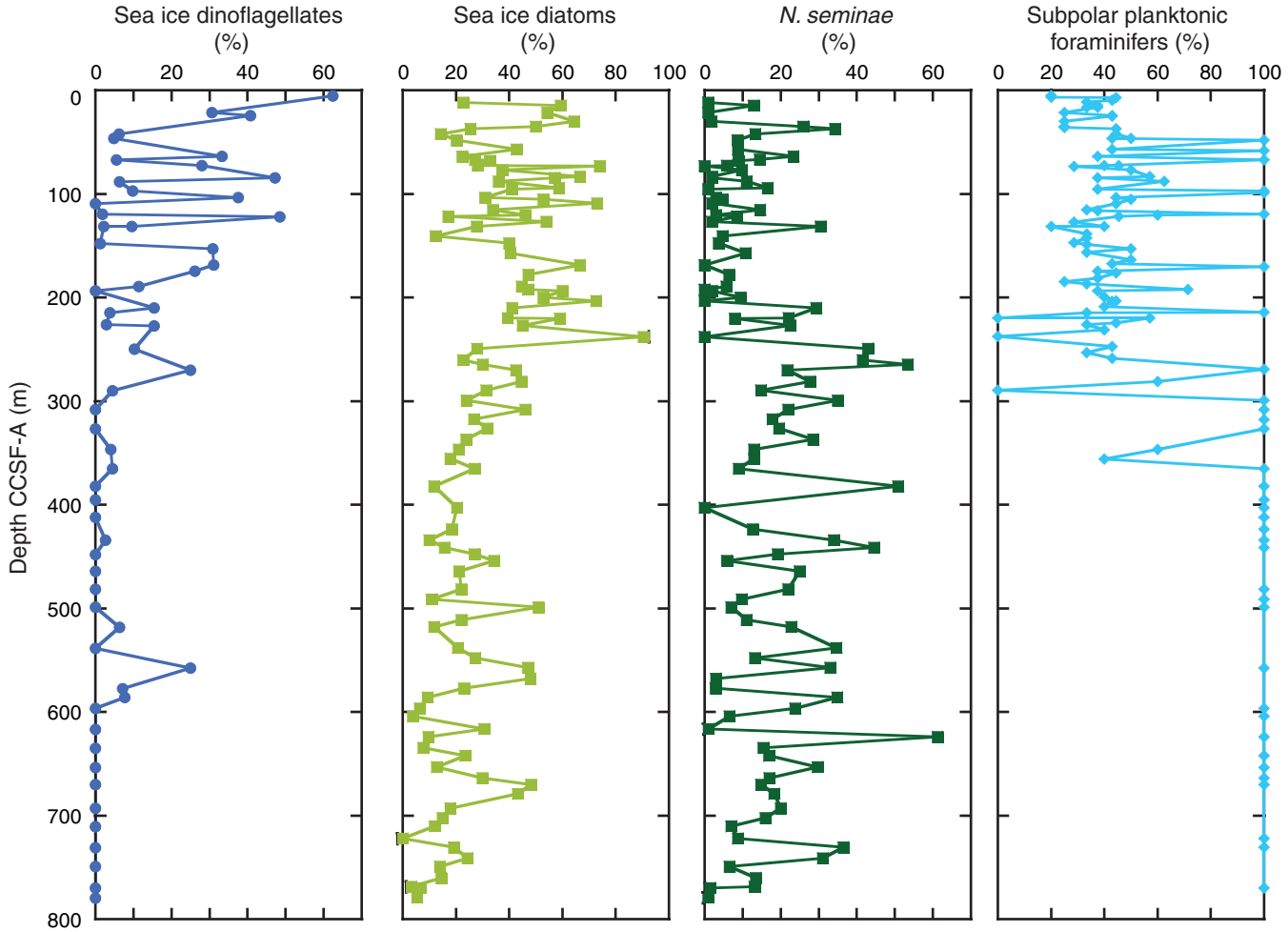

**Figure F16.** Inclination and intensity of remanent magnetization after 20 mT AF demagnetization ($Int_{20\ mT}$), Holes U1343A, U1343C, and U1343D. Intensity data are plotted with STMSL magnetic susceptibility data.

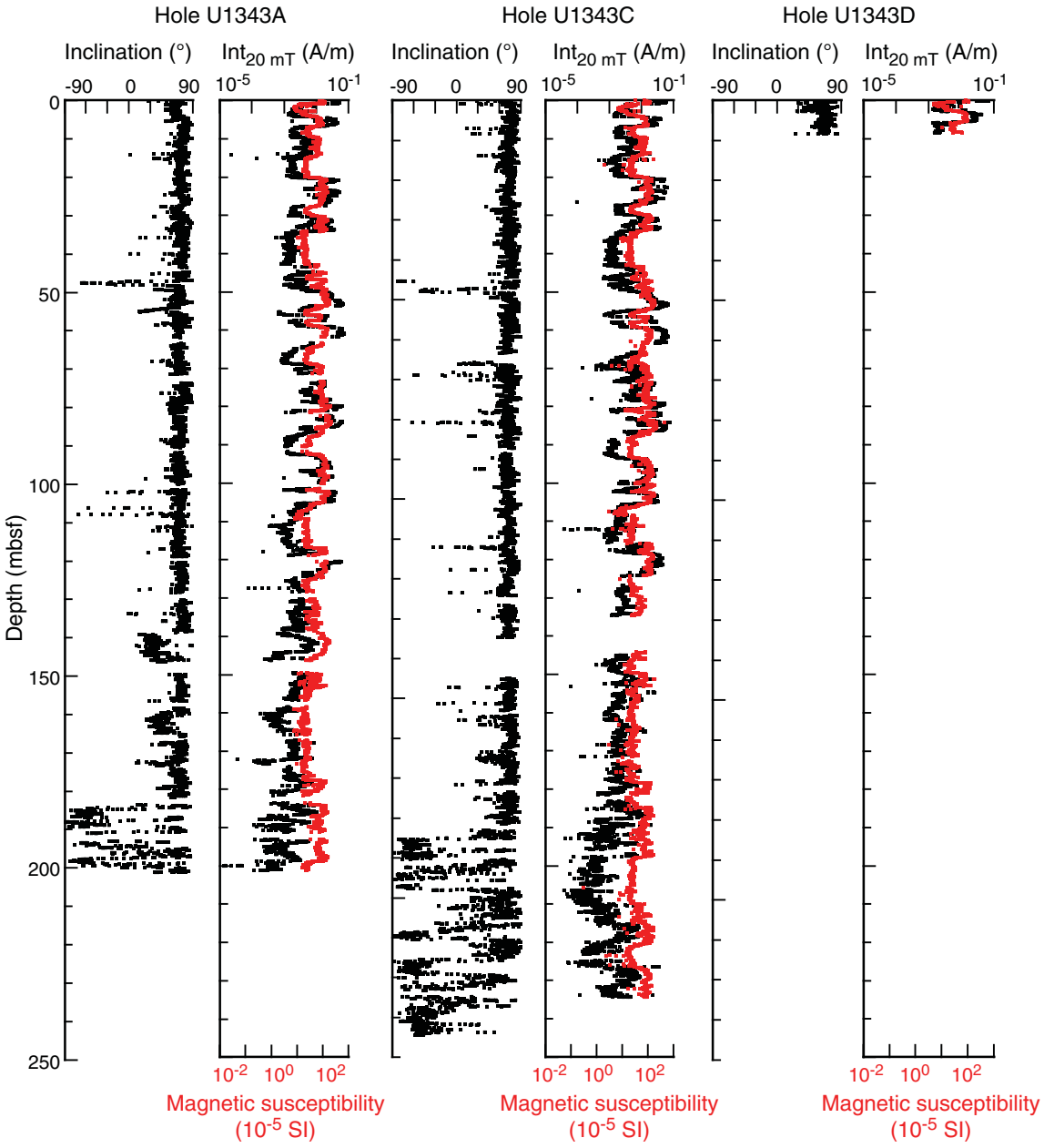

**Figure F17.** Inclination and intensity of remanent magnetization after 20 mT AF demagnetization ($Int_{20\ mT}$), Hole U1343E. Intensity data are plotted with STMSL magnetic susceptibility data.

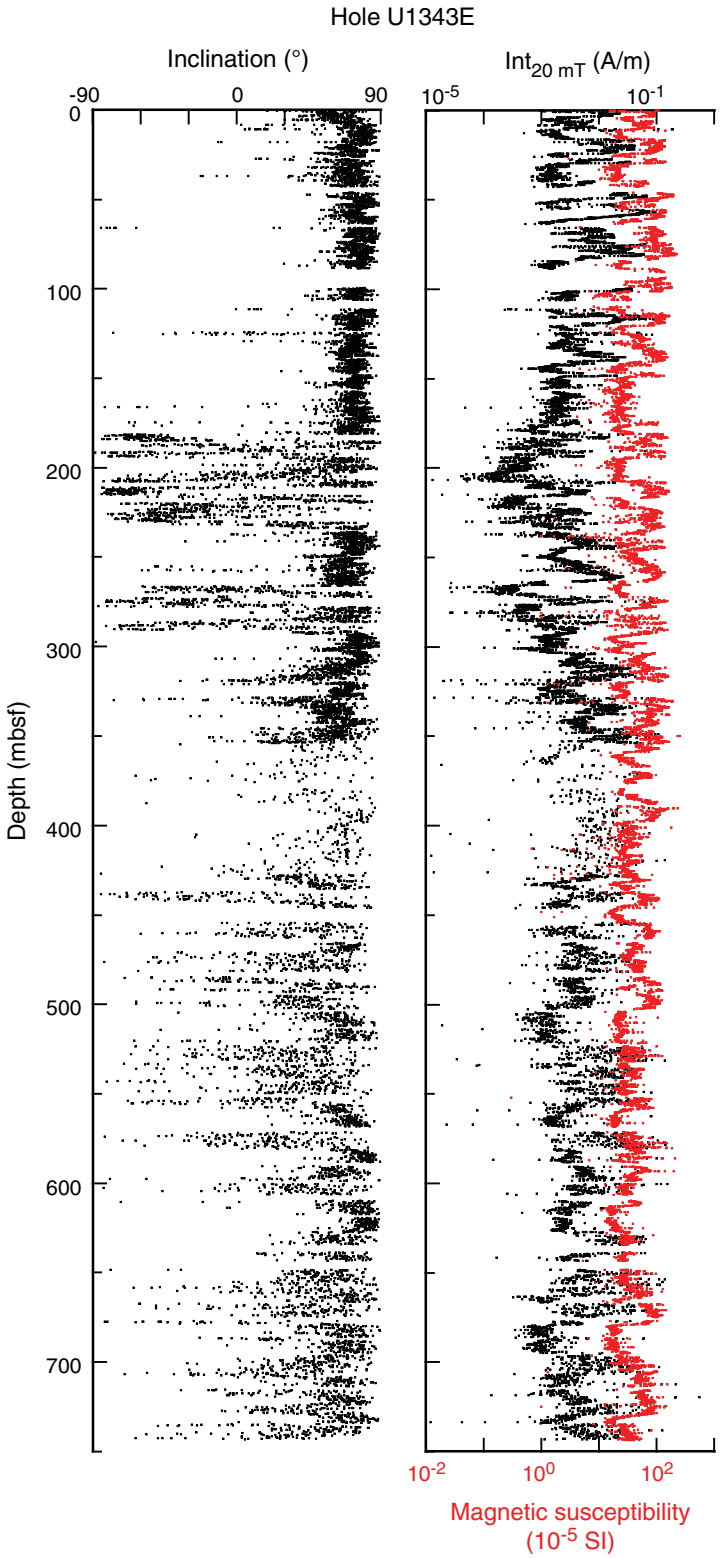

**Figure F18.** Inclination data (dots) and 60 point (corresponding to ~0.5 m) averaged inclination values (solid line), Hole U1343E. Tentative polarity zonation (black = normal polarity, white = reversed polarity, and gray = uncertain polarity) and presumable correlation with the polarity chrons are also shown.

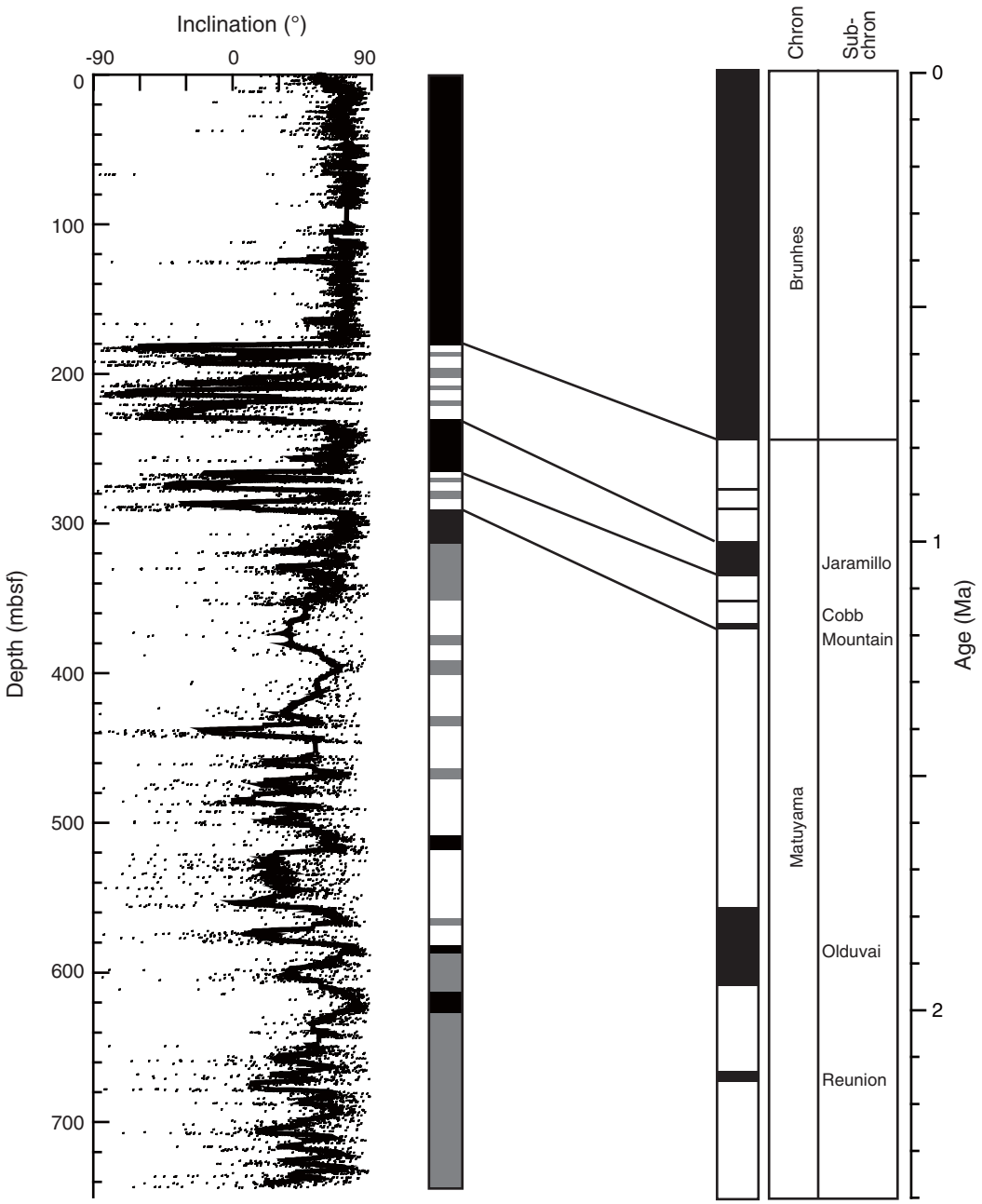

**Figure F19. A.** Intensity of remanent magnetization after 20 mT AF demagnetization ($Int_{20\ mT}$) (black) and magnetic susceptibility (red). **B.** Paleointensity estimates based on normalization of $Int_{20\ mT}$ by magnetic susceptibility. All data are from Holes U1343A, U1343C, U1343D, and U1343E plotted against CCSF-A for the uppermost 100 m. Data are interpolated to have equal spacing of 5 cm.

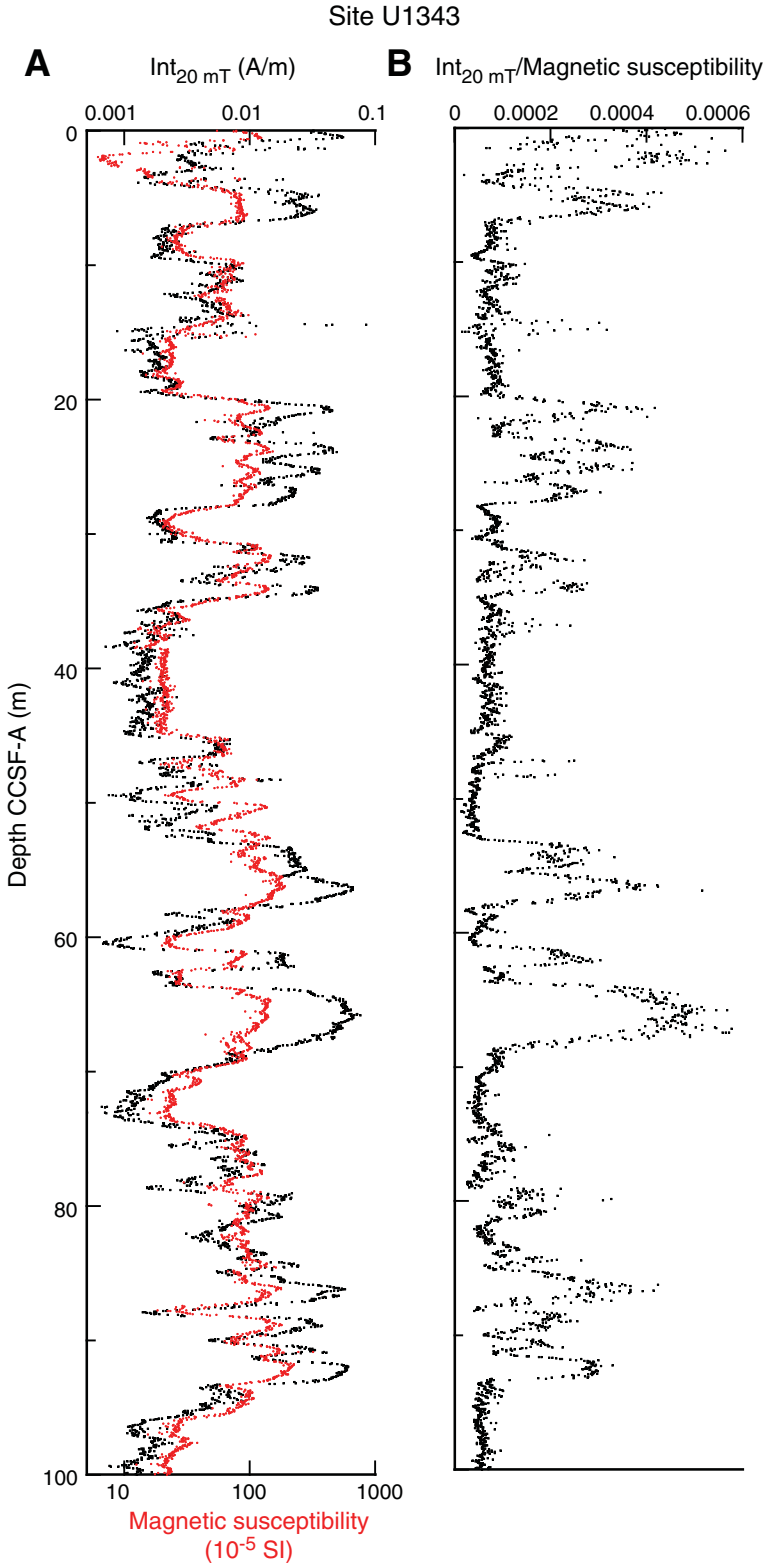

**Figure F20.** Intensity of remanent magnetization after 20 mT AF demagnetization ($Int_{20\ mT}$) plotted against magnetic susceptibility, Holes U1343A, U1343C, U1343D, and U1343E. Data are interpolated to have equal spacing of 5 cm.

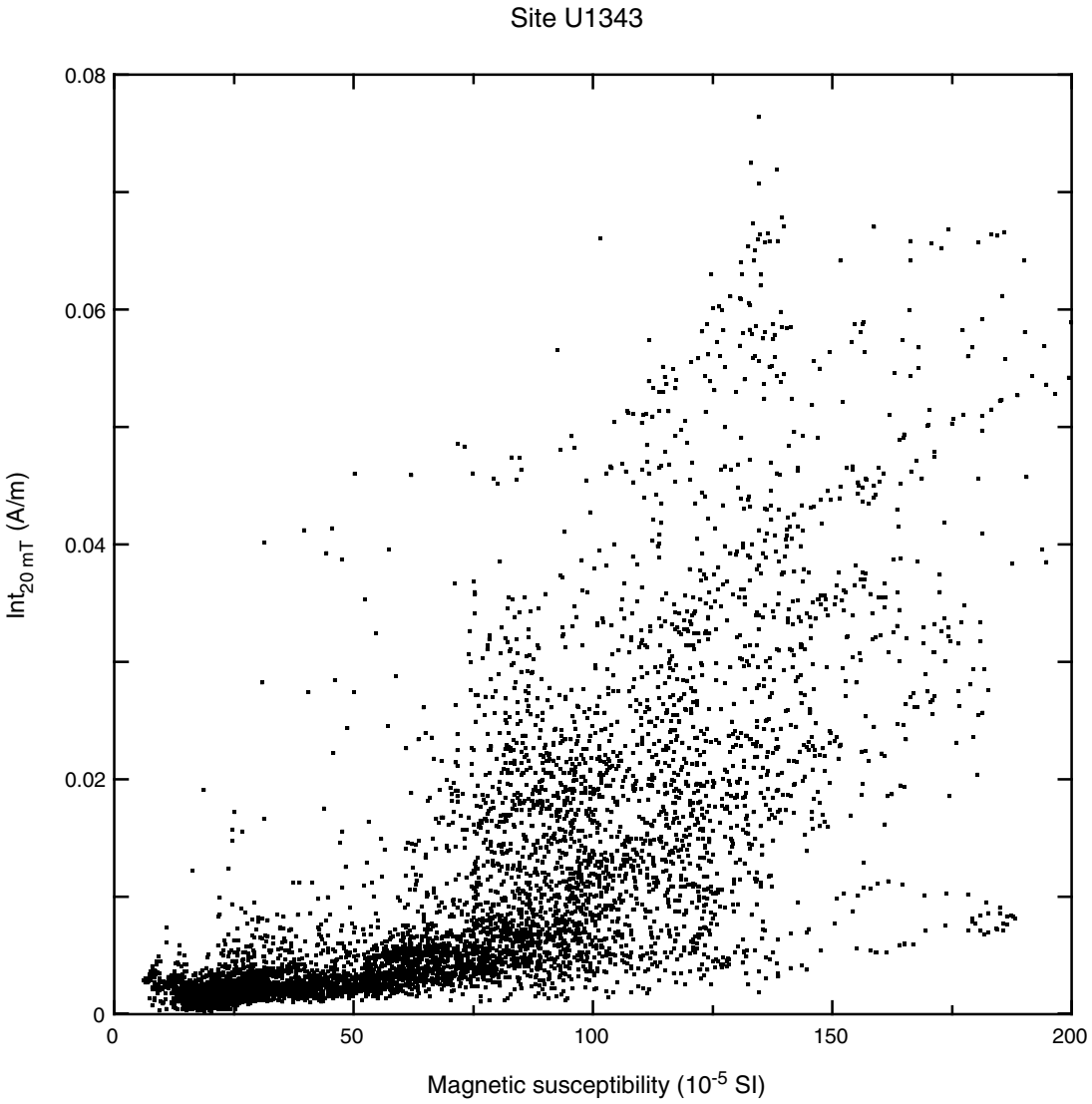

**Figure F21.** Dissolved chemical concentrations, Holes U1343A, U1343B, and U1343E. **A.** Calcium. **B.** Magnesium. **C.** Chloride. **D.** Sodium. **E.** Potassium. **F.** Strontium. **G.** Manganese. **H.** Iron. **I.** Lithium. **J.** Boron. **K.** Silica. **L.** Barium.

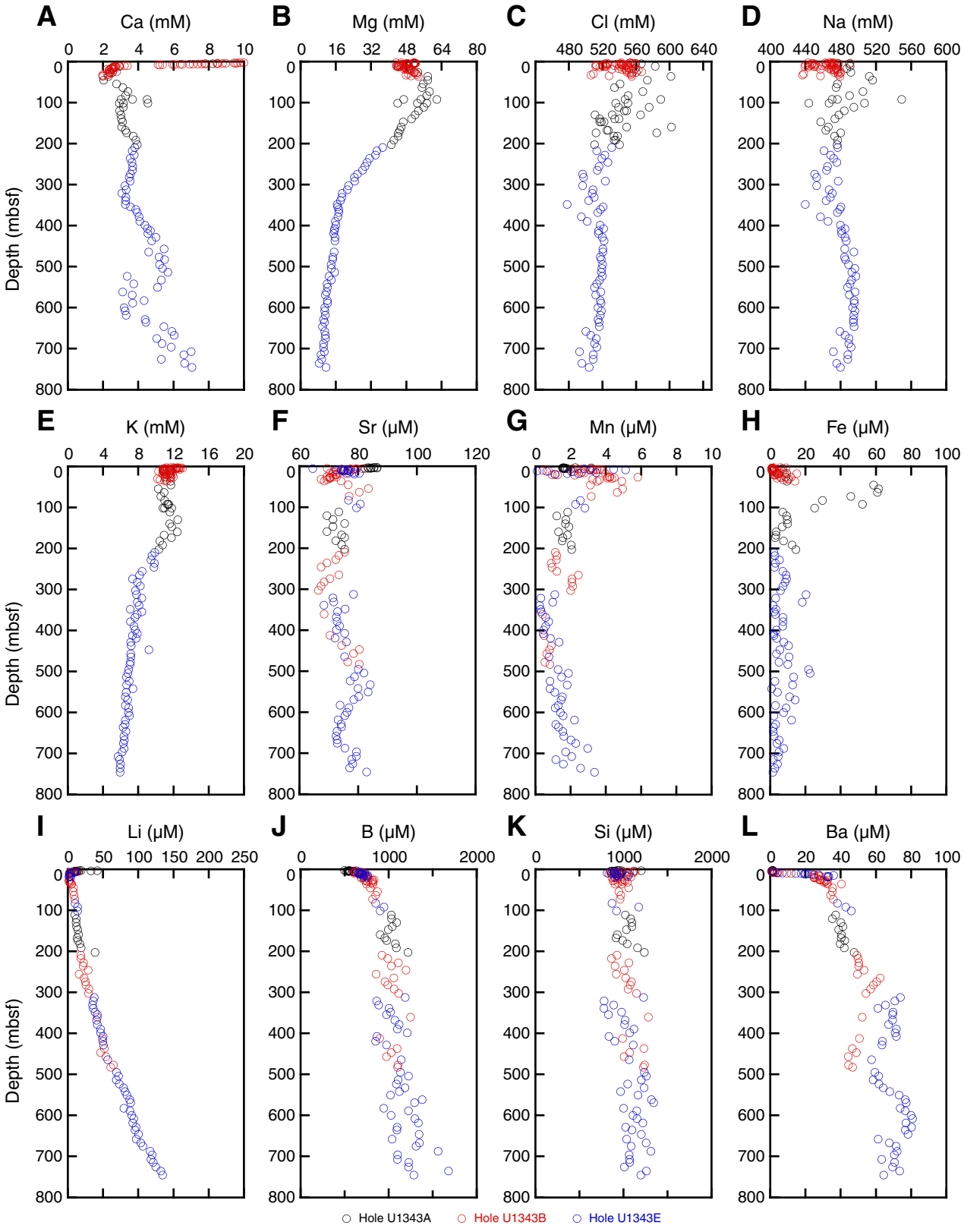

**Figure F22.** Dissolved chemical concentrations, Holes U1343A, U1343B, and U1343E. **A.** Dissolved inorganic carbon (DIC). **B.** pH. **C.** Alkalinity. **D.** Sulfate. **E.** Methane. **F.** Total hydrogen sulfide ($\Sigma H_2S = H_2S + HS^-$). **G.** Phosphate. **H.** Ammonium. **I.** Salinity. Note that $SO_4^{2-}$, $CH_4$, and $\Sigma H_2S$ depth profiles are reported only for the interval 0–15 mbsf.

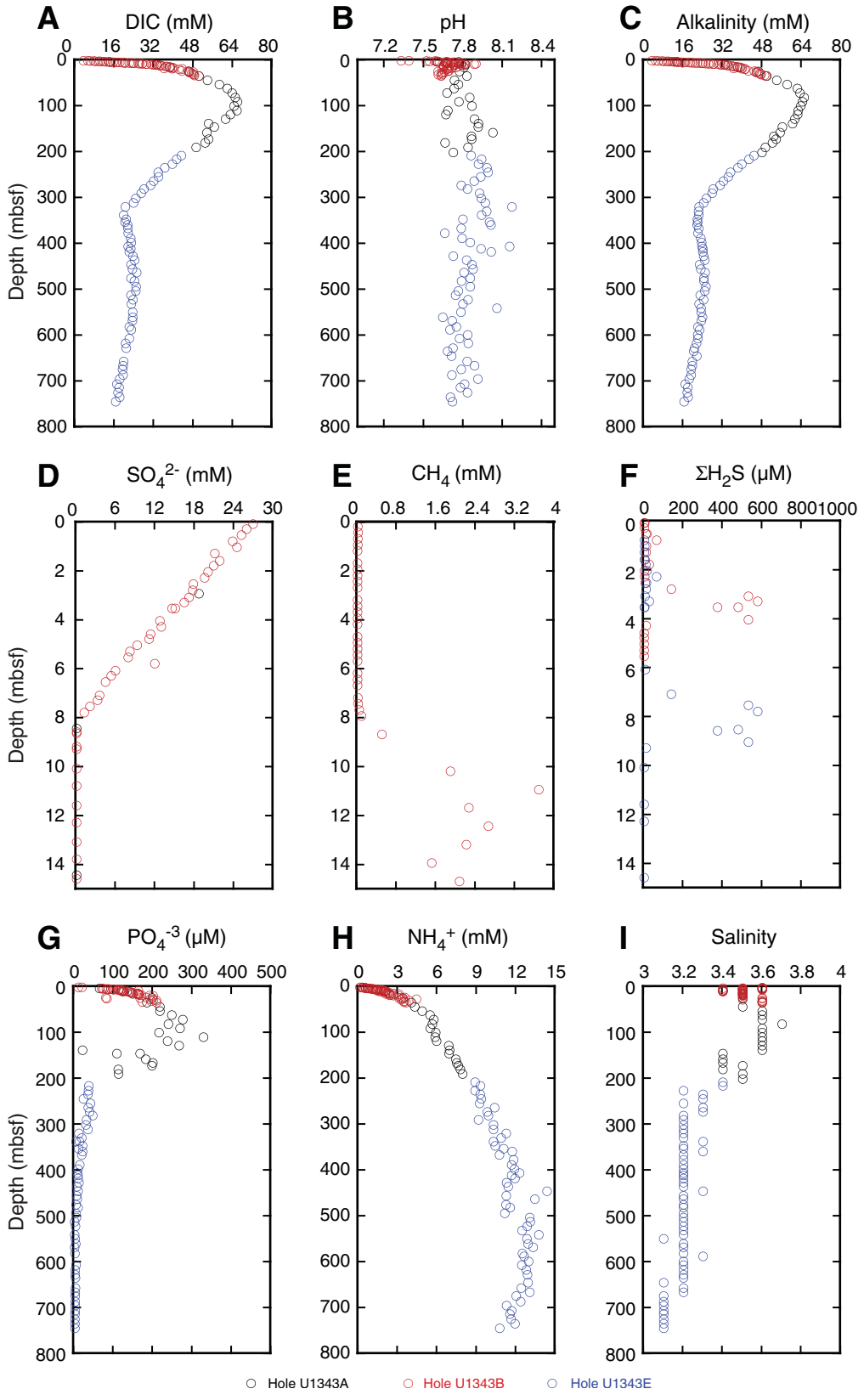

**Figure F23.** Solid-phase chemical concentrations, Holes U1343A and U1343E. **A.** Calcium carbonate ($CaCO_3$). **B.** Total organic carbon (TOC). **C.** Total nitrogen (TN). **D.** Total sulfur (TS).

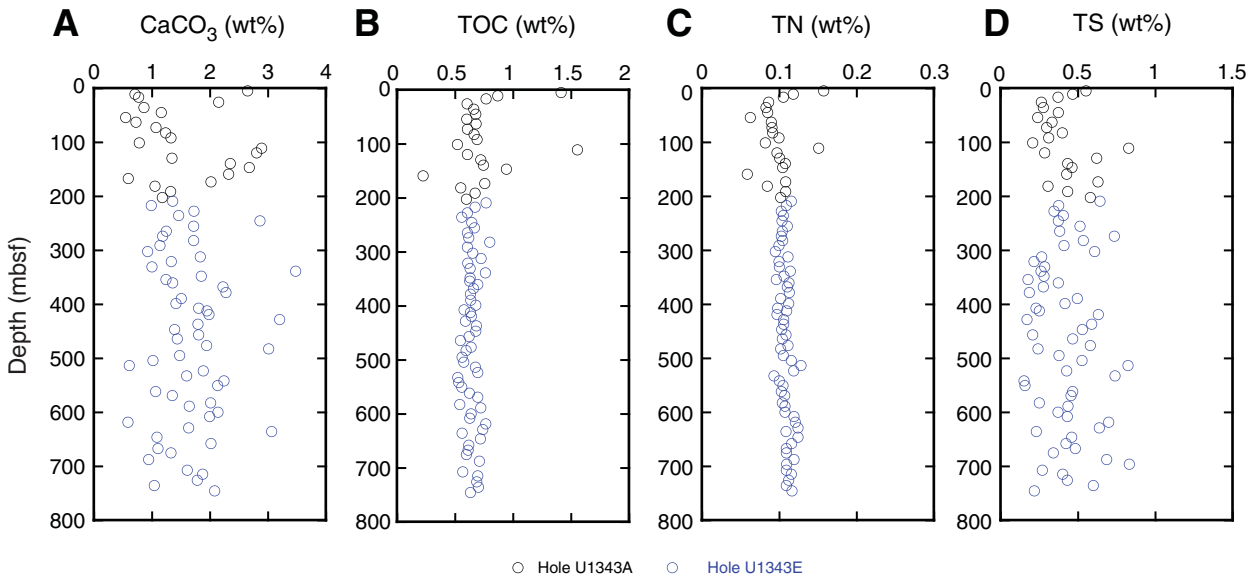

**Figure F24.** Wet bulk density, Hole U1343E. **A.** Downsection distribution of WRMSL GRA wet bulk density. (**Continued on next page.**)

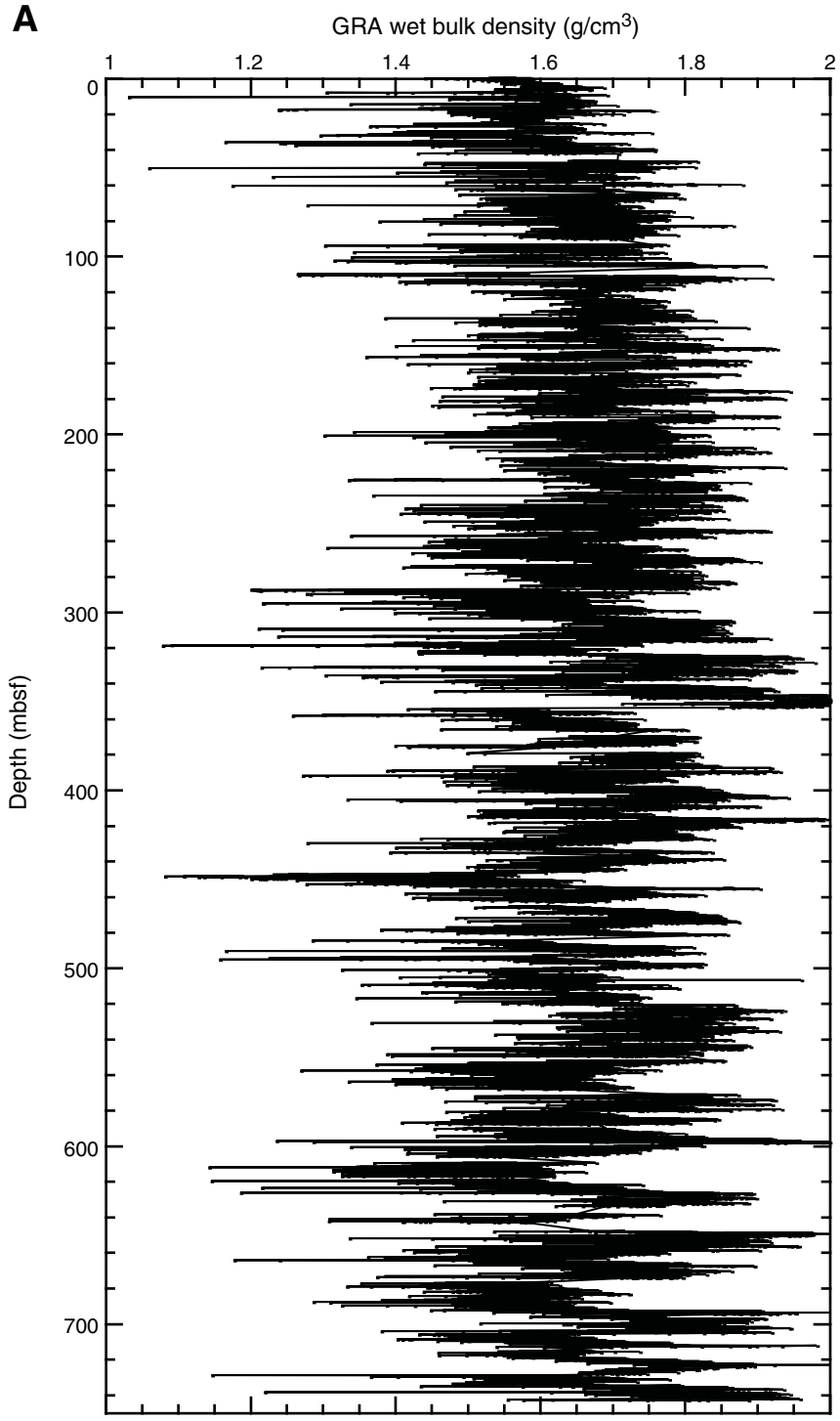

**Figure F24 (continued). B.** Downhole distribution of wet bulk density measured by the triple combination logging tool (see **"Downhole measurements"**).

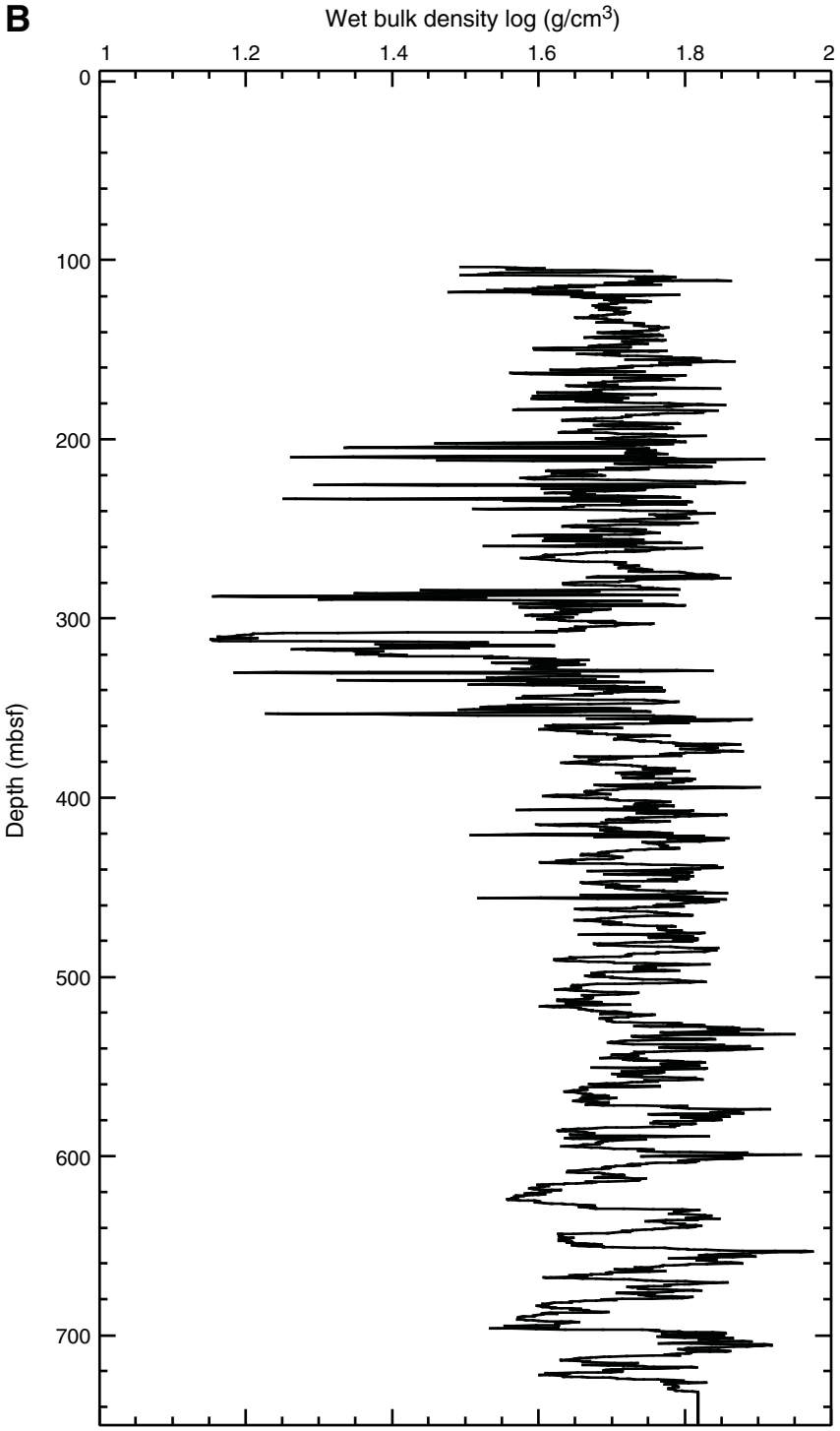

**Figure F25.** Downhole profile of *P*-wave velocity recorded by the Formation MicroScanner (FMS)-sonic logging tool, Hole U1343E (see **"Downhole measurements"**).

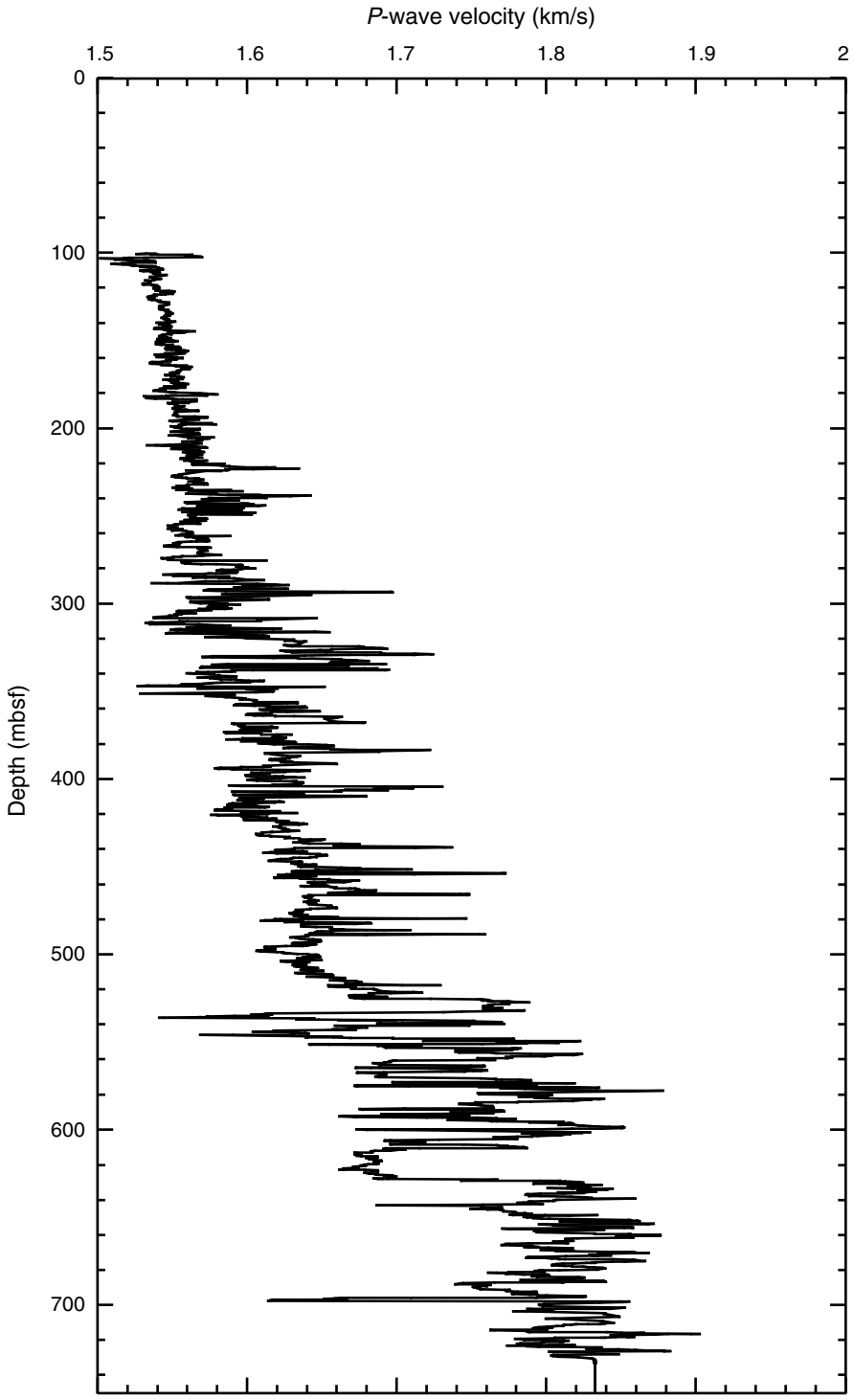

**Figure F26.** Downhole distribution of WRMSL magnetic susceptibility, Hole U1343E.

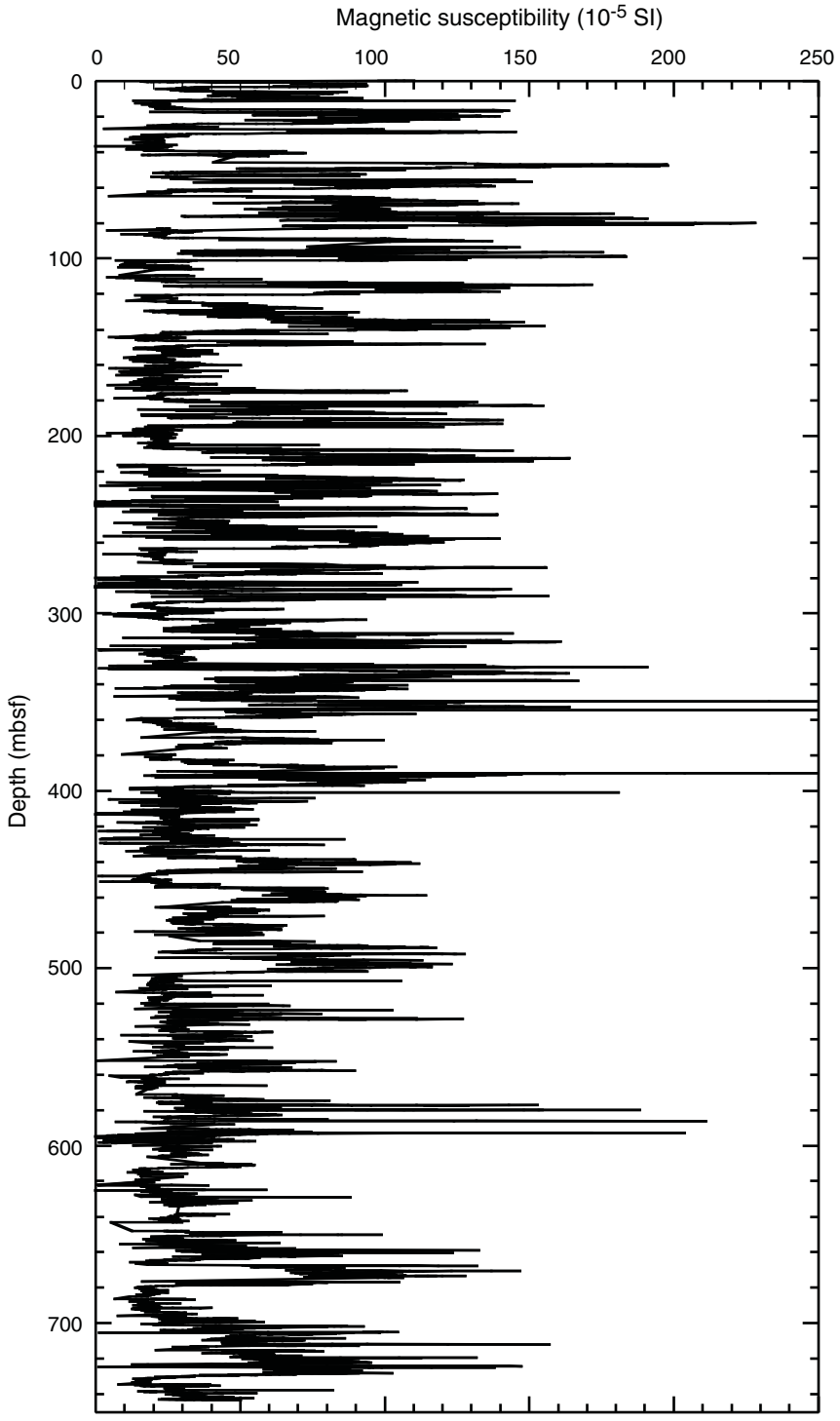

**Figure F27.** Downhole distribution of thermal conductivity measured on Sections 1 or 2 of Hole U1343E cores.

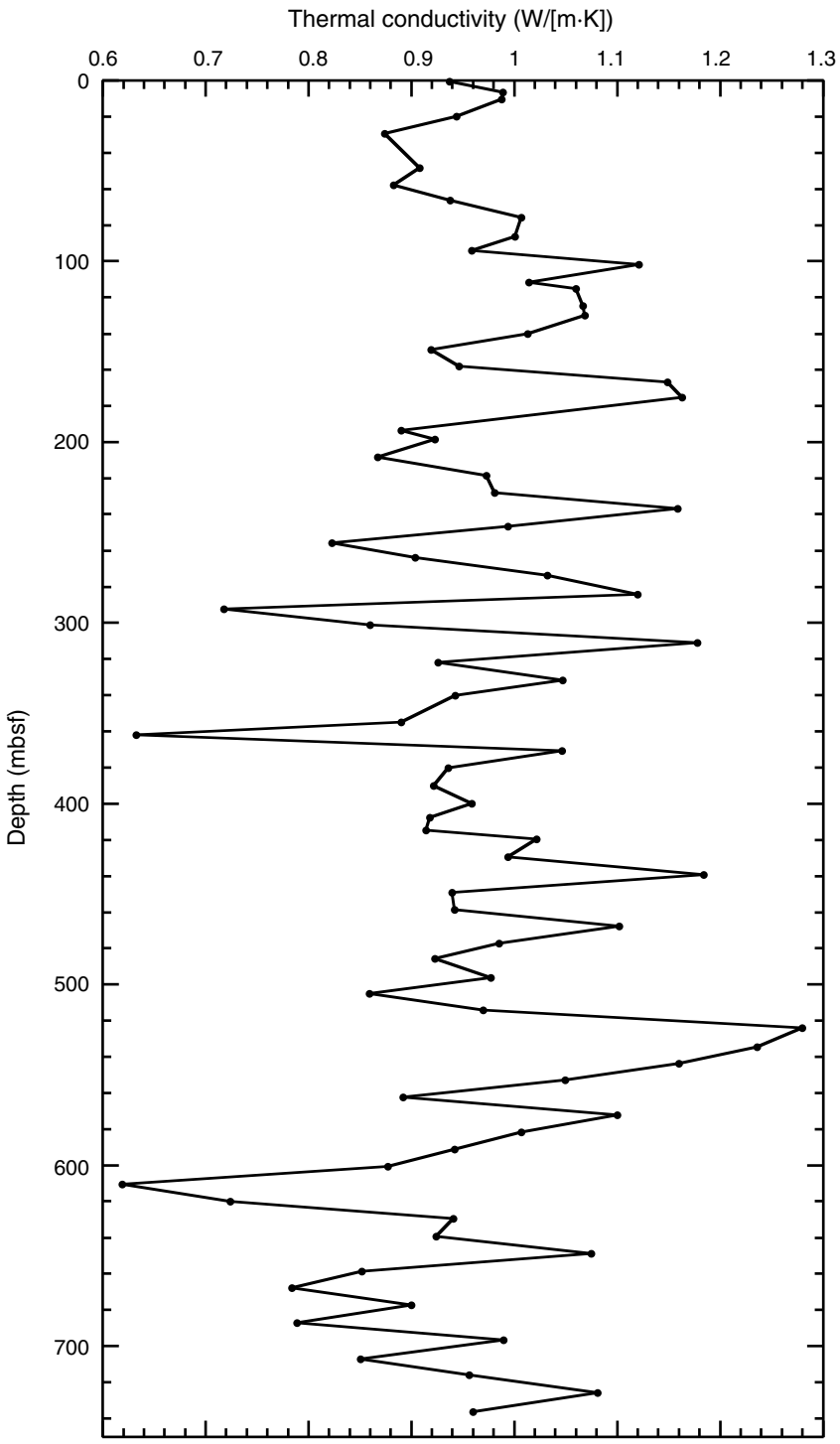

**Figure F28.** Downhole distribution of natural gamma radiation (NGR), Hole U1343E.

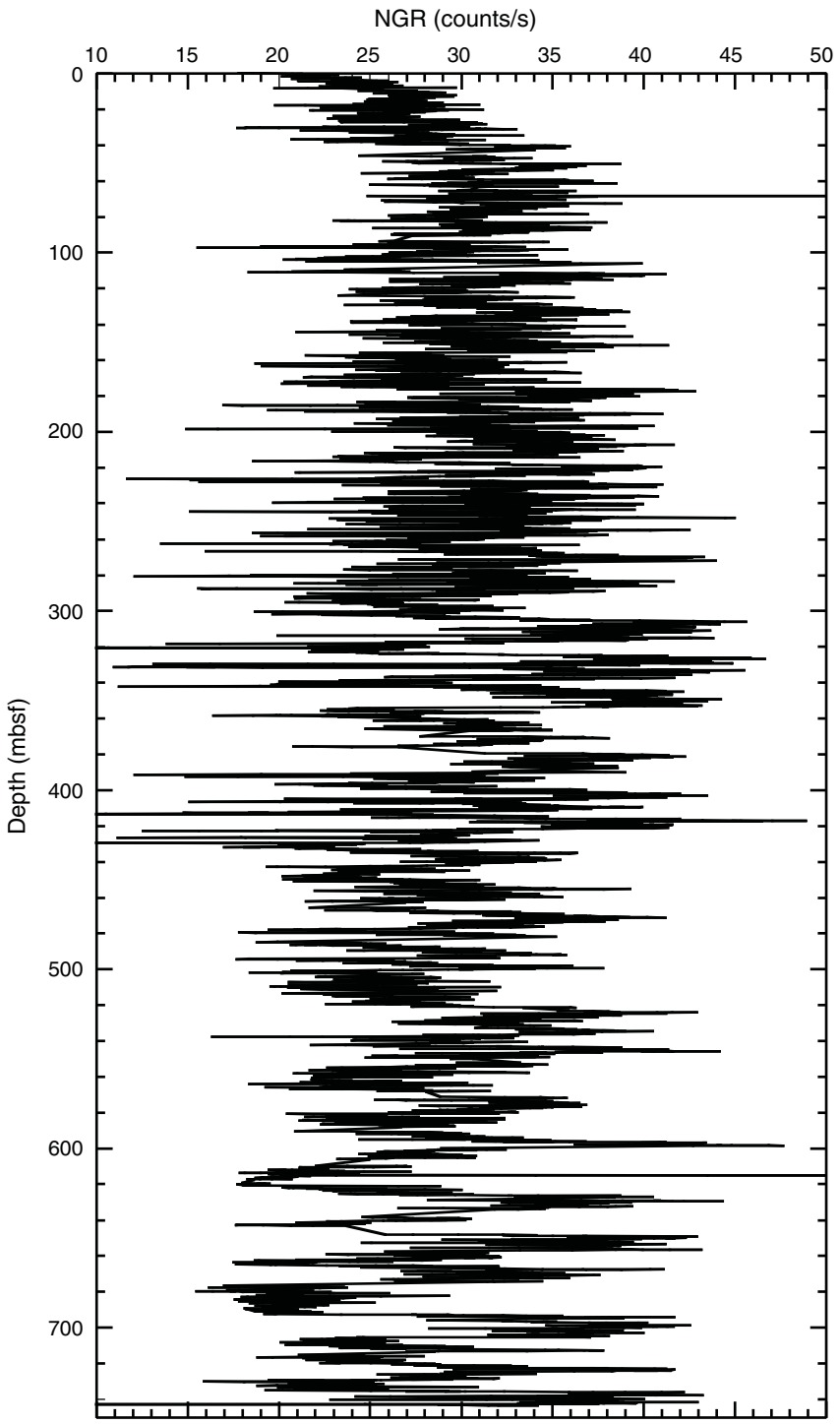

**Figure F29.** Downhole distribution of wet bulk density measured on discrete or moisture and density (MAD) sediment samples, Holes U1343A and U1343E. MAD data should be compared with in situ measurements of bulk density by the triple combination logging tool (see Fig. **F24B** and **"Downhole measurements"**).

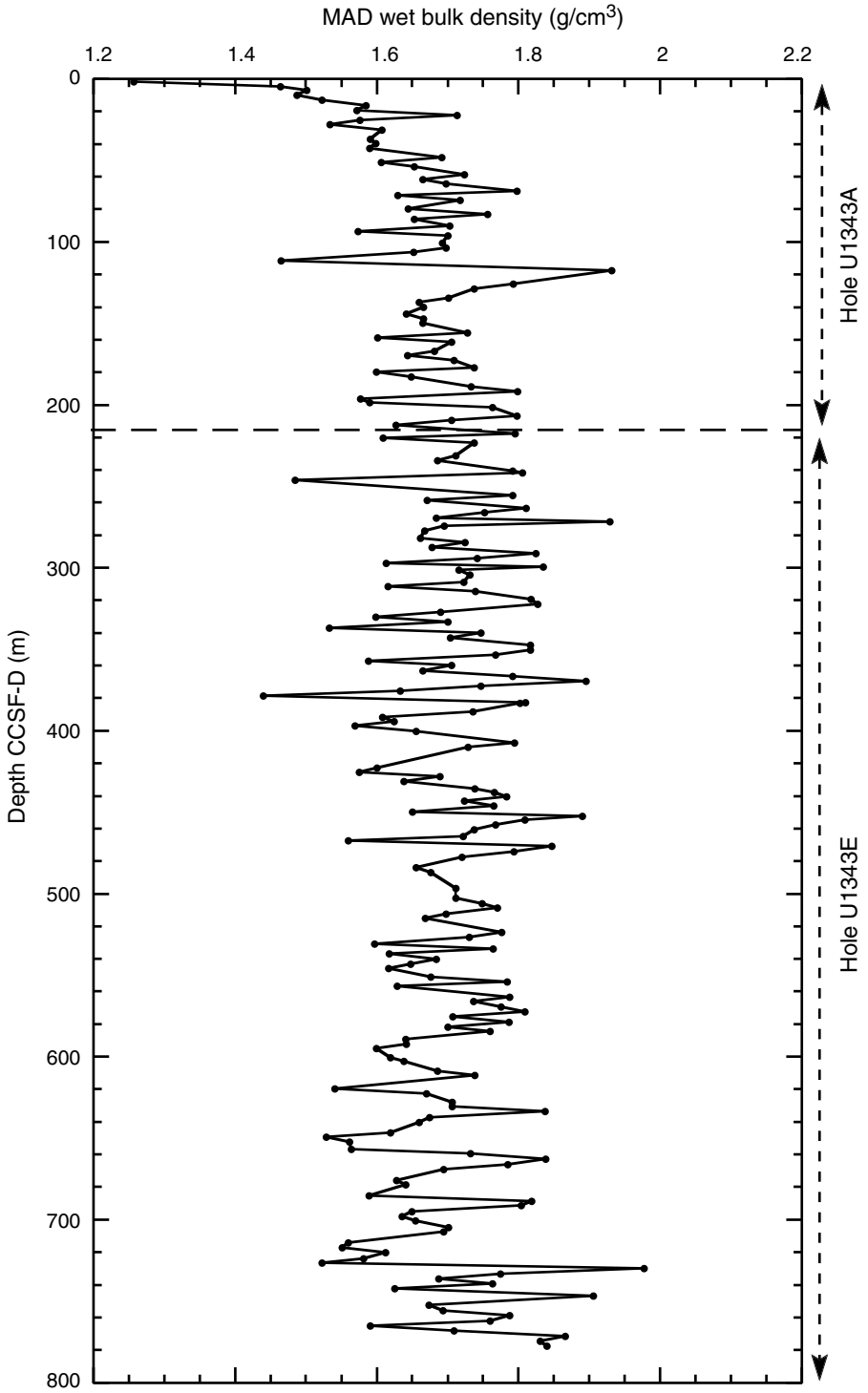

**Figure F30.** Downsection profiles of water content and porosity measured with moisture and density analyses of sediment samples, Holes U1343A and U1343E.

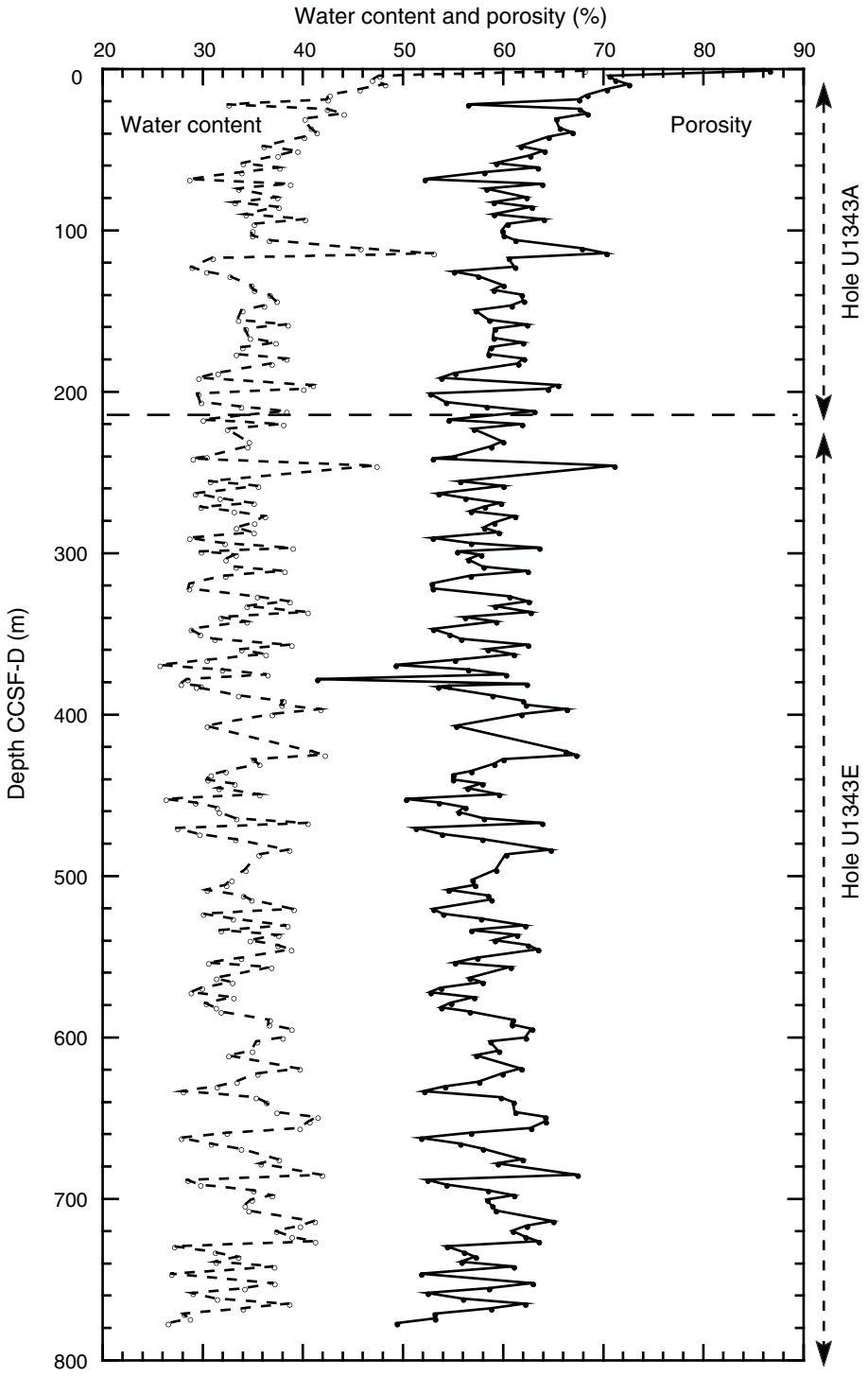

**Figure F31.** Downhole profile of dry grain density measured on discrete samples with the moisture and density system, Holes U1343A and U1343E.

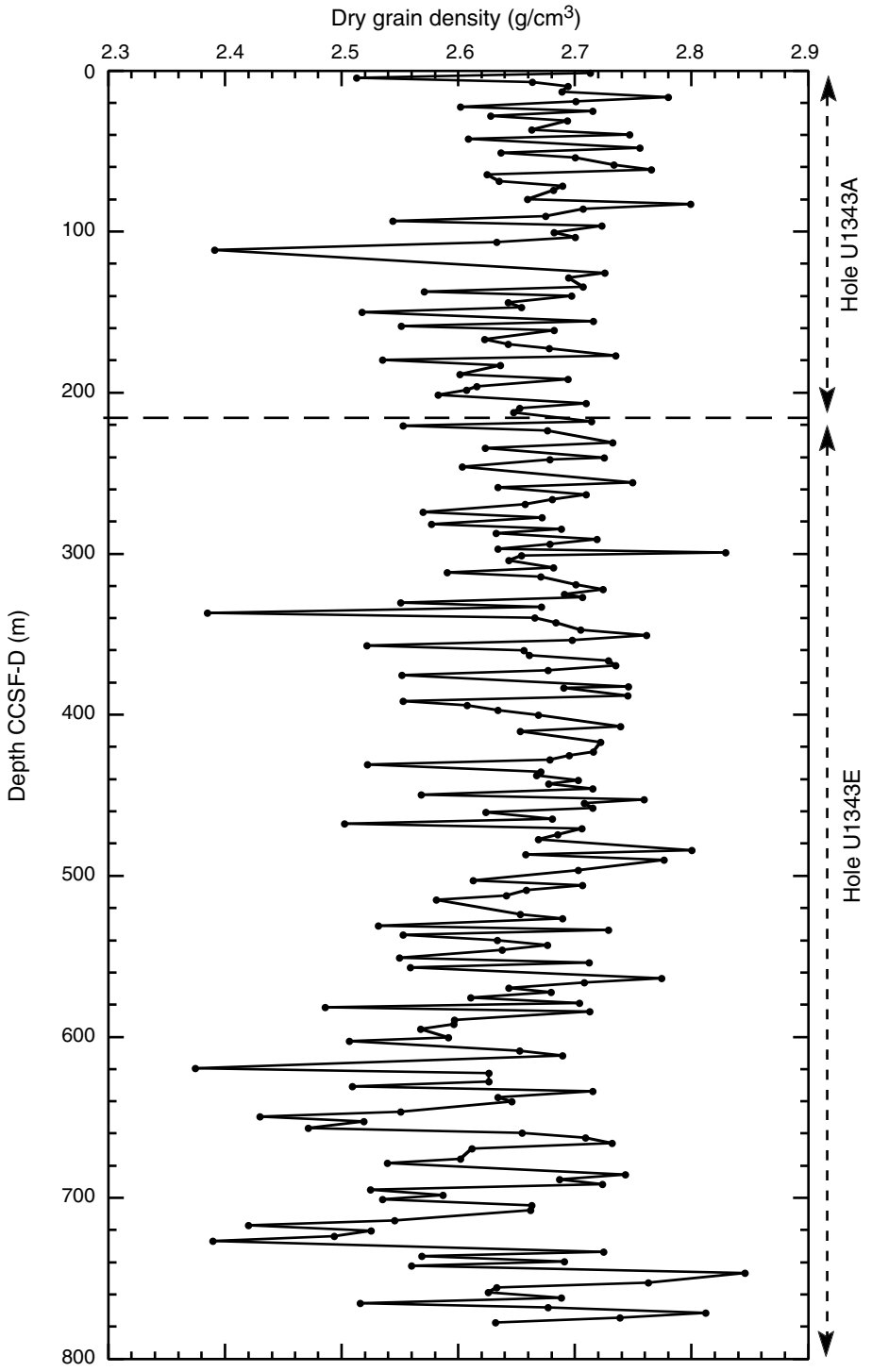

**Figure F32.** WRMSL magnetic susceptibility data vs. composite depth, Site U1343. STMSL magnetic susceptibility data are shown for Hole U1343B because cores from this hole were not run through the WRMSL. For the splice record (top panel), depth on the CCSF-D scale is equivalent to depth on the CCSF-A scale. **A.** 0–90 m CCSF-A. (**Continued on next two pages.**)

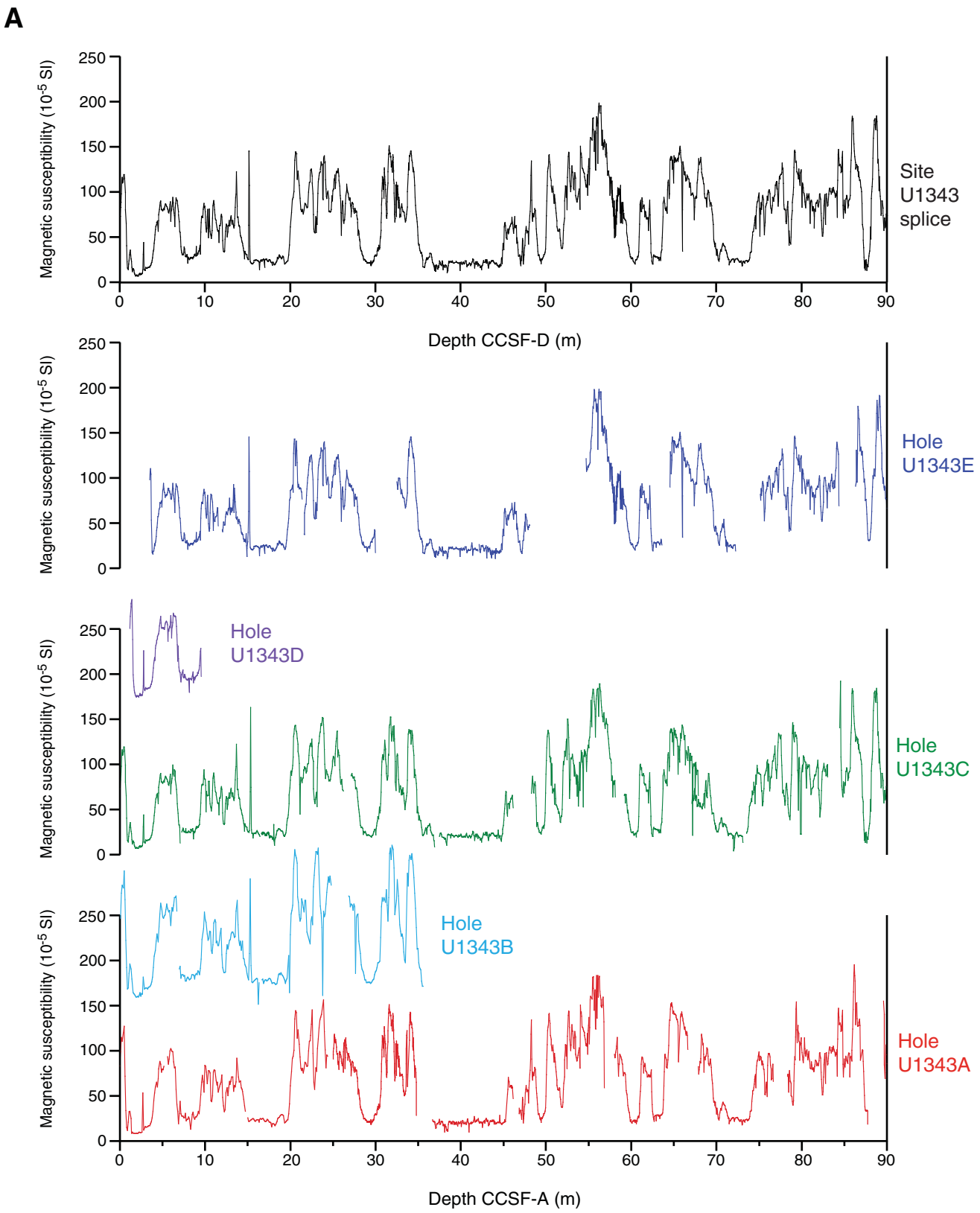

**Figure F32 (continued). B.** 90–180 m CCSF-A. (Continued on next page.)

**B**

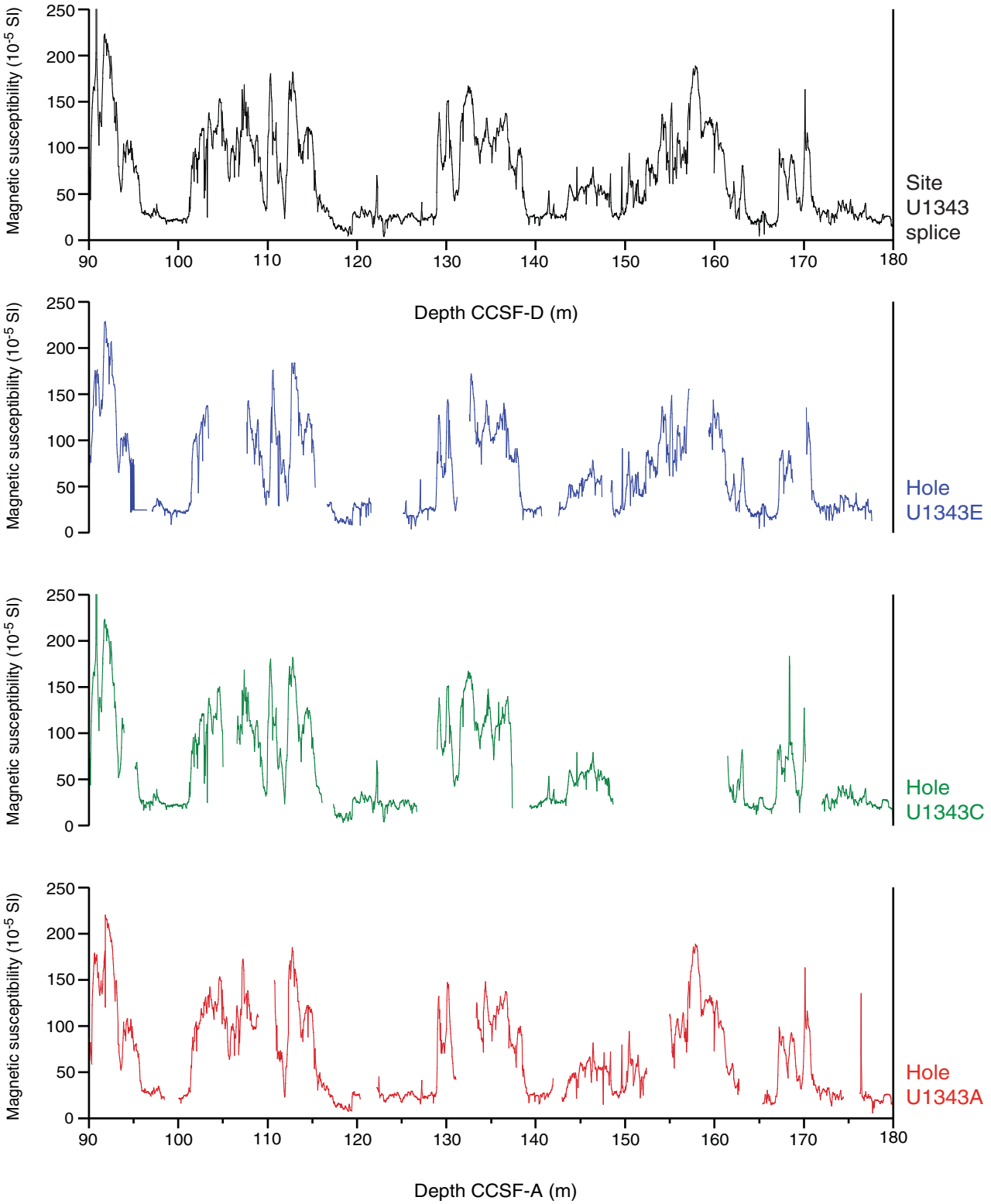

**Figure F32 (continued).** C. 180–270 m CCSF-A.

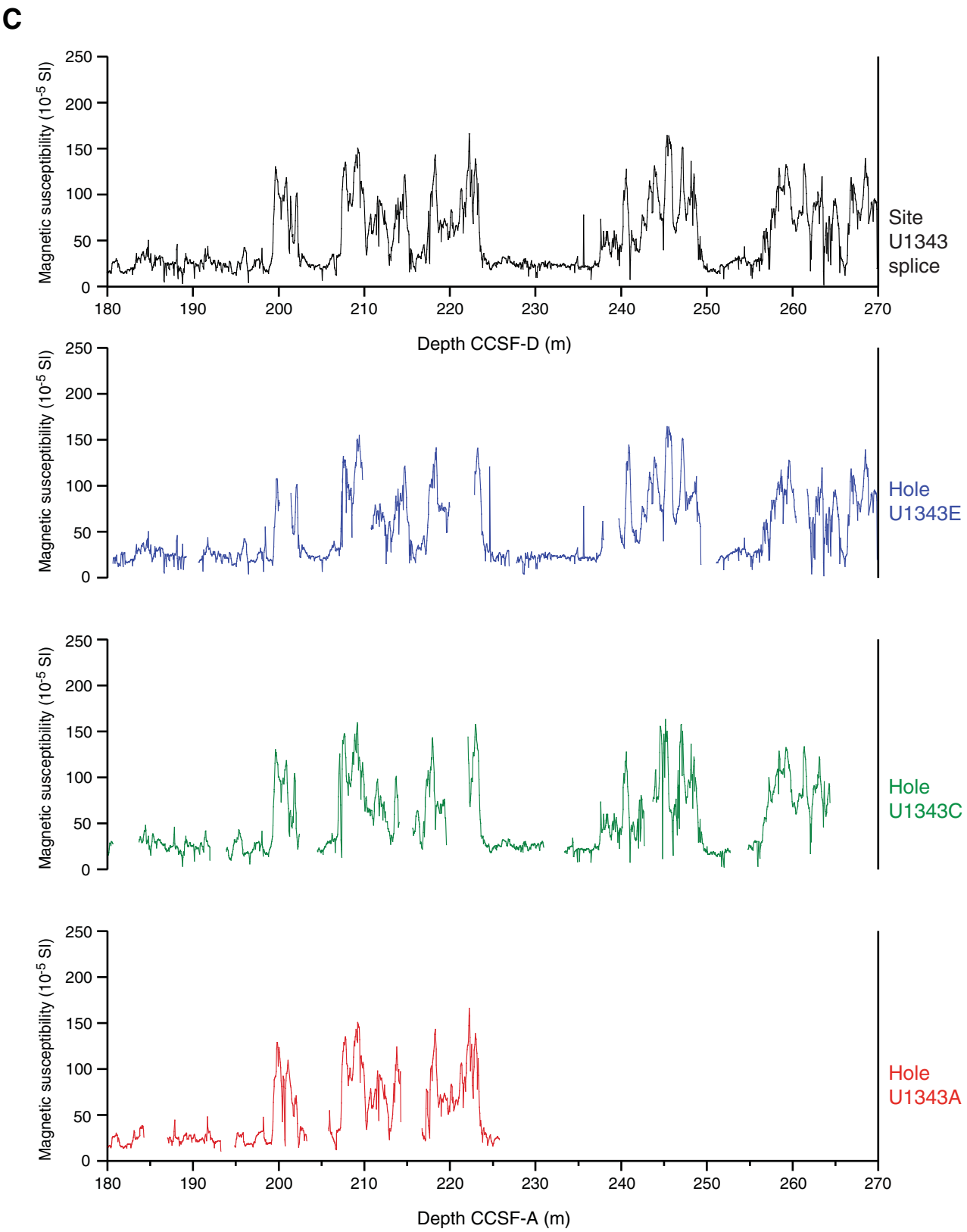

**Figure F33.** WRMSL gamma ray attenuation (GRA) bulk density vs. composite depth, Site U1343. STMSL GRA bulk density data are shown for Hole U1343B because cores from this hole were not run through the WRMSL. For the splice record (top panel), depth on the CCSF-D scale is equivalent to depth on the CCSF-A scale. **A.** 0–90 m CCSF-A. (**Continued on next two pages.**)

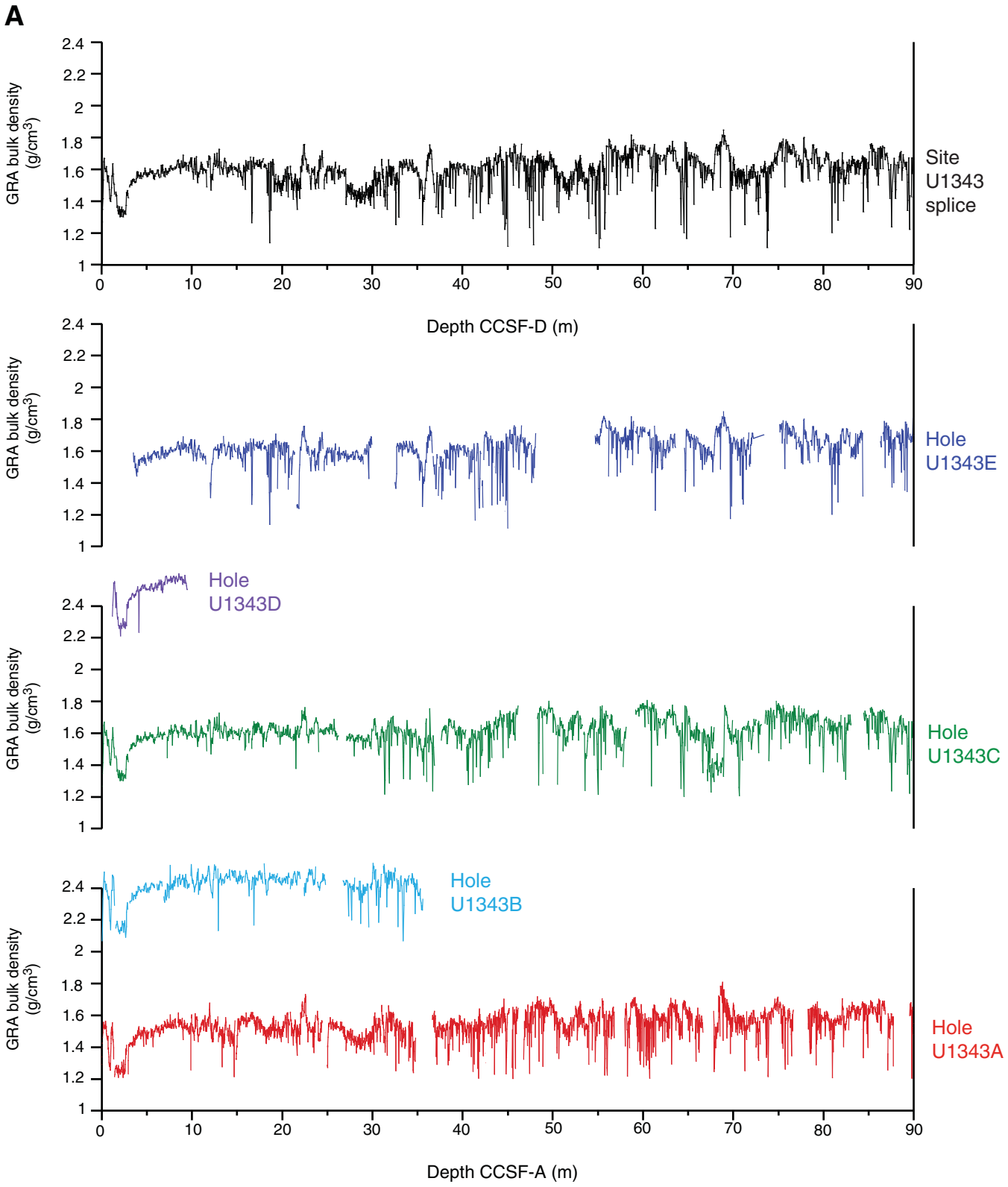

**Figure F33 (continued). B.** 90–180 m CCSF-A. (Continued on next page.)

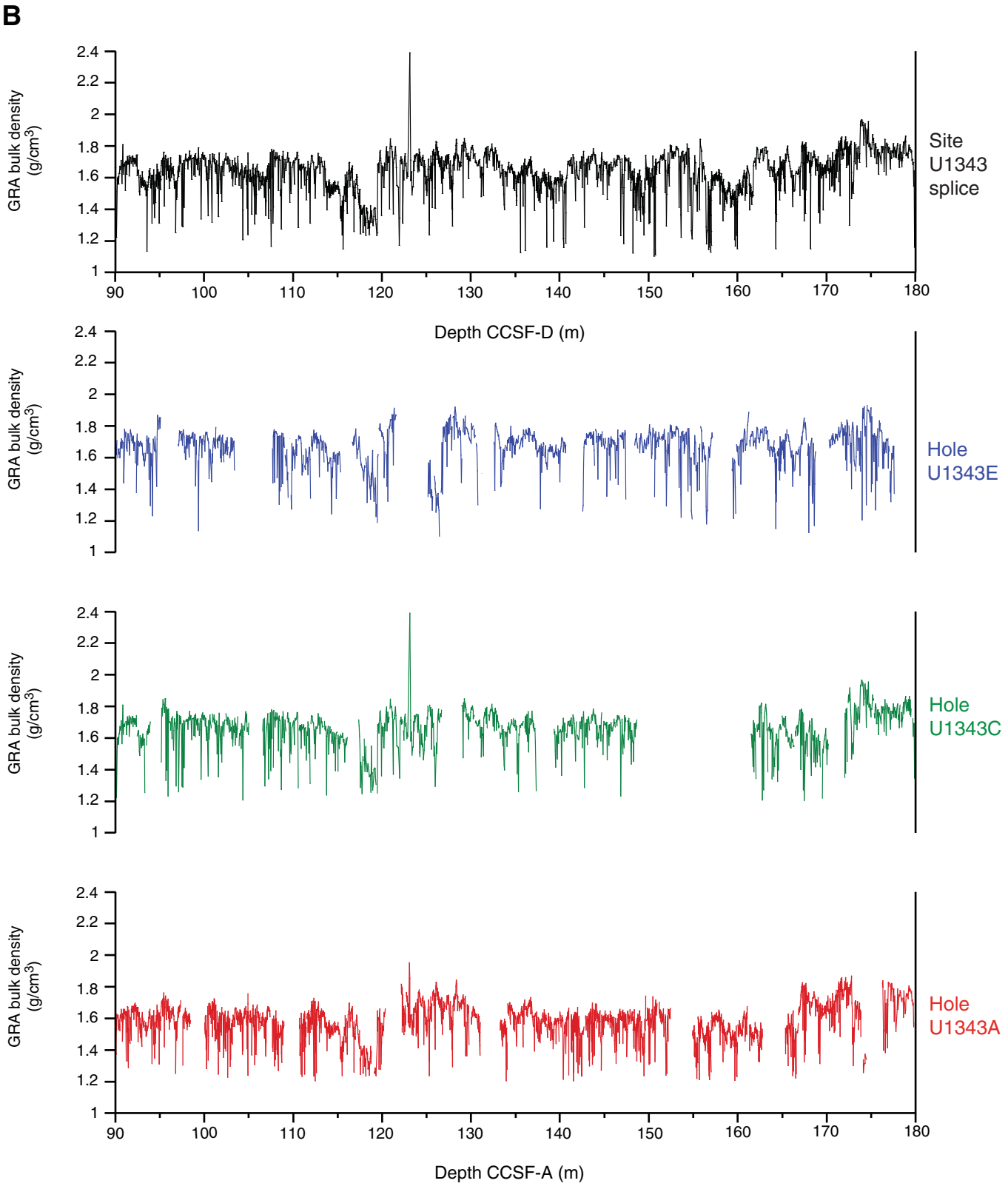

**Figure F33 (continued).** C. 180–270 m CCSF-A.

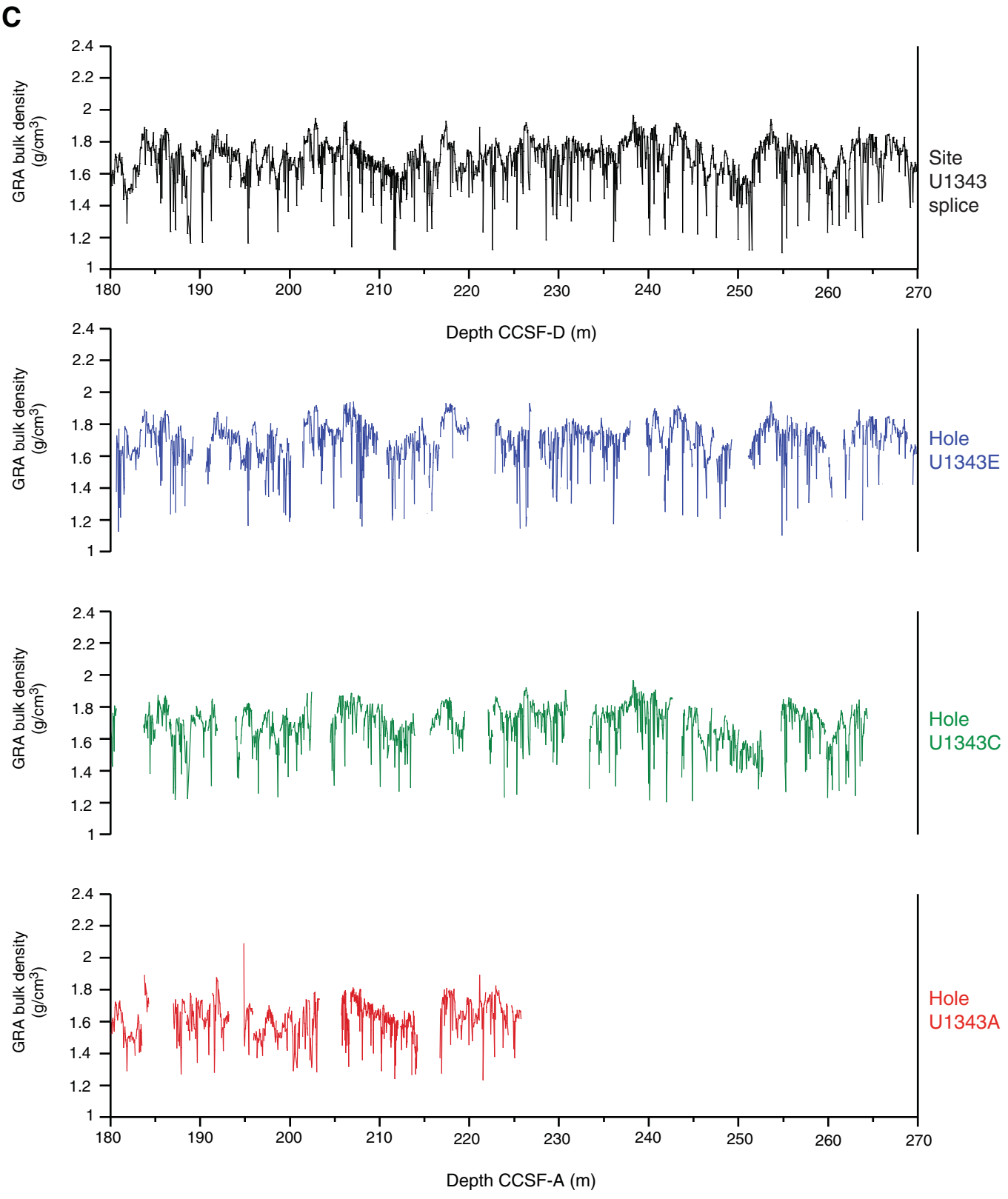

**Figure F34.** Natural gamma radiation (NGR) collected with the Natural Gamma Radiation Logger vs. composite depth, Site U1343. No NGR data are available for Hole U1343B. For the splice record (top panel), depth on the CCSF-D scale is equivalent to depth on the CCSF-A scale. **A.** 0–90 m CCSF-A. (**Continued on next two pages.**)

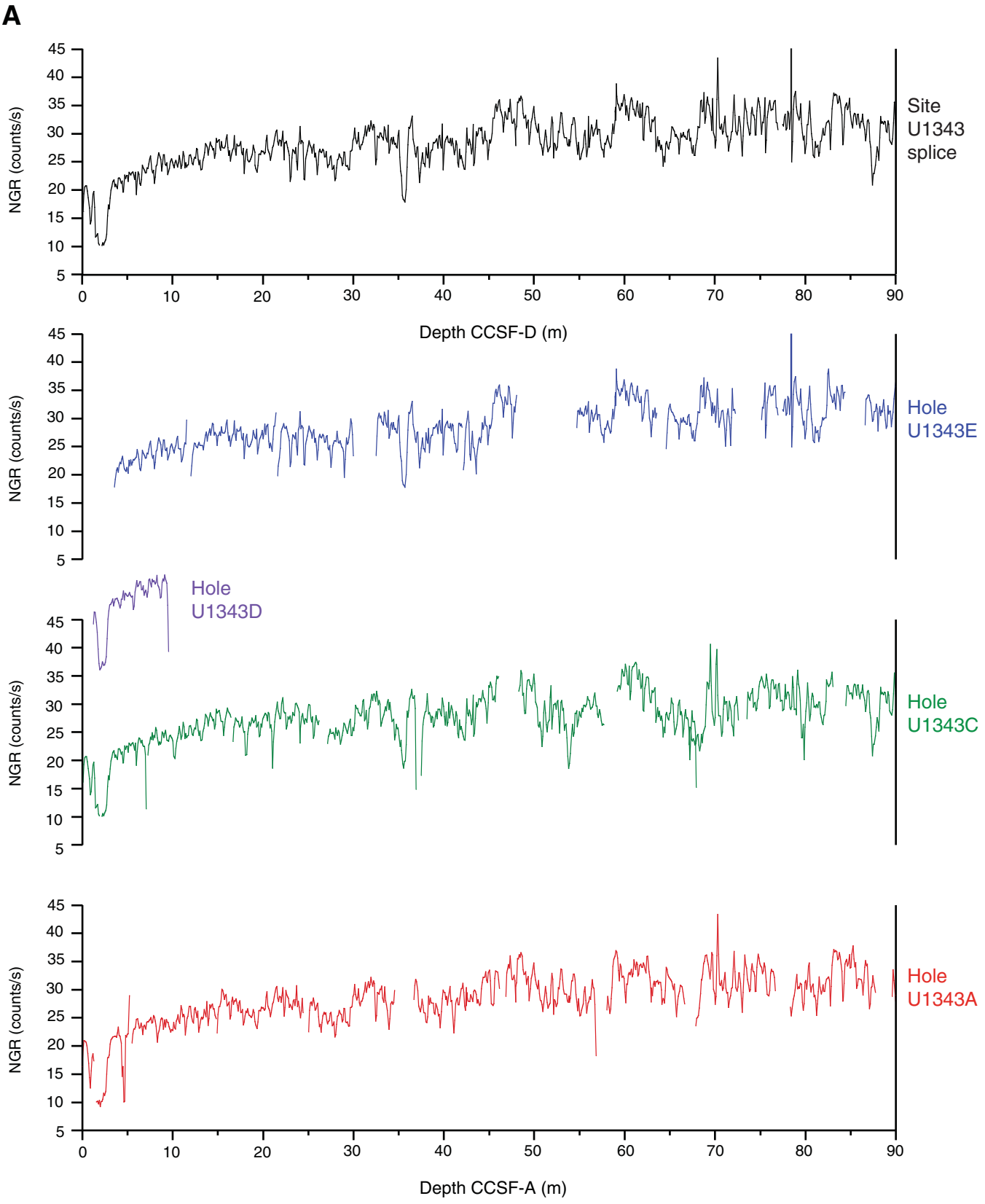

**Figure F34 (continued). B.** 90–180 m CCSF-A. (Continued on next page.)

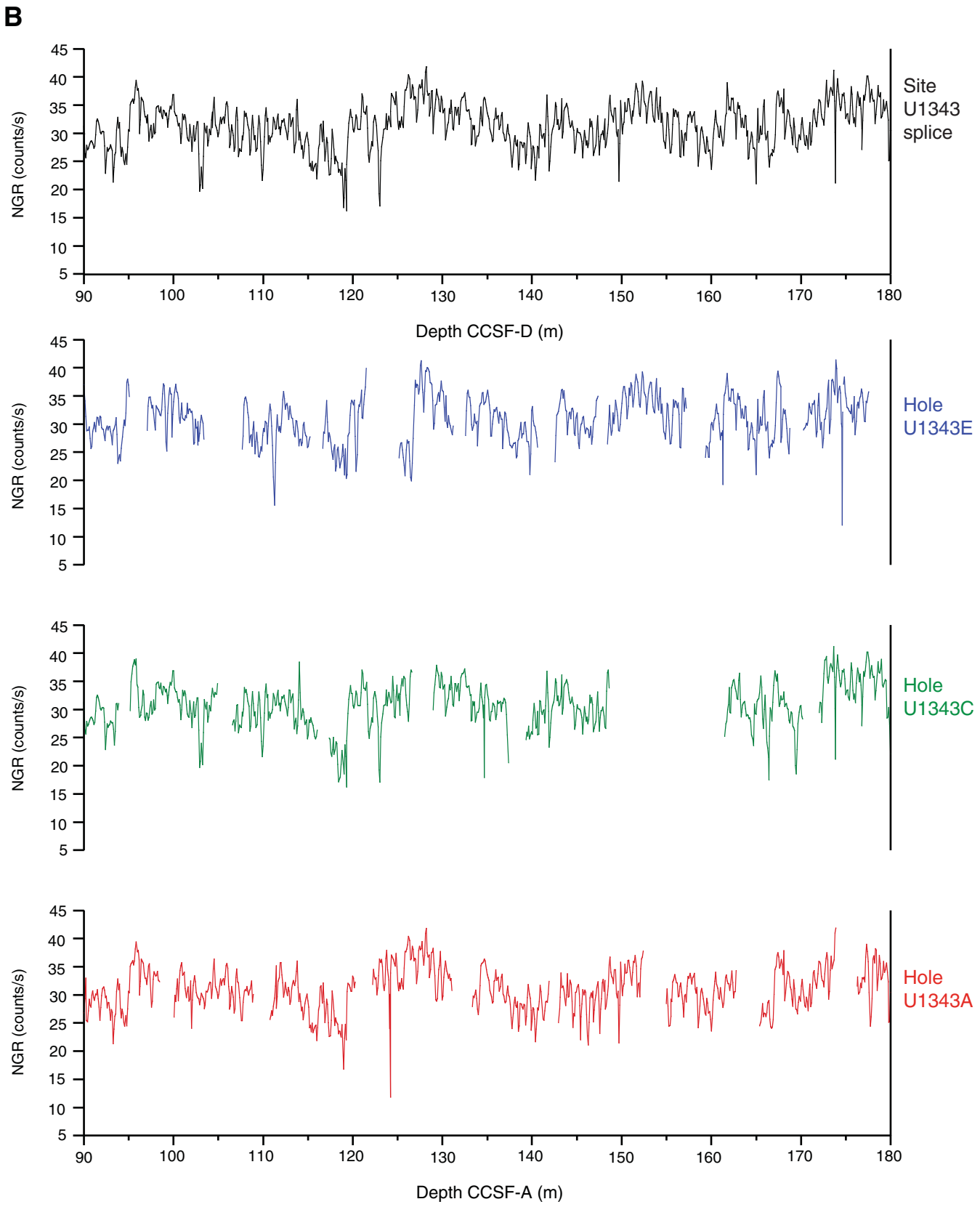

**Figure F34 (continued).** C. 180–270 m CCSF-A.

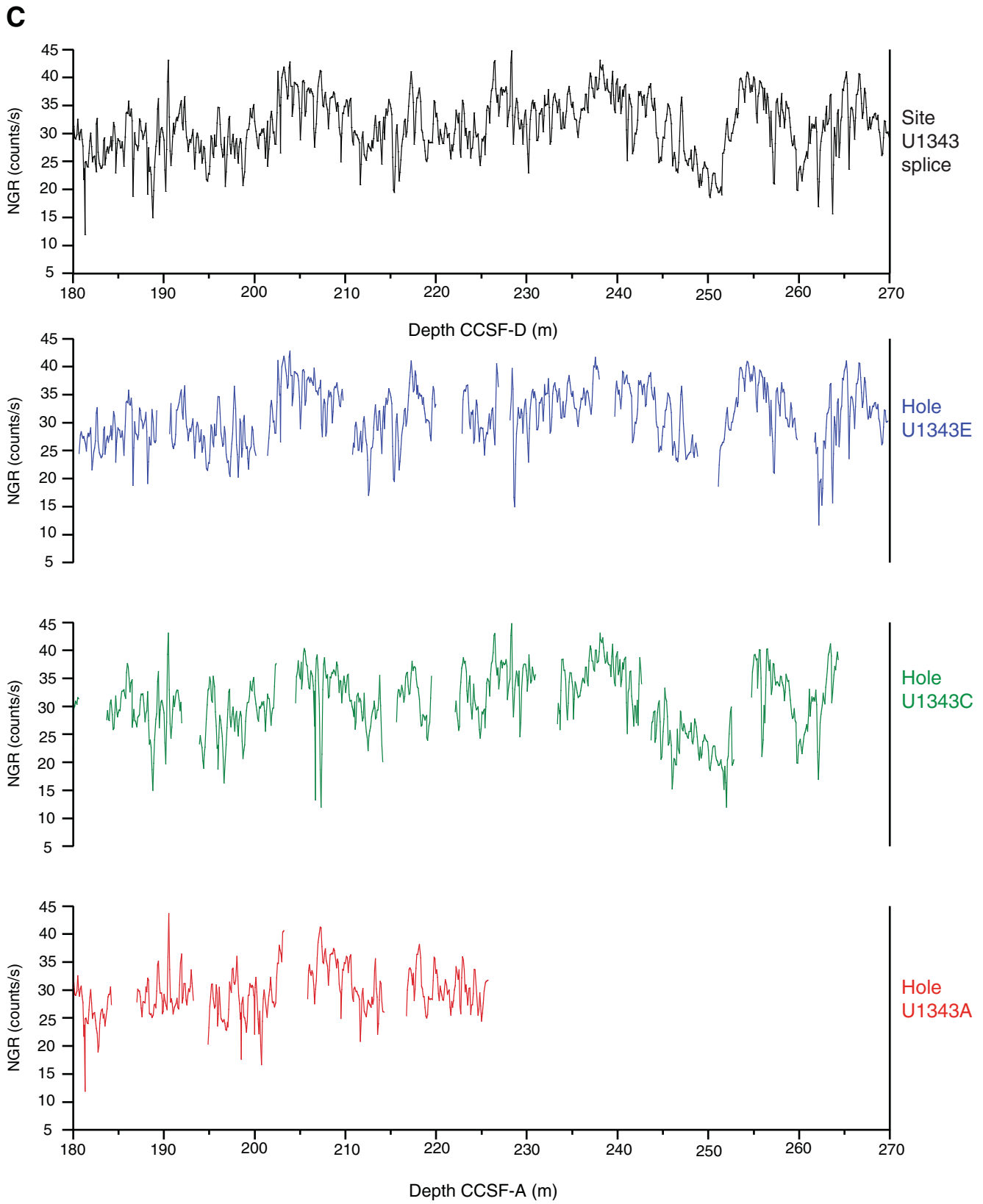

**Figure F35.** Color reflectance parameter b* collected with the SHMSL vs. composite depth, Site U1343. No color reflectance data are available for Hole U1343B. For the splice record (top panel), depth on the CCSF-D scale is equivalent to depth on the CCSF-A scale. **A.** 0–90 m CCSF-A. (**Continued on next two pages.**)

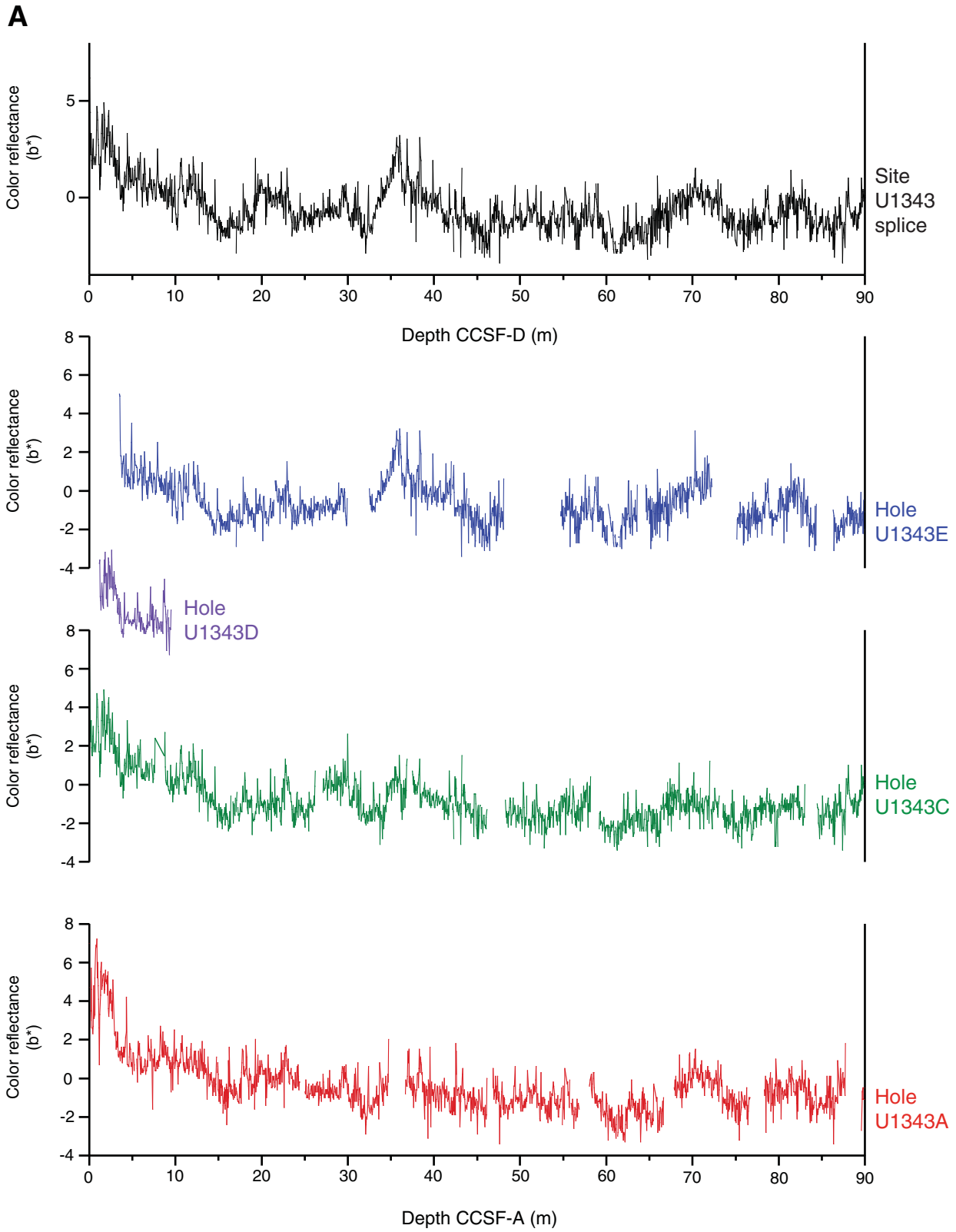

**Figure F35 (continued). B.** 90–180 m CCSF-A. (Continued on next page.)

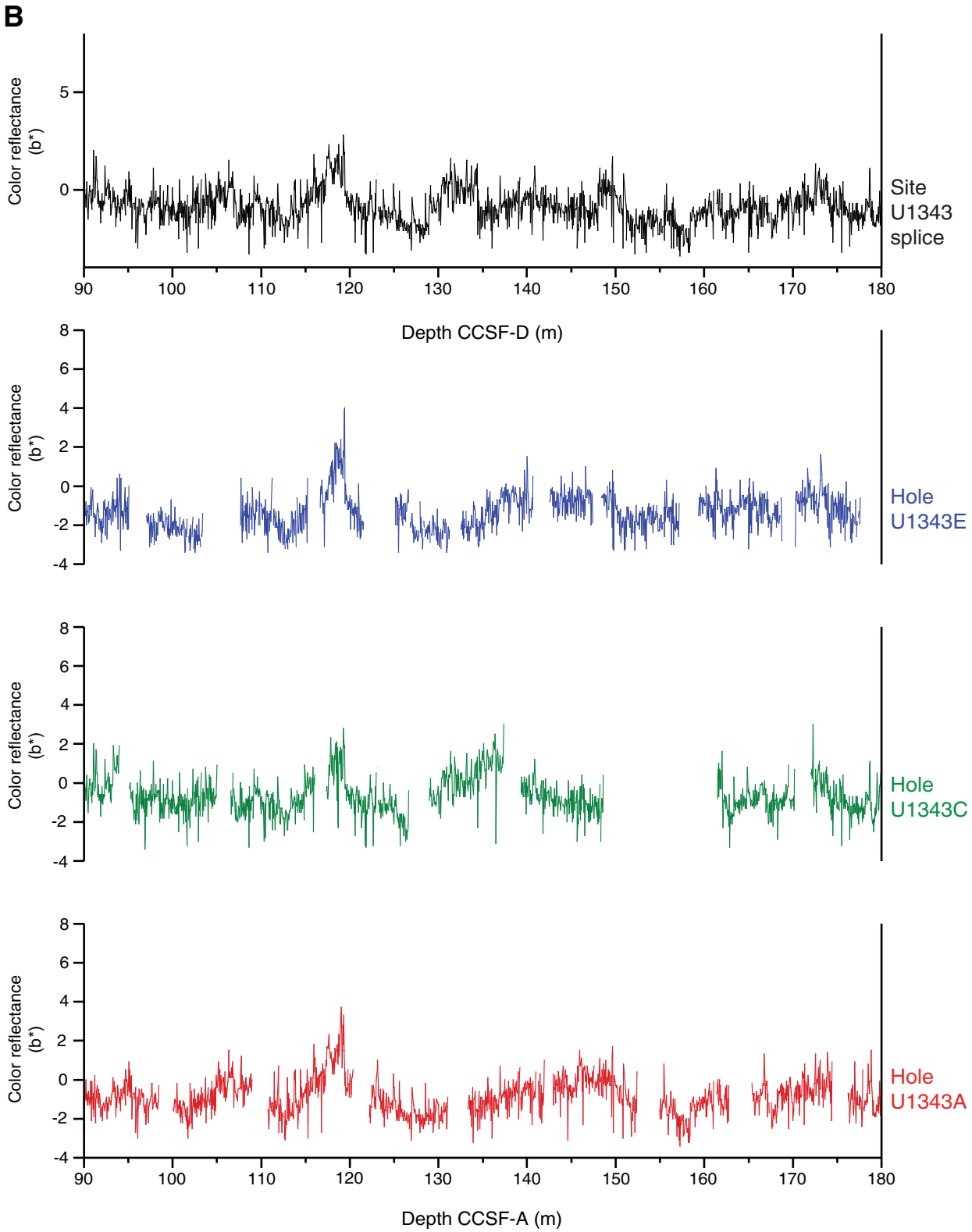

**Figure F35 (continued).** C. 180–270 m CCSF-A.

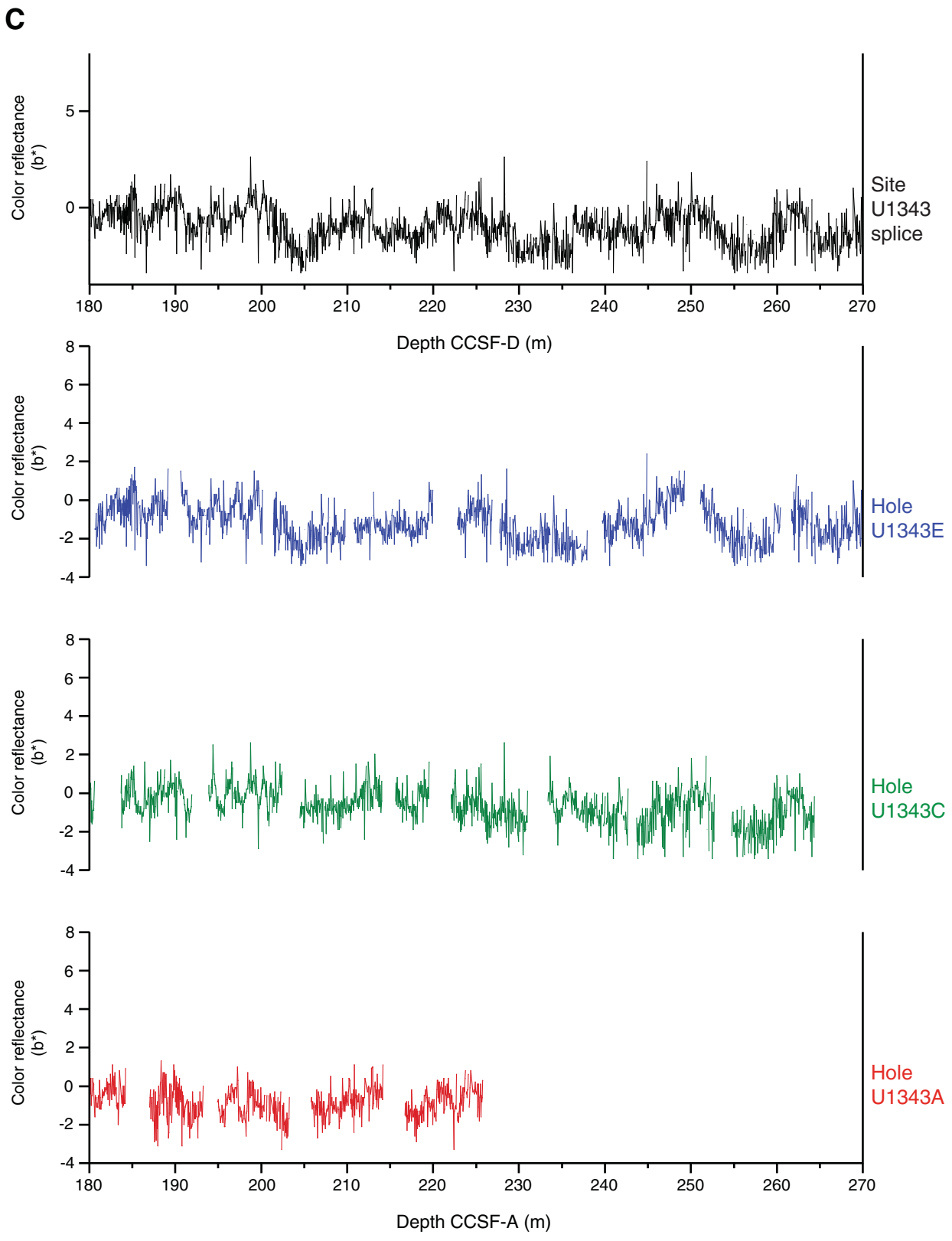

**Figure F36.** Spliced composite records of WRMSL magnetic susceptibility, gamma ray attenuation (GRA) bulk density, natural gamma radiation (NGR), and color reflectance parameter b* vs. splice composite depth, Site U1343. GRA bulk density, NGR, and color reflectance data are smoothed.

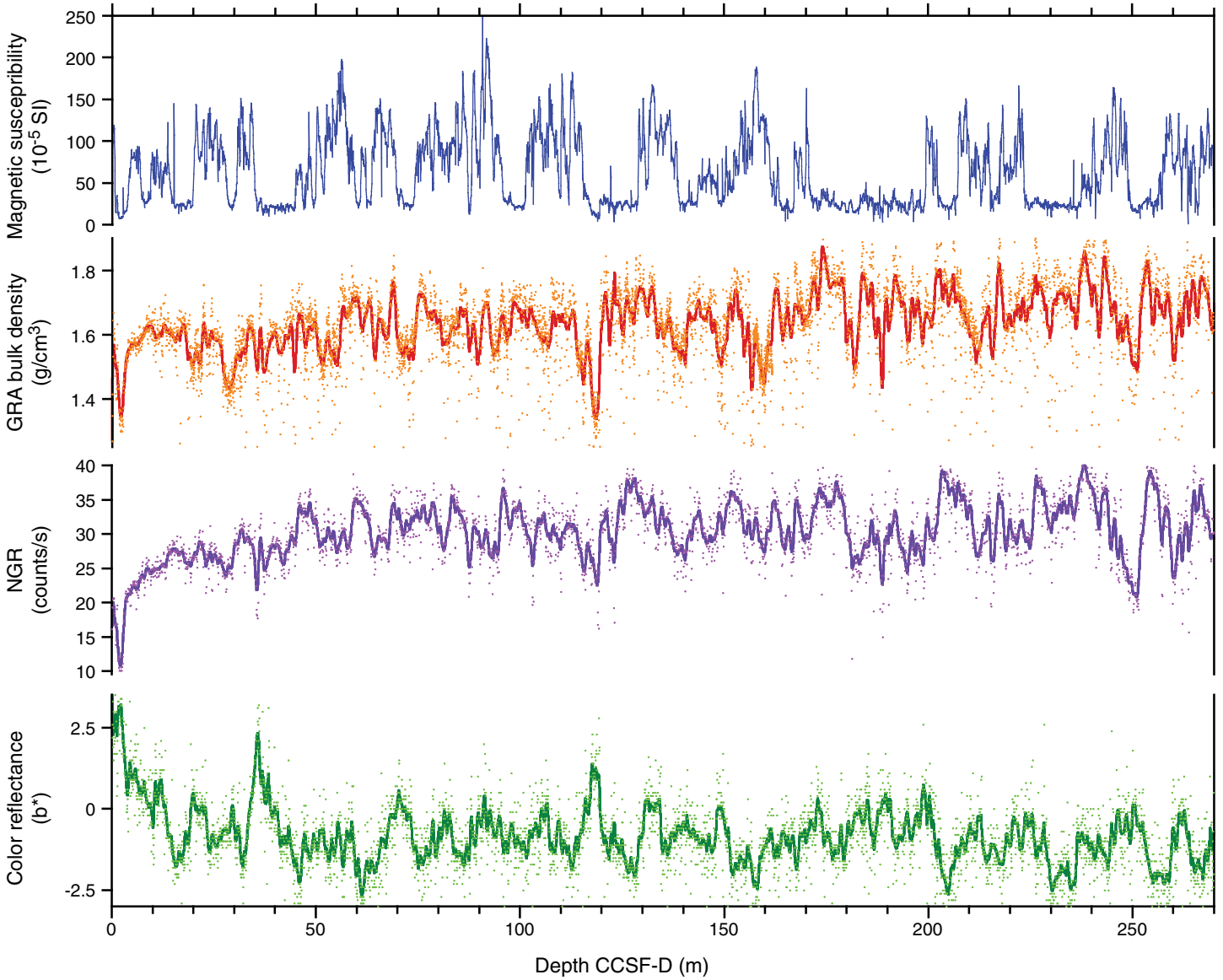

**Figure F37. A.** Mbsf vs. composite (CCSF-A) depth in the splice, Site U1343. **B.** Growth of cumulative depth offset (m) vs. mbsf in the splice. The affine growth factor is 1.03 for the four uppermost cores in each hole (0–36.4 mbsf) and 1.15 for the remainder of the spliced interval.

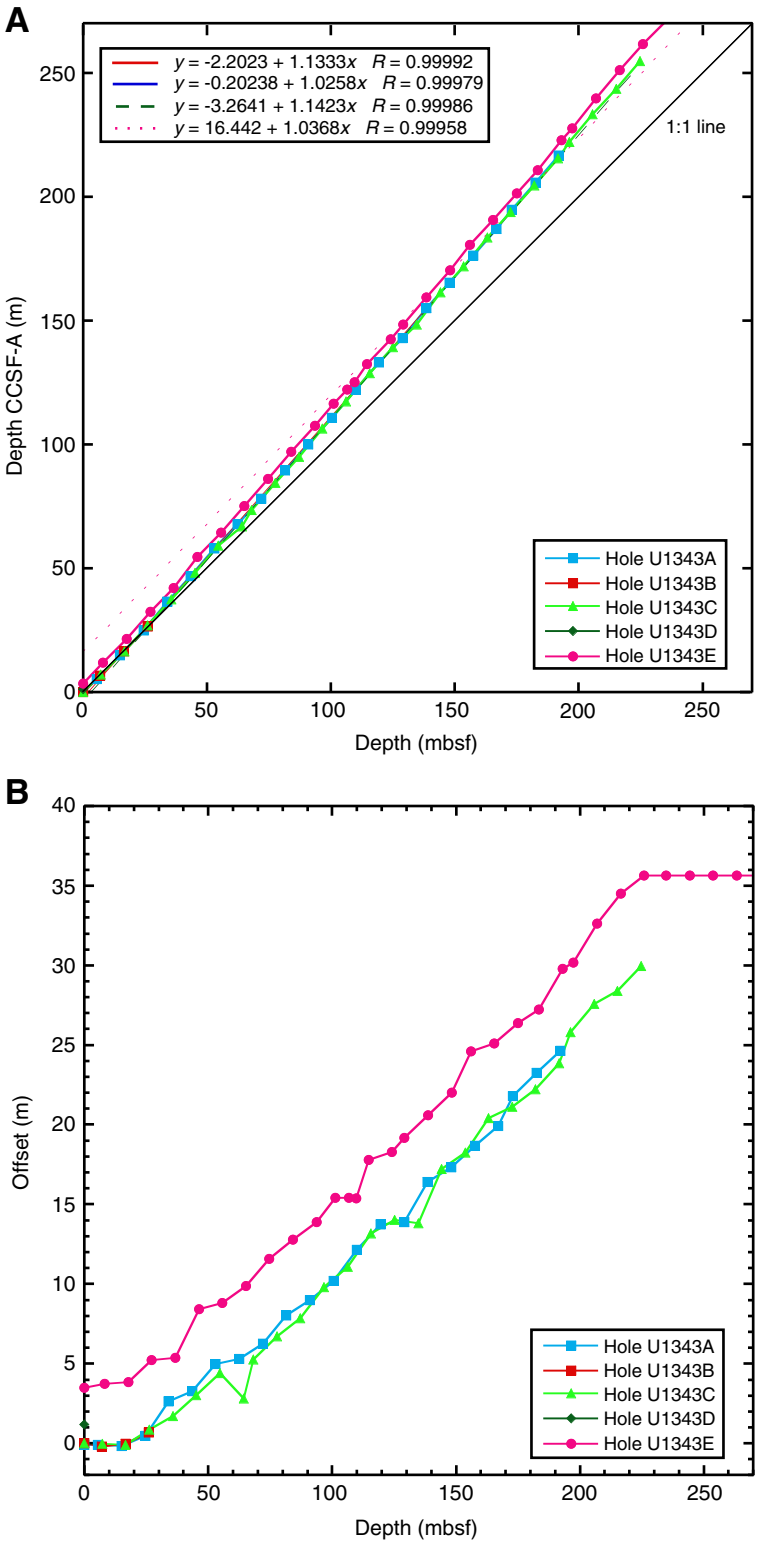

**Figure F38.** Summary of logs recorded by the triple combination tool string, Hole U1343E. HLDS = Hostile Environment Litho-Density Sonde. gAPI = American Petroleum Institute gamma ray units, c/s = counts per second. MAD = moisture and density core data, GRA = gamma ray attenuation bulk density core track measurements, IDPH = deep induction phasor-processed resistivity, IMPH = medium induction phasor-processed resistivity, SFLU = spherically focused resistivity.

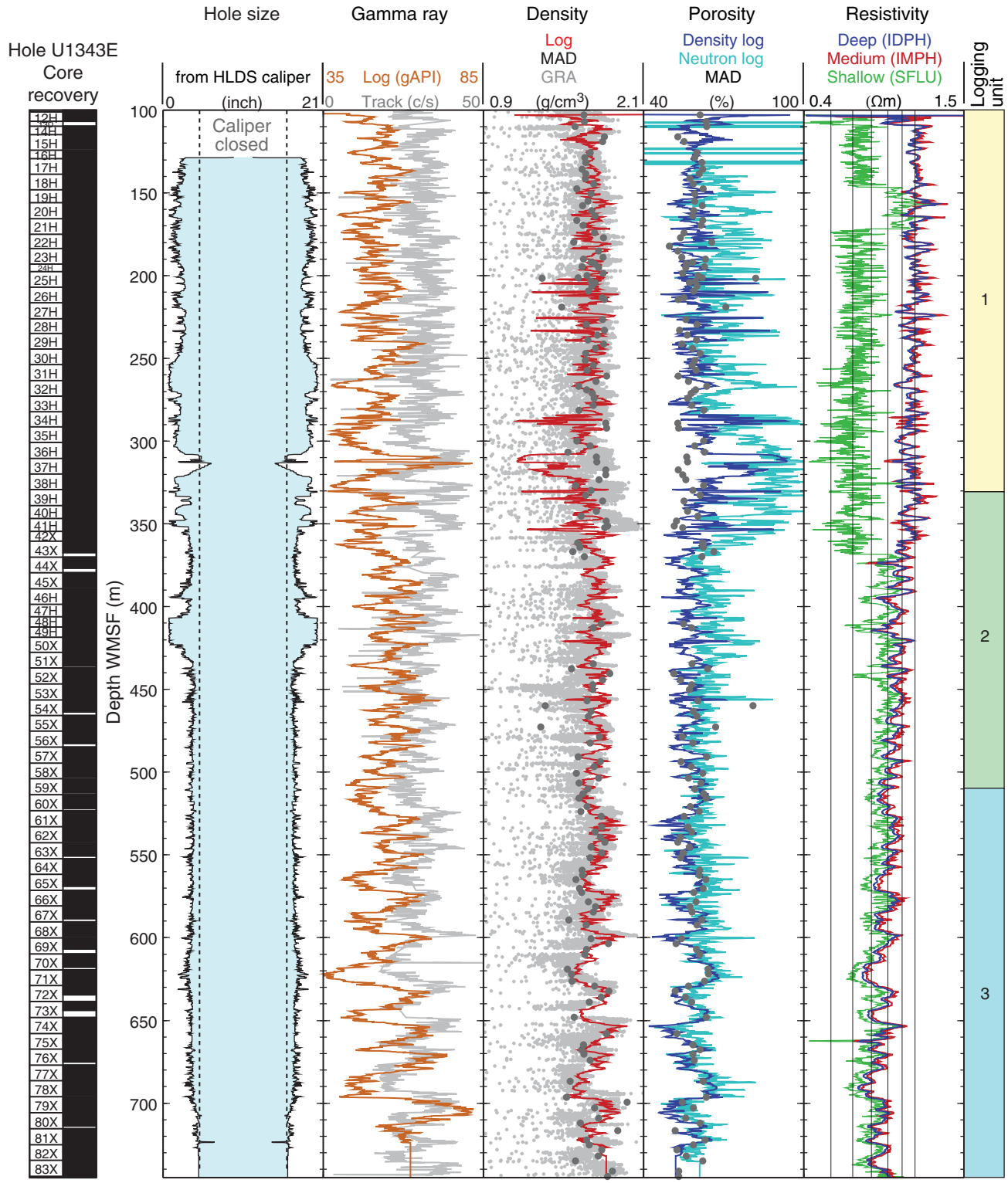

**Figure F39.** Summary of logs recorded during the second pass of the Formation MicroScanner (FMS)-sonic tool string, Hole U1343E. Hole size was calculated by the two orthogonal calipers of the FMS (C1 and C2). High waveform coherence (red in the velocity tracks) is a measure of the reliability of the slowness/time coherence algorithm used to derive compressional ($V_P$) and shear ($V_S$) velocities from the monopole and lower dipole sonic waveforms, respectively. Waveform amplitude is shown to display any amplitude anomalies that could indicate the occurrence of gas hydrate. None were detected. gAPI = American Petroleum Institute gamma ray units. WF = sonic waveform, LD = lower dipole.

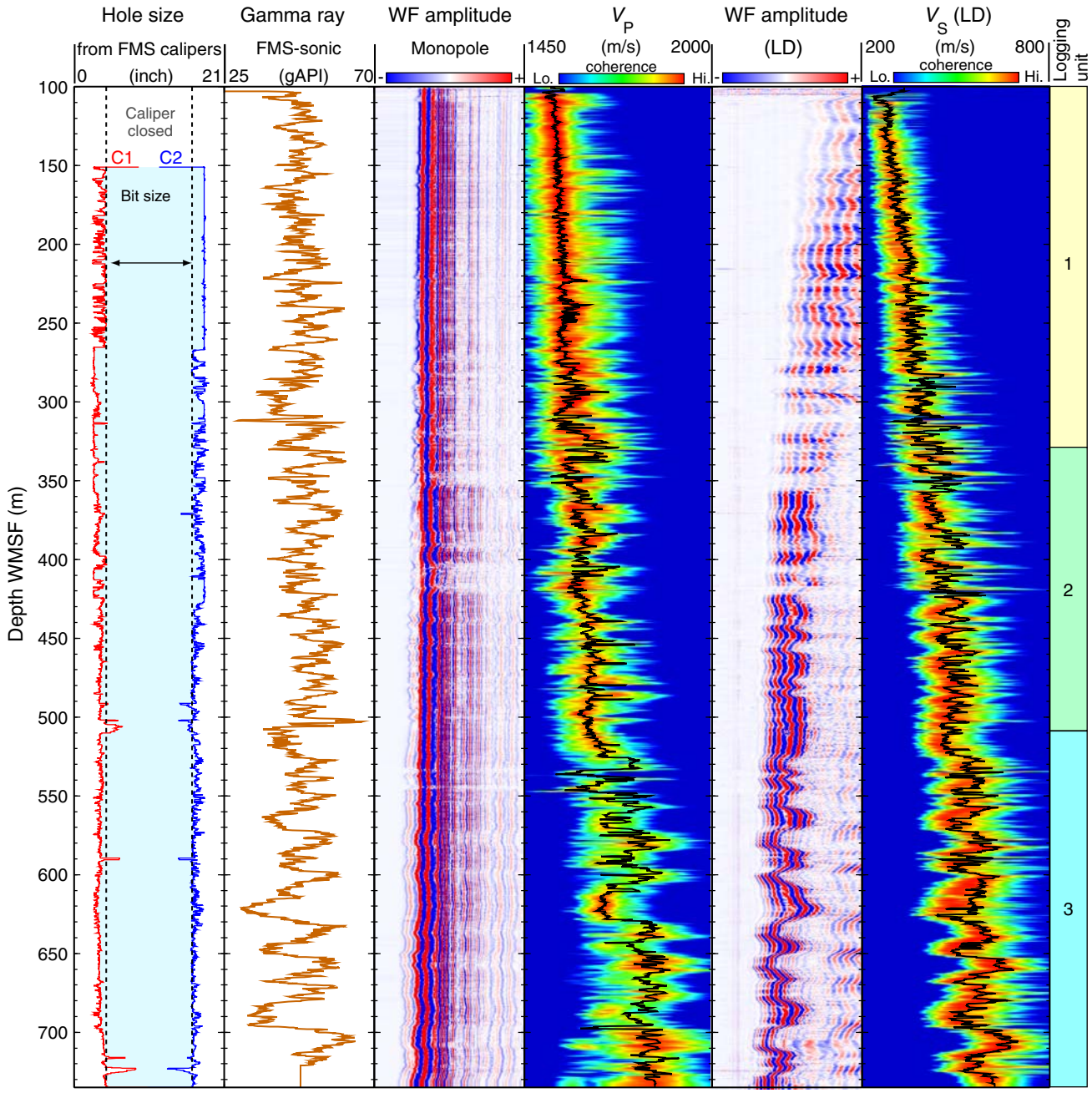

**Figure F40.** Detail of the logs recorded between 280 and 400 m WMSF, illustrating the contradiction between the low-density log values between ~300 and 360 m WMSF—particularly between 307 and 322 m WMSF, where they are much lower than core measurements—and the apparently good contact between the Hostile Environment Litho-Density Sonde (HLDS) and the formation shown by the small HLDS caliper readings in this interval. The caliper logs measured during the main triple combination (triple combo) log (up) and the two Formation MicroScanner (FMS)-sonic passes show the evolution of borehole size during logging operations. The gamma ray attenuation (GRA) logs agree in this interval, except for one log recorded during the main triple combo log. See **"Downhole measurements"** for details. gAPI = American Petroleum Institute gamma ray units. TC = triple combination, MAD = moisture and density, IDPH = deep induction phasor-processed resistivity, IMPH = medium induction phasor-processed resistivity.

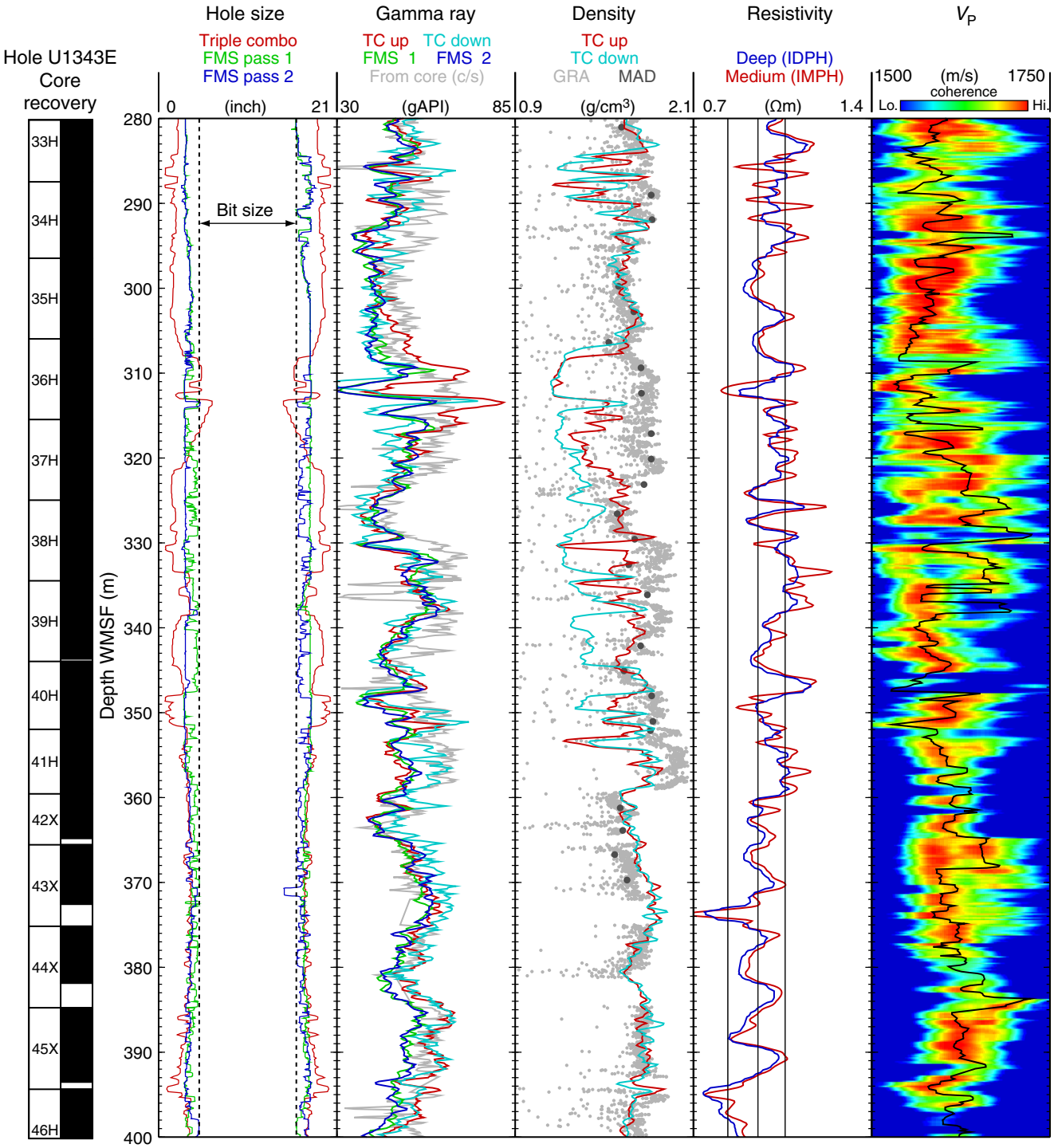

**Figure F41.** Summary of spectral natural gamma ray measurements, Hole U1343E. The area between the two curves shows the contribution of uranium, a common indicator of organic content. gAPI = American Petroleum Institute gamma ray units. CGR = computed gamma ray (gamma ray without uranium contribution), GR = total gamma ray.

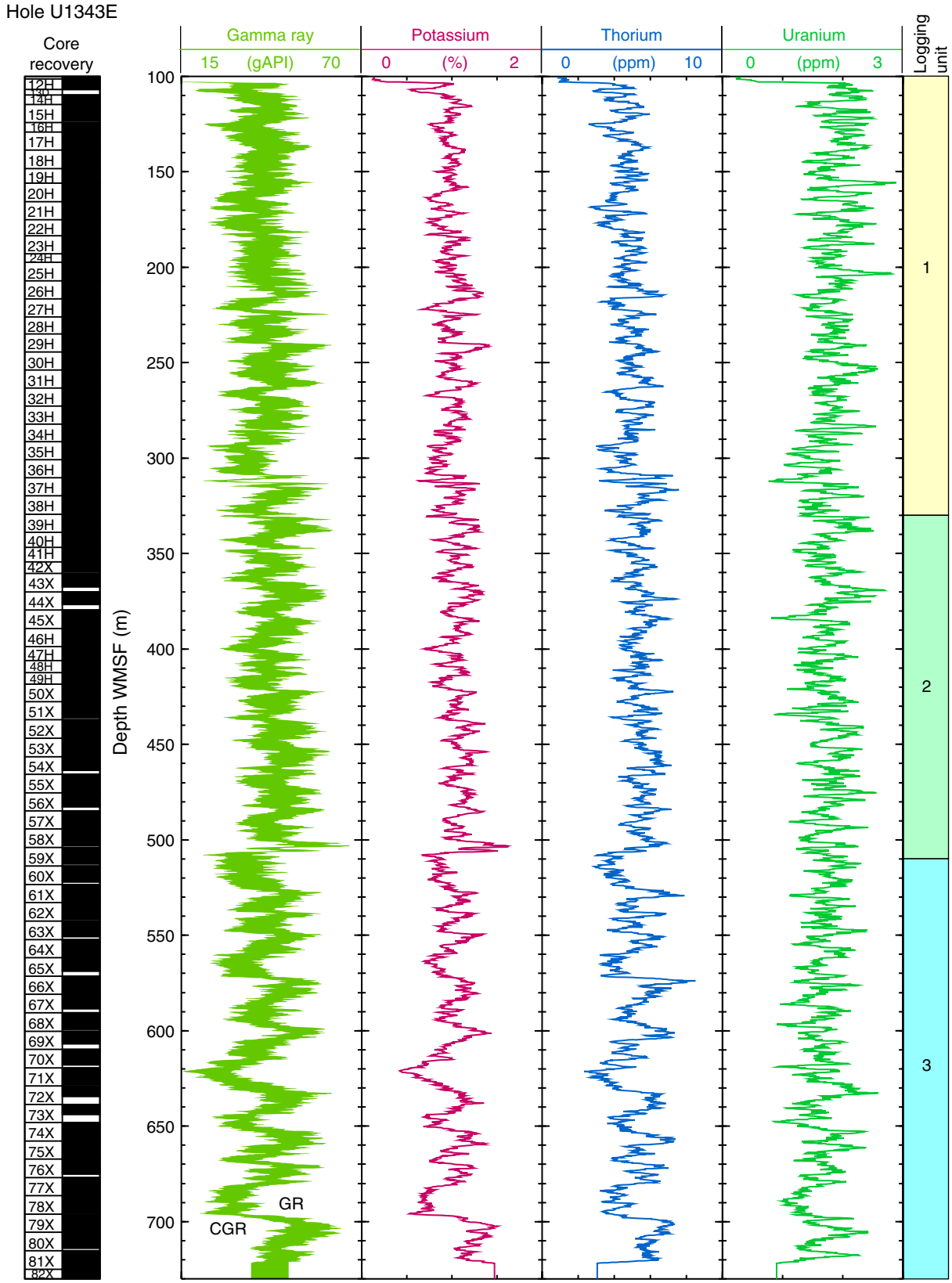

**Figure F42.** Comparison of the synthetic seismogram calculated from density and $V_P$ logs in Hole U1343E and MCS Line Stk1 (Sakamoto et al., 2005) across Site U1343. The gamma ray log is shown as a reference to the other logs and logging units. The density used is a composite of the density log and GRA data from 307 to 360 m WMSF. gAPI = American Petroleum Institute gamma ray units.

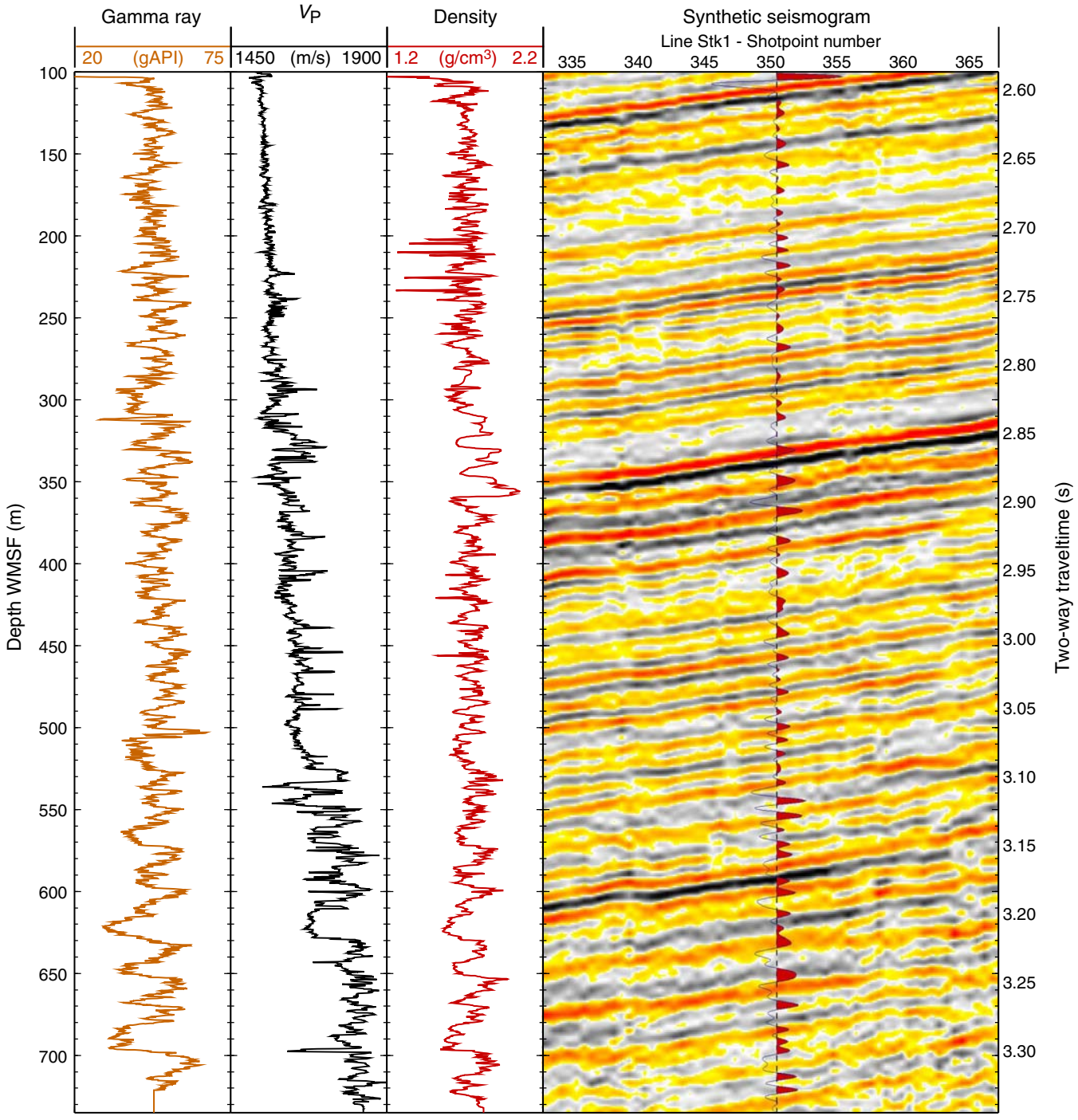

**Figure F43.** Correlation between Formation MicroScanner (FMS) electrical images and core observations in each of the three logging units. **A.** Ash layer in logging Unit 1, Section 323-U1343E-33H-3 (279.2–279.8 m WMSF). **B.** High-density interval in logging Unit 2, Section 323-U1343E-41H-6 (357.358.9 m WMSF). **C.** Dolostone in logging Unit 3, Section 323-U1343E-78X-6 (693.9–694.6 m WMSF). The depths of the core images have been adjusted by 5 m to correct for the difference between the seafloor depth identified by the drillers and by the gamma ray log. The contrast in the core images is enhanced.

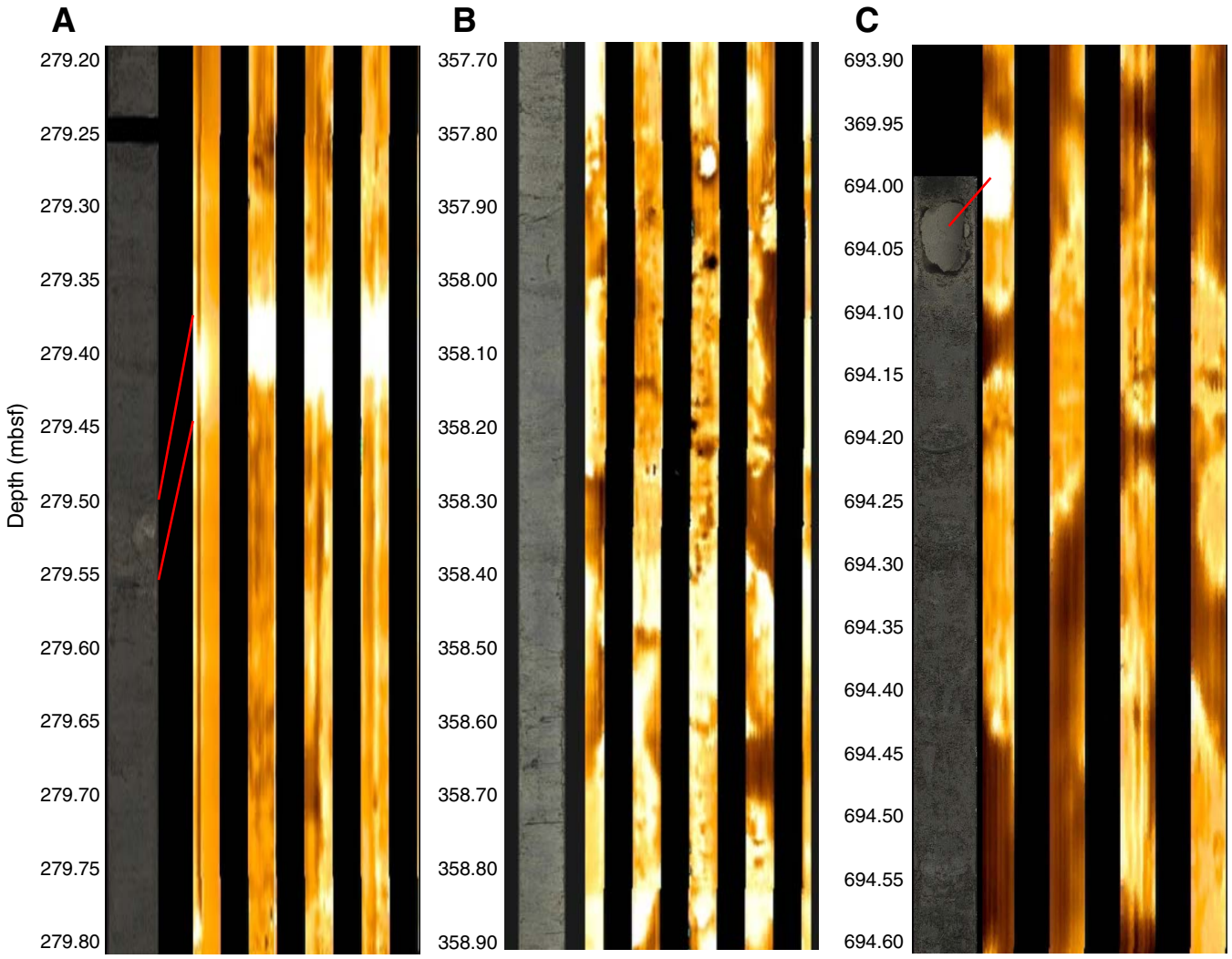

**Figure F44. A.** Records of APCT-3 penetrations and temperature decays, Hole U1343E. **B.** Summary of temperature measurements.

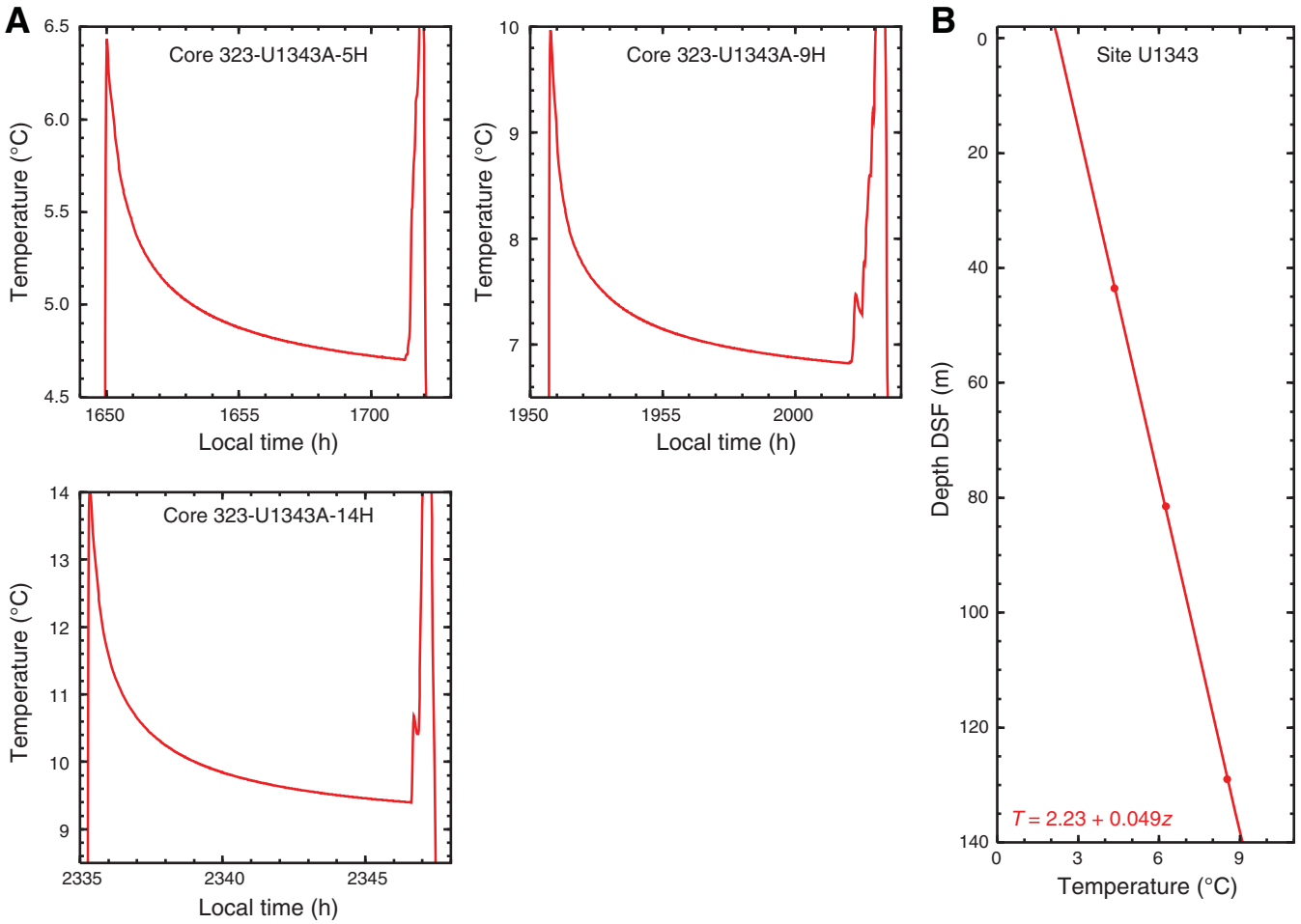

**Table T1.** Coring summary, Holes U1343A, U1343B, U1343C, U1343D, and U1343E. (See table notes.) (Continued on next three pages.)

**Hole U1343A**
Latitude: 57°33.3993′N
Longitude: 175°48.9659′W
Time on hole (h): 24.87
Seafloor (drill pipe measurement from rig floor, m DRF): 1962.4
Distance between rig floor and sea level (m): 11.5
Water depth (drill pipe measurement from sea level, m): 1950.9
Total depth (drill pipe measurement from rig floor, m DRF): 1997.9
Total penetration (mbsf): 201.5
Total length of cored section (m): 201.5
Total core recovered (m): 204.03
Core recovery (%): 101.26
Total number of cores: 22

**Hole U1343B**
Latitude: 57°33.4156′N
Longitude: 175°48.9951′W
Time on hole (h): 4.25
Seafloor (drill pipe measurement from rig floor, m DRF): 1962.4
Distance between rig floor and sea level (m): 11.5
Water depth (drill pipe measurement from sea level, m): 1950.9
Total depth (drill pipe measurement from rig floor, m DRF): 1997.9
Total penetration (mbsf): 35.5
Total length of cored section (m): 35.5
Total core recovered (m): 34.56
Core recovery (%): 97.35
Total number of cores: 4

**Hole U1343C**
Latitude: 57°33.3982′N
Longitude: 175°49.0275′W
Time on hole (h): 22.92
Seafloor (drill pipe measurement from rig floor, m DRF): 1964.2
Distance between rig floor and sea level (m): 11.5
Water depth (drill pipe measurement from sea level, m): 1952.6
Total depth (drill pipe measurement from rig floor, m DRF): 2198.36
Total penetration (mbsf): 234.2
Total length of cored section (m): 234.2
Total core recovered (m): 231.04
Core recovery (%): 98.65
Total number of cores: 26

**Hole U1343D**
Latitude: 57°33.3817′N
Longitude: 175°48.9971′W
Time on hole (h): 1.42
Seafloor (drill pipe measurement from rig floor, m DRF): 1965.7
Distance between rig floor and sea level (m): 11.5
Water depth (drill pipe measurement from sea level, m): 1954.1
Total depth (drill pipe measurement from rig floor, m DRF): 1974.20
Total penetration (mbsf): 8.5
Total length of cored section (m): 8.5
Total core recovered (m): 8.5
Core recovery (%): 100
Total number of cores: 1

**Hole U1343E**
Latitude: 57°33.3814′N
Longitude: 175°48.9974′W
Time on hole (h): 106.82
Seafloor (drill pipe measurement from rig floor, m DRF): 1967.5
Distance between rig floor and sea level (m): 11.5
Water depth (drill pipe measurement from sea level, m): 1956.0
Total depth (drill pipe measurement from rig floor, m DRF): 2711.8
Total penetration (mbsf): 744.3
Total length of cored section (m): 741.3
Total core recovered (m): 700.27
Core recovery (%): 94.47
Total number of cores: 82

**Table T1 (continued).** (Continued on next page.)

| Core | Date (2009) | UTC (h) | Depth DSF (m) Top | Depth DSF (m) Bottom | Length (m) Cored | Length (m) Recovered | Recovery (%) | Comments |
|---|---|---|---|---|---|---|---|---|
| 323-U1343A- | | | | | | | | |
| 1H | 7 Aug | 1405 | 0.0 | 5.5 | 5.5 | 5.49 | 100 | Oriented nonmagnetic barrel |
| 2H | 7 Aug | 1500 | 5.5 | 15.0 | 9.5 | 9.54 | 100 | Oriented nonmagnetic barrel |
| 3H | 7 Aug | 1540 | 15.0 | 24.5 | 9.5 | 9.73 | 102 | Oriented nonmagnetic barrel |
| 4H | 7 Aug | 1620 | 24.5 | 34.0 | 9.5 | 10.26 | 108 | Oriented nonmagnetic barrel |
| 5H | 7 Aug | 1715 | 34.0 | 43.5 | 9.5 | 10.01 | 105 | APCT, oriented nonmagnetic barrel |
| 6H | 7 Aug | 1800 | 43.5 | 53.0 | 9.5 | 10.52 | 111 | Oriented nonmagnetic barrel |
| 7H | 7 Aug | 1840 | 53.0 | 62.5 | 9.5 | 9.29 | 98 | Oriented nonmagnetic barrel |
| 8H | 7 Aug | 1920 | 62.5 | 72.0 | 9.5 | 9.39 | 99 | Oriented nonmagnetic barrel |
| 9H | 7 Aug | 2020 | 72.0 | 81.5 | 9.5 | 10.00 | 105 | APCT, oriented nonmagnetic barrel |
| 10H | 7 Aug | 2100 | 81.5 | 91.0 | 9.5 | 9.50 | 100 | Oriented nonmagnetic barrel |
| 11H | 7 Aug | 2135 | 91.0 | 100.5 | 9.5 | 9.60 | 101 | Oriented nonmagnetic barrel |
| 12H | 7 Aug | 2215 | 100.5 | 110.0 | 9.5 | 10.02 | 105 | Oriented nonmagnetic barrel |
| 13H | 7 Aug | 2300 | 110.0 | 119.5 | 9.5 | 9.42 | 99 | Oriented nonmagnetic barrel |
| 14H | 8 Aug | 0005 | 119.5 | 129.0 | 9.5 | 9.46 | 100 | APCT, oriented nonmagnetic barrel |
| 15H | 8 Aug | 0050 | 129.0 | 138.5 | 9.5 | 10.16 | 107 | Oriented nonmagnetic barrel |
| 16H | 8 Aug | 0135 | 138.5 | 148.0 | 9.5 | 8.71 | 92 | Oriented nonmagnetic barrel |
| 17H | 8 Aug | 0215 | 148.0 | 157.5 | 9.5 | 9.39 | 99 | Oriented nonmagnetic barrel |
| 18H | 8 Aug | 0305 | 157.5 | 167.0 | 9.5 | 8.72 | 92 | Oriented nonmagnetic barrel |
| 19H | 8 Aug | 0345 | 167.0 | 173.0 | 6.0 | 6.90 | 115 | Oriented nonmagnetic barrel |
| 20H | 8 Aug | 0450 | 173.0 | 182.5 | 9.5 | 9.06 | 95 | Oriented nonmagnetic barrel |
| 21H | 8 Aug | 0535 | 182.5 | 192.0 | 9.5 | 9.10 | 96 | Oriented nonmagnetic barrel |
| 22H | 8 Aug | 0625 | 192.0 | 201.5 | 9.5 | 9.76 | 103 | Oriented nonmagnetic barrel |
| | | | | Cored totals: | 201.5 | 204.03 | 101 | |
| 323-U1343B- | | | | | | | | |
| 1H | 8 Aug | 0905 | 0.0 | 7.0 | 7.0 | 6.85 | 98 | Nonmagnetic barrel |
| 2H | 8 Aug | 1045 | 7.0 | 16.5 | 9.5 | 9.87 | 104 | Nonmagnetic barrel |
| 3H | 8 Aug | 1120 | 16.5 | 26.0 | 9.5 | 8.58 | 90 | Nonmagnetic barrel |
| 4H | 8 Aug | 1155 | 26.0 | 35.5 | 9.5 | 9.26 | 97 | Nonmagnetic barrel |
| | | | | Cored totals: | 35.5 | 34.56 | 97 | |
| 323-U1343C- | | | | | | | | |
| 1H | 8 Aug | 1340 | 0.0 | 7.2 | 7.2 | 7.24 | 101 | Oriented nonmagnetic barrel |
| 2H | 8 Aug | 1420 | 7.2 | 16.7 | 9.5 | 9.47 | 100 | Oriented nonmagnetic barrel |
| 3H | 8 Aug | 1455 | 16.7 | 26.2 | 9.5 | 9.90 | 104 | Oriented nonmagnetic barrel |
| 4H | 8 Aug | 1540 | 26.2 | 35.7 | 9.5 | 10.20 | 107 | Oriented nonmagnetic barrel |
| 5H | 8 Aug | 1615 | 35.7 | 45.2 | 9.5 | 9.05 | 95 | Oriented nonmagnetic barrel |
| 6H | 8 Aug | 1655 | 45.2 | 54.7 | 9.5 | 10.31 | 109 | Oriented nonmagnetic barrel |
| 7H | 8 Aug | 1755 | 54.7 | 64.2 | 9.5 | 9.21 | 97 | Oriented nonmagnetic barrel |
| 8H | 8 Aug | 1840 | 64.2 | 68.2 | 4.0 | 6.48 | 162 | Oriented nonmagnetic barrel |
| 9H | 8 Aug | 1920 | 68.2 | 77.7 | 9.5 | 10.15 | 107 | Oriented nonmagnetic barrel |
| 10H | 8 Aug | 2000 | 77.7 | 87.2 | 9.5 | 9.98 | 105 | Oriented nonmagnetic barrel |
| 11H | 8 Aug | 2035 | 87.2 | 96.7 | 9.5 | 10.34 | 109 | Oriented nonmagnetic barrel |
| 12H | 8 Aug | 2115 | 96.7 | 106.2 | 9.5 | 9.98 | 105 | Oriented nonmagnetic barrel |
| 13H | 8 Aug | 2150 | 106.2 | 115.7 | 9.5 | 9.90 | 104 | Oriented nonmagnetic barrel |
| 14H | 8 Aug | 2225 | 115.7 | 125.2 | 9.5 | 8.95 | 94 | Oriented nonmagnetic barrel |
| 15H | 8 Aug | 2315 | 125.2 | 134.7 | 9.5 | 9.84 | 104 | Oriented nonmagnetic barrel |
| 16H | 9 Aug | 0005 | 134.7 | 144.2 | 9.5 | 0.00 | 0 | Oriented nonmagnetic barrel |
| 17H | 9 Aug | 0055 | 144.2 | 153.7 | 9.5 | 9.20 | 97 | Oriented nonmagnetic barrel |
| 18H | 9 Aug | 0145 | 153.7 | 163.2 | 9.5 | 9.45 | 99 | Oriented nonmagnetic barrel |
| 19H | 9 Aug | 0245 | 163.2 | 172.7 | 9.5 | 8.79 | 93 | Oriented nonmagnetic barrel |
| 20H | 9 Aug | 0330 | 172.7 | 182.2 | 9.5 | 9.51 | 100 | Oriented nonmagnetic barrel |
| 21H | 9 Aug | 0425 | 182.2 | 191.7 | 9.5 | 9.95 | 105 | Oriented nonmagnetic barrel |
| 22H | 9 Aug | 0520 | 191.7 | 196.2 | 4.5 | 4.46 | 99 | Oriented nonmagnetic barrel |
| 23H | 9 Aug | 0610 | 196.2 | 205.7 | 9.5 | 9.25 | 97 | Oriented nonmagnetic barrel |
| 24H | 9 Aug | 0745 | 205.7 | 215.2 | 9.5 | 9.84 | 104 | Oriented nonmagnetic barrel |
| 25H | 9 Aug | 0840 | 215.2 | 224.7 | 9.5 | 9.57 | 101 | Oriented nonmagnetic barrel |
| 26H | 9 Aug | 0930 | 224.7 | 234.2 | 9.5 | 10.02 | 105 | Oriented nonmagnetic barrel |
| | | | | Cored totals: | 234.2 | 231.04 | 99 | |
| 323-U1343D- | | | | | | | | |
| 1H | 9 Aug | 1245 | 0.0 | 8.5 | 8.5 | 8.53 | 100.35 | Nonmagnetic barrel |
| | | | | Cored totals: | 8.5 | 8.53 | 100.35 | |
| 323-U1343E- | | | | | | | | |
| 1H | 9 Aug | 1330 | 0.0 | 8.2 | 8.2 | 8.22 | 100 | Steel barrel |
| 2H | 9 Aug | 1430 | 8.2 | 17.7 | 9.5 | 9.60 | 101 | Steel barrel |
| 3H | 9 Aug | 1520 | 17.7 | 27.2 | 9.5 | 8.70 | 92 | Steel barrel |
| 4H | 9 Aug | 1605 | 27.2 | 36.7 | 9.5 | 9.97 | 105 | Steel barrel |
| 5H | 9 Aug | 1645 | 36.7 | 46.2 | 9.5 | 6.36 | 67 | Steel barrel |

**Table T1 (continued).** (Continued on next page.)

| Core | Date (2009) | UTC (h) | Depth DSF (m) Top | Depth DSF (m) Bottom | Length (m) Cored | Length (m) Recovered | Recovery (%) | Comments |
|---|---|---|---|---|---|---|---|---|
| 6H | 9 Aug | 1720 | 46.2 | 55.7 | 9.5 | 9.35 | 98 | Steel barrel |
| 7H | 9 Aug | 1820 | 55.7 | 65.2 | 9.5 | 8.30 | 87 | Steel barrel |
| 8H | 9 Aug | 1850 | 65.2 | 74.7 | 9.5 | 9.69 | 102 | Steel barrel |
| 9H | 9 Aug | 1925 | 74.7 | 84.2 | 9.5 | 9.45 | 99 | Steel barrel |
| 10H | 9 Aug | 2000 | 84.2 | 93.7 | 9.5 | 6.88 | 72 | Steel barrel |
| 11H | 9 Aug | 2030 | 93.7 | 101.2 | 7.5 | 8.07 | 108 | Steel barrel |
| 12H | 9 Aug | 2105 | 101.2 | 106.7 | 5.5 | 5.49 | 100 | Steel barrel |
| 13D | 9 Aug | 2220 | 106.7 | 109.7 | 3.0 | 0.00 | 0 | Steel barrel |
| 14H | 9 Aug | 2335 | 109.7 | 114.7 | 5.0 | 6.35 | 127 | Steel barrel |
| 15H | 10 Aug | 0020 | 114.7 | 124.2 | 9.5 | 8.75 | 92 | Steel barrel |
| 16H | 10 Aug | 0140 | 124.2 | 129.2 | 5.0 | 5.36 | 107 | Nonmagnetic barrel |
| 17H | 10 Aug | 0220 | 129.2 | 138.7 | 9.5 | 9.24 | 97 | Nonmagnetic barrel |
| 18H | 10 Aug | 0300 | 138.7 | 148.2 | 9.5 | 9.61 | 101 | Nonmagnetic barrel |
| 19H | 10 Aug | 0415 | 148.2 | 156.0 | 7.8 | 7.77 | 100 | Nonmagnetic barrel |
| 20H | 10 Aug | 0520 | 156.0 | 165.5 | 9.5 | 8.99 | 95 | Nonmagnetic barrel |
| 21H | 10 Aug | 0605 | 165.5 | 175.0 | 9.5 | 9.67 | 102 | Nonmagnetic barrel |
| 22H | 10 Aug | 0655 | 175.0 | 183.5 | 8.5 | 8.86 | 104 | Nonmagnetic barrel |
| 23H | 10 Aug | 0735 | 183.5 | 193.0 | 9.5 | 9.91 | 104 | Nonmagnetic barrel |
| 24H | 10 Aug | 0855 | 193.0 | 197.5 | 4.5 | 4.57 | 102 | Nonmagnetic barrel |
| 25H | 10 Aug | 0950 | 197.5 | 207.0 | 9.5 | 10.59 | 111 | Nonmagnetic barrel |
| 26H | 10 Aug | 1030 | 207.0 | 216.5 | 9.5 | 10.14 | 107 | Nonmagnetic barrel |
| 27H | 10 Aug | 1105 | 216.5 | 226.0 | 9.5 | 9.61 | 101 | Nonmagnetic barrel |
| 28H | 10 Aug | 1140 | 226.0 | 234.8 | 8.8 | 8.82 | 100 | Nonmagnetic barrel |
| 29H | 10 Aug | 1225 | 234.8 | 244.3 | 9.5 | 10.79 | 114 | Nonmagnetic barrel |
| 30H | 10 Aug | 1405 | 244.3 | 253.8 | 9.5 | 10.01 | 105 | Nonmagnetic barrel |
| 31H | 10 Aug | 1505 | 253.8 | 263.3 | 9.5 | 10.05 | 106 | Nonmagnetic barrel |
| 32H | 10 Aug | 1540 | 263.3 | 272.8 | 9.5 | 9.29 | 98 | Nonmagnetic barrel |
| 33H | 10 Aug | 1620 | 272.8 | 282.3 | 9.5 | 9.60 | 101 | Nonmagnetic barrel |
| 34H | 10 Aug | 1705 | 282.3 | 291.3 | 9.0 | 8.98 | 100 | Nonmagnetic barrel |
| 35H | 10 Aug | 1800 | 291.3 | 300.8 | 9.5 | 10.19 | 107 | Steel barrel |
| 36H | 10 Aug | 1855 | 300.8 | 310.3 | 9.5 | 10.40 | 109 | Steel barrel |
| 37H | 10 Aug | 2005 | 310.3 | 319.8 | 9.5 | 9.99 | 105 | Steel barrel |
| 38H | 10 Aug | 2115 | 319.8 | 329.3 | 9.5 | 10.04 | 106 | Steel barrel |
| 39H | 10 Aug | 2220 | 329.3 | 338.8 | 9.5 | 9.21 | 97 | Steel barrel |
| 40H | 10 Aug | 2340 | 338.8 | 346.8 | 8.0 | 8.04 | 100 | Steel barrel |
| 41H | 11 Aug | 0110 | 346.8 | 354.4 | 7.6 | 7.62 | 100 | Steel barrel, shattered liner |
| 42X | 11 Aug | 0335 | 354.4 | 360.4 | 6.0 | 5.27 | 88 | Steel barrel |
| 43X | 11 Aug | 0425 | 360.4 | 370.0 | 9.6 | 7.02 | 73 | Steel barrel |
| 44X | 11 Aug | 0530 | 370.0 | 379.6 | 9.6 | 6.69 | 70 | Steel barrel |
| 45X | 11 Aug | 0630 | 379.6 | 389.2 | 9.6 | 8.76 | 91 | Steel barrel |
| 46H | 11 Aug | 0730 | 389.2 | 398.7 | 9.5 | 9.47 | 100 | Steel barrel |
| 47H | 11 Aug | 0905 | 398.7 | 406.1 | 7.4 | 7.39 | 100 | Steel barrel |
| 48H | 11 Aug | 1040 | 406.1 | 412.4 | 6.3 | 6.33 | 100 | Steel barrel |
| 49H | 11 Aug | 1200 | 412.4 | 418.5 | 6.1 | 6.14 | 101 | Steel barrel |
| 50X | 11 Aug | 1325 | 418.5 | 427.5 | 9.0 | 10.10 | 112 | Steel barrel |
| 51X | 11 Aug | 1415 | 427.5 | 437.1 | 9.6 | 8.45 | 88 | Steel barrel |
| 52X | 11 Aug | 1500 | 437.1 | 446.8 | 9.7 | 9.11 | 94 | Steel barrel |
| 53X | 11 Aug | 1550 | 446.8 | 456.4 | 9.6 | 9.18 | 96 | Steel barrel |
| 54X | 11 Aug | 1630 | 456.4 | 465.7 | 9.3 | 7.09 | 76 | Steel barrel |
| 55X | 11 Aug | 1720 | 465.7 | 475.3 | 9.6 | 10.00 | 104 | Steel barrel |
| 56X | 11 Aug | 1815 | 475.3 | 484.8 | 9.5 | 7.37 | 78 | Steel barrel |
| 57X | 11 Aug | 1900 | 484.8 | 494.4 | 9.6 | 9.27 | 97 | Steel barrel |
| 58X | 11 Aug | 1945 | 494.4 | 504.0 | 9.6 | 8.58 | 89 | Steel barrel |
| 59X | 11 Aug | 2105 | 504.0 | 513.7 | 9.7 | 8.62 | 89 | Steel barrel |
| 60X | 11 Aug | 2145 | 513.7 | 523.3 | 9.6 | 8.30 | 86 | Steel barrel |
| 61X | 11 Aug | 2240 | 523.3 | 532.9 | 9.6 | 9.21 | 96 | Steel barrel |
| 62X | 11 Aug | 2340 | 532.9 | 542.5 | 9.6 | 8.98 | 94 | Steel barrel |
| 63X | 12 Aug | 0035 | 542.5 | 552.2 | 9.7 | 8.14 | 84 | Steel barrel |
| 64X | 12 Aug | 0140 | 552.2 | 561.8 | 9.6 | 8.95 | 93 | Steel barrel |
| 65X | 12 Aug | 0245 | 561.8 | 571.4 | 9.6 | 7.07 | 74 | Steel barrel |
| 66X | 12 Aug | 0350 | 571.4 | 580.9 | 9.5 | 9.74 | 103 | Steel barrel |
| 67X | 12 Aug | 0440 | 580.9 | 590.5 | 9.6 | 7.70 | 80 | Steel barrel |
| 68X | 12 Aug | 0535 | 590.5 | 600.2 | 9.7 | 8.86 | 91 | Steel barrel |
| 69X | 12 Aug | 0625 | 600.2 | 609.8 | 9.6 | 6.74 | 70 | Steel barrel |
| 70X | 12 Aug | 0715 | 609.8 | 619.4 | 9.6 | 8.20 | 85 | Steel barrel |
| 71X | 12 Aug | 0810 | 619.4 | 629.0 | 9.6 | 8.86 | 92 | Steel barrel |
| 72X | 12 Aug | 0855 | 629.0 | 638.6 | 9.6 | 5.54 | 58 | Steel barrel |
| 73X | 12 Aug | 0940 | 638.6 | 648.2 | 9.6 | 5.29 | 55 | Steel barrel |
| 74X | 12 Aug | 1035 | 648.2 | 657.8 | 9.6 | 9.31 | 97 | Steel barrel |

**Table T1 (continued).**

| Core | Date (2009) | UTC (h) | Depth DSF (m) Top | Depth DSF (m) Bottom | Length (m) Cored | Length (m) Recovered | Recovery (%) | Comments |
|---|---|---|---|---|---|---|---|---|
| 75X | 12 Aug | 1135 | 657.8 | 667.3 | 9.5 | 9.39 | 99 | Steel barrel |
| 76X | 12 Aug | 1225 | 667.3 | 676.9 | 9.6 | 7.76 | 81 | Steel barrel |
| 77X | 12 Aug | 1310 | 676.9 | 686.5 | 9.6 | 9.57 | 100 | Steel barrel |
| 78X | 12 Aug | 1435 | 686.5 | 696.1 | 9.6 | 8.80 | 92 | Steel barrel |
| 79X | 12 Aug | 1530 | 696.1 | 705.7 | 9.6 | 9.72 | 101 | Steel barrel |
| 80X | 12 Aug | 1615 | 705.7 | 715.4 | 9.7 | 8.20 | 85 | Steel barrel |
| 81X | 12 Aug | 1700 | 715.4 | 725.0 | 9.6 | 9.66 | 101 | Steel barrel |
| 82X | 12 Aug | 1755 | 725.0 | 734.6 | 9.6 | 9.51 | 99 | Steel barrel |
| 83X | 12 Aug | 1850 | 734.6 | 744.3 | 9.7 | 9.40 | 97 | Steel barrel |
| | | | | Cored totals: | 741.3 | 700.27 | 94 | |
| | | | | Site totals: | 1221.0 | 1178.43 | 96.5 | |

Notes: DRF = drilling depth below rig floor, mbsf = meters below seafloor, DSF = drilling depth below seafloor. APCT = advanced piston corer temperature tool. UTC = Universal Time Coordinated.

**Table T2.** Datum events of radiolarians, silicoflagellates, diatoms, calcareous nannofossils, ebridians, and planktonic foraminifers, Holes U1343A, U1343C, and U1343E. (**See table notes.**)

| Datum event | Taxon | Age (Ma) | Depth (mbsf) Hole U1343A | Depth (mbsf) Hole U1343C | Depth (mbsf) Hole U1343E | Depth CCSF-A (m) Hole U1343A | Depth CCSF-A (m) Hole U1343C | Depth CCSF-A (m) Hole U1343E |
|---|---|---|---|---|---|---|---|---|
| LO *Lycnocanoma nipponica sakaii* | Radiolarian | 0.05 | 10.3 | 12.0 | 13.0 | 10.2 | 11.9 | 16.6 |
| LO *Distephanus octonarius* | Silicoflagellate | 0.2–0.3 | — | — | 69.4 | — | — | 78.8 |
| LO *Spongodiscus* sp. | Radiolarian | 0.28–0.32 | 76.9 | 83.0 | 79.5 | 82.7 | 89.0 | 90.2 |
| LO *Axoprunum acquilonium* | Radiolarian | 0.25–0.43 | 86.5 | 111.4 | 87.6 | 93.6 | 121.8 | 99.8 |
| LO *Proboscia curvirostris* | Diatom | 0.3 | 76.9 | 74.5 | 69.4 | 82.7 | 78.6 | 78.8 |
| LO *Thalassiosira jouseae* | Diatom | 0.3 | 67.1 | 74.5 | 69.4 | 72.2 | 78.6 | 78.8 |
| LO *Stylatractus universus* | Radiolarian | 0.41–0.51 | 105.6 | 129.8 | 104.2 | 115.1 | 143.5 | 118.9 |
| LO *Pseudoemiliania lacunosa* | Calcareous nannofossil | 0.44 | 109.3 | — | — | 119.5 | — | — |
| LO *Dictyocha subarctios* | Silicoflagellate | 0.6–0.8 | — | 200.8 | 188.6 | — | 217.2 | 215.4 |
| LCO *Actinocyclus oculatus* | Diatom | 0.9 | — | — | 296.4 | — | — | 332.0 |
| LO *Eucyrtidium matuyamai* | Radiolarian | 0.9–1.5 | — | — | 296.4 | — | — | 332.0 |
| LO *Filisphaera filifera* | Dinoflagellate | 1.4–1.7 | — | — | 372.1 | — | — | 407.7 |
| FO *Eucyrtidium matuyamai* | Radiolarian | 1.7–1.9 | — | — | 612.5 | — | — | 648.1 |
| FCO *Proboscia curvirostris* | Diatom | 1.84–1.86 | — | 432.3 | | — | — | 467.9 |
| LO *Stephanopyxis horridus* | Diatom | 1.9–2.0 | — | — | 517.3 | — | — | 552.9 |
| LO *Ammodochium rectangulare* | Ebridian | 1.9 | — | — | 555.9 | — | — | 591.5 |
| LCO *Neodenticula koizumii* | Diatom | 2.0–2.2 | — | — | 680.8 | — | — | 716.4 |
| LO *Neogloboquadrina atlantica* | Planktonic foraminifer | 2.4–2.5 | — | — | 372.1 | — | — | 407.7 |

Notes: For first occurrences (FO), the depth was estimated as the midpoint between the depth at which the species was first observed and the depth of the next sample below. For last occurrences (LO), the depth was estimated as the midpoint between the depth at which the species was last observed and the depth of the next sample above. FCO = first common occurrence, LCO = last common occurrence, — = not applicable.

**Table T3.** Calcareous nannofossil range chart, Holes U1343A, U1343C, and U1343E. (See table notes.) (Continued on next three pages.)

| Core, section, interval (cm) | Martini (1971) zone | Abundance | Preservation | *Coccolithus pelagicus* | *Cyclococcolithus leptoporus* | *Cyclococcolithus leptoporus* (small) | *Dictyococcites* spp. (small) | *Dictyococcites* spp. (medium) | *Emiliania huxleyi* | *Gephyrocapsa* (small) | *Gephyrocapsa* (medium) | *Gephyrocapsa* (large) | *Pseudoemiliania lacunosa* | *Reticulofenestra minuta* | *Reticulofenestra minutula* | *Reticulofenestra pseudoumbilica* (5–7 µm) | *Reticulofenestra pseudoumbilica* (>7 µm) | Other taxa | Comments |
|---|---|---|---|---|---|---|---|---|---|---|---|---|---|---|---|---|---|---|---|
| 323-U1343A- | | | | | | | | | | | | | | | | | | | |
| 1H-CC | | R | M-G | R | | | | | | | | | | | | | | | Slight etching in *Coccolithus pelagicus* |
| 2H-CC | | B | | | | | | | | | | | | | | | | *Thoracosphaera* spp. | |
| 3H-CC | | R | M-G | R | | | | | R | | | | | | | | | | Slight etching in *Coccolithus pelagicus* |
| 4H-CC | | R | M | | | | | | | R | R | | | | | | | | |
| 5H-CC | | B | B | | | | | | | | | | | | | | | | |
| 6H-CC | | B | | | | | | | | | | | | | | | | | |
| 7H-CC | | B | | | | | | | | | | | | | | | | | |
| 8H-4, 55 | | B | | | | | | | | | | | | | | | | | Large quantity of tubular minerals, 4–6 µm long × 1 µm wide, low birefringence |
| 8H-CC | | B | | | | | | | | | | | | | | | | | |
| 9H-CC | NN21 | B | | | | | | | | | | | | | | | | | |
| 10H-6, 52 | | B | | | | | | | | | | | | | | | | | |
| 10H-CC | | B | | | | | | | | | | | | | | | | | Reworked specimen (*Coccolithus pliopelagicus*) |
| 11H-CC | | B | | | | | | | | | | | | | | | | | |
| 12H-6, 67 | | R | G | | | | | | | R | | | | | | | | | Reworked specimens (*Sphenolithus* sp. early to middle Miocene) |
| 12H-6, 75 | | R | M-G | R | | R | | | | R | R | | | | | | | | |
| 12H-7, 10 | | A | G | C | | | | | | D | A | | | | | | | | Gephyrocapsids mostly *Gephyrocapsa caribbeanica,* abundant coccospheres, >10 (usually >25) specimens per FOV |
| 12H-7, 35 | | A | G | A | | | | | | D | A | | | | | | | *Braarudosphaera bigelowii, Syracosphaera* sp. | Gephyrocapsids mostly *Gephyrocapsa caribbeanica,* >10 specimens per FOV, frequent *Coccolithus pelagicus* >10 µm |
| 12H-7, 46 | | C | M-G | R | | R | | | | C | C | | R | | | | | | Gephyrocapsids are *Gephyrocapsa caribbeanica*, more terrigenous material |
| 12H-CC | | R | M-G | | | | | | | R | | | | | | | | | |
| 13H-CC | | R | M | | | | | | | | R | | | | | | | | |
| 14H-CC | | R | M-G | | | | | | | R | | | | | | | | | |
| 15H-CC | | B | | | | | | | | | | | | | | | | | |
| 16H-CC | NN19 | R | M-G | | | | | | | | | | | *R* | | | | | |
| 17H-CC | | R | M | R | | | | | | R | | | | | | | | | Etching in *Coccolithus pelagicus* |
| 18H-CC | | F | M | F | | | | | | | | | | | | | | | Etching in *Coccolithus pelagicus* |
| 19H-CC | | B | | | | | | | | | | | | | | | | | |
| 20H-CC | | B | | | | | | | | | | | | | | | | | |
| 21H-CC | | R | P | R | | | | | | | | | | | | | | | Extreme etching in *Coccolithus pelagicus* |
| 22H-CC | | R | P | | | | | | | | | | | | | | | | |
| 323-U1343C- | | | | | | | | | | | | | | | | | | | |
| 1H-CC | | R | M-G | R | | | | | | | | | | | | | | | |
| 2H-CC | | B | | | | | | | | | | | | | | | | | |
| 3H-CC | | B | | | | | | | | | | | | | | | | | |
| 4H-CC | | B | | | | | | | | | | | | | | | | | |
| 5H-CC | | R | P | | | | | | | | | | | | | | | | |

**Table T3 (continued).** (Continued on next page.)

| Core, section, interval (cm) | Martini (1971) zone | Abundance | Preservation | *Coccolithus pelagicus* | *Cyclococcolithus leptoporus* | *Cyclococcolithus leptoporus* (small) | *Dictyococcites* spp. (small) | *Dictyococcites* spp. (medium) | *Emiliania huxleyi* | *Gephyrocapsa* (small) | *Gephyrocapsa* (medium) | *Gephyrocapsa* (large) | *Pseudoemiliania lacunosa* | *Reticulofenestra minuta* | *Reticulofenestra minutula* | *Reticulofenestra pseudoumbilica* (5–7 µm) | *Reticulofenestra pseudoumbilica* (>7 µm) | Other taxa | Comments |
|---|---|---|---|---|---|---|---|---|---|---|---|---|---|---|---|---|---|---|---|
| 6H-CC | | B | | | | | | | | | | | | | | | | | |
| 7H-CC | | B | | | | | | | | | | | | | | | | | |
| 8H-3, 25 | | A | M-G | A | F | R | | | | F | | | | | | | | | Etching and overgrowth in specimens present in sample |
| 8H-CC | | R | M-G | R | | R | | | | | | | | | | | | | |
| 9H-CC | | R | M-G | | | | | | | R | | | | | | | | | |
| 10H-CC | | A | G | A | | | | | | A | R | | | | | | | *Syracosphaera* spp. | Medium *Gephyrocapsa* is *Gephyrocapsa muellerae* |
| 11H-CC | | B | | | | | | | | | | | | | | | | | |
| 12H-CC | | B | | | | | | | | | | | | | | | | | |
| 13H-CC | | B | | | | | | | | | | | | | | | | | |
| 14H-CC | | F | M-G | | | | | | | F | R | | | | | | | | |
| 15H-CC | | A | M | F | | | | | | D | A | | | | | | | | Severe etching, small pieces might be fragments, >15 coccoliths per FOV |
| 16H-CC | | — | | | | | | | | | | | | | | | | | No recovery |
| 17H-CC | | R | M-G | R | | | | | | | | | | | | | | | |
| 18H-CC | | B | | | | | | | | | | | | | | | | | |
| 19H-CC | | R | M-G | | | | | | | R | | | | | | | | | |
| 20H-CC | | B | | | | | | | | | | | | | | | | | |
| 21H-CC | | B | | | | | | | | | | | | | | | | | |
| 22H-CC | | B | | | | | | | | | | | | | | | | | |
| 23H-CC | | B | | | | | | | | | | | | | | | | | |
| 24H-CC | | B | | | | | | | | | | | | | | | | | |
| 25H-CC | | B | | | | | | | | | | | | | | | | | |
| 26H-CC | | B | | | | | | | | | | | | | | | | | |
| 323-U1343E- | | | | | | | | | | | | | | | | | | | |
| 1H-CC | | F | M | F | | | | | | | | | | | | | | | |
| 2H-CC | | B | | | | | | | | | | | | | | | | | |
| 3H-CC | | R | P | R | | | | | | | | | | | | | | | |
| 4H-CC | | R | M-G | R | | | | | | R | | | | | | | | | |
| 5H-CC | | B | | | | | | | | | | | | | | | | | |
| 6H-CC | | R | M-G | R | | | | | | R | | | | | | | | | |
| 7H-CC | | F | M | F | | R | | | | R | R | | | | | | | | |
| 8H-CC | | B | | | | | | | | | | | | | | | | | Small acicular or tubular minerals with low birefringence |
| 9H-CC | | R | M-G | R | | | | | | R | | | | | | | | | |
| 10H-CC | | R | M-G | | | | | | | R | R | | | | | | | | |
| 11H-CC | | R | M-G | | | | | | | | R | | | | | | | | |
| 12H-CC | | F | P | F | F | | | | | R | R | | | | | | | | Small acicular minerals, low birefringence, ~3 µm long × 0.5 µm wide |
| 13H-CC | | — | | | | | | | | | | | | | | | | | No recovery |
| 14H-CC | | R | M | R | | | | | | R | R | | | | | | | | Small acicular minerals |
| 15H-CC | | R | M-G | | | | | | | R | R | | | | | | | | Small acicular minerals |

**Table T3 (continued).** (Continued on next page.)

| Core, section, interval (cm) | Martini (1971) zone | Abundance | Preservation | *Coccolithus pelagicus* | *Cyclococcolithus leptoporus* | *Cyclococcolithus leptoporus* (small) | *Dictyococcites* spp. (small) | *Dictyococcites* spp. (medium) | *Emiliania huxleyi* | *Gephyrocapsa* (small) | *Gephyrocapsa* (medium) | *Gephyrocapsa* (large) | *Pseudoemiliania lacunosa* | *Reticulofenestra minuta* | *Reticulofenestra minutula* | *Reticulofenestra pseudoumbilica* (5–7 µm) | *Reticulofenestra pseudoumbilica* (>7 µm) | Other taxa | Comments |
|---|---|---|---|---|---|---|---|---|---|---|---|---|---|---|---|---|---|---|---|
| 16H-CC | | R | M-G | R | | | | | | | | | | | | | | | |
| 17H-CC | | B | | | | | | | | | | | | | | | | | |
| 18H-CC | | B | | | | | | | | | | | | | | | | | Reworked specimen *Sphenolithus moriformis* (Miocene) |
| 19H-CC | | R | M-G | | | | | | | R | | | | | | | | | Reworked specimen (*Dictyococcites* sp.; possibly pre-Miocene) |
| 20H-CC | | B | | | | | | | | | | | | | | | | | Small acicular and tubular minerals |
| 21H-CC | | B | | | | | | | | | | | | | | | | | |
| 22H-1, 117 | | A | M-G | A | | | | | | D | C | | | | | | | | |
| 22H-3, 75 | | B | | | | | | | | | | | | | | | | | |
| 22H-CC | | B | | | | | | | | | | | | | | | | | |
| 23H-CC | | B | | | | | | | | | | | | | | | | | |
| 24H-CC | | B | | | | | | | | | | | | | | | | | |
| 25H-CC | | B | | | | | | | | | | | | | | | | | |
| 26H-CC | | B | | | | | | | | | | | | | | | | | |
| 27H-CC | | B | | | | | | | | | | | | | | | | | |
| 28H-CC | | B | | | | | | | | | | | | | | | | | |
| 29H-CC | | B | | | | | | | | | | | | | | | | | Reworked specimens (unidentified) |
| 30H-CC | | B | | | | | | | | | | | | | | | | | |
| 31H-CC | | B | | | | | | | | | | | | | | | | | |
| 32H-CC | | B | | | | | | | | | | | | | | | | | |
| 33H-CC | | B | | | | | | | | | | | | | | | | | |
| 34H-CC | | B | | | | | | | | | | | | | | | | | |
| 35H-CC | | R | M-G | R | | | | | | | R | | | | | | | | Reworked specimens (unidentified) |
| 36H-CC | | B | | | | | | | | | | | | | | | | | |
| 37H-CC | | B | | | | | | | | | | | | | | | | | |
| 38H-CC | | B | | | | | | | | | | | | | | | | | |
| 39H-CC | | B | | | | | | | | | | | | | | | | | |
| 41H-CC | | R | G | | | R | | | | | | | | | | | | | Reworked specimens (unidentified) |
| 43X-CC | | R | M-G | | | | R | | | | | | | | | | | | Reworked specimens (unidentified) |
| 45X-CC | | R | M-G | | | R | | | | | | | | | | | | | Reworked specimens (unidentified) |
| 47HCC | | B | | | | | | | | | | | | | | | | | |
| 49H-CC | | B | | | | | | | | | | | | | | | | | |
| 51X-CC | | B | | | | | | | | | | | | | | | | | Reworked specimens (unidentified) |
| 53X-CC | | B | | | | | | | | | | | | | | | | | |
| 55H-CC | | B | | | | | | | | | | | | | | | | | |
| 57X-CC | | B | | | | | | | | | | | | | | | | | |
| 59X-CC | | B | | | | | | | | | | | | | | | | | |
| 61X-CC | | B | | | | | | | | | | | | | | | | | |
| 63X-CC | | B | | | | | | | | | | | | | | | | | |
| 65X-CC | | B | | | | | | | | | | | | | | | | | |

**Table T3 (continued).**

| Core, section, interval (cm) | Martini (1971) zone | Abundance | Preservation | *Coccolithus pelagicus* | *Cyclococcolithus leptoporus* | *Cyclococcolithus leptoporus* (small) | *Dictyococcites* spp. (small) | *Dictyococcites* spp. (medium) | *Emiliania huxleyi* | *Gephyrocapsa* (small) | *Gephyrocapsa* (medium) | *Gephyrocapsa* (large) | *Pseudoemiliania lacunosa* | *Reticulofenestra minuta* | *Reticulofenestra minutula* | *Reticulofenestra pseudoumbilica* (5–7 µm) | *Reticulofenestra pseudoumbilica* (>7 µm) | Other taxa | Comments |
|---|---|---|---|---|---|---|---|---|---|---|---|---|---|---|---|---|---|---|---|
| 67X-CC | | B | | | | | | | | | | | | | | | | | |
| 69X-CC | | B | | | | | | | | | | | | | | | | | Acicular minerals, low birefringence, >5 µm long |
| 71X-CC | | B | | | | | | | | | | | | | | | | | Small high birefringence minerals (dolomite?) |
| 73X-CC | | F | M | F | | | | | | | | | | | | | | | Etching in *Coccolithus pelagicus*. Lots of small tubular low birefringence minerals |
| 75X-CC | | B | | | | | | | | | | | | | | | | | |
| 77X-CC | | B | | | | | | | | | | | | | | | | | |
| 79X-CC | | B | | | | | | | | | | | | | | | | | |
| 81X-CC | | B | | | | | | | | | | | | | | | | | |
| 83X-CC | | B | | | | | | | | | | | | | | | | | |

Notes: Abundance: D = dominant, A = abundant, C = common, F = few, R = rare, B = barren. Preservation: G = good, M = moderate, P = poor. FOV = field of view.

**Table T4**. Planktonic foraminifer range chart, Holes U1343A, U1343B, U1343C, U1343D, and U1343E. (See table notes.) (Continued on next two pages.)

| Core, section, interval (cm) | Abundance | Preservation | *Globigerina bulloides* | *Globigerina umbilicata* | *Neogloboquadrina atlantica* (sin) | *Neogloboquadrina pachyderma* (dex) | *Neogloboquadrina pachyderma* (sin) | *Turborotalia quinqueloba* | Other observations |
|---|---|---|---|---|---|---|---|---|---|
| 323-U1343A- | | | | | | | | | |
| Mudline | F | G | R | P | | P | F | | Dominant diatoms, few siliciclastics, rare sponge spicules |
| 1H-CC | F | G | | | | | F | | Dominant siliciclastics, rare bubblewalled glass shards |
| 2H-CC | A | G | R | | | P | A | | Dominant siliciclastics, few diatoms |
| 3H-CC | F | G | | | | R | F | | Dominant siliciclastics, rare diatoms |
| 4H-CC | R | G | | | | | R | | Dominant siliciclastics, rare diatoms |
| 5H-CC | F | G | R | | | R | F | | Dominant siliciclastics |
| 6H-CC | F | G | | | | R | F | | Dominant siliciclastics |
| 7H-CC | R | G | R | | | | | | Dominant siliciclastics |
| 8H-4, 55–57 | D | P | F | | | P | D | | Yellow foraminiferal tests |
| 8H-CC | A | G | F | | | P | F | | Pyrite tubes, mica |
| 9H-CC | A | M | A | | | | R | | Yellow foraminiferal tests, pyrite |
| 10H-6, 52–54 | F | P | F | | | | | | Yellow foraminiferal tests |
| 10H-CC | P | G | P | P | | | | | Pyrite, fragments of wood? |
| 11H-CC | A | G | F | | | | A | | Pyrite, mica |
| 12H-7, 35–37 | B | | | | | | | | Benthic foraminiferal ooze, abundant sponge spicules, fish teeth |
| 12H-CC | R | G | R | | | | P | | Pyrite, mica |
| 13H-CC | F | G | | | | | F | | Pyrite, fragments of wood? |
| 14H-CC | F | G | | P | | | F | | Pyrite, fragments of wood? |
| 15H-CC | A | G | A | P | | P | A | | Pyrite |
| 16H-CC | F | G | F | | | | F | | Pyrite, mica |
| 17H-CC | A | G | R | | | P | A | | Dominant siliciclastics, bivalve fragments, and *Scaphander* sp.? |
| 18H-CC | R | M | | | | | R | | Dominant siliciclastics |
| 19H-CC | A | G | R | | | P | A | | Dominant siliciclastics |
| 20H-CC | F | G | P | | | R | F | | Dominant siliciclastics |
| 21H-CC | P | G | | | | | P | | Dominant siliciclastics |
| 22H-CC | F | G | | | | P | F | | Dominant siliciclastics |
| 323-U1343B- | | | | | | | | | |
| Mudline | R | VG | | | | | R | | |
| 1H-CC | A | G | R | | | P | A | | Dominant rock fragments |
| 2H-CC | R | G | R | | | | P | | Abundant pyrite tubes, mica |
| 3H-CC | F | G | | | | | F | | Abundant pyrite tubes, mica |
| 4H-CC | | | R | | | P | F | | Mica |
| 323-U1343C- | | | | | | | | | |
| Mudline | P | G | P | | | | P | | Dominant diatoms, few siliciclastics, rare sponge spicules |
| 1H-CC | A | G | F | | | | A | | Dominant siliciclastics |
| 2H-CC | F | G | P | | | | F | | Dominant siliciclastics |
| 3H-CC | B | | | | | | | | Dominant siliciclastics, rare diatoms |
| 4H-CC | A | G | F | | | | A | | Dominant siliciclastics, rare diatoms |
| 5H-CC | A | M | A | | | | A | | Dominant siliciclastics, rare diatoms |
| 6H-CC | R | G | R | | | | | | Dominant siliciclastics, rare diatoms |
| 7H-CC | B | | | | | | | | Dominant siliciclastics, rare diatoms |
| 8H-CC | A | G | P | | | | A | | Pyrite tubes, yellow foraminifers |
| 9H-CC | F | G | F | | | | R | | Pyrite tubes |
| 10H-CC | B | | | | | | | | Pyrite tubes |
| 11H-CC | | | R | P | | | R | | Pyrite tubes |
| 12H-CC | A | G | R | | | | A | | Dominant siliciclastics, mica, pyrite |
| 13H-CC | A | M | P | | | | A | | Dominant siliciclastics, pyrite |
| 14H-CC | F | G | | | | | F | | Dominant siliciclastics, pyrite |
| 15H-CC | D | M | R | R | | | D | | Dominant siliciclastics, pyrite |
| 16H-CC | | | | | | | | | |
| 17H-CC | R | G | R | | | P | | | Dominant siliciclastics, mica, pyrite |
| 18H-CC | A | G | R | | | | A | | Dominant siliciclastics, mica, pyrite |
| 19H-CC | A | G | A | | | P | P | | Dominant siliciclastics, mica, pyrite |
| 20H-CC | A | G | F | | | F | A | | Dominant siliciclastics, mica, pyrite |
| 21H-CC | P | M | P | | | | | | Dominant siliciclastics, mica, pyrite |

**Table T4 (continued).** (Continued on next page.)

| Core, section, interval (cm) | Abundance | Preservation | *Globigerina bulloides* | *Globigerina umbilicata* | *Neogloboquadrina atlantica* (sin) | *Neogloboquadrina pachyderma* (dex) | *Neogloboquadrina pachyderma* (sin) | *Turborotalia quinqueloba* | Other observations |
|---|---|---|---|---|---|---|---|---|---|
| 22H-CC | F | M | F | | | | R | | Dominant siliciclastics, mica, pyrite |
| 23H-CC | R | M | P | | | | R | | Dominant siliciclastics, pyrite |
| 24H-CC | B | | | | | | | | Abundant siliciclastics, rare pyrite |
| 25H-CC | F | M | | | | P | F | | Dominant siliciclastics, rare diatoms |
| 26H-CC | R | M | | | | | R | | Dominant siliciclastics, rare diatoms |
| 323-U1343D- | | | | | | | | | |
| Mudline | A | VG | R | | | P | A | | Dominant diatoms |
| 1H-CC | F | G | R | | | R | F | | Dominant siliciclastics, rare diatoms, large 1 cm pumice fragment |
| 323-U1343E- | | | | | | | | | |
| Mudline | P | G | P | | | | P | | Mica |
| 1H-CC | D | M | R | | | | D | | Dominant siliciclastics |
| 2H-CC | R | M | | | | | R | | Dominant siliciclastics |
| 3H-CC | R | M | | | | | R | | Dominant siliciclastics, abundant diatoms |
| 4H-CC | D | M | F | | | | A | | Pyrite tubes, yellow foraminiferal tests |
| 5H-CC | P | P | P | | | | | | Pyrite tubes, yellow foraminiferal tests |
| 6H-CC | A | M | R | | | | A | | Few yellow foraminiferal tests, dominant siliciclastics, few diatoms |
| 7H-CC | D | P | A | | | R | D | | Pyrite tubes, yellow foraminiferal tests |
| 8H-CC | A | M | R | | | | A | | Pyrite tubes, yellow foraminiferal tests |
| 9H-CC | A | G | R | | | | A | | Pyrite tubes |
| 10H-CC | A | M | F | | | | A | | Pyrite tubes |
| 11H-CC | F | G | P | | | | F | | Dominant siliciclastics, pyrite tubes |
| 12H-CC | D | M | A | | | | D | | Pyrite tubes, yellow foraminiferal tests |
| 13H -CC | | NA | | | | | | | |
| 14H-CC | D | M | F | P | | | D | | Pyrite tubes, yellow foraminiferal tests |
| 15H-CC | F | M | P | | | | F | | Mica, wood fragments? |
| 16H-CC | A | G | P | | | P | A | | Dominant siliciclastics, few diatoms |
| 17H-CC | P | M | | | | | P | | Dominant siliciclastics, pyrite |
| 18H-CC | F | G | R | | | | F | | Dominant siliciclastics, abundant diatoms, pyrite, large rock fragments >5 mm |
| 19H-CC | A | G | F | R | | R | A | | Dominant siliciclastics, abundant diatoms, pyrite |
| 20H-CC | D | M | R | | | R | D | | Yellow foraminifers, dominant siliciclastics, abundant diatoms, pyrite, large rock fragment >5 mm |
| 21H-CC | R | M | P | | | | R | | Yellow foraminifers, dominant siliciclastics, abundant diatoms, pyrite |
| 22H-CC | F | M | P | | | F | R | | Abundant yellow foraminifers, dominant siliciclastics |
| 23H-CC | A | G | | | | | A | | Dominant siliciclastics |
| 24H-CC | A | G | F | | | R | A | | Dominant siliciclastics |
| 25H-CC | F | G | | | | | F | | Yellow foraminifers, dominant siliciclastics |
| 26H-CC | F | G | R | | | R | F | | Bubblewalled glass shards |
| 27H-CC | F | M | R | | | P | F | | Mica |
| 28H-CC | F | G | F | | | R | | | Pyrite tubes, mica |
| 29H-CC | R | G | R | | | P | P | | Pyrite tubes, mica, fragments of wood? |
| 30H-CC | R | G | | | | | R | | Pyrite tubes, mica |
| 31H-CC | R | G | R | | | R | | | Mica |
| 32H-CC | R | G | R | | | | | | Pyrite tubes, mica |
| 33H-CC | R | M | R | | | | | | Pyrite tubes, mica |
| 34H-CC | F | M | F | | | R | | | Pyrite tubes |
| 35H-CC | B | | | | | | | | |
| 36H-CC | D | G | D | P | | A | F | | Mica |
| 37H-CC | R | G | P | | | | R | | Dominant siliciclastics, pyrite, mica, fragments from bivalves |
| 38H-CC | P | G | P | | | | | | Pyrite, fragments of wood? |
| 39H-CC | B | | | | | | | | |
| 40H-CC | F | M | F | | | F | | | Pyrite |
| 41H-CC | B | | | | | | | | |
| 42X-CC | R | M | | | | R | | | Yellow foraminifers, abundant siliciclastics |
| 43X-CC | P | M | P | | | | | | Abundant siliciclastics, mica, pyrite |
| 44X-CC | R | M | P | | R | R | | | Abundant siliciclastics, mica, pyrite |
| 45X-CC | R | M | R | | | R | | | Abundant siliciclastics, mica, pyrite |
| 46X-CC | A | M | R | | R | A | | | Abundant siliciclastics, mica, pyrite |
| 47X-CC | A | M | R | | P | A | | | Abundant siliciclastics, mica, pyrite |
| 48X-CC | B | | | | | | | | |

**Table T4 (continued).**

| Core, section, interval (cm) | Abundance | Preservation | *Globigerina bulloides* | *Globigerina umbilicata* | *Neogloboquadrina atlantica* (sin) | *Neogloboquadrina pachyderma* (dex) | *Neogloboquadrina pachyderma* (sin) | *Turborotalia quinqueloba* | Other observations |
|---|---|---|---|---|---|---|---|---|---|
| 49X-CC | B | | | | | | | | |
| 50X-CC | B | | | | | | | | |
| 51X-CC | B | | | | | | | | |
| 52X-CC | R | G | | | | R | | | Abundant siliciclastics |
| 53X-CC | R | G | | | | R | | | Abundant siliciclastics |
| 54X-CC | R | G | | | | R | | | Abundant siliciclastics |
| 55X-CC | B | | | | | | | | |
| 56X-CC | B | | | | | | | | Abundant siliciclastics |
| 57X-CC | B | | | | | | | | Abundant siliciclastics |
| 58X-CC | B | | | | | | | | Abundant siliciclastics |
| 59X-CC | B | | | | | | | | Abundant siliciclastics |
| 60X-CC | F | G | F | | | | | | Abundant siliciclastics |
| 61X-CC | B | | | | | | | | Dominant siliciclastics, pyrite |
| 62X-CC | B | | | | | | | | Dominant siliciclastics, pyrite |
| 63X-CC | B | | | | | | | | Dominant siliciclastics, pyrite |
| 64X-CC | R | M | R | | | R | | | Dominant siliciclastics |
| 65X-CC | P | M | P | | | P | | | Dominant siliciclastics |
| 66X-CC | B | | | | | | | | Dominant siliciclastics |
| 67X-CC | R | M | R | | | R | | | Dominant siliciclastics, pyrite, yellow tests |
| 68X-CC | P | M | | | | P | | | Dominant siliciclastics, pyrite, yellow tests |
| 69X-CC | R | M | R | | | R | | | Dominant siliciclastics, pyrite, brown tests |
| 70X-CC | P | M | P | | | | | | Dominant siliciclastics, pyrite |
| 71X-CC | P | G | P | | | | | | Dominant siliciclastics, pyrite |
| 72X-CC | R | M | | | | R | | | Dominant siliciclastics, pyrite |
| 73X-CC | F | G | F | | | | | | Dominant siliciclastics, pyrite, yellow tests |
| 74X-CC | B | | | | | | | | |
| 75X-CC | B | | | | | | | | |
| 76X-CC | B | | | | | | | | |
| 77X-CC | B | | | | | | | | |
| 78X-CC | R | G | R | | | R | | | Dominant siliciclastics, pyrite |
| 79X-CC | | | P | P | | | | | |
| 80X-CC | B | | | | | | | | Dominant siliciclastics, pyrite |
| 81X-CC | B | | | | | | | | |
| 82X-CC | B | | | | | | | | |
| 82X-6 | A | P | A | | | | | | |
| 83X-CC | B | | | | | | | | |

Notes: Abundance: D = dominant, A = abundant, F = few, P = present, R = rare, B = barren. Preservation: VG = very good, G = good, M = moderate, P = poor, B = barren, NA = not applicable. Dex = dextral, sin = sinistral.

**Table T5**. Benthic foraminifer range chart, Holes U1343A and U1343B. (See table notes.)

| Core, section, interval (cm) | Abundance | Preservation | *Brizalina* cf. *spathula* | *Brizalina earlandi* | *Brizalina pygmaea* | *Bulimina* aff. *exilis* | *Bulimina* aff. *mexicana* | *Bulimina* sp. | *Cassidulina laevigata* var. *carinata* | *Cassidulina* sp. | *Cassidulinoides tenuis* | *Cibicidoides* cf. *subhaidingeri* | *Dentalina* sp. | *Eggerella bradyi* | *Elphidium* cf. *batialis* | *Elphidium* sp. | *Epistominella pulchella* | *Fissurina* sp. | *Fursenkoina* sp. | *Glandulina* sp. | *Globobulimina auriculata* | *Globobulimina pacifica* | *Islandiella norcrossi* | *Nodosaria* aff. *pyrula* | *Nodosaria* sp. | *Nonionella labradorica* | *Nonionella turgida* | *Nonionella turgida digitata* | *Planulina ariminensus* | *Procerolagena* cf. *gracillima* | *Pullenia bulloides* | *Pullenia* sp. | *Pygmaeistron* cf. *hispida* | *Pyrgo* sp. | *Reophax dentaliniformis* | *Rhabdammina* sp. | *Stainforthia* aff. *fusiformis* | *Triloculina* cf. *trihedra* | *Triloculina* sp. | *Uvigerina auberiana* | *Uvigerina* cf. *peregrina* | *Uvigerina* cf. *proboscidea* | *Valvulineria* sp. | Undifferentiated agglutinate | Siliciclastics | Other observations |
|---|---|---|---|---|---|---|---|---|---|---|---|---|---|---|---|---|---|---|---|---|---|---|---|---|---|---|---|---|---|---|---|---|---|---|---|---|---|---|---|---|---|---|---|---|
| 323-U1343A- | | | | | | | | | | | | | | | | | | | | | | | | | | | | | | | | | | | | | | | | | | | | | |
| Mudline | F | G | P | R | P | R | | P | | F | | | | | P | | | | | | R | | P | | | R | | R | | | | | P | | | | P | | | R | | P | F | Dominant diatoms, rare sponge spicules |
| 1H-CC | A | G | | | | F | | | | | P | | | | R | | | | | | F | | A | | | R | | P | P | | P | | P | | | | P | | R | P | P | | D | Dominant rock fragments, rare bubble-filled glass shards |
| 2H-CC | A | G | | | | | | | | | | | | | P | | | | | | F | | A | | | | | | | | | | | | | | | | R | | P | | D | Dominant rock fragments, few diatoms |
| 3H-CC | G | G | | | | | | | | | | | | | A | | | | | | R | | F | | | R | | P | | | P | | | | | | | | | | | D | Dominant rock fragments, rare diatoms |
| 4H-CC | A | G | | | | | | | | | | | | | A | | | | | | R | | | | | A | | | | | | | R | | | | | | | | | | D | Dominant rock fragments, rare diatoms |
| 5H-CC | A | G | | P | | R | | | | | R | | | | A | | | | | | R | | F | | | R | | | | | | | | | | | | | A | | | R | D | Dominant rock fragments |
| 6H-CC | F | G | | | | R | | | | | | | | | F | | | | | | R | | R | | | | | | | | P | | | | | | P | | | | | | D | Dominant rock fragments |
| 7H-CC | F | G | | | | P | | | | P | | | | F | P | | | | | | | | P | | | P | | | | | P | | | | | | R | | | | R | | D | Dominant rock fragments |
| 8H-4, 55–57 | A | M | | | | D | | | | | F | | | | R | | | | | | | A | | P | | F | | | | | | | | | | | | | R | | P | | R | Yellow foraminifers |
| 8H-CC | F | G | | | | | | | | | | | | | | | | | | | | | P | | | | | | | | | | | | | | | | F | | | | D | Abundant pyrite tubes, mica |
| 9H-CC | A | M | | P | | F | | | | | A | | | | | | | | | | | F | A | | | R | | P | | | | | | | | | | | F | R | | | D | Yellow pyrite tubes |
| 10H-6, 52–54 | A | P | | | | F | | | | | F | | | | A | | | | | | | A | F | | | F | | | | | | P | | | | | | | R | P | | P | A | Yellow foraminifers |
| 10H-CC | A | G | | | | A | | | | | F | | | | F | | | | | | | F | R | | | R | R | | | P | | | | | | | | | A | | | P | D | Wood, pyrite tubes |
| 11H-CC | F | G | | | | | | | | | P | | | | F | | | | | | | | R | | | R | | | | | | | | | | | | | | | | | D | Abundant pyrite tubes, mica |
| 12H-7, 35–37 | D | G | | A | | D | | | | | | | | | | | | | | | | A | | | | F | | | | | | | | | | | | | | | | | D | Benthic ooze, fish teeth, spicules |
| 12H-CC | A | G | | | | R | | | R | | R | | | | A | | | | | | | F | | | | P | | | | | | | | | | | | | | | | | D | Abundant pyrite tubes, mica |
| 13H-CC | A | G | | | | F | | | | | | | | | R | | | | | | | R | | | | P | | | | | | | | | | | | | | | | P | D | Wood, pyrite tubes |
| 14H-CC | A | G | | | | F | | | | | F | | | | A | | | | | | | R | F | | | F | | | | | | | | | | | | P | | R | | | D | Wood, pyrite tubes |
| 15H-CC | A | G | | | | P | | | | | R | | P | | R | | | | | | | | A | P | | | | | | | F | | | | | | | | | | | | D | Pyrite |
| 16H-CC | A | G | | | | | | | | | R | | | | A | | | | | | | R | F | | | F | | | | | F | | | | | | | | | | | | D | Abundant pyrite tubes, mica |
| 17H-CC | A | G | | P | | A | | P | | | P | P | | | R | P | | | R | | | R | A | | | | | | | | | | P | | | | | | | R | | P | D | Dominant rock fragments, bivalve fragments, and *Scaphander* sp.? |
| 18H-CC | A | G | | | | A | | | | | | F | P | | R | | | | | | | R | R | | | R | | | | | | P | | | | | | | F | | | D | Dominant rock fragments |
| 19H-CC | A | G | | | | A | | | | | R | | P | | A | | | P | | R | | R | R | | | R | | | | | | P | | | | P | | | P | | | D | Dominant rock fragments |
| 20H-CC | D | G | | P | | D | | | | | P | | | | R | | | | | | | F | P | | | R | | | | | | | | | | | | | P | P | | | D | Dominant rock fragments |
| 21H-CC | R | M | | | | R | | | | | P | | | | R | | | | | P | | R | P | | | R | | | R | | | | | | | | | | | | | | D | Dominant rock fragments |
| 22H-CC | F | G | | P | | | | | | | P | | | | F | | | | | | | | | | | R | | | | | | | | | | | | | | A | A | | D | |
| 323-U1343B- | | | | | | | | | | | | | | | | | | | | | | | | | | | | | | | | | | | | | | | | | | | | | |
| Mudline | A | VG | | | | F | | | | | P | | | | | | | | | | P | R | | | P | F | | A | | | | | | P | R | | | | | P | | | F | |
| 1H-CC | A | G | | P | | F | | | R | | R | P | | | A | | P | | | | | F | A | | | | F | | | | | | | | | | P | P | P | P | P | | F | Dominant rock fragments |
| 2H-CC | F | G | | | | | | | P | P | | | | | P | | | | | | | F | P | | | | | | | | | | | | | | P | R | | | P | | A | Abundant pyrite tubes, mica |
| 3H-CC | D | G | | | | | | | | | | | | | D | | | | | | | F | A | | | R | | P | | | P | | | | | | P | | | | | | D | Abundant pyrite tubes, mica |
| 4H-CC | A | G | | | | R | P | | | | P | | | | A | | | | | | | P | | | | R | | F | | | | | | | | | | F | F | | | | D | Mica |

Notes: Abundance: D = dominant, A = abundant, F = few, R = rare, P = present. Preservation: VG = very good, G = good, M = moderate.

**Table T6**. Benthic foraminifer range chart, Holes U1343C and U1343D. (See table notes.)

| Core, section | Abundance | Preservation | *Brizalina* cf. *spathula* | *Brizalina earlandi* | *Bulimina* aff. *exilis* | *Cassidulina laevigata* var. *carinata* | *Cassidulina* sp. | *Cassidulinoides tenuis* | *Cibicidoides* cf. *subhaidingeri* | *Cibicidoides* sp. | *Cribrostomoides subglobosus* | *Eggerella bradyi* | *Elphidium* cf. *batialis* | *Epistominella pulchella* | *Fissurina* sp | *Glandulina* sp. | *Globobulimina auriculata* | *Globobulimina pacifica* | *Globocassidulina* sp. | *Gyroidinoides soldanii* | *Islandiella norcrossi* | *Lagena* sp. | *Lenticulina* sp. | *Nodosaria* sp. | *Nonionella labradorica* | *Nonionella turgida digitata* | *Procerolagena* cf. *gracillima* | *Pullenia* sp. | *Pyrgo* sp. | *Rhabdammina* sp. | *Trifoculina* cf. *trihedra* | *Trifoculina* sp. | *Uvigerina auberiana* | *Uvigerina* cf. *peregrina* | *Valvulineria* sp. | Siliciclastics | Other observations |
|---|---|---|---|---|---|---|---|---|---|---|---|---|---|---|---|---|---|---|---|---|---|---|---|---|---|---|---|---|---|---|---|---|---|---|---|---|
| 323-U1343C- | | | | | | | | | | | | | | | | | | | | | | | | | | | | | | | | | | | | | |
| Mudline | R | G | | P | R | | | | | | R | P | | | | | | R | P | | P | | | | R | P | P | | | | | | | P | P | | |
| 1H-CC | A | G | | | F | R | | | | | | | A | | | | | F | | | R | | | P | P | | | R | | | | P | R | | R | A | Mica |
| 2H-CC | F | G | | | | | | | | | | | | | | | | | | | F | | | | | | | | | | | | P | | P | A | Pyrite tubes, mica, rare glauconite |
| 3H-CC | A | G | | | | | | | | | | | F | | | | | F | | | P | | | | R | | | | | | | | | | A | Pyrite tubes, mica |
| 4H-CC | A | G | | | A | R | | | | | | | | | | | | A | | | P | | | | F | | | | | | | | A | F | A | Pyrite tubes, mica |
| 5H-CC | A | M | | | R | | | | | | | | | | | | | | | P | P | | | | P | | P | F | | | | | R | | A | Pyrite tubes, mica |
| 6H-CC | F | G | | | R | | | | | | | | R | P | | | | R | | | R | | | P | R | | | | | | | | | | D | Mica |
| 7H-CC | R | M | | | | | | R | | | | | | | | | | P | | | R | | P | | | | | | | | P | | | | D | |
| 8H-CC | A | G | | | R | | | P | | | | | D | | | | | A | | | A | | | | P | | | | | | | P | F | R | | F | Pyrite tubes, mica |
| 9H-CC | F | G | | | | | | R | | | | | F | | | | | P | | | F | | | | R | | | | | | | | F | P | | A | Pyrite tubes, mica |
| 10H-CC | F | G | | | R | | | P | | | | | F | | | | | R | | | | | | | | | | | | | | | F | P | | D | Mica |
| 11H-CC | A | G | | | F | | | P | | | | | F | | | | | R | | P | P | | | | | | | | | | | | A | | P | F | Pyrite tubes, mica |
| 12H-CC | A | M | | | F | | | | | | | | A | | P | | | P | | P | R | | | | | | | | | | | | P | R | P | D | Mica, pyrite |
| 13H-CC | F | M | | | R | | | R | | | | | | | | | | P | | | P | | | | | | | P | | | | | | | | F | Pyrite tubes, mica |
| 14H-CC | A | G | | | R | | | R | | | | | A | | P | | | | | | R | | | | | | | | | | | | | R | | D | Pyrite |
| 15H-CC | D | G | | | A | | | F | | | | | | P | | | | F | | | | | | P | A | | | | | | | | | | | F | Orange planktonic foraminifers |
| 16H-CC | | | | | | | | | | | | | | | | | | | | | | | | | | | | | | | | | | | | | |
| 17H-CC | R | G | | | | | | | | | | | | | | | | P | | | | | | | P | | | | | | | P | | R | | D | Pyrite tubes, mica |
| 18H-CC | A | G | | | R | | R | | | | | | A | | | P | | | | | A | | | | R | | | | | | | | | | | D | Mica, pyrite, diatoms |
| 19H-CC | F | G | | | F | R | | | | | | | R | | | | | | | | P | | P | P | R | | | | | | | | | | | D | Pyrite tubes, mica |
| 20H-CC | A | G | | | A | | | | P | | | | | P | | | | R | | | A | | | | R | | | | | | | | | F | | D | Mica, pyrite |
| 21H-CC | F | G | | | F | | | | | | | | F | P | | | | | | | | | | | R | | | | | | | | | | | D | Mica, pyrite |
| 22H-CC | F | M | | | P | | | P | | P | | | F | | | | | P | | | R | | | | | | | | | | | | | | | A | Mica, wood, pyrite |
| 23H-CC | D | M | | | R | | | A | | | | | D | | | | | A | | | P | | P | | F | | | | | | | | | | | D | Pyrite tubes |
| 24H-CC | B | | | | | | | | | | | | | | | | | | | | | | | | | | | | | | | | | | | D | Pyrite, mica |
| 25H-CC | F | M | | | | | | | | | | | F | | | | | | | | | | | | | | | | | | | | | P | | D | Pyrite |
| 26H-CC | R | M | | | | | | | | | | | | | | | | | | | R | | | | | | | | | | | | | | | D | Pyrite tubes |
| 323-U1343D- | | | | | | | | | | | | | | | | | | | | | | | | | | | | | | | | | | | | | |
| Mudline | A | G | P | F | A | | | | | | | | | | | | P | | | | | P | | | R | A | R | | | P | | | | | | D | |
| 1H-CC | F | G | | P | R | | | | | | | | F | | | | | F | | | F | P | | | | | P | | P | | | | F | | R | D | Large 1 cm pumice fragment |

Notes: Abundance: D = dominant, A = abundant, F = few, R = rare, P = present, B = barren. Preservation: G = good, M = moderate.

**Table T7**. Benthic foraminifer and ostracode range chart, Hole U1343E. (See table notes.) (Continued on next two pages.)

| Core, section | Abundance | Preservation | *Alabaminella weddellensis* | *Brizalina* cf. *spathula* | *Brizalina earlandi* | *Brizalina pygmaea* | *Bulimina* aff. *exilis* | *Bulimina* aff. *mexicana* | *Bulimina* sp. | *Cassidulina laevigata* var. *carinata* | *Cassidulina* sp. | *Cassidulinoides tenuis* | *Cibicidoides* cf. *subhaidingeri* | *Cibicidoides* sp. | *Dentalina* sp. | *Elphidium* cf. *batialis* | *Epistominella pulchella* | *Fissurina* sp | *Glandulina* sp. | *Globobulimina auriculata* | *Globobulimina pacifica* | *Globocassidulina* sp. | *Gyroidinoides soldanii* | *Islandiella norcrossi* | *Lagena* sp. | *Lenticulina* sp. | *Nodosaria* aff. *pyrula* | *Nodosaria* sp. | *Nonionella labradorica* | *Nonionella turgida digitata* | *Oridorsalis umbonatus* | *Planulina wuellerstorfi* | *Procerolagena* cf. *gracillima* | *Pullenia bulloides* | *Pullenia* sp. | *Pygmaeseistron* cf. *hispida* | *Pyrgo* sp. | *Quinqueloculina* sp. | *Reophax dentaliniformis* | *Triloculina* cf. *trihedra* | *Triloculina* sp. | *Uvigerina auberiana* | *Uvigerina* cf. *peregrina* | *Valvulineria* sp. | *Krithe* sp. | *Pseudocythere caudata* | Siliciclastics | Other observations |
|---|---|---|---|---|---|---|---|---|---|---|---|---|---|---|---|---|---|---|---|---|---|---|---|---|---|---|---|---|---|---|---|---|---|---|---|---|---|---|---|---|---|---|---|---|---|
| 323-U1343E- | | | | | | | | | | | | | | | | | | | | | | | | | | | | | | | | | | | | | | | | | | | | | |
| Mudline | A | G | | P | P | | P | | | | | | | | | R | | | | | F | | P | | | | A | P | | | | P | | P | | F | | | | | | F | Mica |
| 1H-CC | D | G | | | | | P | | | | | | | | | D | | | | | P | | A | | | | F | R | | | | | | | | | | | R | | | | D | Rare sponge spicules |
| 2H-CC | A | M | | | | | | | | | | | | | | A | | P | | | R | | R | | | | | | | | | | P | | | | | | | | | | D | |
| 3H-CC | A | M | | | | | | | | | | | | | | A | | P | | | R | | P | | | | P | | | | | | | | | | | | P | | | | D | Pyrite tubes |
| 4H-CC | A | M | | | | | P | | | F | | P | | | | P | | | | P | F | | F | | | | R | R | | | | | | | | | | | | | | | A | Pyrite tubes, yellow planktonic foraminifers |
| 5H-CC | D | G | P | | | | A | | | | | A | | | | F | | | | | D | | F | | | P | | | | | | | P | | P | | | | | P | | | | D | |
| 6H-CC | A | M | | | | | P | | | | | | | | | A | | | | | | | F | | | | | | | | | | P | | | | | | | P | | | | D | Pyrite tubes, mutants |
| 7H-CC | D | M | | | | | F | | | | P | A | | | | A | | | | | F | | | | | | F | P | | | | | F | | | | | | P | F | | P | P | F | Pyrite tubes, yellow foraminifers |
| 8H-CC | A | M | | | | | P | | P | | | | | | | F | | | | | F | | A | | | | F | P | | | | | R | | | | | P | A | | R | | A | Pyrite tubes, yellow foraminifers |
| 9H-CC | D | G | | | | | F | | | | | F | | | | D | | | | | A | | A | | | | F | | | | | | R | | | | | | F | R | R | | D | Pyrite tubes |
| 10H-CC | D | M | | | | | R | | | | | F | | | | P | | | | | P | | F | | | | P | | | | | | P | | | | | | D | | P | | D | Pyrite tubes |
| 11H-CC | A | G | | | | | | | | | | | | | | A | | | | | | | | | | | | | | | | | | | | | | | | | | | D | Sandy, some pyrite tubes |
| 12H-CC | D | G | | | | | R | | | | | A | | P | | F | | | | | F | | F | | | | R | | | | | | R | | | | | | F | A | | | D | Pyrite tubes, yellow foraminifers |
| 14H-CC | D | M | | | | | A | | | | | F | | | P | D | | | | | F | | F | | | | F | | | | | P | | F | | | | | | F | | | | F | Pyrite tubes, yellow foraminifers |
| 15H-CC | F | M | | | | | | | | | | | | | | R | | | | | F | | F | | | | F | | | | | | | | | | | | P | | | | | Wood, mica |
| 16H-CC | A | G | | | | | R | | | | P | R | | | P | A | | | | | | | D | | | | P | | | | | | P | | | | | | | R | | | D | Mica |
| 17H-CC | P | M | | | | | | | | | | | | | | P | | | | | | | | | | | | | | | | | | | | | | | | | | | D | Pyrite tubes, yellow foraminifers |
| 18H-CC | A | G | | | | | | | | | | P | | | | A | | | | | R | R | | | | | | R | | | | | | | | | | | P | | | | D | Large rock fragment, pyrite |
| 19H-CC | A | G | | | | | R | | | | | R | | P | | R | | P | | | R | | A | | | | | R | | | | | | | | | | | | P | | | | D | Pyrite |
| 20H-CC | A | G | | | P | | R | | | | | | | | | A | | | | | F | | P | | | | | A | | | | | | | | | | | | R | | | | D | Pyrite, yellow foraminifers, large rock fragment >5 mm |
| 21H-CC | F | M | | | | | R | | | | | | | | | F | | | | | | | R | | | | | | | | | | | | | | | | | | | | | D | Pyrite |
| 22H-CC | A | M | | | R | | A | | | | | P | | | | P | | | P | | | | A | | P | | | P | | | | P | | | | | | | | | | | | D | Pyrite, yellow foraminifers |
| 23H-CC | A | G | | | | | R | | | | | | | | | F | | | | | R | | A | | | | | R | | | | | | | | | | | | | | | | D | |
| 24H-CC | A | G | | | | | | | | | | | | | | R | | | | | | | P | | | | | A | | | | | | | | | | | | P | R | R | | D | |
| 25H-CC | D | G | | | P | | D | | | | | R | | | | R | | P | | | P | | F | P | P | | | | | | | | | | | | | | | | | | | D | Yellow foraminifers, pyrite |
| 26H-CC | A | G | | | | | | | P | | | R | | | | A | | | | | | | | | | | | | | | | | | | | | P | | | R | | | | D | Volcanic glass |
| 27H-CC | A | G | | | | | | | | | | | | | | A | | | | | | | R | | | | | | | | | | | | | | | P | | P | | | | D | Mica |
| 28H-CC | A | G | | | | | | | | | | R | | | | | | | | | | | A | | | | | R | | | | | | | | | | | | | P | | | D | Pyrite tubes, mica |
| 29H-CC | F | G | | | | | | | | | | R | | | | | | | P | | P | | F | | | | | P | | | | | | P | | | | | | | | | | D | Pyrite tubes, mica, wood |
| 30H-CC | R | G | P | | | | | | | | | R | | | | | | | | | | | | | | | | | | | P | | | | | | | | | | | | | | D | Pyrite tubes, mica |
| 31H-CC | A | G | | | | | | | | | | P | | | | A | | | | | | | R | | | | | | | | | | | | | | | | | | | | | D | Mica |
| 32H-CC | P | G | | | | | | | | | | | | | | | | | | P | P | | | | | | | | | | | | | | | | | | | | | | | D | Pyrite tubes, mica |
| 33H-CC | F | G | | | | | | | | | | F | | | | R | | | | | | | | | | | | P | | | | | | P | | | | | | R | | | | D | Pyrite tubes, mica |
| 34H-CC | F | G | P | | | | | | | | | P | | | | | | | | | | | P | | | | | R | | | | | | | | | | | P | | | | R | Pyrite tubes |
| 35H-CC | A | M | | | | | | | | | | | | | | A | | | | | | | | | | | | | | | | | | | | | | | | P | R | | | A | |
| 36H-CC | F | P | | | | | | | | | | R | | | | P | | | | | | | | | | | P | P | | P | | | | | | | | | | | | | | D | Mica |
| 37H-CC | A | G | | | | | | | | | | A | R | | | | | | | | | | F | | | | | | | | | | | | | | | | | | | | | D | Pyrite, mica, fragments from bivalves |
| 38H-CC | A | G | | | | | P | | | | | A | | | | A | | | | | P | | F | | | | | | | | P | | | | | | | | | | | | D | Pyrite, wood |

**Table T7 (continued).** (Continued on next page.)

| Core, section | Abundance | Preservation | *Alabaminella weddellensis* | *Brizalina* cf. *spathula* | *Brizalina earlandi* | *Brizalina pygmaea* | *Bulimina* aff. *exilis* | *Bulimina* aff. *mexicana* | *Bulimina* sp. | *Cassidulina laevigata* var. *carinata* | *Cassidulina* sp. | *Cassidulinoides tenuis* | *Cibicidoides* cf. *subhaidingeri* | *Cibicidoides* sp. | *Dentalina* sp. | *Elphidium* cf. *batialis* | *Epistominella pulchella* | *Fissurina* sp | *Glandulina* sp. | *Globobulimina auriculata* | *Globobulimina pacifica* | *Globocassidulina* sp. | *Gyroidinoides soldanii* | *Islandiella norcrossi* | *Lagena* sp. | *Lenticulina* sp. | *Nodosaria* aff. *pyrula* | *Nodosaria* sp. | *Nonionella labradorica* | *Nonionella turgida digitata* | *Oridorsalis umbonatus* | *Planulina wuellerstorfi* | *Procerolagena* cf. *gracillima* | *Pullenia bulloides* | *Pullenia* sp. | *Pygmaeseistron* cf. *hispida* | *Pyrgo* sp. | *Quinqueloculina* sp. | *Reophax dentaliniformis* | *Triloculina* cf. *trihedra* | *Triloculina* sp. | *Uvigerina auberiana* | *Uvigerina* cf. *peregrina* | *Valvulineria* sp. | *Krithe* sp. | *Pseudocythere caudata* | Siliciclastics | Other observations |
|---|---|---|---|---|---|---|---|---|---|---|---|---|---|---|---|---|---|---|---|---|---|---|---|---|---|---|---|---|---|---|---|---|---|---|---|---|---|---|---|---|---|---|---|---|
| 39H-CC | P | G | | | | | | | | | | | | | | P | | | | | | | P | | | | | | | | | | | | | | | | | | | | A | Mica |
| 40H-CC | F | G | | | | | | | | | | | | | | F | | | | | | | F | | P | | | | | | | | | | | | | | | | | | D | Pyrite, orange benthic foraminifers |
| 41H-CC | R | G | | | | | | | | | | | | | | | | | | | | | R | | | | | | | | | | | | | | | | | | | | A | Mica |
| 42X-CC | D | M | | | | | R | | | | | | R | | | D | | | P | | | | F | | | | P | | | | | | | | | | | | | | | | D | Yellow foraminifers, pyrite |
| 43X-CC | A | M | | | | | A | | | | | | | | | P | | | | | P | | P | A | | | | R | | | | | | | | | | | | | | | A | Pyrite, mica |
| 44X-CC | A | M | | | | | | | | | | | P | | | A | | | | | | | | | | | | | | | | | | | | | | | | | | | | A | Pyrite, mica |
| 45X-CC | F | M | | | | | R | | | | | | | | | F | | | | | R | | | R | | | | | | | | | | | | P | | | | | P | | A | Pyrite |
| 46X-CC | F | M | | | | | R | | | | | | | | | R | | | | | | | | F | | | | | | | | | | | | | | | | | | | | A | Pyrite |
| 47X-CC | A | M | | | | | | | | | | R | | | | A | R | | | | | | | P | | | | P | R | | | | | | | | | | | P | P | | | A | Pyrite |
| 48X-CC | F | G | | | | | | | | | | | | | | F | | | | | | | | P | | | P | | | | | | | | | | | | | | | | | A | Pyrite |
| 49X-CC | A | G | | | | | | | | | | | | | | A | | | | | | | | R | | | R | | | | | | | | | | | | | A | | | | A | Pyrite tubes, mica |
| 50X-CC | F | M | | | | | P | | | | | R | | | | P | | | | | | | | F | | | | | | | | | | | | | | | | | | | | A | Mica |
| 51X-CC | A | M | | | | | | | | | | | | | | A | | | | | | | | | | P | | P | | | | | | | | | | | | P | | | | A | Mica |
| 52X-CC | R | G | | | | | P | | | | | | | | | | | | | | | | | | | | | | | | | | P | | | | | | | P | | | | A | Pyrite tubes, mica |
| 53X-CC | R | G | | | | | P | | | | | P | | | | | | | | | | | | R | | | P | | | | | | | | | | | | | | | | | A | Pyrite |
| 54X-CC | F | G | | | | | | | | | | | | | | F | | | | | | | | | | | | | | | | | | | | | | | | | | | | A | Pyrite tubes, mica |
| 55X-CC | P | G | | | | | | | | | | | | | | | | | | | | | | P | | | | | | | | | | | | | | | | | | | | A | Pyrite |
| 56X-CC | A | G | | | | | A | P | | | | P | | | | F | | | | | | | | A | | | | | | | | | P | | | | | | | | | | A | |
| 57X-CC | A | G | | | | | R | | | | | | | | | | | | | | | | | A | | | | | | | | | | | | | | | | | | | | A | Pyrite |
| 58X-CC | R | G | | | | | | | | | | | | | | | | | | | | | | R | | | | | | | | | | | | | | | | | | | | A | |
| 59X-CC | F | G | | | | | | | | | | R | | | | R | | | | | | | | F | | | | | | | | | | | | | | | | | | | | D | Pyrite |
| 60X-CC | A | G | | | | | P | | | | | R | | | | A | | | | | | | | A | | | | | | | | | | P | | | | | | | | | | A | |
| 61X-CC | P | G | | | | | | | | | | | | | | P | | | | | | | | | | | | | | | | | | P | | | | | | | | P | | D | Pyrite |
| 62X-CC | A | G | P | | | | | | | | | | | | | P | | | | | P | | | A | | | | | | | | | R | | | | | | | | P | | D | Pyrite |
| 63X-CC | A | G | | | | | | | | P | | | | | | A | | | | | | | | R | | | | | | | | | | | | | | | | | | | | D | Pyrite |
| 64X-CC | F | G | | | | | | | | | | | | | | F | | | | | | | | | | | | | | | | | | | | | | | | | | | | D | |
| 65X-CC | F | M | F | | | | R | | | | | | | | | R | | | | | | | | | | | | | | | | | | | | | | | | | | | | D | |
| 66X-CC | B | | | | | | | | | | | | | | | | | | | | | | | | | | | | | | | | | | | | | | | | | | | D | |
| 67X-CC | R | M | | | | | | | | | | | | | | R | | | R | | | | | P | | | | | | | | | | | | | | | P | | P | | | D | Pyrite, yellow foraminifers |
| 68X-CC | A | M | | | | | R | | | | P | | | | | A | | | | | | | | R | | | | | | P | | | | | | | | | | | | | D | Pyrite, yellow foraminifers |
| 69X-CC | A | M | | | | | P | | | | | | | | | A | | | P | | | | | | | | | | R | | | | | | | | | | | | | | | D | Pyrite, mainly brown foraminifers |
| 70X-CC | A | M | | | | | | | | | | | | | | A | | | R | | | | | R | | | | | | | | | | | | | | | | | | | | D | Pyrite |
| 71X-CC | D | G | | | | | R | | | | | P | | | | D | | | P | | | | | A | | | | | | | | | | | | | | | | | | | | D | Pyrite |
| 72X-CC | D | M | | | | | R | | | | | | | | | D | | | R | | | | P | F | | | | | | | | | | | | | | | | | | | | D | Pyrite, few brown-yellow foraminifers |
| 73X-CC | D | M | P | | | | | | | | | | | | | D | | | P | | | | R | R | | | | | | | | | | | | | | | | | R | | | D | Pyrite, yellow foraminifers |
| 74X-CC | F | P | | | | | | | | | | R | | | | | | | | | | | | R | | | | | | | | | | | | | | | | | | | | D | Pyrite tubes, mica |
| 75X-CC | F | P | | | | | | | | | | R | | | | | | | | | | | | F | | | | | | | | | | | | | | | | | | | | A | Pyrite tubes, mica |
| 76X-CC | A | M | | | | | | | | | | | | | | A | | | | | | | | | | | | P | | | P | | | | | | | | | | | | | D | Pyrite tubes |
| 77X-CC | R | M | | | | | | | | | | | | | P | P | | | | | | | | P | | | | | | | | | | | | | | | | P | | | | F | Pyrite tubes |
| 78X-CC | A | G | | | | | R | | | | | P | P | | | A | | P | | | | | | A | | | | | | | | | | | | | | | | | | | | D | Pyrite |
| 79X-CC | P | M | | | | | | | | | | P | | | | | | | | | | | | P | | | | | | | | | | P | | | | | | | | | | |
| 80X-CC | A | M | | | | | | | | | | | P | | | A | | | R | | | | | R | | | | | | | | | | | | | | | | | | | | D | Yellow foraminifers, pyrite |

**Table T7 (continued).**

| Core, section | Abundance | Preservation | *Alabaminella weddellensis* | *Brizalina* cf. *spathula* | *Brizalina earlandi* | *Brizalina pygmaea* | *Bulimina* aff. *exilis* | *Bulimina* aff. *mexicana* | *Bulimina* sp. | *Cassidulina laevigata* var. *carinata* | *Cassidulina* sp. | *Cassidulinoides tenuis* | *Cibicidoides* cf. *subhaidingeri* | *Cibicidoides* sp. | *Dentalina* sp. | *Elphidium* cf. *batialis* | *Epistominella pulchella* | *Fissurina* sp | *Glandulina* sp. | *Globobulimina auriculata* | *Globobulimina pacifica* | *Globocassidulina* sp. | *Gyroidinoides soldanii* | *Islandiella norcrossi* | *Lagena* sp. | *Lenticulina* sp. | *Nodosaria* aff. *pyrula* | *Nodosaria* sp. | *Nonionella labradorica* | *Nonionella turgida digitata* | *Oridorsalis umbonatus* | *Planulina wuellerstorfi* | *Procerolagena* cf. *gracillima* | *Pullenia bulloides* | *Pullenia* sp. | *Pygmaeseistron* cf. *hispida* | *Pyrgo* sp. | *Quinqueloculina* sp. | *Reophax dentaliniformis* | *Triloculina* cf. *trihedra* | *Triloculina* sp. | *Uvigerina auberiana* | *Uvigerina* cf. *peregrina* | *Valvulineria* sp. | *Krithe* sp. | *Pseudocythere caudata* | Siliciclastics | Other observations |
|---|---|---|---|---|---|---|---|---|---|---|---|---|---|---|---|---|---|---|---|---|---|---|---|---|---|---|---|---|---|---|---|---|---|---|---|---|---|---|---|---|---|---|---|---|
| 81X-CC | F | M | | | | | | | | | | | | | | | R | | | | | | F | | | P | | | | | | | | | | | | | | | | | A | Pyrite |
| 82X-CC | R | P | | | | | | | | | | | | | | R | | | | | R | | P | | | | | P | | | | | | | | | | | | | | | A | Mica |
| 82X-6W | A | P | | | | | | | | R | | | | | | F | | | | | | | R | | | | | F | | | | | P | | | | | P | R | | | | F | Abundant shell fragments, yellow foraminifers |
| 83X-CC | F | M | R | | | | | | | | | | | | | | | | | | | | F | | | | | | | | | | | | | | | | | | | | F | Mica |

Notes: Abundance: D = dominant, A = abundant, F = few, R = rare, P = present. Preservation: G = good, M = moderate, P = poor.

**Table T8.** Diatom range chart, Hole U1343A. (See table notes.)

| Core, section, interval (cm) | Depth (mbsf) Top | Depth (mbsf) Bottom | Abundance | Preservation | *Actinocyclus curvatulus* | *Actinocyclus senarius* | *Asteromphalus robustus* | *Aulacoseira* spp. | *Bacteriosira fragilis* | *Chaetoceros* spp. spores | *Coscinodiscus marginatus* | *Coscinodiscus oculus-iridis* | *Cyclotella* spp. | *Delphineis kippae* | *Delphineis surirella* | *Detonula confervacea* | *Diploneis* spp. | *Encyonema lacustre* | *Encyonema* spp. | *Fragilaria* spp. | *Fragilariopsis cylindrus* | *Fragilariopsis oceanica* | *Fragilariopsis* spp. | *Gomphonema* spp. | *Navicula* sp. | *Neodenticula seminae* | *Nitzschia* spp. | *Odontella aurita* | *Palaria sol* | *Paralia sulcata* | *Pinnularia* spp. | *Porosira glacialis* | *Proboscia barboi* | *Proboscia curvirostris* | *Rhizosolenia hebetata* f. *hebetata* | *Rhizosolenia hebetata* f. *hiemalis* | *Rhizosolenia hebetata* f. *semispina* | *Rhizosolenia* sp. | *Stellarima microtrias* | *Stephanopyxis turris* | *Thalassionema bacillaris* | *Thalassionema nitzschioides* | *Thalassiosira antarctica* spore | *Thalassiosira decipiens* | *Thalassiosira eccentrica* | *Thalassiosira gravida* | *Thalassiosira hyalina* | *Thalassiosira jouseae* | *Thalassiosira latimarginata* s.l. | *Thalassiosira lineata* | *Thalassiosira nordenskioeldii* | *Thalassiosira oestrupii* | *Thalassiosira* spp. | *Thalassiothrix longissima* | Diatom zone (NPD) in Yanagisawa and Akiba (1998) |
|---|---|---|---|---|---|---|---|---|---|---|---|---|---|---|---|---|---|---|---|---|---|---|---|---|---|---|---|---|---|---|---|---|---|---|---|---|---|---|---|---|---|---|---|---|---|---|---|---|---|---|
| 323-U1343A- | | | | | | | | | | | | | | | | | | | | | | | | | | | | | | | | | | | | | | | | | | | | | | | | | | | |
| 2H-CC | 14.92 | 15.02 | C | M | C | | | R | R | C | | R | | | R | | | | | | R | C | | R | | C | C | | R | R | | | | | | | | | | | R | A | | | | R | F | | R | | |
| 4H-CC | 34.66 | 34.76 | A | G | F | | | | F | R | | R | | | | | | | | | | F | | | | A | | F | | C | | R | | | R | R | | | | | | A | | | | R | | | | | |
| 5H-1, 48.5 | 34.49 | 34.49 | C-A | M-G | R | | | | | | | | | | | R | | | | | C | R | | | | A | C | | | | | | | | R | | | | | R | C | F | | | | | F | R | | | | *Neodenticula seminae* (NPD12) |
| 6H-CC | 53.92 | 54.02 | A | G | C | R | | | C | C | F | R | | R | | | | | | | | R | | | | C | R | R | | C | | R | | | F | | F | | | | R | A | | | | | C | | | R | |
| 7H-CC | 62.19 | 62.29 | A | G | F | | | | F | F | F | C | | R | R | R | | | | | | C | | | | C | R | C | | R | R | R | | | F | | C | | R | | | C | | R | | | C | | F | C | | |
| 8H-CC | 71.79 | 71.89 | F-C | M | F | | | | C | | R | R | | | R | R | | R | | | F | R | | | | C | F | C | | | | | | | R | R | F | | R | | | A | | | R | A | | | | R | R | |
| 9H-CC | 81.90 | 82.00 | A | G | C | | R | | F | R | | R | | | | | | | R | | | C | R | | R | C | R | F | | R | | | R | R | | | R | | | | C | A | R | | F | | C | R | | R | |
| 11H-CC | 100.50 | 100.60 | C | M | | | | | F | | R | | R | | F | F | | | | | | F | | | | F | | R | R | F | | R | | | | | | R | | | D | | F | | F | F | | | F | | | |
| 12H-CC | 110.42 | 110.52 | F | P | F | | | | C | | R | | | | C | F | R | | | | F | R | | | R | F | | R | | F | | R | | | F | | R | F | R | | | A | | | R | C | F | R | | R | R | *Proboscia curvirostris* (NPD11) |
| 19H-CC | 173.80 | 173.90 | C-A | M | C | | | | | | | | | | | | | | | | | | | | | F | | | C | R | | R | F | F | R | R | R | F | | | A | | | R | | F | | | | R | |
| 20H-CC | 181.96 | 182.06 | C | M | | R | | | | | | | | | F | | | | | R | R | | | | | | R | | C | | | R | | | | | | | | | F | D | | | | | R | R | | | | R | |

Notes: Abundance: D = dominant, A = abundant, C = common, F = few, R = rare. Preservation: G = good, M = moderate, P = poor.

**Table T9.** Diatom range chart, Hole U1343C. (See table notes.)

| Core, section | Depth (mbsf) |  | Abundance | Preservation | *Actinocyclus curvatulus* | *Actinocyclus ochotensis* | *Actinocyclus oculatus* | *Actinoptycus senarius* | *Asteromphalus robustus* | *Bacteriosira fragilis* | *Cocconeis placentula* | *Coscinodiscus marginatus* | *Cyclotella* spp. | *Delphineis* cf. *angustata* | *Delphineis surirella* | *Detonula confervacea* | *Eunotia triodon* | *Eunotia* spp. | *Fragilariopsis cylindrus* | *Fragilariopsis oceanica* | *Navicula* spp. | *Neodenticula koizumii* | *Neodenticula seminae* | *Nitzschia peragalli* | *Nitzschia* spp. | *Odontella aurita* | *Paralia sol* | *Paralia sulcata* | *Pinnularia* spp. | *Porosira glacilis* | *Proboscia alata* | *Proboscia barboi* | *Proboscia curvirostris* | *Psuedopodsira elegans* | *Rhizosolenia borealis* | *Rhizosolenia hebetata* f. *hebetata* | *Rhizosolenia hebetata* f. *hiemalis* | *Rhizosolenia hebetata semispina* | *Rhizosolenia* spp. | *Stauroneis* spp. | *Stephanopyxis* spp. | *Stephanopyxis turris* | *Thalassionema nitzschioides* | *Thalassiosira antarctica* spore | *Thalassiosira antiqua* | *Thalassiosira gravida* | *Thalassiosira hyalina* | *Thalassiosira jouseae* | *Thalassiosira latimarginata* s.l. | *Thalassiosira nordenskioeldii* | *Thalassiosira oestrupii* | *Thalassiosira* spp. | *Thalassiothrix longissima* | Diatom zone (NPD) in Yanagisawa and Akiba (1998) |
|---|---|---|---|---|---|---|---|---|---|---|---|---|---|---|---|---|---|---|---|---|---|---|---|---|---|---|---|---|---|---|---|---|---|---|---|---|---|---|---|---|---|---|---|---|---|---|---|---|---|---|---|---|---|---|
|  | Top | Bottom |  |  |  |  |  |  |  |  |  |  |  |  |  |  |  |  |  |  |  |  |  |  |  |  |  |  |  |  |  |  |  |  |  |  |  |  |  |  |  |  |  |  |  |  |  |  |  |  |  |  |  |  |
| 323-U1343C- |  |  |  |  |  |  |  |  |  |  |  |  |  |  |  |  |  |  |  |  |  |  |  |  |  |  |  |  |  |  |  |  |  |  |  |  |  |  |  |  |  |  |  |  |  |  |  |  |  |  |  |  |  |  |
| 7H-CC | 63.81 | 63.91 | C | M | C | R |  |  | R | R |  | C | R |  | C | F |  |  | R |  |  |  | C |  | F |  |  |  |  | R |  |  |  |  | R | R | F |  | R |  |  | F | R | A |  | F | R | R | F | R |  |  | R | *Neodenticula seminae* (NPD12) |
| 8H-CC | 70.58 | 70.68 | C | M | F |  |  | R |  | R |  | F |  | R | F |  |  |  | F |  |  |  |  |  | F | R |  |  |  |  |  |  |  |  |  | R | R |  |  |  |  |  | F | D |  |  |  |  | F |  |  |  | R |  |
| 9H-CC | 78.25 | 78.35 | C | M | F |  |  |  |  | F |  | R |  |  |  | R |  |  |  |  |  |  | R |  | C |  | R | F | R |  |  |  | F |  |  | R |  |  |  |  |  |  | F | D | R |  |  | R | R | R |  |  |  | Undefined (*Proboscia curvirostris* or *Actinocyclus oculatus*) |
| 10H-CC | 87.58 | 87.68 | C | M |  |  |  |  |  | R |  | R |  | R |  | R |  |  | R |  |  |  | C |  |  |  | R | C | R | R |  |  |  | R |  |  |  |  | R |  |  |  |  | A |  |  | R | C | C |  |  |  |  |  |
| 11H-CC | 97.44 | 97.54 | C | M | R |  |  |  |  |  |  | R |  |  | R | R |  |  | C | F |  |  | F |  | C | R | R |  |  |  |  |  | R | R |  | R | F |  | R |  |  |  | C | A |  | R | R | R | F |  |  |  |  |  |
| 13H-CC | 116.00 | 116.10 | F | M | F |  | R |  |  | R | R | R | F |  |  |  | R | F | F |  |  |  | F |  | F |  |  | C |  | R |  |  |  |  |  | R | R |  |  | R |  |  |  | A |  | R |  | R | C |  | R |  | F |  |
| 19H-CC | 171.89 | 171.99 | C | M | C |  |  |  |  |  |  | F |  | R | C |  |  |  |  |  | F |  |  | F | F |  | F |  |  |  |  | R | F |  | R |  |  |  |  |  | R |  |  | A |  | R |  |  | C |  |  | F | R |  |
| 22H-CC | 196.06 | 196.16 | C | M-P | R |  |  |  |  | C |  |  |  | R | R | F |  | R | C | F |  | R | A | F | C |  | R | R |  |  | R |  |  |  |  | R |  |  | F |  |  |  |  | C |  |  | F | C | R |  |  |  | R |  |
| 26H-CC | 234.62 | 234.72 | A | G | F |  |  |  |  |  |  |  |  |  |  |  |  |  | R | R |  |  | A |  |  |  |  |  |  | F |  | F | F |  |  |  |  | R |  |  |  |  |  | A |  |  |  |  | R |  | R |  |  |  |

Notes: Abundance: D = dominant, A = abundant, C = common, F = few, R = rare. Preservation: G = good, M = moderate, P = poor.

**Table T10.** Diatom range chart, Hole U1343E. This table is available in an oversized format.

**Table T11.** First common occurrences of diatom species *Proboscia curvirostris* and *Proboscia barboi*, Hole U1343E. (See table note.)

| Core, section | Depth (mbsf) Top | Depth (mbsf) Bottom | *Proboscia curvirostris* | *Proboscia barboi* |
|---|---|---|---|---|
| 323-U1343E- | | | | |
| 50X-CC | 428.50 | 428.60 | 30 | 12 |
| 51X-CC | 435.85 | 435.95 | 1 | 10 |
| 52X-CC | 446.16 | 446.21 | 0 | 12 |

Note: The numbers represent counted valve numbers in the coarse fraction (>20 µm) slides prepared for silicoflagellate counting.

**Table T12.** Silicoflagellate and ebridian range chart, Holes U1343C and U1343E. (See table notes.)

| Core, section | Depth (mbsf) Top | Depth (mbsf) Bottom | Abundance | Preservation | Silicoflagellates: Aberrant silicoflagellates | *Dictyocha* cf. *mandrai* | *Dictyocha* spp. | *Dictyocha subarctios* | *Distephanus crux* | *Distephanus medianoctisol* | *Distephanus medianoctisol** | *Distephanus octangulatus* | *Distephanus octonarius* | *Distephanus slavincii* | *Distephanus speculum* | *Distephanus speculum** | Ebridians: *Ammodochium rectangulare* | Zone in Ling (1992) |
|---|---|---|---|---|---|---|---|---|---|---|---|---|---|---|---|---|---|---|
| 323-U1343C- | | | | | | | | | | | | | | | | | | |
| 21H-CC | 192.05 | 192.15 | T | G | | | | | | T | | | | | | | | *Distephanus octonarius* |
| 22H-CC | 196.06 | 196.16 | C | G | | | | | | F | F | | R | | R | R | | |
| 23H-CC | 205.35 | 205.45 | C | G | T | | | T | | T | T | T | | R | F | F | | *Dictyocha subarctios* |
| 24H-CC | 215.44 | 215.54 | C | G | T | | | | | F | R | F | R | R | | | | |
| 25H-CC | 224.67 | 224.77 | C | G | R | | | R | | | | F | | F | | | | |
| 26H-CC | 234.62 | 234.72 | F | G | | | | F | | T | | | R | | | T | | |
| 323-U1343E- | | | | | | | | | | | | | | | | | | |
| 1H-CC | 8.12 | 8.22 | F | M-G | R | | | | | | | R | | | R | T | | |
| 2H-CC | 17.70 | 17.80 | F | M-G | | | | | | | | | | | F | R | | |
| 3H-CC | 26.30 | 26.40 | C | G | | | | | | | T | R | | | F | R | | |
| 4H-CC | 37.07 | 37.17 | C | G | | | | | | T | | C | | | C | R | | *Distephanus octangulatus* |
| 5H-CC | 42.96 | 43.06 | R | G | | | | | | T | | | | | R | | | |
| 6H-CC | 55.45 | 55.55 | A | M-G | R | | | | | R | | A | | | | | | |
| 7H-CC | 63.90 | 64.00 | R | G | | | | | | T | | R | | | | | | |
| 8H-CC | 74.79 | 74.89 | F | M-G | | | | | | | T | | F | | | | | |
| 9H-CC | 84.05 | 84.15 | R | M-G | | | | | | | | R | | | R | | | |
| 10H-CC | 90.90 | 91.00 | F | M-G | | | | | | F | | | | | R | R | | |
| 21H-CC | 175.07 | 175.17 | C | M-G | | | | | | R | | | | | C | F | | *Distephanus octonarius* |
| 22H-CC | 183.76 | 183.86 | F | M | | | | | | R | R | | | | R | | | |
| 23H-CC | 193.31 | 193.41 | C | M | | | | T | | F | R | T | T | R | T | | | |
| 24H-CC | 197.47 | 197.57 | R | M-G | | | | | | | | | | | R | | | |
| 25H-CC | 207.99 | 208.09 | F | G | | | | | | T | | R | R | | T | T | | |
| 26H-CC | 217.04 | 217.14 | C | G | | F | T | R | | F | R | | F | | R | T | | |
| 27H-CC | 226.01 | 226.11 | A | G | T | F | F | F | T | F | R | | F | R | | | | |
| 28H-CC | 234.72 | 234.82 | C | G | | | T | R | | F | | | | | F | R | | *Dictyocha subarctios* |
| 55X-CC | 475.60 | 475.70 | B | | | | | | | | | | | | | | | |
| 56X-CC | 482.57 | 482.67 | R | M | | | | | | R | | | | | T | | | |
| 57X-CC | 493.97 | 494.07 | R | M | | | | | | T | | | | | T | | | |
| 63X-CC | 550.54 | 550.64 | F | P-M | | | | | | | | | | | T | R | | |
| 64X-CC | 561.05 | 561.15 | T | P | | | | | | | | | | | | | T | |
| 65X-CC | 568.77 | 568.87 | R | P | | | | | | | | | | | | T | T | |
| 70X-CC | 617.90 | 618.00 | T | P | | | | | | | | | | | | | T | |
| 71X-CC | 628.16 | 628.26 | T | P | | | | | | | | | | | | T | | |
| 72X-CC | 634.44 | 634.54 | F | P-M | | | | | | | | | | | T | F | R | |
| 73X-CC | 643.79 | 643.89 | F | P-M | | | | | | | | | | | R | F | | *Ammodochium rectangulare* |
| 74X-CC | 657.41 | 657.51 | R | P-M | | | | | | | | | | | | | R | |
| 75X-CC | 667.09 | 667.19 | T | P | | | | | | | | | | | | | T | |
| 76X-CC | 674.96 | 675.06 | R | P | | | | | | | | | | | | | R | |

Notes: Abundance: A = abundant, C = common, F = few, R = rare, T = trace, B = barren. Preservation: G = good, M = moderate, P = poor. * = with short radial spines.

**Table T13.** Radiolarian datum events, Holes U1343A, U1343B, U1343C, U1343D, and U1343E. (See table note.)

| Zone | Marker species | Age (Ma) | Hole U1343A | | | | Hole U1343B | | | | Hole U1343C | | | |
|---|---|---|---|---|---|---|---|---|---|---|---|---|---|---|
| | | | Core, section | | Depth (mbsf) | | Core, section | | Depth (mbsf) | | Core, section | | Depth (mbsf) | |
| | | | Top | Bottom | Top | Bottom | Top | Bottom | Top | Bottom | Top | Bottom | Top | Bottom |
| *Botryostrobus aquilonaris* | T *Lychnocanoma nipponica sakaii* | 0.05 | 1H-CC | 2H-CC | 5.5 | 15.0 | 1H-CC | 2H-CC | 6.9 | 16.9 | 1H-CC | 2H-CC | 7.2 | 16.7 |
| | T *Spongodiscus* sp. | 0.28–0.32 | 8H-CC | 9H-CC | 71.9 | 82.0 | | | | | 9H-CC | 10H-CC | 78.4 | 87.7 |
| | T *Axoprunum acquilonium* | 0.25–0.43 | 9H-CC | 10H-CC | 82.0 | 91.0 | | | | | 12H-CC | 13H-CC | 106.7 | 116.1 |
| *Stylatractus universus* | T *Stylatractus universus* | 0.41–0.51 | 11H-CC | 12H-CC | 100.6 | 110.5 | | | | | 14H-CC | 15H-CC | 124.7 | 135.0 |
| *Eucyrtidium matuyamai* | T *Eucyrtidium matuyamai* | 0.9–1.5 | | | | | | | | | | | | |
| | B *Eucyrtidium matuyamai* | 1.7–1.9 | | | | | | | | | | | | |

Note: T = top, B = bottom.

| Zone | Marker species | Age (Ma) | Hole U1343D | | | | Hole U1343E | | | |
|---|---|---|---|---|---|---|---|---|---|---|
| | | | Core, section | | Depth (mbsf) | | Core, section | | Depth (mbsf) | |
| | | | Top | Bottom | Top | Bottom | Top | Bottom | Top | Bottom |
| *Botryostrobus aquilonaris* | T *Lychnocanoma nipponica sakaii* | 0.05 | | | | | 1H-CC | 2H-CC | 8.2 | 17.8 |
| | T *Spongodiscus* sp. | 0.28–0.32 | | | | | 8H-CC | 9H-CC | 74.9 | 84.2 |
| | T *Axoprunum acquilonium* | 0.25–0.43 | | | | | 9H-CC | 10H-CC | 84.2 | 91.0 |
| *Stylatractus universus* | T *Stylatractus universus* | 0.41–0.51 | | | | | 11H-CC | 12H-CC | 101.8 | 106.7 |
| *Eucyrtidium matuyamai* | T *Eucyrtidium matuyamai* | 0.9–1.5 | | | | | 34H-CC | 35H-CC | 291.3 | 301.5 |
| | B *Eucyrtidium matuyamai* | 1.7–1.9 | | | | | 69X-CC | 70X-CC | 606.9 | 618.0 |

**Table T14.** Radiolarian range chart, Holes U1343A, U1343B, U1343C, U1343D, and U1343E. (See table notes.) (Continued on next three pages.)

| Core, section | Depth (mbsf) Top | Depth (mbsf) Bottom | Abundance | Preservation | *Actinomma boreale* | *Actinomma medianum* | *Amphimelissa setosa* | *Axoprunum acquilonium* | *Botryostrobus aquilonaris* | *Ceratospyris borealis* | *Collosphaera pyloma* | *Cycladophora cornutoides* | *Cycladophora cosma* | *Cycladophora davisiana* | *Cycladophora sakaii* | *Cyrtocapsella japonica* | *Dendrospyris sakaii* | *Dictyophimus bullatus* | *Dictyophimus hirundo* | *Eucyrtidium asanoi* | *Eucyrtidium inflatum* | *Eucyrtidium matuyamai* | *Lamprocyrtis heteroporos* | *Larcopyle butschlii* | *Lipmanella redondoensis* | *Lithelius barbatus* | *Lychnocanoma magnacornuta* | *Lychnocanoma nipponica sakaii* | *Lychnocanoma parallelipes* | *Phormostichoartus fistula* | *Porodiscus circularis* | *Sphaeropyle langii-robusta* group | *Spongodiscus* sp. | *Spongopyle osculosa* | *Spongotrochus glacialis* | *Spongurus pylomaticus* | *Stichocorys delmontensis* | *Stichocorys peregrina* | *Stylatractus universus* | *Stylochlamydium venustum* | *Stylodictya validispina* | *Thecosphaera akitaensis* |
|---|---|---|---|---|---|---|---|---|---|---|---|---|---|---|---|---|---|---|---|---|---|---|---|---|---|---|---|---|---|---|---|---|---|---|---|---|---|---|---|---|
| 323-U1343A- | | | | | | | | | | | | | | | | | | | | | | | | | | | | | | | | | | | | | | | | |
| 1H-CC | 5.38 | 5.48 | C | M | C | | | | | | | | | C | | | | | F | | | | | | | | | | | | F | | | F | | | | | F | F | |
| 2H-CC | 14.92 | 15.02 | F | M | | | | | | F | | | | F | | | | | | | | | F | | | | F | | | | F | | | | | | | | F | F | |
| 3H-CC | 24.60 | 24.73 | F | G | F | | | | | F | | F | | C | | | | | | | | | F | | | | C | | | | | | | | | | | | F | F | |
| 4H-CC | 34.66 | 34.76 | C | M | C | | | | F | C | | | | A | | | | | | | | | F | | | | C | | | | F | | | | | | | | F | F | |
| 5H-CC | 43.91 | 44.01 | F | M | | | | | | F | | | | C | | | | | | | | | F | | | | | | | | F | | | F | | | | | | F | |
| 6H-CC | 53.92 | 54.02 | F | G | | | | | | F | | | | F | | | | | | | | | | | | | F | | | | | | | | | | | | F | F | |
| 7H-CC | 62.19 | 62.29 | F | G | | | | | | | | | | C | | | | | | | | | F | | | | F | | | | | | | F | | | | | F | F | |
| 8H-4 | 67.33 | 67.35 | C | M | | | | | | C | | | | A | | | | | F | | | | F | | | | F | | | | | | | F | | | | | F | F | |
| 8H-CC | 71.79 | 71.89 | F | M | F | F | | | | F | | | | C | | | | | F | | | | F | | | | F | | | | F | | | | | | | | | F | |
| 9H-CC | 81.90 | 82.00 | C | M | F | | | | F | F | | | | C | | | | | | | | | | | | | C | | | | | C | | F | | | | | F | C | |
| 10H-6 | 89.24 | 89.26 | F | M | | | | | | | | | | F | | | | | F | | | | | | | | | | | | | F | | F | | | | | | | |
| 10H-CC | 90.90 | 91.00 | C | M | C | | | F | | F | | | | C | | | | | F | | | | | | | | | | | | F | C | | F | | | | | | | |
| 11H-CC | 100.50 | 100.60 | F | M | F | | | F | | F | | | | | | | | | | | | | | | | | F | | | | F | C | | F | | | | | | F | |
| 12H-7 | 109.53 | 109.55 | F | G | | | | | | F | | | | F | | | | | | | | | | | | | | | | | | F | | | | | | | F | | |
| 12H-CC | 110.42 | 110.52 | F | M | F | | | F | | F | | | | C | | | | | F | | | | | | | | F | | | | | F | | | | | | F | | | |
| 13H-CC | 119.32 | 119.42 | F | M | | | | F | | F | | | | F | | | | | | | | | | | | | | | | | F | | | F | | | | F | | | |
| 14H-CC | 128.86 | 128.96 | F | M | F | | | F | | F | | F | | F | | | | | F | | | | | F | | | | | | | F | F | | F | | | | | | F | |
| 15H-CC | 139.06 | 139.16 | C | M | F | | | F | | C | | | | A | | | | | C | | | | | F | | | | | | | F | C | | F | F | | | | | F | |
| 16H-CC | 147.11 | 147.21 | C | M | F | | | F | | C | | | | F | | | | | F | | | | | | | | | | | | | C | | C | | | | F | | F | |
| 17H-CC | 157.29 | 157.39 | C | M | C | | | F | | C | | F | | F | | | | | F | | | | | | | | | | | | F | C | | | | | F | | F | |
| 18H-CC | 166.12 | 166.22 | F | M | F | | | | F | F | | | | F | | | | | F | | | | | | | | | | | | F | F | | F | F | | F | | F | |
| 19H-CC | 173.80 | 173.90 | C | M | F | | | F | | F | | | | A | | | F | | C | | | | | | | | | | | | F | C | | F | | | F | | F | |
| 20H-CC | 181.96 | 182.06 | C | M | F | | | F | F | C | | F | | F | | | | | F | | | | | | | | | | | | F | F | | F | | | | | F | |
| 21H-CC | 191.50 | 191.60 | F | M | F | | | F | F | | | | | F | | | | | F | | | | | | | | | | | | F | F | | | | | | | F | |
| 22H-CC | 201.66 | 201.76 | C | M | F | | | | | F | | | | C | | | | | F | | | | | F | | | | | | | F | F | | C | F | | | | | F | |
| 323-U1343B- | | | | | | | | | | | | | | | | | | | | | | | | | | | | | | | | | | | | | | | | |
| 1H-CC | 6.72 | 6.85 | C | M | C | | | | | C | | F | | C | | | | | | | | | | | | | | | | | | | | F | | | | | F | F | |
| 2H-CC | 16.77 | 16.87 | F | M | | | | | | F | | | | F | | | | | | | | | | | | | | F | | | | | | F | | | | | | F | |
| 3H-CC | 24.98 | 25.08 | C | M | F | | | | | F | | | | C | | | | | | | | | | | | | | F | | | | | | F | | | | | F | F | |
| 4H-CC | 35.16 | 35.26 | C | M | F | | | | F | C | | | | C | | | | | | | | | | F | | | | C | | | | | | F | | | | | F | F | |
| 323-U1343C- | | | | | | | | | | | | | | | | | | | | | | | | | | | | | | | | | | | | | | | | |
| 1H-CC | 7.14 | 7.24 | F | M | F | | | | | F | | F | | C | | | | | | | | | | | | | | | | | | F | | F | | | | | F | F | |
| 2H-CC | 16.57 | 16.67 | F | M | F | | | | | F | | F | | C | | | | | | | | | | | | | | F | | | | | | F | | | | | | F | |
| 3H-CC | 26.50 | 26.60 | C | M | F | | | | | F | | F | | C | | | | | F | | | | | F | | | | F | | | | | | F | | | | | F | F | |
| 4H-CC | 36.30 | 36.40 | C | M | F | | | | | F | | F | | C | | | | | F | | | | | | | | | C | | | | | | F | | | | | | F | |
| 5H-CC | 44.65 | 44.75 | C | M | F | | | | | C | | F | | C | | | | | | | | | | F | | | | F | | | | | | | | | | | F | C | |
| 6H-CC | 55.41 | 55.51 | C | M | F | | | | | F | | F | | C | | | | | | | | | | F | | | | F | | | | | F | F | | | | | F | C | |
| 7H-CC | 63.81 | 63.91 | F | G | | | F | | | | | | | F | | | | | | | | | | | | | | F | | | | | | | | | | | F | F | |
| 8H-CC | 70.58 | 70.68 | C | M | C | | | | | | | | | C | | | | | | | | | | | | | | C | | | | F | | | | | | | | F | F | |

**Table T14 (continued).** (Continued on next page.)

| Core, section | Depth (mbsf) Top | Depth (mbsf) Bottom | Abundance | Preservation | *Actinomma boreale* | *Actinomma medianum* | *Amphimelissa setosa* | *Axoprunum acquilonium* | *Botryostrobus aquilonaris* | *Ceratospyris borealis* | *Collosphaera pyloma* | *Cycladophora cornutoides* | *Cycladophora cosma* | *Cycladophora davisiana* | *Cycladophora sakaii* | *Cyrtocapsella japonica* | *Dendrospyris sakaii* | *Dictyophimus bullatus* | *Dictyophimus hirundo* | *Eucyrtidium asanoi* | *Eucyrtidium inflatum* | *Eucyrtidium matuyamai* | *Lamprocyrtis heteroporos* | *Larcopyle butschlii* | *Lipmanella redondoensis* | *Lithelius barbatus* | *Lychnocanoma magnacornuta* | *Lychnocanoma nipponica sakaii* | *Lychnocanoma parallelipes* | *Phormostichoartus fistula* | *Porodiscus circularis* | *Sphaeropyle langii-robusta* group | *Spongodiscus* sp. | *Spongopyle osculosa* | *Spongotrochus glacialis* | *Spongurus pylomaticus* | *Stichocorys delmontensis* | *Stichocorys peregrina* | *Stylatractus universus* | *Stylochlamydium venustum* | *Stylodictya validispina* | *Thecosphaera akitaensis* |
|---|---|---|---|---|---|---|---|---|---|---|---|---|---|---|---|---|---|---|---|---|---|---|---|---|---|---|---|---|---|---|---|---|---|---|---|---|---|---|---|---|
| 9H-CC | 78.25 | 78.35 | F | M | | | | | | C | | | | F | | | | | | | | | F | | | | F | | | | F | | | | | | F | F | |
| 10H-CC | 87.58 | 87.68 | C | M | F | | | | F | F | | | | C | | | | | | | | | F | | | | F | | | | F | C | | F | | | | C | C | |
| 11H-CC | 97.44 | 97.54 | F | M | F | | | | | F | | F | | F | | | | | | | | | | | | | | | | | C | | | | | | | | | |
| 12H-CC | 106.58 | 106.68 | F | M | F | | | | | | | | | F | | | | | | | | | F | | | | | | | | C | | F | | | | F | F | |
| 13H-CC | 116.00 | 116.10 | F | M | F | | | F | | F | | | | F | | | | | | | | | | | | | | | | F | C | | | | | | | | |
| 14H-CC | 124.55 | 124.65 | C | M | F | | | F | | F | | F | | C | | | | | F | | | | | F | | | | | | F | F | F | F | F | | | | F | | |
| 15H-CC | 134.94 | 135.04 | F | M | | | | F | | F | | | | | | | | | | | | | | | | | | | | F | C | | F | | | F | | | |
| 17H-CC | 153.30 | 153.40 | F | M | F | | | F | | F | | | | F | | | | | | | | | | | | | | | | F | C | | C | F | | | | F | |
| 18H-CC | 163.05 | 163.15 | C | M | F | | | F | F | F | | | | F | | | | | F | | | | | | | | | | | F | C | | F | | | | | | |
| 19H-CC | 171.89 | 171.99 | F | M | F | | | F | | | | | | C | | | | | F | | | | | | | | | | | F | F | | F | | | | | | |
| 20H-CC | 182.11 | 182.21 | F | M | F | | | F | | F | | F | | | | | | | F | | | | | | | | | | | F | C | | F | | | | | | |
| 21H-CC | 192.05 | 192.15 | F | M | F | | | F | | F | | | | | | | | | F | | | | | | | | | | | F | F | | F | | | | | F | |
| 22H-CC | 196.06 | 196.16 | F | M | F | | | F | | F | | | | F | | | | | F | | | | | | | | | | | F | F | F | F | F | | F | | F | |
| 23H-CC | 205.35 | 205.45 | F | M | F | | | F | | F | | | | F | | | | | | | | | | | | | | | | F | F | | F | F | | | | F | |
| 24H-CC | 215.44 | 215.54 | F | M | F | | | F | | F | | F | | C | | | | | F | | | | | F | | | | | | | F | | F | F | | | | F | |
| 25H-CC | 224.67 | 224.77 | F | P | F | | | F | | | | | | | | | | | | | | | | | | | | | | | F | | F | F | | F | | | |
| 26H-CC | 234.62 | 234.72 | F | M | | | | | | F | | F | | C | | | | | F | | | | | | | | | | | | F | | F | | | | | F | |
| 323-U1343D- | | | | | | | | | | | | | | | | | | | | | | | | | | | | | | | | | | | | | | | | |
| 1H-CC | 8.43 | 8.53 | F | G | F | | | | | F | | | | F | | | | | | | | | | | | | | | | F | | | F | F | | | | F | F | |
| 323-U1343E- | | | | | | | | | | | | | | | | | | | | | | | | | | | | | | | | | | | | | | | | |
| 1H-CC | 8.12 | 8.22 | C | M | F | F | | | | F | | F | | C | | | | | | | | | | F | | | | | | F | | | | | | | | F | F | |
| 2H-CC | 17.70 | 17.80 | C | M | F | | | | | F | | | | C | | | | | F | | | | | F | | | | C | | F | | | | F | | | | F | C | |
| 3H-CC | 26.30 | 26.40 | F | M | | F | | | | F | | | | C | | | | | | | | | | F | | | | | | F | | | | F | | | | F | F | |
| 4H-CC | 37.07 | 37.17 | F | M | F | | | | | F | | | | C | | | | | | | | | | F | | | | | | F | | F | | F | | | | F | F | |
| 5H-CC | 42.96 | 43.06 | F | M | | | | | | C | | | | F | | | | | | | | | | F | | | | | | F | | | | F | | | | F | F | |
| 6H-CC | 55.45 | 55.55 | C | M | | | F | | | C | | F | | C | | | | | | | | | | C | | | | | | F | | F | | | F | | | F | F | |
| 7H-CC | 63.90 | 64.00 | C | M | F | | | | F | F | | | | C | | | | | | | | | | | | | | | | F | | F | | F | F | | | F | F | |
| 8H-CC | 74.79 | 74.89 | F | M | F | | | | | F | | F | | | | | | | | | | | | | | | | | | F | | | | F | | | | F | F | |
| 9H-CC | 84.05 | 84.15 | C | M | C | | | | | F | | F | | C | | | | | F | | | | | | | | | | | F | C | | F | F | | | | | F | |
| 10H-CC | 90.90 | 91.00 | C | G | F | | | F | | C | | F | | F | | | | | | | | | | | | | | | | F | C | | F | | | | | | C | |
| 11H-CC | 101.67 | 101.77 | C | M | C | | F | | F | F | | F | | | | | | | | | | | | F | | | | | | | C | | F | F | | | | C | F | |
| 12H-CC | 106.59 | 106.69 | C | M | F | | | F | F | C | | | | F | | | | | | | | | | | | | | | | F | C | | | | | F | | | |
| 14H-CC | 115.95 | 116.05 | C | M | F | | | F | | C | | F | | A | | | | | F | | | | | F | | | | | | F | C | | F | | | F | | F | |
| 15H-CC | 123.35 | 123.45 | F | M | F | | | F | | F | | F | | C | | | | | F | | | | | | | | | | | F | F | | F | | | F | | | |
| 16H-CC | 129.46 | 129.56 | C | M | F | | | F | | C | | F | | F | | | | | C | | | | | F | | | | | | F | C | | F | F | | | | | |
| 17H-CC | 138.34 | 138.44 | F | M | F | | | | | | | | | C | | | | | F | | | | | | | | | | | | F | | | | | | | | | |
| 18H-CC | 148.21 | 148.31 | F | P | | | | | | F | | | | | | | | | | | | | | | | | | | | | F | | F | | | | | | | |
| 19H-CC | 155.87 | 155.97 | F | M | | | | | | F | | | | F | | | | | F | | | | | F | | | | | | | F | | | | | | | | | |
| 20H-CC | 164.89 | 164.99 | A | M | C | | | F | | C | | | | A | | | | | C | | | | | F | | | | | | C | A | | F | F | | | | F | |
| 21H-CC | 175.07 | 175.17 | C | M | F | | | | | C | | | | C | | | | | F | | | | | | | | | | | F | | | | | | | | F | |
| 22H-CC | 183.76 | 183.86 | F | M | | | | F | | F | | F | | F | | | | | F | | | | | | | | | | | | | F | | F | F | | | | | |

**Table T14 (continued).** (Continued on next page.)

| Core, section | Depth (mbsf) Top | Depth (mbsf) Bottom | Abundance | Preservation | *Actinomma boreale* | *Actinomma medianum* | *Amphimelissa setosa* | *Axoprunum acquilonium* | *Botryostrobus aquilonaris* | *Ceratospyris borealis* | *Collosphaera pyloma* | *Cycladophora cornutoides* | *Cycladophora cosma* | *Cycladophora davisiana* | *Cycladophora sakaii* | *Cyrtocapsella japonica* | *Dendrospyris sakaii* | *Dictyophimus bullatus* | *Dictyophimus hirundo* | *Eucyrtidium asanoi* | *Eucyrtidium inflatum* | *Eucyrtidium matuyamai* | *Lamprocyrtis heteroporos* | *Larcopyle butschlii* | *Lipmanella redondoensis* | *Lithelius barbatus* | *Lychnocanoma magnacornuta* | *Lychnocanoma nipponica sakaii* | *Lychnocanoma parallelipes* | *Phormostichoartus fistula* | *Porodiscus circularis* | *Sphaeropyle langii-robusta* group | *Spongodiscus* sp. | *Spongopyle osculosa* | *Spongotrochus glacialis* | *Spongurus pylomaticus* | *Stichocorys delmontensis* | *Stichocorys peregrina* | *Stylatractus universus* | *Stylochlamydium venustum* | *Stylodictya validispina* | *Thecosphaera akitaensis* |
|---|---|---|---|---|---|---|---|---|---|---|---|---|---|---|---|---|---|---|---|---|---|---|---|---|---|---|---|---|---|---|---|---|---|---|---|---|---|---|---|---|
| 23H-CC | 193.31 | 193.41 | C | M | F | | | F | | F | | F | | A | | | | | F | | | | | | | | | | | | F | C | | F | F | | | | | |
| 24H-CC | 197.47 | 197.57 | F | M | F | | | F | | | | | | C | | | | | F | | | | | | | | | | | | F | F | | F | | | | | | F | |
| 25H-CC | 207.99 | 208.09 | F | M | F | | | | | | | | | F | | | | | F | | | | | | | | | | | | | F | | | | | | | | | |
| 26H-CC | 217.04 | 217.14 | C | G | | | | F | | F | | | | A | | | | | | | | | | F | | | | | | | | F | | F | | | | | F | |
| 27H-CC | 226.01 | 226.11 | C | G | F | | | F | | C | | | | A | | | | | | | | | | | | | | | | | | F | | F | F | | | | | |
| 28H-CC | 234.72 | 234.82 | F | M | F | | | | | F | | F | | C | | | | | | | | | | | | | | | | | | F | | F | F | | | | | |
| 29H-CC | 245.49 | 245.59 | F | M | | | | | | | | | | C | | | | | F | | | | | | | | | | | | | F | | F | | | | | | F | |
| 30H-CC | 254.21 | 254.31 | F | M | F | | | | | F | | | | F | F | | | | | | | | | | | | | | | | F | F | | F | F | | | | | |
| 31H-CC | 263.75 | 263.85 | C | M | F | | | | | F | | F | | | | | | | | | | | | F | | | | | | | | | F | F | | | | | F | |
| 32H-CC | 272.49 | 272.59 | F | M | F | | | | | | | | | F | F | | | | | | | | | | | | | | | | F | | | F | | | | | | F | |
| 33H-CC | 282.20 | 282.30 | F | M | F | | | | | | | | | F | | | | | | | | | | | | | | | | | F | F | | | | | | | | |
| 34H-CC | 291.18 | 291.28 | F | M | F | | | | | F | | | | | | | | | | | | | | F | | | | | | | F | F | F | F | F | | | | | |
| 35H-CC | 301.39 | 301.49 | F | M | F | | | | | | | F | | F | | | | | | | | F | | F | | | | | | | F | | F | F | F | | | | | |
| 36H-CC | 311.10 | 311.20 | F | P | F | | | | | | | | | C | | | | | | | | | | | | | | | | | | | | F | | | | | | | |
| 37H-CC | 320.19 | 320.29 | F | M | F | | | | | | | | | F | | | | | | | | | | | | | | | | | | | | F | | | | | | | |
| 38H-CC | 329.74 | 329.84 | F | P | F | | | | | | | | | | | | | | | | | | | | | | | | | | | | | F | | | | | | | |
| 39H-CC | 338.41 | 338.51 | F | P | F | | | | | | | | | | | | | | | | | | | | | | | | | | | | F | F | | | | | | | |
| 40H-CC | 346.74 | 346.84 | F | M | | | | F | | F | | | | C | F | | | | F | | | | | | | | | | | | F | | | F | | | | | | | |
| 41H-CC | 354.32 | 354.42 | F | P | | | | | | F | | | | | | | | | F | | | | | | | | | | | | | | | F | | | | | | | |
| 42X-CC | 359.57 | 359.67 | F | M | F | | | F | | F | | | | C | F | | | | F | | | F | | | | | | | | | F | | F | F | F | | | | F | F | |
| 43X-CC | 367.32 | 367.42 | F | P | | | | F | | F | | | | F | | | | | | | | | | | | | | | | | | | | | F | | | | | | |
| 44X-CC | 376.59 | 376.69 | F | M | | | | F | | F | | F | | F | | | | | F | | | | | | | | | | | | | | | F | F | | | | | | |
| 45X-CC | 388.26 | 388.36 | F | P | | | | F | | F | | | | | | | | | F | | | | | | | | | | | | | | | F | F | | | | | | |
| 46H-CC | 398.57 | 398.67 | C | M | F | | | F | | F | | F | | C | F | | | | F | | | | | F | | | | | | | | F | | F | C | F | | | | F | |
| 47H-CC | 405.99 | 406.09 | F | M | | | | | | F | | F | | F | F | | | | F | | | | | | | | | | | | | | | F | F | | | | | | |
| 48H-CC | 412.33 | 412.43 | F | M | | | | F | | F | | F | | F | | | | | | | | | | | | | | | | | | | | F | | | | | | F | |
| 49H-CC | 418.44 | 418.54 | F | P | | | | | | | | | | | | | | | | | | | | | | | | | | | | | | | | | | | | F | |
| 50X-CC | 428.50 | 428.60 | F | P | | | | | | | | | | | | | | | | | | | | | | | | | | | | | | F | | | | | | | |
| 51X-CC | 435.85 | 435.95 | F | M | | | | | | | | | | F | | | | | | | | | | F | | | | | | | | | F | F | | | | | F | F | |
| 52X-CC | 446.16 | 446.21 | F | M | | | | F | | F | | F | | C | | | | | | | | | | | | | | | | | | | F | F | | | | | F | | |
| 53X-CC | 455.88 | 455.98 | N | | | | | | | | | | | | | | | | | | | | | | | | | | | | | | | | | | | | | | |
| 54X-CC | 463.39 | 463.49 | F | P | | | | | | F | | | | | | | | | | | | | | | | | | | | | | | | F | | | | | | | |
| 55X-CC | 475.60 | 475.70 | F | P | | | | | | | | | | F | | | | | | | | | | | | | | | | | | | | | | | | | | | |
| 56X-CC | 482.57 | 482.67 | F | P | | | | | | | | | | F | | | | | | | | | | | | | | | | | | | | F | | | | | | | |
| 57X-CC | 493.97 | 494.07 | F | M | | | | | | | | | | | | | | | | | | | | | | | | | | | | | | F | F | | | F | | F | |
| 58X-CC | 502.88 | 502.98 | F | M | | | | F | | F | | | | F | | | | | | | | | | | | | | | | | | | F | F | | | | | F | |
| 59X-CC | 512.52 | 512.62 | F | M | | | | F | | F | | | | | | | | | | | | | | | | | | | | | | | F | F | | | | | F | |
| 60X-CC | 521.90 | 522.00 | F | M | | | | F | | F | | | | | | | | | | | | | | | | | | | | | | | | F | | | | | F | |
| 61X-CC | 532.41 | 532.51 | F | P | | | | F | | | | | | F | | | | | | | | | | | | | | | | | | | | F | | | | | | |
| 62X-CC | 541.78 | 541.88 | F | M | | | | F | | F | | | | F | | | | | F | | | | | | | | | | | | | | | F | | | | | | |
| 63X-CC | 550.54 | 550.64 | F | M | | | | | | F | | | | F | F | | | | F | | | | | | | | | | | | | | | F | | | | | | F | |
| 64X-CC | 561.05 | 561.15 | F | M | | | | F | | | | | | F | | | | | | | | F | | | | | | | | | | | | F | | | | | | |

**Table T14 (continued).**

| Core, section | Depth (mbsf) Top | Depth (mbsf) Bottom | Abundance | Preservation | *Actinomma boreale* | *Actinomma medianum* | *Amphimelissa setosa* | *Axoprunum acquilonium* | *Botryostrobus aquilonaris* | *Ceratospyris borealis* | *Collosphaera pyloma* | *Cycladophora cornutoides* | *Cycladophora cosma* | *Cycladophora davisiana* | *Cycladophora sakaii* | *Cyrtocapsella japonica* | *Dendrospyris sakaii* | *Dictyophimus bullatus* | *Dictyophimus hirundo* | *Eucyrtidium asanoi* | *Eucyrtidium inflatum* | *Eucyrtidium matuyamai* | *Lamprocyrtis heteroporos* | *Larcopyle butschlii* | *Lipmanella redondoensis* | *Lithelius barbatus* | *Lychnocanoma magnacornuta* | *Lychnocanoma nipponica sakaii* | *Lychnocanoma parallelipes* | *Phormostichoartus fistula* | *Porodiscus circularis* | *Sphaeropyle langii-robusta* group | *Spongodiscus* sp. | *Spongopyle osculosa* | *Spongotrochus glacialis* | *Spongurus pylomaticus* | *Stichocorys delmontensis* | *Stichocorys peregrina* | *Stylatractus universus* | *Stylochlamydium venustum* | *Stylodictya validispina* | *Thecosphaera akitaensis* |
|---|---|---|---|---|---|---|---|---|---|---|---|---|---|---|---|---|---|---|---|---|---|---|---|---|---|---|---|---|---|---|---|---|---|---|---|---|---|---|---|
| 65X-CC | 568.77 | 568.87 | F | M | | | | F | | | | | | | | | | | | | | | F | | | | | | | | | F | | | F | | | | F |
| 66X-CC | 581.04 | 581.14 | F | P | | | | | | | | | | | | | | | | | | | | | | | | | | | | F | | F | | | | | | |
| 67X-CC | 588.50 | 588.60 | F | M | | | | F | | | | | | | | | | | | | | | | | | | | | | | | | | F | | | | | | |
| 68X-CC | 599.26 | 599.36 | F | M | | | | F | | | | | | F | | | | | | | | | | | | | | | | | | | | F | | | | | F | |
| 69X-CC | 606.84 | 606.94 | F | G | F | | | F | | | | | | F | | | | | | | | | | | | | | | | | | | | F | | | | | F | |
| 70X-CC | 617.90 | 618.00 | F | P | | | | F | | | | | | | | | | | | | | F | | F | | | | | | | | | | F | F | | | | F | |
| 71X-CC | 628.16 | 628.26 | F | P | | | | F | | | | | | | | | | | | | | | | | | | | | | | | | | F | | | | | | |
| 72X-CC | 634.44 | 634.54 | F | P | | | | F | | | | | | F | | | | | | | | | | | | | | | | | | | | F | | | | | | |
| 73X-CC | 643.79 | 643.89 | F | P | F | | | F | | | | | | | | | | | | | | | | | | | | | | | | | | F | | | | | | |
| 74X-CC | 657.41 | 657.51 | F | P | | | | | | | | | | | | | | | | | | | | | | | | | | | | | | | | | | | F | |
| 75X-CC | 667.09 | 667.19 | F | P | F | | | | | | | | | | | | | | | | | | | | | | | | | | | | | F | | | | | | |
| 76X-CC | 674.96 | 675.06 | F | M | F | | | F | | | | | | F | | | | | | | | | | | | | | | | | | | | | | | | | | |
| 77X-CC | 686.37 | 686.37 | F | P | | | | | | F | | | | | | | | | | | | | | | | | | | | | | | F | | | | | | | |
| 78X-CC | 695.20 | 695.30 | F | P | | | | | | | | | | | | | | | | | | | | | | | | | | | | | | F | | | | | F | |
| 79X-CC | 705.72 | 705.82 | F | P | | | | | | | | | | | | | | | | | | | | | | | | | | | | | | | | | | | | |
| 80X-CC | 713.80 | 713.90 | F | P | | | | | | | | | | | | | | | | | | | | | | | | | | | | | | F | | | | | | |
| 81X-CC | 724.96 | 725.06 | F | M | | | | | | | | | | F | | | | | | | | | | | | | | | | | | F | | | | | | | | |
| 82X-CC | 734.41 | 734.51 | F | P | | | | | | | | | | | | | | | | | | | | | | | | | | | | | | F | | | | | F | |
| 83X-CC | 743.90 | 744.00 | F | P | | | | | | F | | | | | | | | | | | | | | | | | | | | | | | | F | | | | | | |

Notes: Abundance: A = abundant, C = common, F = few, N = none. Preservation: G = good, M = moderate, P = poor.

**Table T15.** Dinoflagellate cyst, pollen, and palynomorph range chart, Holes U1343A and U1343E. (See table notes.) (Continued on next page.)

| Core, section | Depth (mbsf) Top | Depth (mbsf) Bottom | Preservation | Marine: Dinoflagellate cysts | Marine: Organic lining of foraminifers | Pollen and spores: *Picea* | Pollen and spores: *Pinus* | Pollen and spores: Pollen (trees) | Pollen and spores: Pollen (shrubs) | Pollen and spores: Pollen (herbs) | Pollen and spores: Total pollen | Pollen and spores: Spores of *Sphagnum* | Pollen and spores: Spores of pteridophytes | Fresh water: *Botryococcus* + *Pediastrum* | Fresh water: *Hallodinium* | Fresh water: Tintinnids | Reworked palynomorphs | Dinoflagellate cyst assemblages: *Bitectatodinium tepikiense* | *Brigantedinium cariacoense* | *Brigantedinium simplex* | *Brigantedinium* spp. | *Dubridinium* spp. | *Filisphaera filifera* | *Impagidinium pallidum* | *Impagidinium* spp. | *Islandinium* cf. *brevispinosum* | *Islandinium minutum* | *Islandinium* morphotype *cesare* | *Nematosphaeropsis lemniscata* | *Operculodinium centrocarpum* | *Operculodinium centrocarpum* - Arctic morphotype | *Operculodinium centrocarpum* var. short processes | *Pentapharsodinium dalei* | *Polykrikos* - Arctic morphotype | *Polykrikos schwartzii* | *Protoperidinium americanum* | *Quinquecuspis concreta* | *Selenopemphix quanta* | *Spiniferites elongatus* | *Spiniferites ramosus* | *Trinovantedinium variabile* | *Votadinium spinosum* |
|---|---|---|---|---|---|---|---|---|---|---|---|---|---|---|---|---|---|---|---|---|---|---|---|---|---|---|---|---|---|---|---|---|---|---|---|---|---|---|---|---|
| 323-U1343A- | | | | | | | | | | | | | | | | | | | | | | | | | | | | | | | | | | | | | | | | | |
| 1H-CC | 5.4 | 5.5 | G | C | R | F | R | C | R | R | C | R | R | F | R | R | R | R | R | F | A | | | R | | R | D | | | | R | | R | R | | | | | | R |
| 3H-CC | 24.6 | 24.7 | G | C | F | C | R | C | R | | C | F | F | R | R | | R | | R | A | A | | | | | F | D | | | | R | | F | R | | R | R | | R | | |
| 5H-CC | 43.9 | 44.0 | G | C | R | C | | C | | R | C | F | F | R | | | R | | R | A | D | R | | | | F | R | | | | R | | | | | R | | | | |
| 7H-CC | 62.2 | 62.3 | G | A | C | F | R | A | R | | A | C | A | C | | | F | | R | A | D | | | | | R | F | | | | | | | | | | | | | | |
| 8H-4 | 67.3 | 67.4 | G | C | R | C | R | C | R | R | C | R | R | R | R | | | | R | A | D | | | | | | A | | | | R | A | | | | | | | | |
| 9H-CC | 81.9 | 82.0 | G | C | C | C | R | C | R | | C | C | C | | | | R | | R | A | D | | | | | | F | | | | A | | | | | | | | | |
| 10H-6 | 89.2 | 89.3 | G | A | R | R | | R | R | R | F | R | R | R | | | | | F | A | D | | | | | R | A | | | | | | | | | | | | | |
| 11H-CC | 100.5 | 100.6 | G | C | R | C | | C | F | | C | C | F | C | | | C | | F | A | D | | | | | | | | | | | | | | | | | | | |
| 12H-7 | 109.5 | 109.6 | G | A | C | F | | F | C | R | C | C | | C | | | R | | F | D | D | | | | | R | R | R | | | | | | R | R | R | R | | | |
| 13H-CC | 119.3 | 119.4 | G | A | | C | | C | F | R | C | C | F | F | | | R | | F | D | D | | | | | | R | | | | | | | | | R | | | | |
| 15H-CC | 139.1 | 139.2 | M | C | R | C | | C | R | R | C | R | R | | | | F | | R | A | D | | | | R | | D | | | | | | | | | | | | | R |
| 17H-CC | 157.3 | 157.4 | M | C | C | | | | R | R | F | R | | F | | | F | | | R | D | | | | | R | A | F | A | | | | | | | | | | | | |
| 19H-CC | 173.8 | 173.9 | P | C | R | R | | R | R | R | F | R | R | R | | | R | | F | D | D | | | | | | | | | | | | | | | | | | | |
| 21H-CC | 191.5 | 191.6 | M | A | F | F | | F | R | | F | R | | | | | C | | F | A | D | | | | | | R | | | | | | | | | | | | | |
| 22H-CC | 201.7 | 201.8 | M | A | C | C | F | C | C | R | C | C | R | C | | | C | | R | A | D | | | | | | R | | | | F | | | | | | | | | |
| 323-U1343E- | | | | | | | | | | | | | | | | | | | | | | | | | | | | | | | | | | | | | | | | | |
| 2H-CC | 17.7 | 17.8 | G | C | C | C | R | C | F | R | C | R | C | R | | | F | | F | A | D | | | | | R | A | | | | | | | | R | | | | | |
| 4H-CC | 37.1 | 37.2 | G | A | C | F | | F | R | R | C | | R | F | | | R | | R | A | D | | | | | | F | | | | R | | | R | | | | | | |
| 6H-CC | 55.5 | 55.6 | M | F | F | C | R | C | F | R | C | C | C | F | | | R | | | | P | | | | | | A | | | | P | P | | | | | | | | |
| 8H-CC | 74.8 | 74.9 | M | C | R | R | R | R | R | | F | R | R | R | | | R | | R | F | D | | | | | | D | | | | | | R | | | | | | | |
| 10H-CC | 90.9 | 91.0 | G | C | F | F | | C | R | R | C | C | R | C | | R | F | | | A | D | | | | | | D | | | | | | | | | | | | | |
| 12H-CC | 106.6 | 106.7 | G | A | C | C | | C | R | R | C | R | R | R | | | R | | R | A | D | | | | | | D | | | | | | | | | R | | | | |
| 14H-CC | 116.0 | 116.1 | G | C | C | C | R | C | R | | C | C | R | R | | | R | | R | A | D | | | | | | A | | | | | | | | | R | | | | |
| 16H-CC | 129.5 | 129.6 | G | A | C | A | R | A | F | | A | F | C | C | | | R | | R | A | D | | | | | | R | | | | R | | | | | R | | | | |
| 18H-CC | 148.2 | 148.3 | G | A | C | C | | C | R | R | C | F | R | R | | | R | | R | A | D | | | | | | D | | | | | | | | | R | | | | |
| 20H-CC | 164.9 | 165.0 | M | A | F | R | | R | | | R | R | R | R | | | R | | R | F | D | R | | | | | A | | | | R | | | | | R | | | R | |
| 22H-CC | 183.8 | 183.9 | G | C | R | | | | R | | R | R | | | | | | | F | D | D | | | | | | A | | | | | | | | | | | | | |
| 24H-CC | 197.5 | 197.6 | G | C | | | | | R | R | F | C | | C | | | R | | R | A | D | | | | | | A | | | | R | | | | | | | | | |
| 26H-CC | 217.0 | 217.1 | G | C | C | R | R | F | R | | F | F | C | F | | | R | | F | A | D | | | | | | A | | | | F | | | | | R | | | | |
| 28H-CC | 234.7 | 234.8 | M | C | C | F | R | F | R | R | C | F | R | C | | | R | | F | A | D | | | | | | A | | F | | | | | | | | | | | |
| 30H-CC | 254.2 | 254.3 | M | C | F | C | | C | F | | C | R | F | R | | | R | | R | D | D | | | | | | R | | | | | | | | | | | | | |
| 32H-CC | 272.5 | 272.6 | M | C | | C | | C | | | C | F | F | F | | | F | | A | A | D | | | | | | | | | | | | | | | | | | | |
| 34H-CC | 291.2 | 291.3 | M | C | | R | | R | R | | F | | R | | | | R | | F | A | D | | | | | | | | | | | | | | | | | | | |

**Table T15 (continued).**

| Core, section | Depth (mbsf) Top | Depth (mbsf) Bottom | Preservation | Marine: Dinoflagellate cysts | Marine: Organic lining of foraminifers | Pollen and spores: *Picea* | Pollen and spores: *Pinus* | Pollen and spores: Pollen (trees) | Pollen and spores: Pollen (shrubs) | Pollen and spores: Pollen (herbs) | Pollen and spores: Total pollen | Pollen and spores: Spores of *Sphagnum* | Pollen and spores: Spores of pteridophytes | Fresh water: *Botryococcus* + *Pediastrum* | Fresh water: *Hallodinium* | Fresh water: Tintinnids | Reworked palynomorphs | Dinoflagellate cyst assemblages: *Bitectatodinium tepikiense* | Dinoflagellate cyst assemblages: *Brigantedinium cariacoense* | Dinoflagellate cyst assemblages: *Brigantedinium simplex* | Dinoflagellate cyst assemblages: *Brigantedinium* spp. | Dinoflagellate cyst assemblages: *Dubridinium* spp. | Dinoflagellate cyst assemblages: *Filisphaera filifera* | Dinoflagellate cyst assemblages: *Impagidinium pallidum* | Dinoflagellate cyst assemblages: *Impagidinium* spp. | Dinoflagellate cyst assemblages: *Islandinium* cf. *brevispinosum* | Dinoflagellate cyst assemblages: *Islandinium minutum* | Dinoflagellate cyst assemblages: *Islandinium* morphotype *cesare* | Dinoflagellate cyst assemblages: *Nematosphaeropsis lemniscata* | Dinoflagellate cyst assemblages: *Operculodinium centrocarpum* | Dinoflagellate cyst assemblages: *Operculodinium centrocarpum* - Arctic morphotype | Dinoflagellate cyst assemblages: *Operculodinium centrocarpum* var. short processes | Dinoflagellate cyst assemblages: *Pentapharsodinium dalei* | Dinoflagellate cyst assemblages: *Polykrikos* - Arctic morphotype | Dinoflagellate cyst assemblages: *Polykrikos schwartzii* | Dinoflagellate cyst assemblages: *Protoperidinium americanum* | Dinoflagellate cyst assemblages: *Quinquecuspis concreta* | Dinoflagellate cyst assemblages: *Selenopemphix quanta* | Dinoflagellate cyst assemblages: *Spiniferites elongatus* | Dinoflagellate cyst assemblages: *Spiniferites ramosus* | Dinoflagellate cyst assemblages: *Trinovantedinium variabile* | Dinoflagellate cyst assemblages: *Votadinium spinosum* |
|---|---|---|---|---|---|---|---|---|---|---|---|---|---|---|---|---|---|---|---|---|---|---|---|---|---|---|---|---|---|---|---|---|---|---|---|---|---|---|---|---|---|
| 36H-CC | 311.1 | 311.2 | M | C | R | R | R | F | | | F | | | R | | | R | | | A | A | D | | | | | R | | | | | | | | | | | | |
| 38H-CC | 329.7 | 329.8 | G | C | C | C | F | C | R | | C | C | R | F | | | F | | | A | D | D | | | | | R | | | | | | | | | | | | |
| 40H-CC | 346.7 | 346.8 | G | C | C | C | C | C | F | | C | F | R | R | | | R | | | F | A | D | | | | | | | | R | | | | | | | | |
| 42X-CC | 359.6 | 359.7 | G | C | F | C | C | C | R | | C | C | F | C | | R | R | A | R | A | A | D | | | | | | | | R | | | | | | | | |
| 44X-CC | 376.6 | 376.7 | M | C | R | C | R | C | | | C | C | C | | | | R | | | | A | D | | A | | | | | | | | | | | | | | |
| 46H-CC | 398.6 | 398.7 | G | A | F | C | C | C | | R | C | C | C | F | | | R | | R | R | A | D | R | | | | R | | | | | | | | | | | |
| 48H-CC | 412.3 | 412.4 | M | C | F | C | | C | | | C | R | F | | | | | | | A | D | A | | | | | | | | | | | | | R | | | |
| 50X-CC | 428.5 | 428.6 | M | C | F | C | | C | C | | C | | F | | | | F | | | A | D | | | | | | | | | | | | | | | | | |
| 52X-CC | 446.2 | 446.2 | P | R | R | C | F | C | F | R | C | C | R | R | | | R | | | P | P | | | | | | | | | | | | | | | | | |
| 54X-CC | 463.4 | 463.5 | G | A | F | C | | C | F | | C | F | F | C | | | R | | R | F | D | D | | | | | | | | | | | | | R | | R | |
| 56X-CC | 482.6 | 482.7 | M | C | F | R | | R | R | | F | F | | R | | | | | | A | D | F | | | | | F | | | | | | | | | | | |
| 58X-CC | 502.9 | 503.0 | M | C | F | C | | C | | | C | | F | F | | | R | | | P | P | | | | | | | | | | | | | | | | | |
| 60X-CC | 521.9 | 522.0 | P | C | F | F | | F | | | F | | | | | | | | F | | D | | | | | | A | | | | | | | | F | | | |
| 62X-CC | 541.8 | 541.9 | M | C | C | C | | C | R | | C | | R | F | | | | | | F | D | F | | F | | | F | | | | | | | | | | | |
| 63X-CC | 550.5 | 550.6 | M | C | F | C | | C | | R | C | | F | | | | F | | | F | F | D | | | | | F | | | | | | | | | | | |
| 64X-CC | 561.1 | 561.2 | M | A | | C | | C | | | C | F | C | | | | C | | | | D | D | | | | | | | | | | | | | | | | |
| 66X-CC | 581.0 | 581.1 | P | C | R | C | R | C | | | C | R | C | R | | | C | | | A | D | A | | | | | | | | | | | | | | | | |
| 68X-CC | 599.3 | 599.4 | G | C | R | F | | F | | | F | | | | | | | | | D | D | R | | | | | | | | | | | | | | | | |
| 70X-CC | 617.9 | 618.0 | M | C | | C | | C | R | | C | | R | R | | | | | | | P | | | | | | | | | | | | | | | | | |
| 72X-CC | 634.4 | 634.5 | P | F | F | C | | C | R | | C | R | R | | | | C | | | | P | | | | | | | | | | | | | | | | | |
| 74X-CC | 657.4 | 657.5 | M | C | | C | | C | | F | C | C | F | | | | C | | | P | P | | | | | | | | | | | | | | | | | |
| 76X-CC | 675.0 | 675.1 | M | C | | C | F | C | F | | C | C | | F | | | C | | | | P | | | | | | | | | | | | | | | | | |
| 78X-CC | 695.2 | 695.3 | G | A | R | F | | F | | | F | F | R | R | | | R | | | R | F | D | | | | | | | | | | | | | | | | |
| 80X-CC | 713.8 | 713.9 | M | F | F | C | | C | R | R | C | | | F | | | F | | | | P | P | P | | | | | | | | | | | | | | | |
| 82X-CC | 734.4 | 734.5 | M | F | | R | | R | F | | C | R | R | | | | F | | | | P | P | P | | | | | | | | | | | | | | | |
| 84X-CC | 743.9 | 744.0 | P | F | | F | | F | F | | C | | F | | | | F | | | | P | | | | | | | | | | | | | | | | | |

Notes: Absolute abundance: A = abundant (>2000/cm$^3$), C = common (>200/cm$^3$), F = few (>100/cm$^3$), R = rare (<100/cm$^3$). Relative abundance of dinoflagellate cysts: D = dominant (>30%), A = abundant (>10%), F = few (>5%), R = rare (<5%), P = occurrence (when counts are <20). Preservation: G = good, M = moderate, P = poor.

**Table T16.** Chron ages and preliminary depths, Holes U1343A, U1343C, and U1343E. (See table notes.)

| Event | Age (ka) | Hole U1343A | | | Hole U1343C | | | Hole U1343E | | |
|---|---|---|---|---|---|---|---|---|---|---|
| | | Core, section, interval (cm) | Depth (mbsf) | Sed. rate (cm/k.y.) | Core, section, interval (cm) | Depth (mbsf) | Sed. rate (cm/k.y.) | Core, section, interval (cm) | Depth (mbsf) | Sed. rate (cm/k.y.) |
| | | 323-U1343A- | | | 323-U1343C- | | | 323-U1343E- | | |
| | 0 | | 0 | 23.6 | | 0 | 23.7 | | 0 | 23.2 |
| B Brunhes | 781 | 21H-2, 90 | 184.4 | | 21H-3, 60 | 185 | | 22H-5, 65 | 181.37 | 23.3 |
| T Jaramillo | 998 | | | | | | | 28H-5 (T) | 232 | 46.4 |
| B Jaramillo | 1072 | | | | | | | 32H-4, 70 | 266.33 | 24.9 |
| T Cobb Mountain | 1173 | | | | | | | 35H-2 (T) | 291.48 | |

Notes: B = bottom, T = top. Sed. rate = sedimentation rate.

**Table T17.** Moisture and density, Holes U1343A and U1343E. (Continued on next two pages.)

| Core, section, interval (cm) | Depth (mbsf) | Density (g/cm$^3$) | | | Void ratio | Water content (%) | Porosity (%) |
|---|---|---|---|---|---|---|---|
| | | Dry grain | Wet bulk | Dry bulk | | | |
| 323-U1343A- | | | | | | | |
| 2H-4, 29–31 | 10.3 | 2.71 | 1.49 | 0.74 | 2.65 | 49.97 | 72.59 |
| 2H-6, 29–31 | 13.3 | 2.71 | 1.52 | 0.80 | 2.38 | 47.33 | 70.37 |
| 3H-2, 29–31 | 16.8 | 2.80 | 1.58 | 0.88 | 2.17 | 44.22 | 68.43 |
| 3H-4, 29–31 | 19.8 | 2.72 | 1.57 | 0.88 | 2.09 | 44.03 | 67.61 |
| 4H-1, 29–31 | 24.8 | 2.73 | 1.58 | 0.88 | 2.09 | 43.98 | 67.69 |
| 4H-5, 29–31 | 30.8 | 2.71 | 1.61 | 0.94 | 1.89 | 41.64 | 65.36 |
| 5H-1, 29–31 | 34.3 | 2.68 | 1.59 | 0.92 | 1.92 | 42.30 | 65.71 |
| 5H-3, 29–31 | 37.3 | 2.75 | 1.59 | 0.90 | 2.05 | 43.26 | 67.16 |
| 5H-5, 29–31 | 40.2 | 2.62 | 1.59 | 0.93 | 1.82 | 41.57 | 64.54 |
| 6H-2, 29–31 | 45.0 | 2.77 | 1.69 | 1.06 | 1.62 | 37.39 | 61.77 |
| 6H-4, 29–31 | 48.0 | 2.65 | 1.61 | 0.95 | 1.79 | 40.91 | 64.17 |
| 7H-2, 29–31 | 53.9 | 2.75 | 1.72 | 1.12 | 1.46 | 35.24 | 59.33 |
| 7H-4, 29–31 | 56.8 | 2.78 | 1.67 | 1.02 | 1.74 | 39.04 | 63.49 |
| 8H-4, 29–31 | 66.5 | 2.70 | 1.63 | 0.98 | 1.77 | 40.17 | 63.92 |
| 9H-2, 29–31 | 73.8 | 2.67 | 1.64 | 1.01 | 1.66 | 38.82 | 62.34 |
| 9H-4, 29–31 | 76.8 | 2.81 | 1.76 | 1.15 | 1.45 | 34.50 | 59.13 |
| 9H-6, 29–31 | 79.7 | 2.73 | 1.50 | 0.77 | 2.56 | 49.02 | 71.92 |
| 10H-2, 29–31 | 82.6 | 2.69 | 1.70 | 1.10 | 1.45 | 35.53 | 59.10 |
| 10H-4, 29–31 | 85.5 | 2.55 | 1.57 | 0.92 | 1.78 | 41.70 | 64.07 |
| 10H-6, 29–31 | 88.5 | 2.74 | 1.70 | 1.08 | 1.53 | 36.40 | 60.46 |
| 11H-2, 29–31 | 91.9 | 2.69 | 1.69 | 1.08 | 1.50 | 36.25 | 59.93 |
| 11H-4, 29–31 | 94.8 | 2.71 | 1.70 | 1.08 | 1.51 | 36.25 | 60.10 |
| 11H-6, 29–31 | 97.6 | 2.64 | 1.65 | 1.02 | 1.58 | 37.96 | 61.23 |
| 12H-2, 29–31 | 101.6 | 2.75 | 1.66 | 1.00 | 1.74 | 39.29 | 63.50 |
| 12H-4, 29–31 | 104.6 | 2.58 | 1.59 | 0.93 | 1.76 | 41.13 | 63.73 |
| 13H-2, 29–31 | 110.9 | 2.68 | 1.81 | 1.26 | 1.12 | 30.00 | 52.90 |
| 13H-4, 29–31 | 113.8 | 2.74 | 1.79 | 1.23 | 1.23 | 31.48 | 55.11 |
| 14H-2, 29–31 | 120.7 | 2.72 | 1.70 | 1.09 | 1.50 | 36.13 | 60.04 |
| 14H-4, 29–31 | 123.6 | 2.58 | 1.66 | 1.05 | 1.44 | 36.45 | 59.10 |
| 14H-6, 29–31 | 126.5 | 2.71 | 1.67 | 1.03 | 1.62 | 38.04 | 61.90 |
| 15H-2, 29–31 | 130.5 | 2.65 | 1.64 | 1.01 | 1.64 | 38.74 | 62.11 |
| 15H-4, 29–31 | 133.3 | 2.67 | 1.67 | 1.04 | 1.56 | 37.43 | 60.89 |
| 15H-6, 29–31 | 136.1 | 2.52 | 1.66 | 1.08 | 1.34 | 35.22 | 57.27 |
| 16H-2, 29–31 | 139.4 | 2.73 | 1.73 | 1.13 | 1.42 | 34.76 | 58.66 |
| 16H-4, 29–31 | 142.4 | 2.56 | 1.60 | 0.96 | 1.66 | 39.91 | 62.42 |
| 16H-6, 29–31 | 145.2 | 2.69 | 1.71 | 1.10 | 1.45 | 35.53 | 59.18 |
| 17H-2, 29–31 | 149.8 | 2.63 | 1.68 | 1.08 | 1.44 | 35.97 | 59.09 |
| 17H-4, 29–31 | 152.6 | 2.65 | 1.64 | 1.01 | 1.63 | 38.63 | 61.99 |
| 17H-6, 29–31 | 155.6 | 2.69 | 1.71 | 1.11 | 1.43 | 35.22 | 58.80 |
| 18H-2, 29–31 | 158.7 | 2.75 | 1.74 | 1.14 | 1.41 | 34.52 | 58.58 |
| 18H-4, 29–31 | 161.4 | 2.54 | 1.60 | 0.96 | 1.64 | 39.75 | 62.11 |
| 18H-6, 29–31 | 164.4 | 2.65 | 1.65 | 1.02 | 1.60 | 38.23 | 61.54 |
| 19H-2, 29–31 | 169.0 | 2.61 | 1.73 | 1.17 | 1.23 | 32.62 | 55.23 |
| 19H-4, 29–31 | 171.9 | 2.70 | 1.80 | 1.25 | 1.17 | 30.66 | 53.86 |
| 20H-2, 29–31 | 174.4 | 2.63 | 1.58 | 0.91 | 1.90 | 42.51 | 65.49 |
| 20H-4, 29–31 | 177.0 | 3.41 | 2.23 | 1.72 | 0.98 | 22.82 | 49.61 |
| 20H-6, 29–31 | 179.9 | 2.59 | 1.76 | 1.22 | 1.12 | 30.64 | 52.76 |
| 21H-2, 29–31 | 183.8 | 2.72 | 1.80 | 1.24 | 1.19 | 30.93 | 54.33 |
| 21H-4, 29–31 | 186.6 | 2.66 | 1.71 | 1.11 | 1.40 | 35.06 | 58.40 |
| 21H-6, 29–31 | 189.4 | 2.68 | 1.64 | 1.00 | 1.69 | 39.23 | 62.83 |
| 22H-2, 29–31 | 193.2 | 2.72 | 1.80 | 1.24 | 1.20 | 31.12 | 54.59 |
| 22H-4, 29–31 | 196.1 | 2.56 | 1.61 | 0.98 | 1.63 | 39.41 | 61.93 |
| 22H-6, 29–31 | 198.9 | 2.69 | 1.74 | 1.15 | 1.33 | 33.66 | 57.10 |
| 323-U1343E- | | | | | | | |
| 23H-2, 29–31 | 184.9 | 2.72 | 1.65 | 1.00 | 1.72 | 39.22 | 63.18 |
| 23H-4, 29–31 | 187.7 | 2.63 | 1.73 | 1.16 | 1.28 | 33.15 | 56.06 |
| 23H-6, 29–31 | 189.8 | 2.70 | 1.76 | 1.19 | 1.26 | 32.40 | 55.82 |
| 24H-2, 29–31 | 194.7 | 2.67 | 1.68 | 1.06 | 1.52 | 36.78 | 60.27 |
| 24H-3, 29–31 | 196.2 | 2.78 | 1.34 | 0.50 | 4.57 | 62.77 | 82.06 |
| 25H-2, 29–31 | 198.2 | 2.71 | 1.71 | 1.10 | 1.47 | 35.72 | 59.50 |
| 25H-4, 29–31 | 201.2 | 2.75 | 1.71 | 1.10 | 1.50 | 35.90 | 60.02 |
| 25H-6, 29–31 | 204.2 | 2.63 | 1.69 | 1.08 | 1.43 | 35.73 | 58.83 |
| 26H-2, 29–31 | 208.1 | 2.74 | 1.79 | 1.23 | 1.23 | 31.52 | 55.14 |
| 26H-3, 29–31 | 209.3 | 2.69 | 1.81 | 1.26 | 1.13 | 30.06 | 53.00 |
| 26H-6, 29–31 | 213.8 | 2.62 | 1.49 | 0.76 | 2.44 | 48.80 | 70.90 |
| 27H-4, 29–31 | 221.3 | 2.76 | 1.79 | 1.22 | 1.26 | 31.87 | 55.77 |

**Table T17 (continued).** (Continued on next page.)

| Core, section, interval (cm) | Depth (mbsf) | Density (g/cm$^3$) | | | Void ratio | Water content (%) | Porosity (%) |
|---|---|---|---|---|---|---|---|
| | | Dry grain | Wet bulk | Dry bulk | | | |
| 27H-6, 29–31 | 224.3 | 2.64 | 1.67 | 1.06 | 1.50 | 36.80 | 60.05 |
| 28H-2, 29–31 | 227.8 | 2.71 | 1.81 | 1.26 | 1.15 | 30.35 | 53.57 |
| 28H-4, 29–31 | 230.8 | 2.70 | 1.75 | 1.18 | 1.29 | 32.86 | 56.31 |
| 28H-6, 29–31 | 233.8 | 2.67 | 1.68 | 1.07 | 1.49 | 36.36 | 59.82 |
| 29H-2, 29–31 | 236.2 | 2.72 | 1.80 | 1.24 | 1.19 | 30.88 | 54.27 |
| 29H-4, 29–31 | 238.9 | 2.75 | 1.74 | 1.14 | 1.40 | 34.32 | 58.37 |
| 29H-6, 27–29 | 241.9 | 2.68 | 1.67 | 1.04 | 1.58 | 37.57 | 61.20 |
| 30H-2, 27–29 | 246.1 | 2.59 | 1.66 | 1.06 | 1.45 | 36.46 | 59.16 |
| 30H-4, 28–30 | 249.0 | 2.70 | 1.72 | 1.13 | 1.39 | 34.53 | 58.16 |
| 30H-6, 28–30 | 252.0 | 2.64 | 1.68 | 1.07 | 1.47 | 36.37 | 59.59 |
| 31H-2, 27–29 | 255.6 | 2.73 | 1.82 | 1.28 | 1.13 | 29.74 | 53.00 |
| 31H-4, 32–34 | 258.6 | 2.69 | 1.74 | 1.16 | 1.32 | 33.39 | 56.82 |
| 31H-6, 26–28 | 261.5 | 2.65 | 1.61 | 0.96 | 1.75 | 40.41 | 63.66 |
| 32H-2, 29–31 | 263.8 | 2.63 | 1.67 | 1.06 | 1.47 | 36.39 | 59.47 |
| 32H-4, 29–31 | 265.9 | 2.66 | 1.72 | 1.12 | 1.37 | 34.51 | 57.82 |
| 32H-6, 29–31 | 268.8 | 2.65 | 1.73 | 1.15 | 1.30 | 33.45 | 56.56 |
| 33H-2, 29–31 | 273.3 | 2.69 | 1.72 | 1.13 | 1.38 | 34.50 | 58.06 |
| 33H-4, 29–31 | 276.0 | 2.60 | 1.62 | 0.98 | 1.66 | 39.58 | 62.46 |
| 34H-2, 29–31 | 284.0 | 2.71 | 1.82 | 1.28 | 1.12 | 29.78 | 52.88 |
| 34H-4, 27–28 | 286.9 | 2.73 | 1.82 | 1.28 | 1.14 | 29.89 | 53.24 |
| 34H-6, 29–31 | 289.8 | 2.69 | 2.27 | 2.00 | 0.34 | 11.57 | 25.61 |
| 35H-4, 29–31 | 294.8 | 2.56 | 1.60 | 0.96 | 1.67 | 40.09 | 62.58 |
| 35H-6, 29–31 | 297.8 | 2.68 | 1.70 | 1.09 | 1.45 | 35.66 | 59.21 |
| 36H-2, 29–31 | 301.4 | 2.39 | 1.53 | 0.89 | 1.69 | 41.94 | 62.76 |
| 36H-4, 29–31 | 304.4 | 2.67 | 1.75 | 1.17 | 1.28 | 32.93 | 56.19 |
| 36H-6, 29–31 | 307.4 | 2.69 | 1.75 | 1.17 | 1.30 | 33.00 | 56.43 |
| 37H-2, 29–31 | 312.1 | 2.71 | 1.82 | 1.27 | 1.13 | 29.89 | 53.04 |
| 37H-4, 29–31 | 315.1 | 2.77 | 1.82 | 1.26 | 1.21 | 30.80 | 54.65 |
| 37H-6, 29–31 | 318.1 | 2.71 | 1.77 | 1.20 | 1.26 | 32.35 | 55.84 |
| 38H-2, 29–31 | 321.5 | 2.53 | 1.59 | 0.95 | 1.67 | 40.29 | 62.51 |
| 38H-4, 29–31 | 324.5 | 2.67 | 1.71 | 1.11 | 1.41 | 35.09 | 58.47 |
| 38H-6, 29–31 | 327.5 | 2.67 | 1.67 | 1.04 | 1.57 | 37.57 | 61.10 |
| 39H-2, 29–31 | 331.1 | 2.74 | 1.79 | 1.23 | 1.23 | 31.53 | 55.19 |
| 39H-6, 29–31 | 337.1 | 2.69 | 1.75 | 1.17 | 1.30 | 33.13 | 56.53 |
| 40H-2, 29–31 | 340.1 | 2.56 | 1.63 | 1.02 | 1.52 | 37.82 | 60.32 |
| 40H-4, 29–31 | 343.0 | 2.70 | 1.82 | 1.28 | 1.10 | 29.49 | 52.40 |
| 40H-6, 29–31 | 346.0 | 2.68 | 1.83 | 1.30 | 1.06 | 28.85 | 51.52 |
| 41H-1, 29–31 | 347.1 | 2.76 | 1.81 | 1.25 | 1.20 | 30.89 | 54.60 |
| 41H-6, 29–31 | 352.8 | 2.74 | 1.74 | 2.15 | 1.44 | 33.50 | 58.90 |
| 42X 2, 29–31 | 356.2 | 2.56 | 1.61 | 0.97 | 1.63 | 39.47 | 62.00 |
| 42X 4, 29–31 | 358.8 | 2.62 | 1.62 | 0.99 | 1.65 | 39.26 | 62.30 |
| 43X 2, 29–31 | 361.7 | 2.65 | 1.57 | 0.89 | 1.97 | 43.20 | 66.28 |
| 43X 4, 29–31 | 364.7 | 2.68 | 1.66 | 1.02 | 1.62 | 38.27 | 61.87 |
| 47H-6, 29–31 | 405.2 | 2.71 | 1.78 | 1.22 | 1.22 | 31.58 | 55.01 |
| 48H-2, 29–31 | 407.5 | 2.69 | 1.72 | 1.13 | 1.38 | 34.40 | 57.92 |
| 51X-2, 29–31 | 429.2 | 2.69 | 1.72 | 1.13 | 1.39 | 34.56 | 58.13 |
| 51X-4, 29–31 | 432.2 | 2.51 | 1.56 | 0.91 | 1.77 | 41.97 | 63.94 |
| 51X-6, 29–31 | 435.2 | 2.71 | 1.85 | 1.32 | 1.05 | 28.45 | 51.32 |
| 52X-2, 29–31 | 438.9 | 2.69 | 1.79 | 1.24 | 1.17 | 30.77 | 53.90 |
| 52X-4, 29–31 | 441.9 | 2.68 | 1.72 | 1.13 | 1.38 | 34.48 | 57.92 |
| 52X-6, 29–31 | 444.8 | 2.65 | 1.72 | 1.13 | 1.33 | 34.06 | 57.17 |
| 53X-4, 29–31 | 451.6 | 2.67 | 1.68 | 1.06 | 1.52 | 36.88 | 60.36 |
| 53X-6, 29–31 | 454.6 | 2.81 | 1.36 | 0.53 | 4.27 | 60.86 | 81.04 |
| 54X-2, 29–31 | 458.2 | 2.68 | 1.71 | 1.11 | 1.42 | 35.20 | 58.71 |
| 54X-4, 29–31 | 461.1 | 2.68 | 1.69 | 1.07 | 1.50 | 36.38 | 59.94 |
| 55X-2, 29–31 | 467.5 | 1.95 | 1.33 | 0.64 | 2.02 | 51.53 | 66.92 |
| 55X-4, 29–31 | 470.5 | 3.62 | 2.89 | 2.60 | 0.39 | 10.02 | 28.27 |
| 55X-6, 29–31 | 473.5 | 2.67 | 1.77 | 1.21 | 1.20 | 31.57 | 54.57 |
| 56X-2, 29–31 | 477.1 | 2.65 | 1.70 | 1.10 | 1.41 | 35.30 | 58.55 |
| 57X-2, 29–31 | 485.4 | 2.64 | 1.61 | 0.96 | 1.76 | 40.50 | 63.71 |
| 57X-4, 29–31 | 488.4 | 2.66 | 1.78 | 1.22 | 1.18 | 31.14 | 54.03 |
| 57X-6, 29–31 | 491.4 | 2.70 | 1.73 | 1.14 | 1.37 | 34.19 | 57.81 |
| 58X-2, 29–31 | 495.5 | 2.54 | 1.60 | 0.96 | 1.65 | 39.88 | 62.20 |
| 58X-4, 29–31 | 498.5 | 2.74 | 1.76 | 1.18 | 1.32 | 32.99 | 56.84 |
| 58X-6, 29–31 | 501.3 | 2.56 | 1.62 | 0.99 | 1.59 | 38.89 | 61.42 |
| 59X-2, 29–31 | 504.7 | 2.64 | 1.68 | 1.08 | 1.45 | 35.98 | 59.20 |
| 59X-4, 29–31 | 507.7 | 2.69 | 1.65 | 1.01 | 1.67 | 38.84 | 62.52 |
| 59X-6, 29–31 | 510.6 | 2.65 | 1.62 | 0.97 | 1.74 | 40.22 | 63.51 |

**Table T17 (continued).**

| Core, section, interval (cm) | Depth (mbsf) | Density (g/cm$^3$) | | | Void ratio | Water content (%) | Porosity (%) |
|---|---|---|---|---|---|---|---|
| | | Dry grain | Wet bulk | Dry bulk | | | |
| 60X-2, 29–31 | 515.5 | 2.56 | 1.68 | 1.09 | 1.35 | 35.07 | 57.42 |
| 60X-4, 29–31 | 518.5 | 2.57 | 1.63 | 1.01 | 1.55 | 38.18 | 60.76 |
| 60X-6, 29–31 | 521.5 | 2.72 | 1.78 | 1.22 | 1.23 | 31.68 | 55.21 |
| 61X-2, 29–31 | 525.1 | 3.37 | 2.44 | 2.03 | 0.66 | 16.66 | 39.68 |
| 61X-4, 29–31 | 528.1 | 2.79 | 1.79 | 1.21 | 1.31 | 32.47 | 56.68 |
| 61X-6, 29–31 | 530.8 | 2.72 | 1.74 | 1.14 | 1.38 | 34.17 | 57.95 |
| 62X-2, 29–31 | 534.1 | 2.65 | 1.78 | 1.22 | 1.17 | 31.04 | 53.82 |
| 62X-4, 29–31 | 537.1 | 2.69 | 1.81 | 1.27 | 1.12 | 29.86 | 52.78 |
| 62X-6, 29–31 | 540.1 | 2.62 | 1.71 | 1.12 | 1.33 | 34.27 | 57.14 |
| 63X-2, 29–31 | 543.4 | 2.71 | 1.79 | 1.23 | 1.21 | 31.43 | 54.85 |
| 63X-4, 29–31 | 546.4 | 2.49 | 1.70 | 1.15 | 1.17 | 32.44 | 53.88 |
| 64X-2, 29–31 | 554.0 | 2.61 | 1.64 | 1.02 | 1.56 | 38.05 | 60.99 |
| 64X-4, 29–31 | 557.0 | 2.61 | 1.64 | 1.02 | 1.56 | 37.98 | 60.91 |
| 64X-6, 29–31 | 559.6 | 2.58 | 1.59 | 0.95 | 1.72 | 40.63 | 63.27 |
| 65X-3, 29–31 | 565.1 | 2.60 | 1.62 | 0.98 | 1.65 | 39.39 | 62.28 |
| 65X-5, 29–31 | 567.5 | 2.51 | 1.64 | 1.04 | 1.42 | 36.73 | 58.76 |
| 66X-2, 29–31 | 573.2 | 2.66 | 1.69 | 1.08 | 1.48 | 36.22 | 59.63 |
| 66X-4, 29–31 | 576.2 | 2.70 | 1.74 | 1.15 | 1.34 | 33.77 | 57.34 |
| 66X-6, 29–31 | 579.2 | 2.70 | 1.72 | 1.13 | 1.39 | 34.55 | 58.16 |
| 67X-3, 29–31 | 584.2 | 2.38 | 1.54 | 0.91 | 1.62 | 41.12 | 61.86 |
| 67X-5, 29–31 | 587.2 | 2.64 | 1.67 | 1.06 | 1.50 | 36.76 | 59.94 |
| 68X-2, 29–31 | 592.3 | 7.38 | 1.71 | 1.14 | 1.36 | 33.40 | 57.60 |
| 68X-4, 29–31 | 595.3 | 2.52 | 1.71 | 1.15 | 1.19 | 32.55 | 54.24 |
| 68X-6, 29–31 | 598.3 | 2.72 | 1.84 | 1.30 | 1.09 | 29.07 | 52.16 |
| 69X-2, 29–31 | 602.0 | 2.64 | 1.67 | 1.06 | 1.49 | 36.57 | 59.82 |
| 69X-4, 29–31 | 605.0 | 2.66 | 1.66 | 1.03 | 1.57 | 37.67 | 61.06 |
| 70X-4, 29–31 | 614.0 | 2.44 | 1.53 | 0.87 | 1.80 | 43.01 | 64.23 |
| 70X-6, 29–31 | 617.0 | 2.53 | 1.56 | 0.90 | 1.80 | 42.15 | 64.27 |
| 71X-2, 29–31 | 621.2 | 2.48 | 1.56 | 0.92 | 1.69 | 41.13 | 62.84 |
| 71X-4, 29–31 | 624.2 | 2.66 | 1.73 | 1.15 | 1.32 | 33.59 | 56.82 |
| 71X-6, 29–31 | 627.2 | 2.72 | 1.84 | 1.31 | 1.08 | 28.88 | 51.87 |
| 72X-2, 29–31 | 630.8 | 2.74 | 1.78 | 1.21 | 1.26 | 31.97 | 55.72 |
| 72X-4, 29–31 | 633.8 | 2.62 | 1.69 | 1.10 | 1.38 | 35.07 | 58.02 |
| 73X-4, 29–31 | 643.1 | 2.55 | 1.58 | 0.93 | 1.74 | 41.11 | 63.47 |
| 74X-2, 29–31 | 650.0 | 2.74 | 1.59 | 0.92 | 2.07 | 41.90 | 67.50 |
| 74X-4, 29–31 | 653.0 | 2.70 | 1.82 | 1.28 | 1.10 | 29.54 | 52.46 |
| 75X-2, 29–31 | 659.6 | 2.53 | 1.65 | 1.05 | 1.41 | 36.33 | 58.51 |
| 75X-4, 29–31 | 662.6 | 2.60 | 1.64 | 1.01 | 1.57 | 38.27 | 61.12 |
| 75X-6, 29–31 | 665.4 | 2.54 | 1.65 | 1.06 | 1.41 | 36.16 | 58.44 |
| 76X-2, 29–31 | 669.1 | 2.67 | 1.70 | 1.10 | 1.44 | 35.47 | 58.94 |
| 77X-4, 29–31 | 681.7 | 2.43 | 1.55 | 0.91 | 1.66 | 41.18 | 62.38 |
| 78X-4, 29–31 | 691.3 | 2.39 | 1.52 | 0.87 | 1.75 | 42.74 | 63.57 |
| 78X-6, 29–31 | 694.3 | 3.12 | 1.98 | 1.42 | 1.19 | 28.18 | 54.42 |
| 79X-2, 29–31 | 697.9 | 2.74 | 1.73 | 1.13 | 1.42 | 34.66 | 58.64 |
| 79X-6, 29–31 | 703.9 | 2.70 | 1.76 | 1.19 | 1.27 | 32.45 | 55.89 |
| 80X-2, 29–31 | 707.0 | 2.57 | 1.63 | 1.00 | 1.57 | 38.50 | 61.09 |
| 80X-5, 29–31 | 711.4 | 2.86 | 1.91 | 1.38 | 1.07 | 27.81 | 51.80 |
| 81X-2, 29–31 | 717.2 | 2.78 | 1.67 | 1.03 | 1.70 | 38.52 | 62.97 |
| 81X-4, 29–31 | 720.2 | 2.64 | 1.69 | 1.09 | 1.42 | 35.44 | 58.62 |
| 81X-6, 29–31 | 723.2 | 2.63 | 1.79 | 1.25 | 1.11 | 30.07 | 52.51 |
| 82X-2, 29–31 | 726.8 | 2.70 | 1.76 | 1.19 | 1.27 | 32.58 | 56.01 |
| 82X-4, 29–31 | 729.8 | 2.52 | 1.59 | 0.95 | 1.65 | 40.06 | 62.23 |
| 83X-2, 29–31 | 736.1 | 2.82 | 1.87 | 1.32 | 1.14 | 29.17 | 53.17 |
| 83X-4, 29–31 | 739.1 | 2.75 | 1.83 | 1.29 | 1.14 | 29.77 | 53.21 |
| 83X-6, 29–31 | 742.0 | 2.64 | 1.84 | 1.33 | 0.98 | 27.49 | 49.42 |

**Table T18.** Affine table indicating the amount that each core in each hole needs to be offset in order to construct a continuous record, Site U1343. (**Continued on next two pages.**)

| Core | Depth (mbsf) Top | Depth (mbsf) Bottom | Offset (m) | Depth CCSF-A (m) Top | Depth CCSF-A (m) Bottom | Recovered (m) | Recovery (%) |
|---|---|---|---|---|---|---|---|
| 323-U1343A- | | | | | | | |
| 1H | 0.00 | 5.49 | –0.10 | –0.10 | 5.39 | 5.49 | 100 |
| 2H | 5.50 | 15.04 | –0.09 | 5.41 | 14.95 | 9.54 | 100 |
| 3H | 15.00 | 24.73 | –0.16 | 14.84 | 24.57 | 9.73 | 102 |
| 4H | 24.50 | 34.76 | 0.46 | 24.96 | 35.22 | 10.26 | 108 |
| 5H | 34.00 | 44.01 | 2.62 | 36.62 | 46.63 | 10.01 | 105 |
| 6H | 43.50 | 54.02 | 3.26 | 46.76 | 57.28 | 10.52 | 111 |
| 7H | 53.00 | 62.29 | 4.97 | 57.97 | 67.26 | 9.29 | 98 |
| 8H | 62.50 | 71.89 | 5.29 | 67.79 | 77.18 | 9.39 | 99 |
| 9H | 72.00 | 82.00 | 6.26 | 78.26 | 88.26 | 10.00 | 105 |
| 10H | 81.50 | 91.00 | 8.03 | 89.53 | 99.03 | 9.50 | 100 |
| 11H | 91.00 | 100.60 | 8.97 | 99.97 | 109.57 | 9.60 | 101 |
| 12H | 100.50 | 110.52 | 10.18 | 110.68 | 120.70 | 10.02 | 105 |
| 13H | 110.00 | 119.42 | 12.13 | 122.13 | 131.55 | 9.42 | 99 |
| 14H | 119.50 | 128.96 | 13.75 | 133.25 | 142.71 | 9.46 | 100 |
| 15H | 129.00 | 139.16 | 13.88 | 142.88 | 153.04 | 10.16 | 107 |
| 16H | 138.50 | 147.21 | 16.41 | 154.91 | 163.62 | 8.71 | 92 |
| 17H | 148.00 | 157.39 | 17.33 | 165.33 | 174.72 | 9.39 | 99 |
| 18H | 157.50 | 166.22 | 18.66 | 176.16 | 184.88 | 8.72 | 92 |
| 19H | 167.00 | 173.90 | 19.93 | 186.93 | 193.83 | 6.90 | 115 |
| 20H | 173.00 | 182.06 | 21.79 | 194.79 | 203.85 | 9.06 | 95 |
| 21H | 182.50 | 191.60 | 23.24 | 205.74 | 214.84 | 9.10 | 96 |
| 22H | 192.00 | 201.76 | 24.64 | 216.64 | 226.40 | 9.76 | 103 |
| 323-U1343B- | | | | | | | |
| 1H | 0.00 | 6.85 | 0.01 | 0.01 | 6.86 | 6.85 | 98 |
| 2H | 7.00 | 16.87 | –0.19 | 6.81 | 16.68 | 9.87 | 104 |
| 3H | 16.50 | 25.08 | –0.02 | 16.48 | 25.06 | 8.58 | 90 |
| 4H | 26.00 | 35.26 | 0.67 | 26.67 | 35.93 | 9.26 | 97 |
| 323-U1343C- | | | | | | | |
| 1H | 0.00 | 7.24 | 0.00 | 0.00 | 7.24 | 7.24 | 101 |
| 2H | 7.20 | 16.67 | –0.04 | 7.16 | 16.63 | 9.47 | 100 |
| 3H | 16.70 | 26.60 | –0.11 | 16.59 | 26.49 | 9.90 | 104 |
| 4H | 26.20 | 36.40 | 0.86 | 27.06 | 37.26 | 10.20 | 107 |
| 5H | 35.70 | 44.75 | 1.71 | 37.41 | 46.46 | 9.05 | 95 |
| 6H | 45.20 | 55.51 | 3.03 | 48.23 | 58.54 | 10.31 | 109 |
| 7H | 54.70 | 63.91 | 4.41 | 59.11 | 68.32 | 9.21 | 97 |
| 8H | 64.20 | 70.68 | 2.82 | 67.02 | 73.50 | 6.48 | 162 |
| 9H | 68.20 | 78.35 | 5.26 | 73.46 | 83.61 | 10.15 | 107 |
| 10H | 77.70 | 87.68 | 6.71 | 84.41 | 94.39 | 9.98 | 105 |
| 11H | 87.20 | 97.54 | 7.87 | 95.07 | 105.41 | 10.34 | 109 |
| 12H | 96.70 | 106.68 | 9.79 | 106.49 | 116.47 | 9.98 | 105 |
| 13H | 106.20 | 116.10 | 11.08 | 117.28 | 127.18 | 9.90 | 104 |
| 14H | 115.70 | 124.65 | 13.19 | 128.89 | 137.84 | 8.95 | 94 |
| 15H | 125.20 | 135.04 | 14.04 | 139.24 | 149.08 | 9.84 | 104 |
| 16D | 134.70 | 134.70 | 13.79 | 148.49 | 148.49 | 0.00 | 0 |
| 17H | 144.20 | 153.40 | 17.22 | 161.42 | 170.62 | 9.20 | 97 |
| 18H | 153.70 | 163.15 | 18.24 | 171.94 | 181.39 | 9.45 | 99 |
| 19H | 163.20 | 171.99 | 20.42 | 183.62 | 192.41 | 8.79 | 93 |
| 20H | 172.70 | 182.21 | 21.11 | 193.81 | 203.32 | 9.51 | 100 |
| 21H | 182.20 | 192.15 | 22.24 | 204.44 | 214.39 | 9.95 | 105 |
| 22H | 191.70 | 196.16 | 23.85 | 215.55 | 220.01 | 4.46 | 99 |
| 23H | 196.20 | 205.45 | 25.82 | 222.02 | 231.27 | 9.25 | 97 |
| 24H | 205.70 | 215.54 | 27.60 | 233.30 | 243.14 | 9.84 | 104 |
| 25H | 215.20 | 224.77 | 28.41 | 243.61 | 253.18 | 9.57 | 101 |
| 26H | 224.70 | 234.72 | 29.98 | 254.68 | 264.70 | 10.02 | 105 |
| 323-U1343D- | | | | | | | |
| 1H | 0.00 | 8.53 | 1.16 | 1.16 | 9.69 | 8.53 | 100 |
| 323-U1343E- | | | | | | | |
| 1H | 0.00 | 8.22 | 3.48 | 3.48 | 11.70 | 8.22 | 100 |
| 2H | 8.20 | 17.80 | 3.72 | 11.92 | 21.52 | 9.60 | 101 |
| 3H | 17.70 | 26.40 | 3.82 | 21.52 | 30.22 | 8.70 | 92 |
| 4H | 27.20 | 37.17 | 5.24 | 32.44 | 42.41 | 9.97 | 105 |
| 5H | 36.70 | 43.06 | 5.37 | 42.07 | 48.43 | 6.36 | 67 |
| 6H | 46.20 | 55.55 | 8.42 | 54.62 | 63.97 | 9.35 | 98 |
| 7H | 55.70 | 64.00 | 8.82 | 64.52 | 72.82 | 8.30 | 87 |

**Table T18 (continued).** (Continued on next page.)

| Core | Depth (mbsf) Top | Depth (mbsf) Bottom | Offset (m) | Depth CCSF-A (m) Top | Depth CCSF-A (m) Bottom | Recovered (m) | Recovery (%) |
|---|---|---|---|---|---|---|---|
| 8H | 65.20 | 74.89 | 9.87 | 75.07 | 84.76 | 9.69 | 102 |
| 9H | 74.70 | 84.15 | 11.56 | 86.26 | 95.71 | 9.45 | 99 |
| 10H | 84.20 | 91.08 | 12.80 | 97.00 | 103.88 | 6.88 | 72 |
| 11H | 93.70 | 101.77 | 13.89 | 107.59 | 115.66 | 8.07 | 108 |
| 12H | 101.20 | 106.69 | 15.40 | 116.60 | 122.09 | 5.49 | 100 |
| 13D | 106.70 | 106.70 | 15.39 | 122.09 | 122.09 | 0.00 | 0 |
| 14H | 109.70 | 116.05 | 15.37 | 125.07 | 131.42 | 6.35 | 127 |
| 15H | 114.70 | 123.45 | 17.78 | 132.48 | 141.23 | 8.75 | 92 |
| 16H | 124.20 | 129.56 | 18.28 | 142.48 | 147.84 | 5.36 | 107 |
| 17H | 129.20 | 138.44 | 19.16 | 148.36 | 157.60 | 9.24 | 97 |
| 18H | 138.70 | 148.31 | 20.58 | 159.28 | 168.89 | 9.61 | 101 |
| 19H | 148.20 | 155.97 | 22.02 | 170.22 | 177.99 | 7.77 | 100 |
| 20H | 156.00 | 164.99 | 24.59 | 180.59 | 189.58 | 8.99 | 95 |
| 21H | 165.50 | 175.17 | 25.09 | 190.59 | 200.26 | 9.67 | 102 |
| 22H | 175.00 | 183.86 | 26.36 | 201.36 | 210.22 | 8.86 | 104 |
| 23H | 183.50 | 193.41 | 27.21 | 210.71 | 220.62 | 9.91 | 104 |
| 24H | 193.00 | 197.57 | 29.78 | 222.78 | 227.35 | 4.57 | 102 |
| 25H | 197.50 | 208.09 | 30.18 | 227.68 | 238.27 | 10.59 | 111 |
| 26H | 207.00 | 217.14 | 32.61 | 239.61 | 249.75 | 10.14 | 107 |
| 27H | 216.50 | 226.11 | 34.51 | 251.01 | 260.62 | 9.61 | 101 |
| 28H | 226.00 | 234.82 | 35.62 | 261.62 | 270.44 | 8.82 | 100 |
| 29H | 234.80 | 245.59 | 35.62 | 270.42 | 281.21 | 10.79 | 114 |
| 30H | 244.30 | 254.31 | 35.62 | 279.92 | 289.93 | 10.01 | 105 |
| 31H | 253.80 | 263.85 | 35.62 | 289.42 | 299.47 | 10.05 | 106 |
| 32H | 263.30 | 272.59 | 35.62 | 298.92 | 308.21 | 9.29 | 98 |
| 33H | 272.80 | 282.40 | 35.62 | 308.42 | 318.02 | 9.60 | 101 |
| 34H | 282.30 | 291.28 | 35.62 | 317.92 | 326.90 | 8.98 | 100 |
| 35H | 291.30 | 301.49 | 35.62 | 326.92 | 337.11 | 10.19 | 107 |
| 36H | 300.80 | 311.20 | 35.62 | 336.42 | 346.82 | 10.40 | 109 |
| 37H | 310.30 | 320.29 | 35.62 | 345.92 | 355.91 | 9.99 | 105 |
| 38H | 319.80 | 329.84 | 35.62 | 355.42 | 365.46 | 10.04 | 106 |
| 39H | 329.30 | 338.51 | 35.62 | 364.92 | 374.13 | 9.21 | 97 |
| 40H | 338.80 | 346.84 | 35.62 | 374.42 | 382.46 | 8.04 | 100 |
| 41H | 346.80 | 354.42 | 35.62 | 382.42 | 390.04 | 7.62 | 100 |
| 42X | 354.40 | 359.67 | 35.62 | 390.02 | 395.29 | 5.27 | 88 |
| 43X | 360.40 | 367.42 | 35.62 | 396.02 | 403.04 | 7.02 | 73 |
| 44X | 370.00 | 376.69 | 35.62 | 405.62 | 412.31 | 6.69 | 70 |
| 45X | 379.60 | 388.36 | 35.62 | 415.22 | 423.98 | 8.76 | 91 |
| 46H | 389.20 | 398.67 | 35.62 | 424.82 | 434.29 | 9.47 | 100 |
| 47H | 398.70 | 406.09 | 35.62 | 434.32 | 441.71 | 7.39 | 100 |
| 48H | 406.10 | 412.43 | 35.62 | 441.72 | 448.05 | 6.33 | 100 |
| 49H | 412.40 | 418.54 | 35.62 | 448.02 | 454.16 | 6.14 | 101 |
| 50X | 418.50 | 428.60 | 35.62 | 454.12 | 464.22 | 10.10 | 112 |
| 51X | 427.50 | 435.95 | 35.62 | 463.12 | 471.57 | 8.45 | 88 |
| 52X | 437.10 | 446.21 | 35.62 | 472.72 | 481.83 | 9.11 | 94 |
| 53X | 446.80 | 455.98 | 35.62 | 482.42 | 491.60 | 9.18 | 96 |
| 54X | 456.40 | 463.49 | 35.62 | 492.02 | 499.11 | 7.09 | 76 |
| 55X | 465.70 | 475.70 | 35.62 | 501.32 | 511.32 | 10.00 | 104 |
| 56X | 475.30 | 482.67 | 35.62 | 510.92 | 518.29 | 7.37 | 78 |
| 57X | 484.80 | 494.07 | 35.62 | 520.42 | 529.69 | 9.27 | 97 |
| 58X | 494.40 | 502.98 | 35.62 | 530.02 | 538.60 | 8.58 | 89 |
| 59X | 504.00 | 512.62 | 35.62 | 539.62 | 548.24 | 8.62 | 89 |
| 60X | 513.70 | 522.00 | 35.62 | 549.32 | 557.62 | 8.30 | 86 |
| 61X | 523.30 | 532.51 | 35.62 | 558.92 | 568.13 | 9.21 | 96 |
| 62X | 532.90 | 541.88 | 35.62 | 568.52 | 577.50 | 8.98 | 94 |
| 63X | 542.50 | 550.64 | 35.62 | 578.12 | 586.26 | 8.14 | 84 |
| 64X | 552.20 | 561.15 | 35.62 | 587.82 | 596.77 | 8.95 | 93 |
| 65X | 561.80 | 568.87 | 35.62 | 597.42 | 604.49 | 7.07 | 74 |
| 66X | 571.40 | 581.14 | 35.62 | 607.02 | 616.76 | 9.74 | 103 |
| 67X | 580.90 | 588.60 | 35.62 | 616.52 | 624.22 | 7.70 | 80 |
| 68X | 590.50 | 599.36 | 35.62 | 626.12 | 634.98 | 8.86 | 91 |
| 69X | 600.20 | 606.94 | 35.62 | 635.82 | 642.56 | 6.74 | 70 |
| 70X | 609.80 | 618.00 | 35.62 | 645.42 | 653.62 | 8.20 | 85 |
| 71X | 619.40 | 628.26 | 35.62 | 655.02 | 663.88 | 8.86 | 92 |
| 72X | 629.00 | 634.54 | 35.62 | 664.62 | 670.16 | 5.54 | 58 |
| 73X | 638.60 | 643.89 | 35.62 | 674.22 | 679.51 | 5.29 | 55 |
| 74X | 648.20 | 657.51 | 35.62 | 683.82 | 693.13 | 9.31 | 97 |
| 75X | 657.80 | 667.19 | 35.62 | 693.42 | 702.81 | 9.39 | 99 |
| 76X | 667.30 | 675.06 | 35.62 | 702.92 | 710.68 | 7.76 | 81 |

**Table T18 (continued).**

| Core | Depth (mbsf) Top | Depth (mbsf) Bottom | Offset (m) | Depth CCSF-A (m) Top | Depth CCSF-A (m) Bottom | Recovered (m) | Recovery (%) |
|---|---|---|---|---|---|---|---|
| 77X | 676.90 | 686.47 | 35.62 | 712.52 | 722.09 | 9.57 | 100 |
| 78X | 686.50 | 695.30 | 35.62 | 722.12 | 730.92 | 8.80 | 92 |
| 79X | 696.10 | 705.82 | 35.62 | 731.72 | 741.44 | 9.72 | 101 |
| 80X | 705.70 | 713.90 | 35.62 | 741.32 | 749.52 | 8.20 | 85 |
| 81X | 715.40 | 725.06 | 35.62 | 751.02 | 760.68 | 9.66 | 101 |
| 82X | 725.00 | 734.51 | 35.62 | 760.62 | 770.13 | 9.51 | 99 |
| 83X | 734.60 | 744.00 | 35.62 | 770.22 | 779.62 | 9.40 | 97 |

**Table T19.** Splice table indicating tie points between holes, Site U1343. Sampling along the splice should be used to construct a continuous record.

| Hole, core, section, interval (cm) | Depth mbsf | Depth CCSF-D (m) | | Hole, core, section, interval (cm) | Depth mbsf | Depth CCSF-D (m) |
|---|---|---|---|---|---|---|
| 323- | | | | 323- | | |
| U1343C-1H-5, 9.3 | 6.09 | 6.09 | Tie to | U1343E-1H-2, 111.3 | 2.61 | 6.09 |
| U1343E-1H-5, 133.9 | 7.34 | 10.82 | Tie to | U1343C-2H-3, 66.4 | 10.86 | 10.82 |
| U1343C-2H-6, 75.5 | 15.46 | 15.41 | Tie to | U1343E-2H-3, 48.7 | 11.69 | 15.41 |
| U1343E-2H-5, 142.4 | 15.62 | 19.35 | Tie to | U1343A-3H-3, 150.9 | 19.51 | 19.35 |
| U1343A-3H-6, 42.9 | 22.93 | 22.77 | Tie to | U1343E-3H-1, 125.1 | 18.95 | 22.77 |
| U1343E-3H-4, 147.8 | 23.68 | 27.49 | Tie to | U1343A-4H-2, 103.7 | 27.04 | 27.49 |
| U1343A-4H-6, 98.8 | 32.99 | 33.45 | Tie to | U1343E-4H-1, 100.9 | 28.21 | 33.45 |
| U1343E-4H-6, 145.0 | 36.15 | 41.39 | Tie to | U1343C-5H-3, 102.7 | 39.68 | 41.39 |
| U1343C-5H-5, 137.9 | 42.97 | 44.68 | Tie to | U1343E-5H-2, 110.5 | 39.31 | 44.68 |
| U1343E-5H-5, 10.1 | 42.30 | 47.67 | Tie to | U1343A-6H-1, 91.8 | 44.42 | 47.67 |
| U1343A-6H-7, 109.3 | 53.27 | 56.53 | Tie to | U1343E-6H-2, 40.8 | 48.11 | 56.53 |
| U1343E-6H-6, 44.7 | 53.98 | 62.40 | Tie to | U1343C-7H-3, 34.6 | 57.99 | 62.40 |
| U1343C-7H-5, 75.7 | 61.32 | 65.73 | Tie to | U1343E-7H-1, 121.3 | 56.91 | 65.73 |
| U1343E-7H-4, 138.6 | 61.44 | 70.25 | Tie to | U1343A-8H-3, 23.0 | 64.96 | 70.25 |
| U1343A-8H-6, 108.1 | 70.25 | 75.54 | Tie to | U1343E-8H-1, 47.1 | 65.67 | 75.54 |
| U1343E-8H-6, 90.4 | 72.52 | 82.40 | Tie to | U1343A-9H-3, 113.9 | 76.14 | 82.40 |
| U1343A-9H-5, 132.7 | 79.25 | 85.50 | Tie to | U1343C-10H-2, 35.8 | 78.80 | 85.50 |
| U1343C-10H-7, 87.8 | 86.60 | 93.30 | Tie to | U1343A-10H-3, 149.1 | 85.27 | 93.30 |
| U1343A-10H-6, 112.2 | 89.32 | 97.36 | Tie to | U1343C-11H-2, 95.0 | 89.49 | 97.36 |
| U1343C-11H-7, 67.7 | 96.67 | 104.53 | Tie to | U1343A-11H-4, 105.4 | 95.56 | 104.53 |
| U1343A-11H-6, 104.5 | 98.36 | 107.33 | Tie to | U1343C-12H-1, 84.6 | 97.55 | 107.33 |
| U1343C-12H-6, 25.7 | 103.94 | 113.72 | Tie to | U1343A-12H-3, 71.7 | 103.55 | 113.72 |
| U1343A-12H-7, 26.5 | 109.09 | 119.27 | Tie to | U1343C-13H-2, 133.4 | 108.19 | 119.27 |
| U1343C-13H-6, 66.9 | 113.45 | 124.53 | Tie to | U1343A-13H-3, 37.9 | 112.40 | 124.53 |
| U1343A-13H-6, 113.0 | 117.58 | 129.71 | Tie to | U1343C-14H-1, 81.4 | 116.51 | 129.71 |
| U1343C-14H-5, 37.4 | 121.83 | 135.03 | Tie to | U1343A-14H-2, 91.8 | 121.28 | 135.03 |
| U1343A-14H-6, 96.9 | 127.14 | 140.89 | Tie to | U1343C-15H-2, 23.6 | 126.85 | 140.89 |
| U1343C-15H-7, 57.4 | 134.06 | 148.11 | Tie to | U1343A-15H-4, 124.1 | 134.23 | 148.11 |
| U1343A-15H-7, 21.2 | 137.47 | 151.35 | Tie to | U1343E-17H-2, 151.1 | 132.19 | 151.35 |
| U1343E-17H-6, 106.6 | 137.72 | 156.87 | Tie to | U1343A-16H-2, 134.6 | 140.47 | 156.87 |
| U1343A-16H-6, 69.4 | 145.58 | 161.99 | Tie to | U1343E-18H-3, 71.8 | 141.41 | 161.99 |
| U1343E-18H-7, 56.2 | 146.83 | 167.42 | Tie to | U1343A-17H-2, 58.9 | 150.09 | 167.42 |
| U1343A-17H-6, 34.7 | 155.62 | 172.94 | Tie to | U1343C-18H-2, 58.5 | 154.71 | 172.94 |
| U1343C-18H-6, 71.1 | 160.77 | 179.01 | Tie to | U1343A-18H-3, 46.6 | 160.35 | 179.01 |
| U1343A-18H-6, 8.3 | 164.17 | 182.84 | Tie to | U1343E-20H-2, 75.1 | 158.25 | 182.84 |
| U1343E-20H-6, 58.7 | 163.73 | 188.31 | Tie to | U1343C-19H-4, 29.6 | 167.90 | 188.31 |
| U1343C-19H-6, 81.5 | 171.18 | 191.60 | Tie to | U1343E-21H-2, 37.6 | 166.52 | 191.60 |
| U1343E-21H-5, 107.6 | 171.70 | 196.78 | Tie to | U1343C-20H-3, 82.1 | 175.67 | 196.78 |
| U1343C-20H-6, 119.7 | 180.42 | 201.53 | Tie to | U1343E-22H-1, 16.6 | 175.17 | 201.53 |
| U1343E-22H-4, 113.2 | 180.35 | 206.71 | Tie to | U1343A-21H-1, 97.7 | 183.48 | 206.71 |
| U1343A-21H-7, 39.7 | 190.09 | 213.32 | Tie to | U1343E-23H-3, 20.0 | 186.11 | 213.32 |
| U1343E-23H-6, 109.9 | 190.58 | 217.79 | Tie to | U1343A-22H-2, 20.1 | 193.15 | 217.79 |
| U1343A-22H-6, 111.3 | 199.70 | 224.34 | Tie to | U1343C-23H-3, 38.2 | 198.52 | 224.34 |
| U1343C-23H-6, 127.6 | 203.32 | 229.14 | Tie to | U1343E-25H-2, 104.8 | 198.96 | 229.14 |
| U1343E-25H-7, 81.4 | 206.22 | 236.41 | Tie to | U1343C-24H-4, 52.7 | 208.81 | 236.41 |
| U1343C-24H-7, 92.2 | 213.70 | 241.30 | Tie to | U1343E-26H-2, 93.4 | 208.69 | 241.30 |
| U1343E-26H-6, 135.2 | 214.81 | 247.42 | Tie to | U1343C-25H-4, 30.0 | 219.01 | 247.42 |
| U1343C-25H-7, 12.7 | 223.26 | 251.66 | Tie to | U1343E-27H-1, 65.0 | 217.15 | 251.66 |
| U1343E-27H-5, 123.3 | 223.73 | 258.25 | Tie to | U1343C-26H-3, 129.9 | 228.27 | 258.25 |
| U1343C-26H-7, 52.3 | 233.30 | 263.28 | Tie to | U1343E-28H-2, 15.7 | 227.66 | 263.28 |
| U1343E-28H-6, 79.2 | 234.29 | 269.92 | Append | U1343E-29H-1, 0.0 | 234.80 | 270.42 |

**Table T20.** Temperature data, Site U1343. (See table note.)

| Core | Depth (mbsf) | Thermal resistance ($m^2K/W$) | $T$ (°C) | $T_s$ (°C) | Remarks |
|---|---|---|---|---|---|
| 323-U1343A- | | | | | |
| 5H | 43.5 | 45.28 | 4.34 | 2.04 | Calm sea |
| 9H | 81.5 | 83.09 | 6.25 | 2.02 | Calm sea |
| 14H | 129.0 | 134.79 | 8.53 | 2.10 | Calm sea |

Note: $T$ = formation temperature, $T_s$ = seafloor temperature.